Dual regulation of APC/C activity by Rca1

DISSERTATION

ZUR ERLANGUNG DES DOKTORGRADES

DER NATURWISSENSCHAFTEN (DR. RER. NAT.)

DER FAKULTÄT FÜR BIOLOGIE UND VORKLINISCHE MEDIZIN

DER UNIVERSITÄT REGENSBURG

vorgelegt von

Matthias Kies

aus Eschenbach i. d. OPf.

im Jahr

2017

Die vorliegende Doktorarbeit wurde von November 2013 bis Mai 2017 am Institut für Biochemie, Genetik und Mikrobiologie an der Universität Regensburg angefertigt.

Das Promotionsgesuch wurde eingereicht am:

05.05.2017

Die Arbeit wurde angeleitet von:

Prof. Dr. Frank Sprenger

Unterschrift:

Für meine Eltern

Table of contents

1 Abstract

The Anaphase-Promoting Complex/Cyclosome (APC/C) drives degradation of a large variety of mitotic cell cycle regulators. Therefore, tight regulation of APC/C activity plays a central role in proper cell cycle progression. Suppression of APC/C activity during G2-phase is crucial for entry into mitosis. This is achieved 1) by Cdk-dependent phosphorylation of the APC/C activator subunit Fzr, which renders Fzr unable to interact with the APC/C, and 2) by direct inhibition of APC/C-Fzr by Regulator of Cyclin A1 (Rca1). Previous studies suggest that not only the C-terminal part, but also the central localized F-box in Rca1 is fundamental for APC/C-Fzr inhibition. F-box proteins usually recruit substrates to SCF complexes, causing their polyubiquitination and subsequent degradation. To identify such substrates, an Rca1 precipitate from S2R+ cells was analyzed by mass spectrometry. Rca1 was found in complex with SCF components and other cell cycle regulators including Dacapo (Dap) and Skp2. Rca1 binds polyubiquitinated substrates in an F-box dependent manner *in vivo* giving evidence for a functional SCF-Rca1 complex. To analyze, whether SCF-Rca1 affects the protein stability of Dap and Skp2, a method for the stability analysis of GFP-labeled proteins during cell cycle progression of S2R+ cells was established. Dap stability was analyzed using a cell cycle inactive GFP-tagged version of Dap that lacks destabilization by CRL4-Cdt2 during S-phase (GFP-Dap-dCDI-dPIPa). Downregulation of Rca1 activity by RNAi resulted in upregulation of GFP-Dap-dCDI-dPIPa protein levels. Conversely, overexpression of Rca1 stimulated degradation of GFP-Dap-dCDI-dPIPa in an F-box dependent manner. Overexpression of CycE enhanced the interaction between Rca1 and Dap-dCDI-dPIPa, and further destabilized GFP-Dap-dCDI-dPIPa. These studies indicate that SCF-Rca1 functions synergistically with CycE/Cdk2 to target Dap for degradation. Two candidate Cdk phosphorylation sites in Dap, S205 and S214, were mutated but these mutations did neither affect the stability nor did they impair the interaction with Rca1. Interaction analyses with different truncated Rca1 and Dap constructs have revealed that the N-terminal part of Dap and the central region in Rca1 are required for their interaction. Loss of Rca1 binding by deletion of N-terminal residues in GFP-Dap-dCDI-dPIPa resulted in its complete stabilization. Flow cytometric based *in vivo* APC/C-Fzr activity assays in S2R+ cells were used to analyze the functional interaction between SCF-Rca1 and Dap. Loss of the F-box reduced APC/C-Fzr inhibition. However, this defect in APC/C-Fzr inhibition was suppressed by RNAi-mediated downregulation of Dap activity. Taken together, these studies provide a model, in which SCF-Rca1 targets Dap for degradation to release CycE/Cdk2 activity for APC/C-Fzr inhibition. To analyze the biochemical inhibition of APC/C-Fzr by Rca1 in more detail, an *in vitro* APC/C-Fzr ubiquitination assay was further developed. Experiments in the past failed to purify active *Drosophila* APC/C-Fzr from transgenic embryos. Therefore, a stable S2R+ cell line expressing a GFP-tagged APC/C component, Cdc16-MYC-TEV-GFP, was established. In addition, Fzr was *in vitro* translated in reticulocyte lysate and purified from baculovirus-infected SF-21 cells. APC/C-Fzr-dependent ubiquitination activity was detected to some extend by using Cdc16 precipitate treated with *in vitro* translated Fzr.

2 Introduction

2.1 The eukaryotic cell cycle

Each organism on earth either consists of a single cell or a body that is composed of a vast variety of highly specialized cell types. Reproduction of cells constitutes a fundamental aspect in each organism's life. In unicellular organisms, cell division results in an entire new organism, whereas in multicellular organisms, cell divisions fulfill several functional aspects, such as sexual reproduction, growth, development and maintenance of life. During embryonic development, a high number of cells arises from a single founder cell through cell divisions, thereby forming differentiated cell communities used for the formation of tissues and organs. After completion of development, cell divisions are required for replacement of injured and aged cells. The process of cell division is highly regulated and evolutionarily conserved from unicellular organisms, such as yeast, to higher multicellular organisms, such as humans. A highly precisely regulated cell machinery, known as the cell cycle ensures that events during cell division occur in a timely ordered fashion. In eukaryotes, the typical cell cycle is divided into four distinct phases: G1-, S-, G2- and M-phase (see Figure 1).

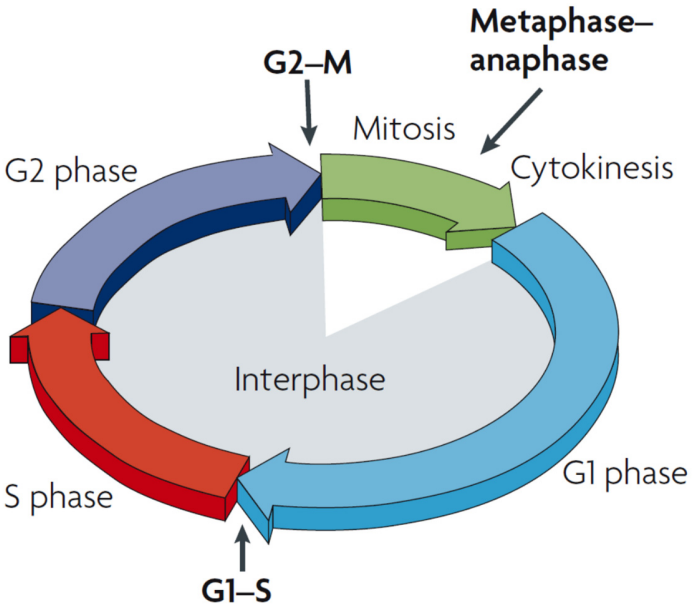

Figure 1 | The standard eukaryotic cell cycle
The standard eukaryotic cell cycle consists of four distinct phases: G1-, S-, G2- and M-phase. During S-phase DNA replication occurs, whereas a series of distinct processes during M-phase promote the formation of two genetically identical daughter cells. The M-phase is comprised of mitosis (nuclear division) and cytokinesis (cell division). The two gap phases (G1- and G2-phase) prepare the cell for the upcoming phase. Cell growth takes place during interphase, which includes G1-, S- and G2-phase. Cell cycle progression is governed by three major transitions that function in a switch-like manner. The G1/S transition initiates entry into S-phase, the G2/M transition regulates entry into mitosis and the metaphase-to-anaphase transition controls segregation of the sister chromatids into the new daughter cells and stimulates exit from mitosis (1, 2).

During S-phase, the genetic material is replicated resulting in chromosomes that consist of two identical sister chromatids. Equal distribution of the replicated sister chromatids into two new daughter cells occurs during the following M-phase. Two gap phases, G1- and G2-phase, separate S- and M-phases for growth and preparation. During G1-phase, the first phase of the cell cycle, the cell grows and prepares for the following S-phase by synthesizing substrates required for DNA synthesis. However, when growth factors and nutrients are low, the cell exits the cell cycle and enters the G0 phase, a quiescent stage, which keeps the cell in a non-proliferative state. After completion of S-phase, the G2-phase follows, where cell growth continues and synthesis of proteins required for entry into M-phase takes place. The first three phases of the cell cycle (G1-, S- and G2-phase) together are known as interphase and describe the period between

the M-phase of successive cell cycles. The M-phase is composed of mitosis and cytokinesis. Mitosis leads to the division of the nucleus and is regulated by five consecutive stages (prophase, prometaphase, metaphase, anaphase and telophase). In prophase, the first stage of mitosis, the sister chromatids are prepared for their segregation by condensation of the chromatin. Furthermore, the two centrosomes separate and migrate to opposite sides of the nucleus. The separated centrosomes initiate the assembly of the mitotic spindle required for sister chromatid segregation. During the next phase, the prometaphase, the nuclear envelope breaks down, the sister chromatids become attached to the mitotic spindle and their migration to the central region of the mitotic spindle (metaphase plate) begins. In metaphase, all sister chromatids are attached to the mitotic spindle and aligned at the metaphase plate. During anaphase, the mitotic spindle promotes the segregation of the sister chromatids to the opposite poles of the cell. The final stage of mitosis occurs during telophase, when the mitotic spindle is disassembled, the single-chromatid chromosomes become decondensed and the nuclear envelope is reformed around the chromosomes. After mitosis, cell division is completed by cytokinesis, which physically divides the cytoplasm of the proliferating cell into two daughter cells sharing the same genetic information (1).

2.2 Cell cycle regulation during *Drosophila* embryogenesis

Different types of cell cycle regulation are established during development of the *Drosophila* embryo. After fertilization, embryogenesis begins with 13 rapid synchronous nuclear divisions that occur in a common cytoplasm called a syncytium. These divisions cycles lack gap phases and consist only of alternating S- and M-phases (10, 11). The first eight divisions take place in the central portion of the egg. After that, most of the nuclei begin to migrate to the surface as they continue to divide. Some nuclei remain in the interior of the embryo to differentiate into yolk nuclei. After two further divisions (cycles 8 – 10) in synchrony with the migrating nuclei, yolk nuclei cease dividing and become polyploid (12). After nine divisions, a few nuclei move to the posterior pole of the embryo, where they form separate pole cells, the precursors of the germ cells, during division cycle 10. Meanwhile, the remaining migrating nuclei are evenly distributed in a monolayer under the cell membrane of the embryo, where they execute four further divisions (cycles 10 – 13) to form a syncytial blastoderm. During cell cycle 14, cellularization is initiated by the formation of a plasma membrane between all of the peripheral nuclei. The formed cells are progenitors of future somatic tissues. Following cellularization, gastrulation movement begins (10). From now on, maternal components are exhausted and cell cycle progression requires active transcription (13, 14). The following cell divisions (cycles 14 – 16) are no longer synchronous. Instead, for the first time, a G2-phase is established during cell cycle 14 and entry into mitosis occurs in a spatiotemporal pattern of 25 mitotic domains (15). The duration of the G2 phase, in which cells of each domain reside, depends on the zygotic expression of String (Stg). Stg belongs to the family of Cdc25 phosphatases, which trigger mitotic entry by immediate activation of mitotic Cdk1 (16-18). Following mitosis 16, the first G1 phase is established in cell cylce 17. Most of the epidermal cells exit the cell cycle and arrest in G1 until end of embryogenesis (18). Only cells of the developing nervous system enter S-phase and continue to divide (19). Other cell types, including dorsal cells as well as cells forming internal organs such as the gut and salivary glands switch their mitotic cycles to endoreplication cycles (20). Endoreplication cycles are special cell cycle variants, in which cells undergo continuing rounds of DNA replication consisting only of G- and S-phases, thereby becoming polyploid (21).

2.3 Cyclin-dependent kinases (Cdks) drive cell cycle progression

The cell cycle is a complex machinery that requires strict regulation to ensure that specific events during cell cycle progression are triggered in a timely ordered fashion. Three switch-like transitions are distributed throughout the cell cycle that are precisely controlled by several cell cycle regulators (2). These transitions are primarily controlled by cyclin-dependent kinases (Cdks) that function as key regulators during cell division (1, 2, 4-6). Cdks are serine/threonine kinases that primarily phosphorylate proteins on the minimal consensus motif S/T-P, with the optimal sequence being S/T-P-X-R/K (6). An alternative phosphorylation motif is the so-called non-S/T-P motif consisting of the minimal consensus sequence S/T-X-X-R/K (22). Cdks are inactive alone and require binding of regulatory subunits, known as cyclins, to become active (1). However, cyclin binding result only in partial activation of Cdks. For complete activity, Cdks must be in a particular phosphorylation state. This is achieved by Cdk-activating kinases (CAKs) that stimulate Cdk activity by phosphorylation of a threonine residue adjacent to the kinase active site (T161). Furthermore, members of the Wee1 kinase family inhibit activated cyclin-bound Cdk complexes through phosphorylation of specific tyrosine and threonine residues (Tyr15 in all Cdks, Tyr15 and Thr14 in Cdks of higher eukaryotes). Cdk activity is regained by phosphatases of the Cdc25 family that remove the inhibitory phosphate groups (1, 2).

Beside activation, cyclins also confer substrate specificity to the bound Cdks. This is well characterized for E- and A-type cyclins, which contain a hydrophobic patch that mediates binding to specific substrates through interaction with the cy motif consisting of the short sequence R-X-L (6). In contrast, D-type cyclins possess a L-X-C-X-E motif that is required for association with members of the pocket protein family (23, 24). Recruitment of target substrates with several Cdk phosphorylation sites can be stimulated by cyclin-dependent kinase subunits (Cks). Cks are highly conserved small adaptor proteins that interact with Cyc/Cdk complexes. Due to a phosphate anion-binding site, Cks proteins are additionally able to associate with phosphorylated residues, thereby allowing multi-phosphorylation of already phosphorylated target substrates (25). Mammals possess two Cks proteins, Cks1 and Cks2 (26), whereas in *Drosophila* Cks function is provided by the corresponding homologues Cks85A and Cks30A (27, 28). Another control of substrate recognition is achieved by subcellular localization of cyclin-bound Cdk complexes (6). For instance, E-type and A-type cyclins activate Cdks in the nucleus (29-31), while CycB1, a B-type cyclin, traffics between the cytoplasm and the nucleus to stimulate phosphorylation of substrates in both compartments (30-32) .

Cdk activity plays a central role in three major transitions that are distributed throughout the cell cycle (see Figure 1). These transitions behave in a switch-like manner and are based on all-or-none responses that induce an irreversible series of events when a certain threshold of Cdk activity is reached. The decision to enter a new division cycle is made at the restriction point (mammals) or Start (yeast) in late G1-phase. Once a cell passes this “point of no return”, it is committed to a new round of the cell cycle and mitogenic stimuli are no longer required to drive progression through the cell cycle (33). Following the restriction point/Start, an increase in Cdk activity stimulates the G1/S transition (2, 34, 35). Upon DNA replication, a rapid release of high Cdk activity triggers the transition from G2- to M-phase by which mitotic processes are initiated (1, 2). Conversely, initiation of the metaphase-to-anaphase transition, which promotes exit from mitosis is induced by Cdk inactivation (1, 2).

In contrast to Cdks that are present throughout the cell cycle, different types of cyclins are synthesized and destroyed during specific cell cycle stages, resulting in periodic oscillations of active Cyclin/Cdk

complexes (1, 2, 4-6). In yeast, cell division cycles are driven by a single Cdk, Cdc28 (*Schizosaccharomyces pombe*)/Cdc2 (*Saccharomyces cerevisiae*), and different cyclins that are expressed at specific cell cycle stages (1). During evolution, the number of Cdks and cyclins increased, resulting in a large variety of different Cyc/Cdk complexes (4). In mammals, three interphase Cdks (Cdk2, Cdk4 and Cdk6), a mitotic Cdk (Cdk1) and ten cyclins that belong to four different classes (D-type: CycD1, D2 and D3; E-type: CycE1, E2; A-type: CycA1, A2 and B-type: CycB1, B2 and B3) are directly involved in cell cycle progression (1, 2, 4-6). The different cyclin classes that contribute to cell divisions are well conserved among eukaryotes, only the number of cyclin subtypes varies. For instance, *Drosophila* possesses only one version of the cyclin types D, E and A (CycD, CycE and CycA), and two versions of B-type cyclins (CycB and CycB3) (1). According to the classical model of the mammalian cell cycle, specific Cyclin/Cdk complexes function during distinct stages of the cell cycle in order to trigger various events in their sequential order (see Figure 2).

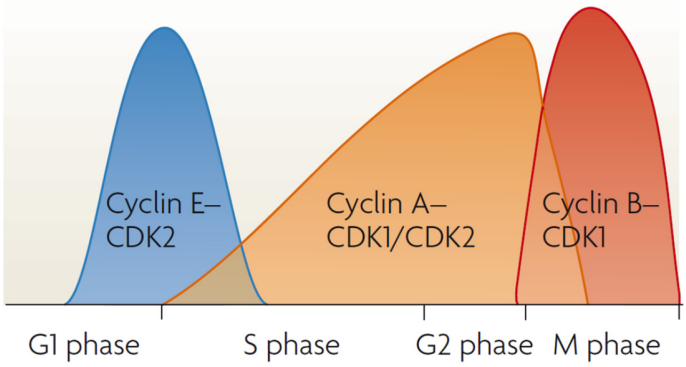

Figure 2 | Classical model of mammalian cell cycle regulation by specific Cyc/Cdk complexes
Level of cyclin accumulation controls the activity of specific Cyc/Cdk complexes during cell cycle progression. Upon mitogenic stimulation, Cdk4 and Cdk6 complexed with D-type cyclins regulate progression through G1-phase (not shown) (3). CycE/Cdk2 activity stimulates entry into S-phase. CycA/Cdk2 plays an important role in S-phase progression. Finally, onset of mitosis requires both CycA/Cdk1 and CycB/Cdk1 activity (2, 4-6).

Upon stimulation by growth factors, Cdk4 and Cdk6 are activated by D-type cyclins and play an important role for progression through G1-phase (36). Entry into S-phase is stimulated by CycE/Cdk2 activity, while continuation and completion of S-phase depends on CycA/Cdk2 activity. Both CycA and CycB complexed with Cdk1 are required for progression through mitosis (1, 2, 4-6). Although this model of cell cycle regulation is widely distributed and accepted, studies with Cdk-knockout mice demonstrated that cell cycle progression in most cell types does not require the interphase Cdks, Cdk2, Cdk4 and Cdk6. Only highly specialized cell types depend on these Cdk types (2, 4). Cdk2-null mice are viable and does not reveal any cell cycle defects in proliferating cells (37, 38). Even triple knockout embryos for *cdk2*, *cdk4* and *cdk6* developed normally until mid-gestation, but subsequently died due to heart and haematopoietic defects. In contrast, embryos lacking Cdk1 activity were not able to perform any cell divisions (39). Thus, Cdk activity provided by the mitotic Cdk, Cdk1, is essential and sufficient to drive the mammalian cell cycle. Furthermore, studies with cyclin-knockout mice showed that D-type and E-type cyclins are dispensable for cell cycle progression (40, 41). Only loss of CycA2 or CycB1, respectively, resulted in lethality (42, 43). These studies suggest that only Cdk1, together with CycA2 and CycB1, is required for triggering events involved in cell division. Given that expression of both CycA and CycB steadily rise during interphase (1), together with the fact that a single cyclin is able to promote cell cycle progression of fission yeast (44), a minimal threshold level was established, in which the level of Cdk activity controls the entry into different cell cycle stages (see Figure 3).

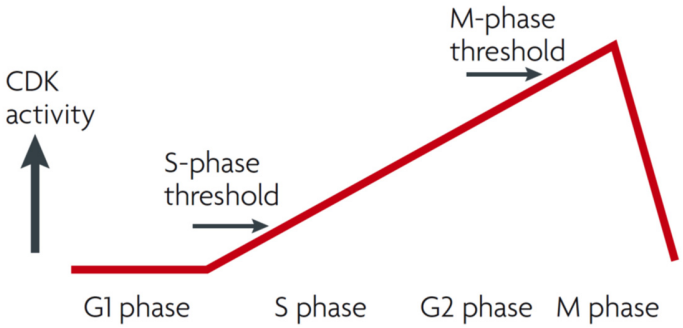

Figure 3 | Minimal threshold model for general cell cycle regulation
Entry into S- or M-phase, respectively, are triggered by different thresholds of Cdk1 activity. Threshold required for S-phase entry is accomplished by CycA or CycE complexed with Cdk1 or Cdk2. The M-phase threshold is fulfilled by CycA and CycB in conjunction with Cdk1 (2).

Low Cdk1 activity is sufficient for initiation of S-phase, whereby an increase in Cdk1 activity during S- and G2-phase stimulates entry into mitosis. Threshold for initiation of S-phase is achieved by low levels of CycA, while accumlation of CycA and CycB during interphase is necessary to trigger entry into mitosis. The requirement of only Cdk1 for proper cell cycle progression indicates that the basic principles in cell cycle regulation are highly conserved from yeast to higher eukaryotes.

2.4 Checkpoints monitor cell cycle progression

Proper cell cycle progression by Cyc/Cdk complexes is essential for the maintenance of life, as failure in cell cycle regulation may cause severe defects including unscheduled proliferation, genomic instability and chromosomal instability, leading in the worst case to death. Therefore, critical processes during progression through the cell cycle are monitored by checkpoints. These checkpoints control whether cell cycle events have been completed successfully without any complications before progression into the next cell cycle phase takes place. When this is not the case, and inconvenient conditions prevent appropriate cell divisions, the corresponding checkpoint is activated. Activation of checkpoints triggers arrest of the cell cycle through induction of several signal transduction pathways that modulate Cdk activity. Progression through the cell cycle is halted until all failures compromising genomic integrity are completely eliminated (4).

The DNA damage checkpoint protects the cell from endogenous (reactive cellular metabolites) and environmental factors (ionizing or ultraviolet radiation, chemicals and drugs) that affect the integrity of the genomic DNA. Whenever unreplicated or damaged DNA is detected, signaling pathways pause cell cycle progression, thereby giving the cell time to repair the damage before cell division processes are resumed. Cell cycle arrests due to DNA damage occur during G1- or G2-phase (4, 45). Upon successful DNA replication, the spindle assembly checkpoint that functions at the metaphase-to-anaphase transition ensures proper distribution of sister chromatids during mitosis. Only when all chromosomes are bipolarly attached to the mitotic spindle during metaphase, processes resulting in chromosome segregation are initiated. This includes the downregulation of Cdk activity, which contributes to the elimination of sister chromatid cohesion, thereby allowing the migration of sister chromatids to opposite poles of the cell. As long as the chromosomes are not correctly aligned to the mitotic spindle, Cdk activity is sustained by preventing CycB degradation (4).

2.5 Regulation of the G1-S transition

The G1/S transition is characterized by a switch-like transcriptional activation of G1/S genes that drive entry into S-phase. In the mammalian system, G1/S gene transcription is regulated by members of the E2F

family of transcription factors. E2F family members are divided into activator E2Fs (E2F1, E2F2 and E2F3a) stimulating expression of G1/S genes and repressor E2Fs (E2F3b, E2F4, E2F5, E2F6, E2F7, and E2F8) that inhibit the expression of the same G1/S genes (34). DNA binding to promoters of E2F target genes requires association with any member of the DP protein family (DP1 and DP2) (46), except E2F7 and E2F8, which bind DNA independently of the DP proteins (47, 48). During early G1-phase, E2F transcription factors interact with members of the pocket protein family (RB, p107 and p130) to inhibit transcription (34). Activator E2F proteins are bound and inhibited by RB (49), while the E2F repressor proteins E2F4 and E2F5 associate with p107 and p130 to form transcriptional repressor complexes (50). In contrast, the repressor proteins E2F6, E2F7 and E2F8 do not require binding of pocket proteins to function as transcriptional repressors (47, 51, 52). An increase in Cdk activity during late G1-phase triggers transcriptional activation of G1/S genes (34). Cdk activity is initially promoted by Cdk4 and Cdk6, which become activated by the accumulation of D-type cyclins in response to growth factors (36). Phosphorylation of the pocket proteins by D-type cyclin-conjugated Cdk4/6 results in their release from the bound E2F transcription factors (9, 34). E2F repressors are replaced by E2F activator proteins, thereby inducing the transcription of G1/S genes, with CycE belonging to the first subset of G1/S proteins that is expressed (53). CycE activates Cdk2 and drives further phosphorylation of the pocket proteins (9, 34). Furthermore, E2F activator proteins stimulate their own transcription (54). By this, a positive feedback loop system is established that induces G1/S gene expression in a switch-like manner (see Figure 4).

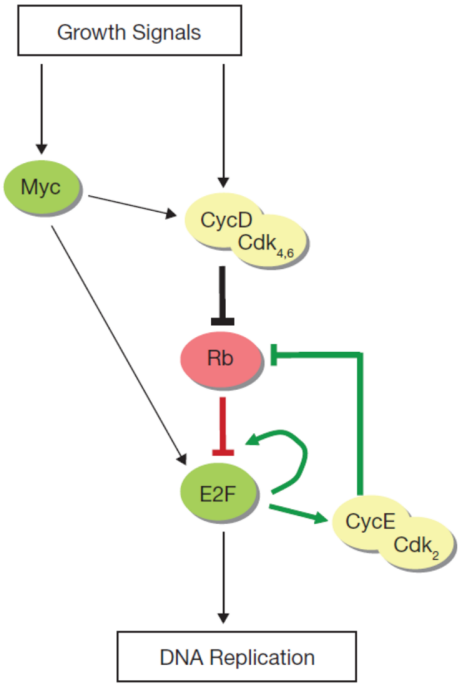

Figure 4 | A bistable RB-E2F switch regulates entry into S-phase
DNA replication is initiated by a feedback system that transforms growth signals into a bistable switch in response to growth signals. Here, a simplified version of the G1/S switch involving the core components RB and E2F is shown. During G1-phase, E2F transcription factors are bound and inhibited by RB. Growth factors induce RB inactivation by CycD/Cdk4 and CycD/Cdk6, thereby releasing E2F activity that stimulates entry into S-phase through transcriptional activation of DNA replication genes. Positive feedback loops ensure rapid accumulation of G1/S gene products. E2F stimulates its own activity by directing its own transcription and the transcription of *cycE*, which results in further Cdk activity driving Rb inhibition (9).

Upon transcriptional activation of G1/S genes, transcription is inactivated through several negative feedback loops. Expression of the E2F target gene *cyclin A* stimulates CycA/Cdk2 activity during S-phase, resulting in inhibition of the activator E2F1 by phosphorylation (55). Both CycA/Cdk2 and CycE/Cdk2 mediate degradation of the cyclin-dependent kinase inhibitor p27, thereby further enhancing Cdk2 activity (56, 57). Another negative feedback loop is established by the E2F target gene *skp2* that stimulates formation of SCF-Skp2, which targets E2F1 for degradation (58). Furthermore, accumulation of the E2F

targets E2F6, E2F7 and E2F8 during S-phase contributes to inactivation of G1/S gene transcription (34). The RB-E2F pathway controlling the G1/S transition is functionally conserved among eukaryotes, but differs in its complexity. In *Drosophila*, G1/S gene transcription is regulated by two members of the E2F transcription family, E2F1 and E2F2, a single DP protein and two pocket proteins, RBF1 and RBF2 (59). E2F1 activates G1/S gene transcription, while E2F2 function as transcriptional repressor (60, 61).

As in the mammalian system, in *Drosophila*, entry into S-phase requires Cdk activation. CycD/Cdk4 was identified as kinase able to provide Cdk activity during G1-Phase. However, Cdk4 activity is not critical for triggering the switch into S-phase, since loss of Cdk4 did not disturb proper cell cycle progression (62). Entry into S-phase rather depends on CycE/Cdk2 activity. Embryos mutant for *cycE* displayed a G1-phase arrest, while ectopic overexpression of CycE induced entry into S-phase (63, 64). Studies with mutant embryos have shown that in mitotically dividing cells, CycE stimulates E2F1 dependent transcription of DNA replication genes (65). CycE was also identified as an E2F1 target gene product in endocycling cells (66), suggesting that G1/S switch is also established in *Drosophila*. During S-phase, CycE/Cdk2 stimulates its own inactivation by phosphorylation of CycE, which is recognized by SCF-Ago for degradation (67, 68). CycA plays an important role for S-phase entry as well. Overexpression of CycA or loss of the CycA/Cdk1 inhibitor Roughex accelerated the G1/S transition (69, 70).

2.6 Entry into mitosis

Entry into mitosis is triggered by abrupt activation of Cdk1 at the end of G2-phase (1). Studies in the mammalian system suggest that the release of high Cdk1 activity is achieved through a switch-like feedback system that relies on the interplay of Cdk1 regulatory proteins (71). During G2-phase, mitotic Cdk1 is kept in an inactive state by inhibitory phosphorylations on Tyr15 and Thr14. These phosphorylations are catalyzed by two kinases, Tyr15 by Wee1 (35) and both Tyr15 and Thr14 by Myt1 (72). Inhibition of both enzymes drives premature entry into mitosis (73). Before mitosis, members of the Cdc25 phosphatase family (Cdc25A, Cdc25B and Cdc25C) activate Cdk1 by removing the inhibitory phosphate groups (74). A switch-like mechanism for Cdk1 activation is established by positive feedback loops that involve Cdk1-mediated regulation of the Cdc25 proteins as well as the kinases Wee1 and Myt1 (see Figure 5).

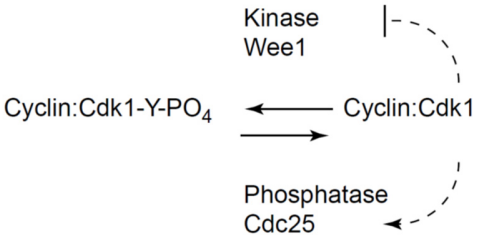

Figure 5 | A molecular switch controls entry into mitosis
Inhibitory phosphorylations catalyzed by Wee1-related kinases keep Cdk1 in an inactive state (Cyclin:Cdk1-Y-PO_4) during G2-phase. Before mitosis, dephosphorylation by Cdc25-related phosphatases activate Cdk1 (Cyclin:Cdk1). Inhibition of Wee1 kinases and activation of Cdc25 phosphatases through phosphorylation by Cdk1 generates a positive feedback system that allows a switch-like activation of Cdk1 (7).

Phosphorylation by Cdk1 activates Cdc25 phosphatases, but inhibits the kinase activity of Wee1 and Myt1. Thus, once a small portion of Cdk1 becomes active, a sudden increase in Cdk1 activation follows, providing the Cdk1 activity required for robust progression through mitosis (1, 7, 71). Removal of inhibitory phosphate groups is regarded as initiator of the feedback system. Overexpression of a non-phosphorylatable version of Cdk1 (T14A and Y15F) caused rapid cell cycles with abortive mitoses (75). Cdc25A is sufficient to trigger the switch into mitosis. Deletion of the other Cdc25 isoforms, Cdc25B and Cdc25C, did not affect normal cell cycle progression in mice (76). However, the mechanism that initiate

activation of Cdc25 phosphatases to trigger the switch from a state of “no Cdk1 activity” to a state of “high Cdk1 activity” is not well understood. Studies in human culture cells point to CycA/Cdk2 as an essential component of such a trigger mechanism (1, 77). CycA2 raises during S-phase (1, 2, 4-6) and its downregulation resulted in a G2-phase arrest due to inhibitory phosphorylation on CycB/Cdk1 (77). Furthermore, CycA2/Cdk2 activity was not inhibited upon downregulation of CycB1 expression. Therefore, it is possible that CycA/Cdk2 initiates activation of Cdc25 phosphatases to trigger abrupt CycB/Cdk1 activation in late G2-phase. In addition, CycB/Cdk1 promotes its activation by stimulating the activity of members of the Polo-like kinase (Plk) family that support phosphorylation of Cdc25 phosphatases (1, 78, 79).

In *Drosophila*, CycA, B and B3 in conjunction with Cdk1 contribute to progression through mitosis (1, 80). *In vivo* analyses of diverse mutant embryos have demonstrated the functional role of each cyclin. Embryos mutant for *cycA* were lethal due to a G2-phase arrest before mitosis 16 during embryogenesis when maternal contributions are exhausted. Thus, CycA is essential for mitosis (81-83). *cycB* mutant embryos were viable and displayed only minor defects in cell cycle progression, such as delay of mitosis or slightly abnormal mitotic spindles. Loss of CycB3 did not produce abnormalities during cell divisions. However, *cycB cycB3* double mutants were lethal and showed defects in mitotic spindle assembly. Mutation of both *cycA* and *cycB3* resulted in embryonic lethality with additional failures in chromosome condensation (80). *cycA cycB* double mutant embryos even arrested before mitosis 15, a stage during which maternal supplied cyclin transcripts are still present (80, 81). Altogether, these studies indicate that all three cyclins cooperate to regulate progression through mitosis, with each cyclin possessing major functions during mitosis. CycA is mainly responsible for triggering mitosis, whereas CycB is particularly important for proper formation of the mitotic spindle. CycB3 plays a major role in chromosome condensation (80).

In *Drosophila*, two different Cdc25 homologues exists, String (Stg) and Twine. However, only Stg is responsible for Cdk1 activation in mitosis (17). Twine plays an important role in controlling Cdk1 activity in meiotic cells (84). As suggested for the mammalian system, activation of Stg plays also a critical role in triggering immediate entry into mitosis. During embryogenesis, when cells arrest in G2-phase of cell cycle 14, Stg expression is required to drive cells into mitosis (16, 17).

2.7 The ubiquitin proteasome pathway mediates degradation of cell cycle regulators

Cell divisions are driven by the coordinated up- and downregulation of cell cycle regulatory proteins at specific stages of the cell cycle. The presence of cell cycle proteins at non-desirable time points during the cell cycle might cause severe defects on the viability and functionality of the cell. In the worst case, the cell cycle regulatory system becomes uncontrolled resulting in highly proliferating and genetically unstable cells that finally give rise to cancer. Therefore, the existence of a system that regulates degradation of regulatory proteins in a temporally and spatially specific manner constitutes an essential part in proper cell cycle progression (85). The ubiquitin proteasome pathway mediates the degradation of specific proteins and belongs to the major proteolytic mechanisms in eukaryotic cells. In this pathway, the formation of specific polyubiquitin (polyUb) chains on target proteins label them for degradation by the 26S proteasome (see Figure 6). Ubiquitin (Ub) is a small protein of 76 residues and is highly conserved among eukaryotes (86). The attachment of monoubiquitin on substrates, a process known as ubiquitination, are catalyzed by a cascade of enzymatic reactions that involve the three enzymes E1 (ubiquitin-activating enzyme), E2 (ubiquitin-conjugating enzyme) and E3 (ubiquitin-ligase). In these

reactions, an isopeptide bond between the carboxyl group of the C-terminus of Ub (G76) and the ε-amino group of a lysine residue within the substrate is formed. Repeated ubiquitination of the previously added Ub results in the formation of polyUb chains. Due to the presence of seven lysine residues in Ub, seven different types of lysine linkages (K6, K11, K27, K29, K33, K48, K63) can exist in polyUb chains. The lysine residue that is utilized for linkage determines the fate of the target substrate. PolyUb chains that consist of Ub linked by K6, K11, K29 and K48 target substrates for proteolytic destruction by the 26S proteasome. However, K48-conjugated polyUb chains are the primary signal for degradation (87). In contrast, K63 linkages are involved in non-proteolytic processes, such as protein trafficking (88), DNA repair (89) and inflammation (90).

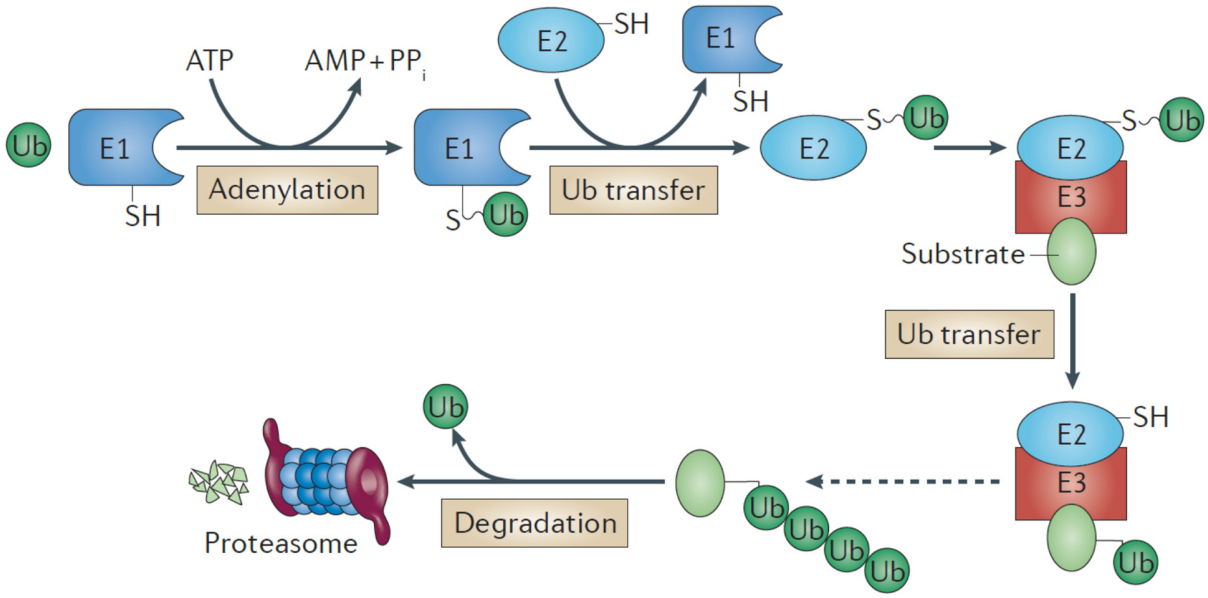

Figure 6 | The ubiquitin proteasome pathway
The ubiquitin proteasome pathway mediates degradation of proteins by the 26S proteasome. Polyubiquitin (polyUb) chains are assembled on target proteins by the subsequent action of three enzymes: E1 (ubiquitin-activating enzyme), E2 (ubiquitin-conjugating enzyme) and E3 (ubiquitin-ligase). First, the E1 catalyzes the formation of an Ubiquitin (Ub) adenylate intermediate (adenylation), which is then transferred to the catalytical cysteine in E1. This creates a reactive thioester bond between E1 and the C-terminus of Ub, thereby releasing AMP and pyrophosphate (PP_i). Next, the activated Ub is transferred to a cysteine residue in E2. Finally, E3 that is associated with a target substrate catalyzes the transfer of the E2-bound Ub to a lysine residue in the substrate. Multiple cycles of Ub transfers to the previously attached Ub (preferentially through K48-linkages) leads to the formation of polyUb chains (dashed arrow), which are recognized by the 26S proteasome for degradation. The tilde (~) represents a high-energy bond (91).

The E1 enzyme catalyzes the initial step of the ubiquitination process, the ATP-dependent activation of Ub. This is achieved by two subsequent reactions. First, the E1 binds ATP and Ub and catalyzes the formation of an Ub adenylate via adenylation of its carboxy-terminal glycine residue, thereby releasing pyrophosphate. Next, the catalytic cysteine in E1 attacks the Ub adenylate, resulting in a covalent E1~Ub thioester and release of AMP. The high-energy thioester bond (~) prepares Ub for further transfer reactions (92, 93). The number of E1 enzymes that function in Ub activation depends on the organism. For instance, in human, two E1 enzymes, Ube1 and Ube6, were identified. In *Drosophila*, Uba1 is the sole E1 enzyme (93).

The second step of the ubiquitination cascade is accomplished by the transfer of the activated Ub in E1∼Ub to an E2 enzyme. Upon E1∼Ub binding, a catalytic cysteine in E2 attacks the E1∼Ub thioester in a transthioesterification reaction, resulting in E2∼Ub, in which Ub is again covalently linked via a high-energy thioester bond (94). In contrast to E1 enzymes, E2 enzymes comprise a large family that is defined by a conserved core ubiquitin conjugation (UBC) domain containing the catalytic cysteine (95). In human, 37 members of the E2 family are present, whereas *Drosophila* possesses 32 different E2 proteins (96).

The final step in the ubiquitination process requires the action of an E3 enzyme, which catalyzes the transfer of the active Ub from a specific E2∼Ub complex to a lysine residue within a specific target substrate. By this, an isopeptide bond is formed between the Ub C-terminus and the ε-amino lysine of the substrate. Repeated ubiquitination of a lysine residue of the previously added Ub leads to the formation of a polyUb conjugated substrate. All E3 enzymes belong to three classes according to the domain structure they contain: (1) HECT (homologous to to the E6AP carboxyl terminus) domain containing E3s, (2) RING (really interesting new gene) and (3) RBR (RING-between-RING) domain containing E3s (97). The E3 families differ in the mechanism of Ub transfer. RING E3s transfer the Ub directly to the substrate by binding E2∼Ub and the target substrate simultaneously (98, 99). The RING domain associates with the E2-Ub complex and stimulates the Ub transfer. Ring E3s are further subdivided into single-subunit and multi-subunit E3 ligases (100). In contrast to RING E3s, HECT E3s ubiquitinate their substrates in a two-step reaction. After binding of E2∼Ub via the HECT domain, an E3∼Ub thioester intermediate on a catalytic cysteine residue within the HECT domain is first established, before the Ub is finally transferred to the target substrate (101). RBR E3s share features with both RING and HECT E3 ligases, using a RING-HECT hybrid mechanism for ubiquitination. RBR domain consists of two RING domains, RING1 and RING2, which are separated by a conserved IBR (in-between-ring) domain. RING1 functions as interaction site for E2∼Ub, while RING2 contains the catalytic cysteine residue for the formation of an E3∼Ub thioester intermediate (102). Since all E3 enzymes contain individual domains for substrate recognition, E3s are primarily involved in the selection of their target substrates. The mammalian genome encodes for more than 600 E3s to cover the ubiquitination of the vast variety of target substrates (103). In contrast, E2 enzymes determine the type of lysine linkage during ubiquitination, and thereby the fate of the substrate (104).

Polyubiquitinated proteins, especially those that are linked through K48, are degraded by the 26S proteasome, which consists of two sub-complexes, the 20S core particle (CP) and two 19S regulatory particle (RP). The CP is capped by one or two RPs. The 20S CP is composed of four rings (two outer α- and two inner β-rings). Each ring consists of seven distinct subunits, α1-α7 and β1- β7, respectively. The outer α-rings function as entrance for the substrate and the removal of degraded peptides. The inner β-rings provide proteolytic activity by the β-subunits β1, β2 and β5. The 19S RP is divided into two sub-structures, the base and the lid complex. The lid complex consists of Rpn subunits (Rpn3, Rpn5-9, Rpn11, Rpn12 and Rpn15). The base complex contains six AAA-ATPase subunits (Rpt1-Rpt6) and non-ATPase subunits (Rpn1, Rpn2, Rpn10 and Rpn13) (105, 106). ATPase activity is necessary for unfolding and translocation of the protein to be degraded into the 20S RP, where degradation into short peptides takes place (107). Recognition of polyubiquitinated substrates is accomplished by intrinsic receptors, 19S RP subunits (Rpn13, Rpn1, Rpn10, Rpt5 and Rpn15), and extra-proteasomal shuttle proteins (Rad23, Dsk2 and Ddi1) that recruit polyubiquitinated substrates to the 26S proteasome. Shuttle proteins associate with polyubiquitin chains via their UBA domain, and interact with 19S RP subunits via their UBL domain (108). Poly-Ub chains consisting of at least four Ub are required to provide an efficient signal for recognition (109). During proteasomal degradation, polyubiquitin chains are disassembled by members of the DUB (deubiquitinating enzymes) family (110). The 19S RP subunit Rpn11 functions as integral DUB of the 26S

proteasome (111), whereas Uch37 (112) and Ubp6 (113) associate with 19S RP subunits. Released polyubiquitin chains are broken down to single Ub monomers by the DUB protein IsoT, which thereby refills the pool of available free Ub for further protein modifications (114).

2.8 The Anaphase Promoting Complex/Cyclosome (APC/C)

The anaphase promoting complex or cyclosome (APC/C) is a multi-subunit E3 ligase that belongs to the family of RING E3s. The vertebrate APC/C is a high molecular weight complex (1.22 MDa) that consists of 19 conserved subunits, of which 5 are present in two copies (see Figure 7). The subunits divide the complex into three structural domains: 1) the platform, which functions as scaffold for the different subunits, 2) the catalytic core, that binds an E2 enzyme to catalyze substrate ubiquitination, and 3) the tetratricopeptide repeat (TPR), also known as the arc lamp, which serves as further scaffold that associates with APC/C regulatory proteins (115).

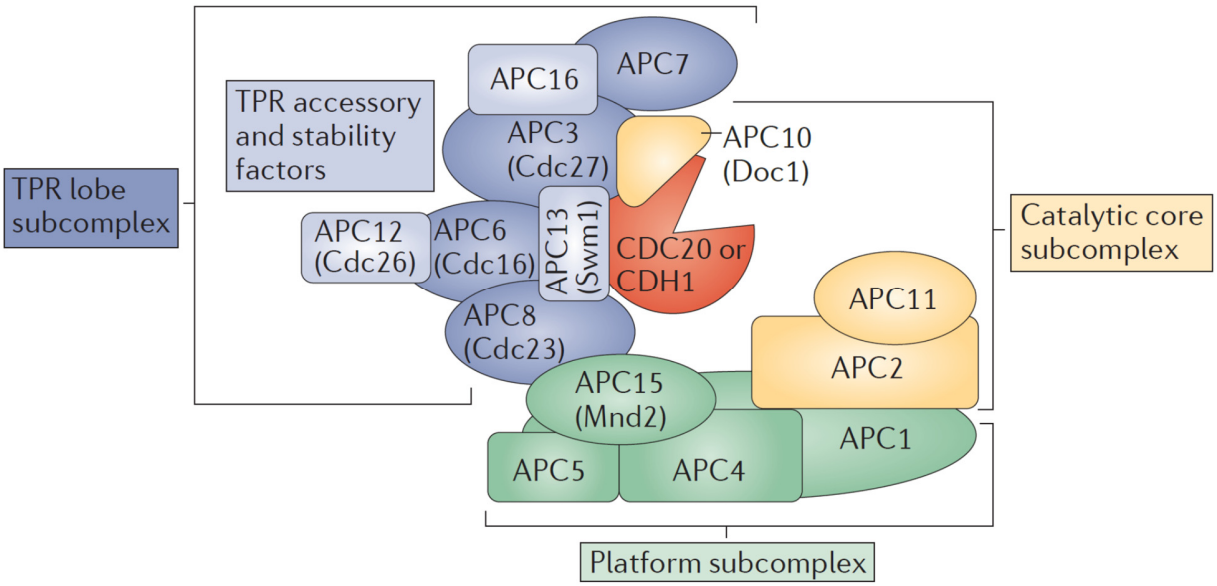

Figure 7 | Schematic structure of the APC/C complex bound to its co-activator subunit Cdc20/Cdh1
The APC/C is a multi-subunit RING-type E3 ligase that consists of several conserved subunits (19 subunits, of which 5 exist as duplicates), which divide the complex in three functional parts: 1) The platform (green subunits), 2) the catalytic core (yellow subunits), and 3) tetratricopeptide repeat (TPR) lobe (dark blue subunits), which is stabilized by TPR accessory and stability factors (light blue subunits). APC3, APC6, APC7, APC8 and APC12 are present as dimers. The platform and the TPR lobe have scaffolding functions. APC11 mediates binding to the E2 enzyme. Substrate recruitment occurs via APC10 and the associated co-activator subunit Cdc20/Cdh1 (red subunit) (115).

In vertebrate, the APC/C interacts with three distinct E2 enzymes (UBCH5, UBCH10 and UBE2S) via the RING domain of APC11 (116). Together, UBCH5/UBCH10 and UBE2S stimulate the formation of polyubiquitin chains on bound target substrates. Both UBCH5 and UBCH10 bind to the APC/C to catalyze the initial attachment of short polyubiquitin chains on specific lysine residues within the target substrate (117). During cell cycle progression, UBCH10 plays a more prominent role than UBCH5. Loss of UBCH5 did not show any mitotic defects in mammalian cells (118). Furthermore, UBCH10 is more efficient in ubiquitination than UBCH5 (117). In *Drosophila*, UbcD1/Effete (119) and Vihar (120) represent homologues of UBCH5 and UBCH10, respectively. After the assembly of short polyubiquitin chains, they are elongated

by UBE2S resulting in long polyubiquitin chains that target the substrate to the 26S proteasome for degradation (121, 122). UBE2S interacts with the APC/C scaffold subunit APC2, its co-activator subunit Cdc20 or Cdh1 and binds on a specific surface in the RING domain of APC11 that does not compete with association of the initiator E2 enzymes (116, 123).

APC/C is an essential cell cycle regulator, since it mediates progression through the cell cycle by targeting other critical cell cycle regulators for degradation (see

Figure 8). APC/C substrates are degraded in a timely and ordered fashion to ensure controlled activation of cell cycle events. This is achieved by several regulatory mechanisms including binding of regulatory proteins to the APC/C, phosphorylation of APC/C subunits and subcellular localization of the APC/C (85).

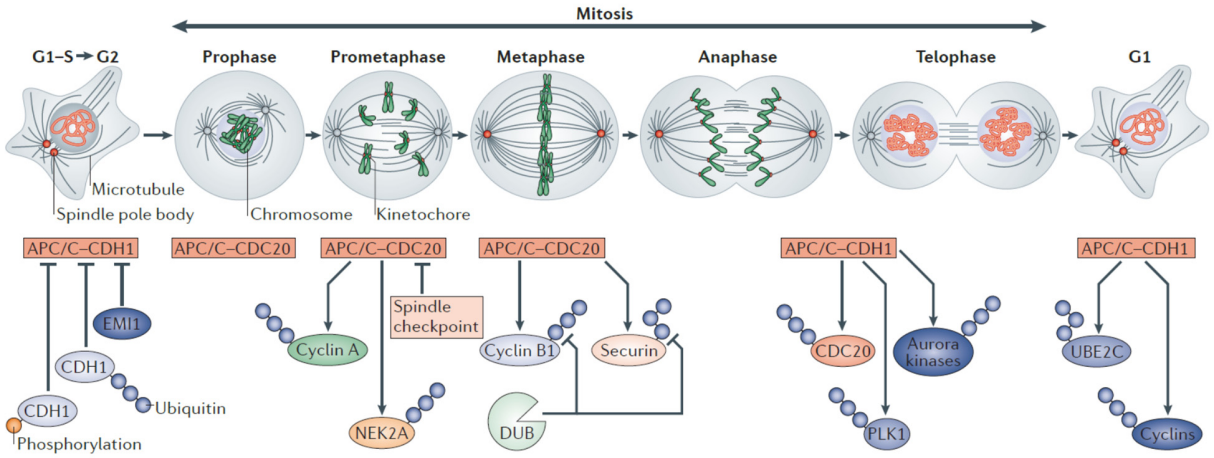

Figure 8 | Regulation of APC/C activity during cell cycle progression
Timely ordered degradation of APC/C substrates during cell cycle progression is primarily regulated by the APC/C co-activator subunits Cdc20 and Cdh1, respectively. Cdc20 activates APC/C during early mitosis, while Cdh1 keeps the APC/C active during late mitosis and G1-phase. Upon entry into mitosis, APC/C-Cdc20 targets early mitotic substrates for degradation, such as Cyclin (Cyc) A and NEK2A. Destruction of the APC/C-Cdc20 substrates CycB1 and Securin is inhibited by the Spindle checkpoint. When sister chromatids are bipolarly attached to the mitotic spindle during metaphase, the spindle checkpoint is inactivated and degradation of CycB1 and Securin is stimulated, leading to exit from mitosis and cytokinesis. In late mitosis, APC/C-Cdh1 becomes activated and mediates degradation of additional late mitotic substrates including Cdc20, Plk1 and Aurora kinases. Degradation of cyclins establishes a stable G1-phase. In late G1-phase, Cdk activity is upregulated and APC/C-Cdh1 activity is downregulated by APC/C-Cdh1 dependent destruction of UBE2C (UBCH10) and Cdh1, inactivation of Cdh1 by Cdk mediated phosphorylation and direct APC/C-Cdh1 inhibition by Emi1 (115)

Catalytic activity and substrate specificity of the APC/C requires the interaction with one of the activator subunits, Cdc20 or Cdh1. Cdh1 binds to APC1, APC3 and APC8 through different sequence elements (C-box, IR-tail, KLLR motif) in its N-terminal domain (124). Similar binding applies to Cdc20 (125). Substrate recognition by these co-activators occurs via specific degradation signals (degrons) within the target substrate. The most common degrons in APC/C substrates are the D-box with the minimal consensus sequence R-X-X-L (126) and the KEN-box named after its core sequence K-E-N (127). D-box and KEN-box interact with specific sites on the surface of a well conserved WD40 β-propeller domain in Cdc20/Cdh1 (128). Binding of the KEN-box occurs by the co-activator alone (128), whereas in the case of the D-box, a bipartite D-box receptor is generated by the co-activator and the APC/C subunit APC10 (129). Although D-box and KEN-box are required, they are often not sufficient to mediate substrate degradation (130). Together, Cdc20 and Cdh1 restrict APC/C activity to late mitosis and G1-phase. Co-activator dependent

activation of APC/C is regulated by phosphorylation. Phosphorylated Cdh1 is not able to interact with APC/C (131). In contrast, APC/C phosphorylation at multiple sites is required for Cdc20 binding (131, 132). During early mitosis, CycB1/Cdk1 in complex with Cks1 and the kinase Plk1 drive APC/C-Cdc20 assembly by phosphorylation of APC/C subunits (133-135). In *Drosophila*, Fzy and Fzr represent the homologues of Cdc20 and Cdh1, respectively (1).

APC/C activity during mitotic progression is also regulated by its subcellular localization. In early mitosis, Emi1 mediated inhibition of APC/C-Cdc20 at spindle poles prevents local degradation of CycB. This results in high CycB/Cdk1 activity at the spindle poles, which stimulates assembly of the mitotic spindle (136).

Upon entry into mitosis, ubiquitination of the APC/C substrates Securin and CycB1 is inhibited by the spindle assembly checkpoint (SAC) until all chromosomes are correctly attached to the mitotic spindle. As long as unattached kinetochores are present, the SAC is active and prevents transition into metaphase, which is characterized by separation of the sister chromatids. SAC dependent cell cycle arrest in anaphase is well conserved among eukaryotes and is mediated by the mitotic checkpoint complex (MCC) (137). In vertebrates, the MCC consists of the subunits Mad2, BubR1, Bub3 and Cdc20 (138). During early mitosis, the MCC is catalyzed by several functional proteins (SAC module) that are assembled on unattached kinetochores (139). Briefly, the formation of the MCC complex is achieved by several steps. During interphase, Mad2 binds to Mad1, transforming Mad2 from the open conformation (O-Mad2) into the closed conformation (C-Mad2). Upon entry into mitosis, the kinases Aurora B, Mps1 and Bub1 promote the recruitment of Mad1-C-Mad2 to unattached kinetochores, where it interacts with O-Mad2 and Cdc20, thereby catalyzing the formation of a C-Mad2-Cdc20 complex. C-Mad2-Cdc20 is released and associates with the subcomplex BubR1-Bub3, resulting in an active MCC. MCC interacts with the inside of the APC/C, and by this, inhibits ubiquitination of its target substrates CycB1 and Securin (137). APC/C inhibition is achieved by BubR1 and Mad2. BubR1 contains two separate KEN-box motifs, KEN1 and KEN2. KEN1 blocks recruitment of KEN-box substrates by occupying the KEN-box receptor on Cdc20 (140). KEN2 is required for displacement of Cdc20 in APC/C, which prevents the formation of a functional bi-partite D-box receptor and blocks recruitment of D-box substrates (141, 142). Recognition of target substrates is also inhibited by Mad2, which interacts with the Cdc20 binding site on APC/C, and hence prevents its activation by Cdc20 (143, 144). Furthermore, rearrangement of Cdc20 promotes its own ubiquitination and subsequent degradation, which counteracts the continuous expression of Cdc20 (145).

Some substrates, such as CycA and the NEK2A kinase escape the SAC, and therefore are degraded during early mitosis when bipolar attachment of the chromosomes to the spindle is not yet accomplished. Recruitment of these substrates to a SAC inhibited APC/C-Cdc20 complex is achieved through the formation of alternative binding sites on APC/C-Cdc20. In the case of CycA, CycA binding is additionally promoted by CKS proteins that target Cdk-associated CycA complexes to phosphorylated APC/C (146, 147). NEK2A, a kinase that is required for centrosome disjunction at the G2/M transition (148), interacts via its C-terminal MR dipeptide with the APC/C independent of Cdc20 (149, 150). When all sister chromatids are properly attached to the mitotic spindle during metaphase, the SAC is inactivated via downregulation of MCC activity, and the anaphase is initiated. This is achieved by several mechanisms. Recruitment of SAC components to the kinetochore is inhibited by the phosphatase PP1 (151). Formation of the MCC is prevented by the removal of SAC components from kinetochores by the minus-end directed motor protein dynein (152). Furthermore, the MCC is disassembled by p31, which binds to Mad2 and inhibits its activation, thereby releasing free Cdc20 (153). Finally, released Cdc20 together with newly synthesized Cdc20 stimulates abrupt APC/C activation, and in the absence of the MCC, degradation of late APC/C

mitotic substrates including CycB1 and Securin is initiated (115). Securin functions as inhibitor of the Separase, whose activity triggers sister chromatid separation by cleaving Rad21, a component of the cohesin complex. Cohesin is a highly conserved multi-subunit protein complex consisting of four subunits (Smc1, Smc3, Rad21 and Scc3) that form a ring-like structure, which is assembled around sister chromatids to keep them together until their separation (154). Cleavage of Rad21 at the metaphase-to-anaphase transition breaks the ring-like structure enabling the mitotic spindle to pull the sister chromatids apart from each other (155). Degradation of CycB1 leads to Cdk1 inactivation and activation of Cdk-counteracting phosphatases, such as PP2A, PP1 and members of the Cdc14 family, which together promote exit from mitosis and cytokinesis (156).

During anaphase, APC/C activation is switched from Cdc20 to Cdh1. Dephosphorylation of Cdh1 and APC/C-Cdc20 mediated degradation of the Cdh1-interacting protein MAD2L2 stimulates the association of Cdh1 with APC/C (131, 157, 158). During late mitosis and subsequent G1-phase, APC/C-Cdh1 keeps degradation of APC/C-Cdc20 substrates, such as cyclins, but also mediates degradation of further substrates including Cdc20, Plk1 and Aurora kinases and Geminin (159). Plk1 plays an important role in the assembly of a bipolar spindle and cytokinesis (79). Aurora kinases are implicated in several processes during mitosis, such as centrosome maturation, bipolar spindle assembly and the proper attachment of kinetochores to the mitotic spindle (160). Geminin is an inhibitor of the replication factor Cdt1. Geminin degradation is essential to stimulate the assembly of pre-replication complexes on DNA required for its replication during S-phase (161).

Entry into a new cell cycle requires inhibition of APC/C-Cdh1 at the G1/S transition. This is achieved by several mechanisms. Activation of Cdk2 by CycE and CycA stimulates phosphorylation of Cdh1, which prevents its binding to APC/C (162-164). Furthermore, APC/C-Cdh1 inactivates itself by mediating the degradation of its E2 enzymes UBCH10 and UBE2S upon depletion of the other APC/C substrates (159, 165), and its co-activator subunit Cdh1 (166). Furthermore, APC/C activity is directly inhibited by Emi1, whose expression is initiated at the G1/S transition (167-169).

2.9 The SCF complex

SCF complexes are member of the RING family of E3 ligases and are named according to their three core subunits Skp1, Cul1 and an exchangeable F-box protein. In these E3 ligases, Cul1 is the scaffold protein that interacts N-terminally with the adaptor protein Skp1 and C-terminally with Rbx1 that contains a RING domain for recruitment of an E2 enzyme. F-box proteins are characterized by a 40 amino acid motif, the F-box domain, which binds to Skp1 (170). F-box proteins function as substrate recognition subunits by targeting specific substrates to the SCF complex for polyubiquitination and subsequent degradation (see Figure 9). Depending on the structure of the substrate binding site, F-box proteins are divided into three different classes: (1) FBXWs (F-box WD-40 repeat domain) that interact with phosphorylated substrates through a WD-40 repeat domain, which forms a β-propeller like structure, (2) FBXLs (F-box leucine rich repeat), which bind phosphorylated and non-phosphorylated substrates, sometimes in complex with other subunits, via their leucine-rich repeat (LRR) domain, and (3) FBXOs (F-box and other domains) that contain substrate interaction domains other than WD-40 repeats or LRRs (171-173). The specificity of SCF complexes to certain substrates is regulated at the level of substrate recruitment (170). In most cases, this is achieved by phosphorylation of the target substrate, which generates a phosphodegron that is recognized by the F-box protein (170). However, binding of phosphorylated substrates can also depend on the presence of accessory proteins. For instance, the interaction between the F-box protein Skp2 and its

phosphorylated target substrate p27 is mediated by Cks1, which was initially identified as accessory subunit for Cdk kinases (174-176). Modification of the substrate is not always necessary. For instance, binding of the degrons CP110 and RRM2 to the F-box protein CycF does not require their previous phosphorylation (177, 178). However, phosphorylation of RRM2 at another region is required to promote binding to the unmodified degron indicating that control of degron access constitutes a further regulatory mechanism for substrate recognition (177). Beside phosphorylation, several other mechanisms exist that restrict SCF activity to specific conditions, concerning subcellular localization of both F-box protein and target substrate, stabilization and activation of F-box proteins by small molecules, temporal regulation of F-box expression and different covalent modifications, such as glycosylation and methylation (170).

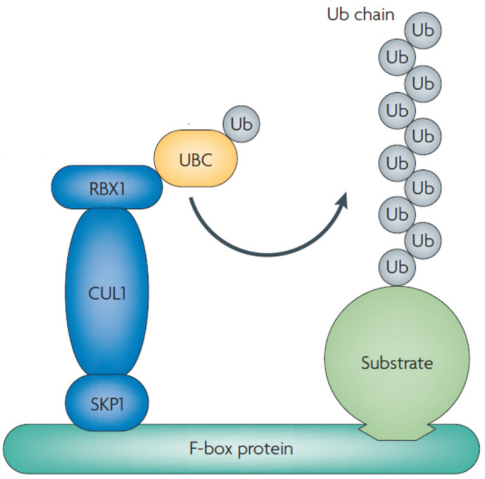

Figure 9 | Schematic presentation of SCF mediated polyubiquitination of target substrates
SCF (SKP1-Cul1-FBP) complexes belong to the family of multi-subunit RING-type E3 ligases, which are composed of the three core subunits Skp1, Cul1 and Rbx1. Cul1 functions as scaffold protein that interacts with Skp1 and Rbx1. An interchangeable F-box protein associates with Skp1 via its F-box domain and recruits specific substrates to the SCF complex. Usually, recruitment requires previous phosphorylation of the target substrate. Rbx1 associates with an ubiquitin-conjugating enzyme (UBC) providing an active ubiquitin for the assembly of polyubiquitin chains on bound target substrates. Figure adapted from Welcker and Clurman (8).

In addition to the high variety of mechanisms specifically regulating substrate recruitment, the assembly of substrate specific SCF complexes is controlled in an unspecific manner. Around 70 F-box proteins are present in humans that compete for binding to the Cul1 core protein (172, 179). Thus, F-box proteins must be exchangeable to guarantee the formation of all required SCF complexes. This is achieved by Cand1, a protein exchange factor that drives assembly and disassembly of SCF complexes dependent on the presence of target substrates. Activation of SCF complexes requires the Ubc12 catalyzed neddylation of the ubiquitin-like protein Nedd8 on Cul1. When substrates are depleted and SCF complexes are not associated with their target substrate, neddylation is reversed by the COP9 signalosome. Cand1 interacts with deneddylated SCF complexes, thereby inducing the dissociation of the Skp1-F-box-protein heterodimer, leaving behind a Cand1-Cul1-Rbx1 complex. This ternary complex is able to associate with another pair of Skp1 and F-box protein, resulting in the assembly of a new SCF-complex able to mediate the degradation of other substrates. This allows a dynamic exchange of different F-box proteins, which fulfills the requirement for the degradation of the large variety of different substrates (180, 181).

SCF-complexes play a prominent role in cell cycle progression, since loss of their regulation is often linked with cancer (170). The most well studied F-box proteins involved in the mammalian cell cycle system are Skp2, FBXW7 and β-TRCP. SCF-Skp2 promotes entry into S-phase by mediating the degradation of the CKI family members p21, p27 and p57 (182-184). Overexpression of Skp2 causes tumorigenesis and correlates with a high variety of cancer types (185). In contrast, SCF-FBXW7 functions predominantly as tumor suppressor by downregulating growth promoting substrates, such as the S-phase initiator CycE (8, 186). SCF-β-TRCP is implicated in both stimulation and inhibition of cell cycle progression. Upon entry into a new

cycle, SCF-β-TRCP promotes the degradation of growth inhibitors (for instance Wee1), whereas during mitosis, it drives destruction of growth promoters including Emi1 and Cdc25A. Although SCF-β-TRCP provides tumor suppressor activity, a vast majority of tumors is characterized by overexpression of β-TRCP (170).

2.10 Cyclin-dependent kinase inhibitors

During cell cycle progression, Cdk activity is regulated by cyclin-dependent kinase inhibitors (CKI). In mammals, two families of CKIs exist, the inhibitor of Cdk4 (INK4) family and the Cdk interacting protein/kinase inhibitor protein (CIP/KIP) family. INK4 family members (p15, p16, p18 and p19) specifically binds and inhibits Cdk4 and Cdk6 during G1 phase, while members of the CIP/KIP family (p21, p27 and p57) are capable of inhibiting all Cdks during different cell cycle stages (187). All members of the CIP/KIP family share a conserved terminal Cdk inhibitor domain (CDI) that interacts with Cyc/Cdk complexes for inhibition (188). A crystal structure of p27 bound to CycA/Cdk2 revealed that Cdk inhibition occurs by binding both the cyclin subunit to block substrate recruitment and the catalytic region of Cdk to prevent ATP binding (189). The CIP/KIP CKIs are differentially expressed during cell cycle progression and control different aspects in the cell cycle. p21 is present during G1- and G2-phase and mediates a block in cell cycle progression in response to DNA damage (183). This is accomplished by stabilization of the transcription factor p53 by DNA damage-induced kinase cascades involving the kinases ATM and Chk2. Accumulation of p53 results in upregulation of p21, which induces a cell cycle arrest in G1-phase (190). Mice lacking p21 developed normally and did not display any defects in cell proliferation, indicating that p21 is not essential for proper cell cycle progression. However, p21 deficient cells failed to establish a DNA damage-induced G1-phase arrest (191). In contrast to p21, p27 expression is induced in mitogen-starved cells and promotes exit from the cell cycle (192, 193). Moreover, loss of p27 in mice caused an increase in their body size, indicating that p27 is required for cell growth regulation (194). Unlike p21 and p27, p57 is expressed in specific tissues and plays a prominent role during embryogenesis (188). Loss of p57 in mice embryos caused hyperplasia in several tissues and cells failed to differentiate due to uncontrolled cell proliferation (195). p57 is also upregulated upon serum starvation (196) and is mainly present in terminally differentiated cells to promote exit from the cell cycle (197). Progression through the cell cycle requires downregulation of CKI activity. Several E3 ligases mediate degradation of the different CIP/KIP family members during specific cell cycle stages. SCF-Skp2 becomes active at the G1/S transition and targets all three CKI proteins, p21, p27 and p57, for degradation during S- and G2-phase (182-184). Recognition of these CKIs depends on the co-factor Cks1, which together with Skp2 provides a binding platform for recruitment of the CKI protein (175, 198, 199). Furthermore, SCF-Skp2 targets only CKIs that are bound to a Cyc/Cdk2 complex (56, 200-203). In case of p27 and p57, Cdk2 mediated phosphorylation on a specific residue (p27: T187 by CycE/Cdk2, p57: T310) is additionally required for interaction with SCF-Skp2 (200, 204). In contrast, phosphorylation of p21 on S130 stimulates recruitment to SCF-Skp2, but this is not a strict requirement for SCF-Skp2 mediated degradation (198). Degradation of p21 is not only mediated by SCF-Skp2. During S-phase, p21 interact with chromatin-bound PCNA via its PIP-degron, which recruits the E3 ligase CRL4-Cdt2 for polyubiquitination (205-209). Furthermore, p21 contains a D-box which recruits p21 to APC/C-Cdc20 during prometaphase for degradation (210).

Beside SCF-Skp2, CRL4-Cdt2 and APC/C-Cdc20, several more E3 ligases stimulate the degradation of the CIP/KIP proteins during cell cycle progression. Recognition by the E3 ligases is regulated by a large variety of different kinases through phosphorylations of specific residues (183, 184). Moreover, although p21, p27

and p57 are indispensable for blocking cell cycle progression, these CKIs are also implicated in a variety of cell cycle independent processes, including transcription, apoptosis and migration (183, 187).

In *Drosophila*, Dap functions as single homologue of the mammalian CIP/KIP proteins p21, p27 and p57, with highest conservation in regions that are implicated in inhibition of Cyc/Cdk complexes. Dap is most similar to p21, sharing 26 % identity to rat p21 (211). In contrast to the mammalian CKIs that inhibit a broad range of different Cyc/Cdk complexes, Dap is specific for CycE/Cdk2 (212). Dap plays an important role during embryogenesis, since Dap expression promotes exit from the cell cycle in several tissues during development including cells of the mesoderm, epidermis and the nervous system (212). In *dap* mutant embryos, most epidermal cells failed to arrest in G1-phase of cell cycle 17 at the end of embryogenesis and underwent an additional round of cell division before becoming quiescent (211, 212). Premature entry into S-phase was also observed upon overexpression of CycE (63, 64). Consistent with the role of Dap as CycE/Cdk2 inhibitor, overexpression of Dap blocked entry into S-phase in cells posterior to the morphogenetic furrow in the developing eye imaginal disc (211). Premature Dap expression in the epidermis resulted in a precocious G1-phase arrest of cell cycle 16, which was rescued by overexpression of CycE (212).

Expression of Dap during embryonic development has been shown to depend on CycE activity. In *cycE* mutants, Dap expression was reduced in the nervous system. Furthermore, *dap* transcripts and Dap proteins were upregulated upon overexpression of CycE in eye and wing imaginal discs. The same was observed in ovarian nurse cells indicating that CycE also regulates Dap protein levels in endocycling cells. The expression of a beta-galactosidase reporter controlled by the endogenous *dap* promoter region was stimulated, when CycE was overexpressed suggesting that CycE regulates Dap expression at the transcriptional level (213).

Like the mammalian p21, Dap contains a PIP-degron and is targeted for degradation by CRL4-Cdt2 during S-phase. Expression of a PIP-degron Dap mutant in S2-cells resulted in its accumulation during S-phase. However, S-phase stabilization of Dap did not disrupt mitotic cell cycles in epidermal and imaginal discs. In contrast, overexpression of a PIP-degron Dap mutant impaired endocycle progression in several tissues such as midgut, ovarian follicle cells and salivary glands. Based on mathematical model studies, it was shown that Dap degradation during S-phase is required for adjustment of the G1-phase length to allow proper oscillation of CycE activity during endocycle progression (214).

Beside CRL4-Cdt2, Dui et al. presented evidence that the E3 ligase SCF-Skp2 also targets Dap for degradation to ensure proper cell cycle progression. The F-box protein Skp2 interacted with Dap and Dap protein levels were dependent on Skp2 activity. While Skp2 overexpression reduced Dap protein levels, Dap protein levels were increased by RNAi against *skp2* in extracts of S2 cells and in extracts of the *Drosophila* eye tissue. The same regulation of Dap stability by Skp2 was observed in wing imaginal discs. Furthermore, Skp2 stimulated Dap polyubiquitination *in vivo*. In addition, *skp2* and *dap* have been shown to interact genetically since developmental defects during eye and wing development caused by *skp2* knockdown were rescued by knockdown of *dap* (215). However, Dap as SCF-Skp2 target substrate is controversially discussed. Ghorbani et al. did not observe any upregulation of Dap protein levels by *skp2* knockdown in extracts from larvaes and mitotic tissues (216). Consistent with this, the protein stability of a cell cycle inactive version of Dap was not influenced by different Skp2 expression levels in S2R+ cells. Dap is required for the establishment of a stable G1-phase (211, 212). In this context, detailed cell cycle analyses provided evidence against Dap being a SCF-Skp2 target substrate. Overexpression of Skp2 delayed

G1/S transition, whereas Skp2 downregulation shortened G1-phase (T. Rössler, personal communication, June 27, 2016).

Like Dap, Roughex (Rux) functions as another CKI that is required for the establishment and maintenance of a stable G1-phase. However, Rux does not show any homology to the mammalian CKI family members p21, p27 and p57. Furthermore, Rux only binds and inhibits mitotic Cdk1 conjugated with CycA or CycB. Consistent with this, ectopic S-phase induction during G1-phase 17 in epidermal cells by overexpression of a stable version of CycA was blocked by overexpression of Rux (70). In *rux* mutants, cells of the developing eye imaginal disc failed to establish a stable G1-phase and immediately entered S-phase, thereby producing unorganized ommatidia structures that result in a rough eye phenotype. The *rux* phenotype was dominantly suppressed by mutations in *cycA* indicating that Rux promotes a stable G1-phase by preventing premature activation of CycA/Cdk1 (217).

CycE/Cdk2 activity is thought to promote Rux degradation at the G1/S transition. Rux is phosphorylated by CycE/Cdk2 *in vitro* and it becomes destabilized upon CycE overexpression in eye imaginal discs (218).

2.11 The APC/C inhibitor Emi1

Progression through cell cycles are driven by oscillating periods of cyclin expression and destruction. Degradation of cyclins is mediated by the APC/C in conjunction with its co-activator subunit Cdc20 or Cdh1, respectively. APC/C-Cdc20 is partially active in early mitosis and becomes fully activated at the metaphase-to-anaphase transition. In anaphase, Cdc20 is replaced by Cdh1, and APC/C-Cdh1 triggers exit from mitosis and remains active until late G1-phase. Entry into a new cycle requires APC/C-Cdh1 inactivation to allow the accumulation of mitotic cyclins that trigger entry into mitosis (1).

In vertebrates, APC/C activity is restrained by Emi1, which binds to and inhibits both APC/C-Cdc20 and APC/C-Cdh1 (167, 169, 219, 220). However, the interaction between APC/C-Cdh1 and Emi1 is much stronger than it is the case for APC/C-Cdc20 (169). *In vivo* studies in *Xenopus* egg extracts have demonstrated the essential role of Emi1 in proper cell cycle progression. Removal of Emi1 in *Xenopus* cycling extracts failed to enter mitosis due to permanent APC/C-Cdc20 mediated degradation of CycB1 during interphase (219). Overexpression of Emi1 prevented degradation of mitotic cyclins, which resulted in a mitotic block caused by a permanently inactive APC/C-Cdc20 (169, 219). Emi1 is induced by E2F transcription factors at the G1/S transition to stimulate APC/C-Cdh1 inhibition during S- and G2-phase, thereby allowing accumulation of APC/C substrates, such as CycA, CycB1 and the DNA replication inhibitor Geminin (168, 169, 219). Emi1 is not only required for entry into mitosis, but also prevents rereplication through stabilization of the rereplication inhibitors CycA and Geminin, both APC/C substrates (167, 221). Upon entry into mitosis, Emi1 is targeted for degradation by SCF-βTRCP (222).

Emi1 is divided into three domains, the N-terminal domain (Emi1-NT), the central localized F-box and the C-terminal domain (Emi1-CT) (219). Emi1 harbors several functional domains, of which most reside in Emi1-CT consisting of a D-box, linker, zinc-binding region (ZBR) and a C-terminal RL-tail (223). These domains together mediate efficient binding to the APC/C (220) and are also sufficient to inhibit APC/C activity (117, 169, 219, 223). Recent structural studies based on NMR and electron microscopy were able to reveal the binding sites on APC/C-Cdh1 that associate with Emi1 for direct inhibition (124, 223). This structural insights in combination with several different *in vitro* ubiquitination assays uncovered the mechanisms through which Emi1 mediates efficient APC/C inhibition (117, 220). Briefly, all domains in

Emi1-CT act synergistically to inhibit both recruitment and ubiquitination of APC/C-Cdh1 target substrates (see Figure 10). To achieve this, each domain occupies distinct sites on APC/C-Cdh1.

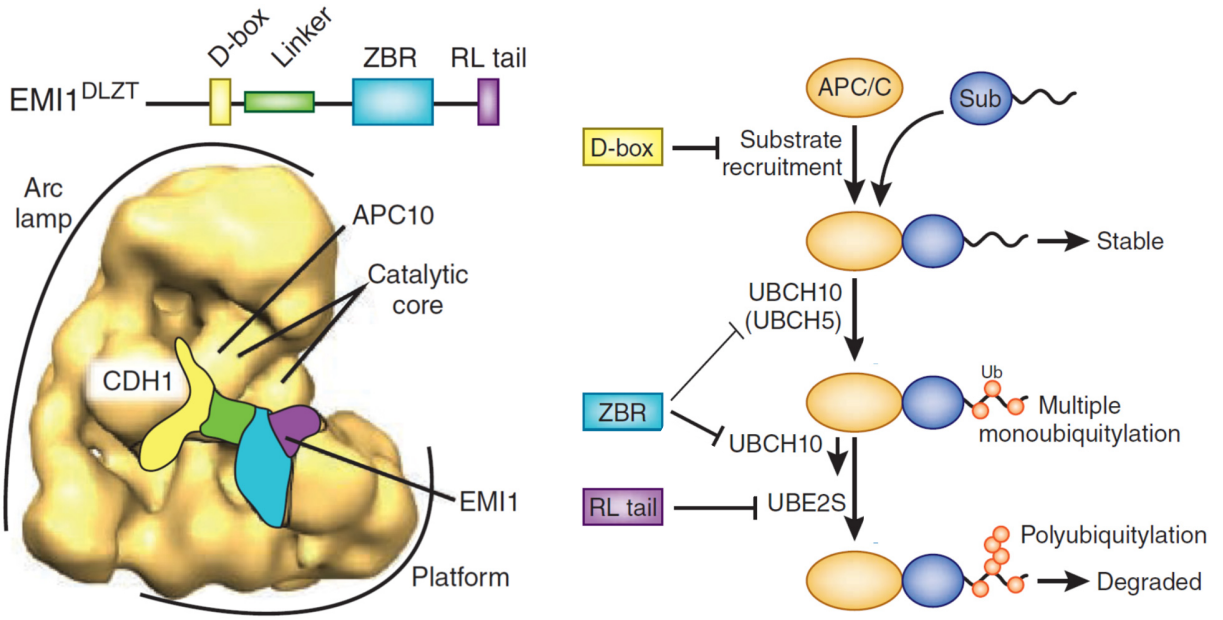

Figure 10 | Mechanism of APC/C-Cdh1 inhibition by Emi1
Several domains in the C-terminal part of Emi1 (DLZT) synergize to inhibit APC/C-Cdh1 activity. Each domain binds to a distinct region of the APC/C-Cdh1 complex and fulfils a specific inhibitory function. The D-box (yellow) blocks substrate access to the D-box receptor, the ZBR (cyan) together with the linker region (green) inhibits initial ubiquitination catalyzed by UBCH5 and UBCH10, whereas the RL-tail (purple) prevents polyubiquitination by competing with binding of the ubiquitin elongation E2 enzyme UBE2S (117, 124, 223). Sub: substrate. Figure adapted from Hiroyuki Yamano (224).

The D-box blocks access of D-box substrates by interacting with the D-box receptor formed by the subunit APC10 and Cdh1. Although the D-box alone possesses only weak binding affinity to APC/C-Cdh1, loss of the D-box eliminated the ability of Emi1 to inhibit ubiquitination (117, 220, 223). When a D-box substrate is already bound to APC/C-Cdh1, the assembly of polyububiquitin chains is prevented by the linker, ZBR and the C-terminal RL-tail (117). The ZBR resembles the structure of an in-between-RING domain (223) and interacts with the APC/C core subunits APC2 and APC11, while the adjacent linker is associated with APC2 (124). Deletion of the linker sequence or its replacement with a glycine-rich sequence impaired APC-Cdh1 inhibition *in vitro* (223). Both ZBR and the adjacent linker block the UBCH5/UBCH10 binding site on APC11, but not the site specific for UBE2S recruitment (124). In agreement with this, *in vitro* formation of initial short polyubiquitin chains catalyzed by UBCH5/UBCH10 depends on a functional ZBR, while chain elongation by UBE2S is not affected (117). Notably, Emi1 harboring a non-functional ZBR was ubiquitinated by APC/C-Cdh1 *in vitro* and degraded *in vivo*. Both effects were eliminated by additional loss of the D-box indicating that Emi1 was converted from an APC/C-Cdh1 inhibitor to an APC/C-Cdh1 target substrate. Thus, it is conceivable that Emi1 does not only function as APC/C-Cdh1 inhibitor during interphase and early mitosis, but itself can also be a target substrate of APC/C. However, the mechanisms that trigger the switch from Emi1 as APC/C inhibitor to Emi1 as APC/C target substrate are still unknown, but might include phosphorylations on specific sites of Emi1 (220). Ubiquitin chain elongation by UBE2S is inhibited by the C-terminal RL-tail, which competes with the RL-tail of UBE2S for binding to APC2 (124). Deletion of the RL-

tail completely eliminated the ability of Emi1 to inhibit the Ube2S-catalyzed polyubiquitination of an ubiquitin linked APC/C target substrate *in vitro* (117).

In comparison to Emi1-CT, Emi1-NT does not bind APC/C-Cdh1 (220). This agrees with the inability of Emi1-NT to inhibit APC/C-Cdc20 and APC/C-Cdh1 (117, 219, 220, 223). Rather, Emi1-NT is responsible for regulatory functions of Emi1, such as its degradation during mitosis. Whereas Emi1-NT was degraded in prophase, similar to full-length Emi1, Emi1-CT remained stable in mitotic *Xenopus* egg extracts causing an arrest in prometaphase (219, 225). Addition of a D-box peptide did not prevent Emi1 degradation during mitosis and Emi1 stability was not affected upon supplement of Cdh1 in *Xenopus* interphase extracts. Thus, Emi1 degradation is not mediated by APC/C (169, 219). Instead, Emi1 is targeted for degradation by SCF-βTrCP during prophase (225). Recruitment to βTrCP is directed by a consensus D-S-G-X-X-S degron motif. Recognition of βTrCP substrates requires phosphorylation of both serine residues within the degron sequence (226). In Emi1, the βTrCP degron is phosphorylated by Plk1, whose activity is enhanced by CycB/Cdk1, which drives phosphorylation of one or several S-P consensus sites in Emi1-NT (222, 227). Overexpression of a non-degradable Emi1 mutant carrying a mutated βTrCP degron caused a mitotic arrest in prometaphase, which was accompanied by severe mitotic defects, including spindle abnormalities, chromosome overcondensation and centrosome overduplication (225). During S- and G2-phase, SCF-βTrCP-dependent degradation of Emi1 is prevented by Evi5, which binds adjacent to the D-S-G-X-X-S degron, thereby blocking both degron phosphorylation by Plk1 and subsequent βTrCP binding (228).

Between Emi1-NT and Emi1-CT, Emi1 harbors an F-box domain, which is required for interaction with the SCF component Skp1 (169, 219) suggesting that Emi1 targets substrate for degradation as part of an SCF complex. However, so far, SCF-Emi1 target substrates were not identified and the F-box has neither been shown to be involved in APC/C inhibition nor does it possess any regulatory functions. Thus, the purpose of the F-box domain is still unclear and remains to be elucidated.

2.12 Rca1, the *Drosophila* homologue of Emi1

In *Drosophila*, *rca1* was initially identified in a screen for dominant suppressors of the *rux[3]* eye phenotype (229). Rux is a CKI that specifically inhibits Cdk1 activity (see section 2.10). In *rux* mutants, cells failed to establish a stable G1-phase in cells of the eye imaginal disc due to premature activation of CycA/Cdk1 resulting in a rough eye phenotype. Beside *cycA* and the *cdc25* homologues *string* and *twine,* heterozygous mutations in *rca1* were also found to dominantly suppress the *rux[3]* mutant phenotype by restoration of a normal G1-phase (69, 217). Several genetic experiments revealed a genetic interaction between *rca1* and *cycA*. Rca1 overexpression stimulated the accumulation of CycA protein levels leading to premature entry into S-phase. In wildtype embryos, most epidermal arrest in G1-phase upon mitosis 16. Both *rca1* and *cyca* mutant embryos failed to perform this final division, and therefore exhibited a reduced number of epidermal cells. Some of these cells initiated endoreduplication indicating that loss of either Rca1 or CycA drives conversion of a mitotic cycle to an endoreduplication cycle. This is supported by the observation of large nuclei in *rca1* mutant cell clones in wing imaginal discs (229, 230). Thus, Rca1 and CycA prevent endoreduplication and are essential cell cycle regulators that drive entry into mitosis. A phenotype before mitosis 16 is likely obscured by maternally provided transcripts. The similarity between the phenotypes of *cyca* and *rca1* mutants is the reason for the gene name *rca1*, which is an abbreviation for *regulator of Cyclin A 1* (229).

Rca1 is required to prevent premature degradation of mitotic cyclins during interphase. In *rca1* mutants, CycA and CycB protein levels were strongly reduced before mitosis 16 when compared to wildtype embryos. However, only overexpression of CycA, but not CycB, suppressed the *rca1* mutant phenotype indicating that CycA is the limiting factor for entry into mitosis. CycA levels were also reduced in *rca1* mutant clones that were generated in wing imaginal discs. Furthermore, these cells exhibited growth defects demonstrating that Rca1 plays a general important role for cell proliferation (230). In contrast, overexpression of Rca1 increased CycA and CycB protein levels in eye imaginal discs (231). Several genetic experiments revealed that Rca1 functions as APC/C-Fzr inhibitor during interphase to allow accumulation of mitotic cyclins. As observed in *rca1* mutants, Fzr overexpression resulted in premature degradation of CycA and CycB in G2-phase of epidermal cells, and therefore failed to execute mitosis 16 (163, 230). The accumulation of mitotic cyclins was restored by overexpression of Rca1 demonstrating that Rca1 negatively regulates Fzr activity. Consistent with this, the *rca1* mutant phenotype was suppressed in *rca1 fzr* double mutants (230). Furthermore, Rca1 was found in complex with Fzr and the APC/C subunit Cdc27 (230).

Rca1 and its human homologue hEmi1 share the same arrangement of functional domains (see Figure 11). Both proteins contain an F-box in their central region and own a C-terminal part that consists of a APC/C degron (D-box/KEN-box), linker region, zinc-binding region (ZBR) and RL-tail. The C-terminal part of Emi1 have been shown to be essential for direct APC/C-Cdh1 inhibition (see section 2.11), suggesting that Rca1 directly inhibits APC/C-Fzr activity in the same manner as Emi1. Indeed, overexpression of the C-terminal part of Rca1 restored mitosis 16 in *rca1[2]* mutants, whereas Rca1 harboring a disrupted ZBR or lacking part of the linker region did not allow entry into mitosis (231).

In wildtype embryos, Rca1 is degraded during G1-phase, likely to allow APC/C-Fzr mediated degradation of CycA, thereby preventing premature S-phase induction (230). Consequently, epidermal cells in the terminal G1-phase lack both Rca1 and CycA (231). Live cell imaging analyses in S2R+ cells have demonstrated that Rca1 behaves like an APC/C-Fzr substrate during G1-phase suggesting that APC/C-Fzr promotes its own activation during G1-phase by targeting its inhibitor Rca1 for degradation. This is dependent on a small KEN-box containing region (residues 204-298) in Rca1 (232). This is in agreement with *in vivo* studies in embryos that have shown that the region between residue 203 and 255 is required to mediate degradation in G1-phase (231). However, the mechanisms that convert Rca1 from an APC/C-Fzr inhibitor to an APC/C-Fzr substrate are still under investigation.

Studies on Rca1 have revealed that the F-box plays an important role in the regulation of the G1/S transition. Rca1 overexpression resulted in ectopic S-phases in cells of the developing eye imaginal disc in an F-box dependent manner. In contrast to full-length Rca1, overexpression of Rca1 lacking F-box did not result in CycA accumulation during G1-phase and did not induce a rough eye phenotype. Flow cytometric analyses of wing imaginal discs have revealed that the F-box stimulates transition into S-phase. Consistently, in *rca1[2]* mutant clones, cell proliferation defects were complemented by Rca1 overexpression, but only partially by Rca1 lacking the F-box (231).

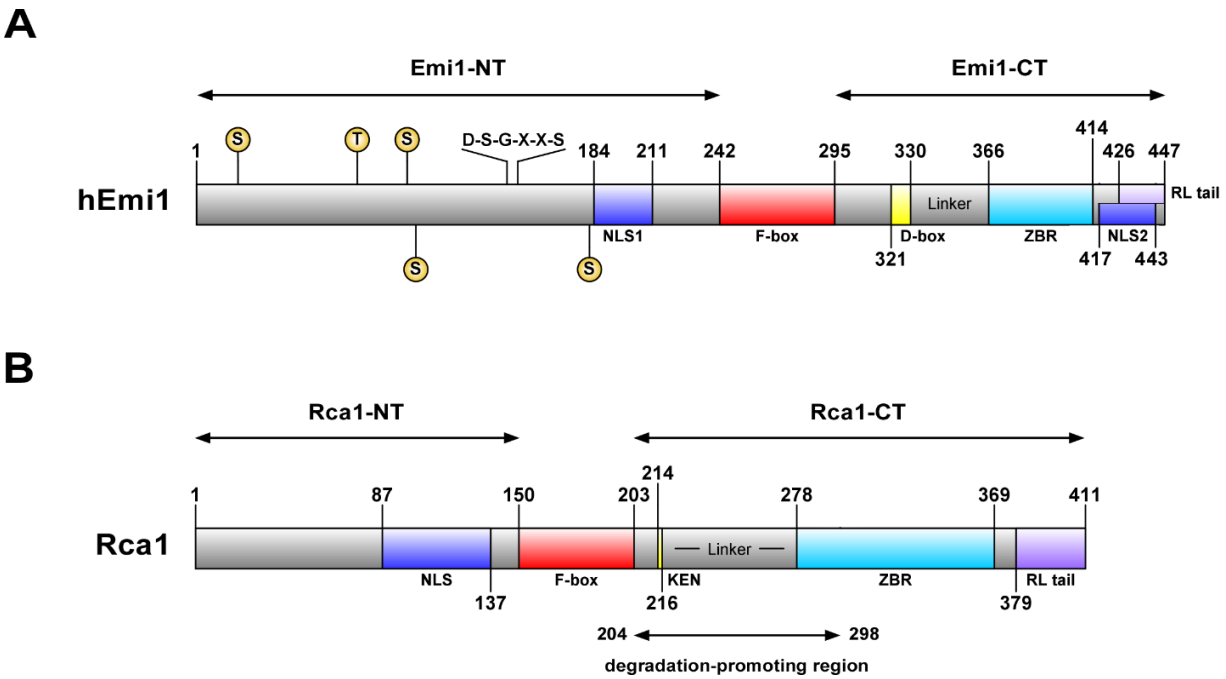

Figure 11 | Schematic illustration of domains in Rca1 and its human homologue hEmi1
Rca1 and hEmi1 share the same order of functional domains. Both Emi1 (A) and Rca1 (B) are divided into three different sections. The N-terminal part (Rca1-NT/Emi1-NT), the central localized F-box and the C-terminal part (Rca1-CT/Emi1-CT). **(A)** The location of the D-box (yellow), linker region and ZBR (cyan) were determined according to Frye et al. (223), whereas for the RL-tail (purple), Yamano's definition about the length and position of the RL-tail was used (224). The F-box (red) was determined by using the SMART database (233). NLS domains (blue) were predicted by using the cNLS Mapper (234): Score NLS1: 5.7, NLS2: 5.1. Both the D-S-G-X-X-S motif and Cdk phosphorylation sites in Emi-NT mediate degradation during mitosis by SCF-βTrCP (222, 225, 228). **(B)** Rca1 was aligned to hEmi1 to determine the location of the F-box, linker region, ZBR and RL-tail. Rca1 carries a KEN-box instead of a functional D-box, both representing APC/C degrons (yellow). The NLS domain described in Rca1 contains several predicted NLS domains with scores between 5 and 7. The degradation-promoting region (204-298) mediates instability during G1-phase (232). ZBR: zinc-binding region.

However, the F-box is not only involved in the regulation of the G1/S boundary. Phenotypic analyses of different EMS-induced *rca1* alleles have revealed that the F-box is also essential for entry into mitosis. *rca1* mutants carrying the F-box point mutation M182T failed to execute the terminal mitosis 16 in epidermal cells during embryogenesis (235). The same phenotype was observed in *rca1[2]* mutants upon endogenous expression of Rca1 lacking the F-box under the control of the *rca1* promoter region (236). Interestingly, overexpression of Rca1 without F-box prevented premature degradation of CycA and restored mitosis 16 in *rca1[2]* mutants (231). Thus, the F-box function becomes essential at endogenous expression levels, while overexpression makes the F-box indispensable for entry into mitosis.

F-box proteins are often implicated in the proteasomal degradation of specific proteins by acting as substrate recognition components of SCF complexes (170). An interaction between Rca1 and the SCF core component SkpA component was identified by a genome-wide yeast two hybrid screen of the fly proteome (237). Further analysis demonstrated that the interaction to the SCF components Cul1 and SkpA is F-box dependent suggesting that Rca1 might function as part of an SCF complex to target specific substrates for degradation (231). Rca1 inhibits APC/C-Fzr activity during G2-phase to allow CycA accumulation (230). Overexpression of Rca1 stimulated accumulation of CycA in G1-phase cells of the eye imaginal disc in an F-box dependent manner. Thus, an SCF-Rca1 complex might be required to promote degradation of an

APC/C-Fzr stimulator. CycE/Cdk2 is known to inhibit APC/C-Fzr activity. The failure of *Drosophila* embryos to enter mitosis 16 due to Fzr overexpression was rescued by overexpression of CycE (163). Furthermore, CycE overexpression restored entry into mitosis in *rca1[2]* mutant embryos (230). Dap functions as CycE/Cdk2 inhibitor (211, 212), suggesting that Dap stimulates APC/C-Fzr activity by preventing APC/C-Fzr inhibition by CycE/Cdk2. Thus, Dap represents a potential target substrate of SCF-Rca1. Consistent with this, ectopic S-phases by Rca1 overexpression were not prevented by Dap overexpression in eye imaginal discs. However, a downregulation of Dap protein levels were not detected (231). Therefore, whether Dap is targeted for degradation by SCF-Rca1 to inhibit APC/C-Fzr activity remains to be elucidated in detail and was the main topic in this thesis.

3 Results

3.1 Identification of Rca1 interaction partners

3.1.1 Aim

According to studies on the vertebrate homologue Emi1 (117, 167-169, 219-221, 223, 224), Rca1 binds and inhibits APC/C-Fzr activity through direct interactions with different APC/C-Fzr subunits (230). However, physical interactions studies suggest that Rca1 might also function as part of an SCF complex that targets other cell cycle regulators for degradation during cell cycle progression (231, 236). *In vivo* studies on *rca1 dap* double mutant *Drosophila* embryos provided evidence for a genetic interaction between *rca1* and *dap*. Importantly, the outcome of the genetic interaction was F-box dependent turning Dap into a potential SCF-Rca1 target substrate (236).

To confirm the interaction between Rca1 and APC/C-Fzr components, and to identify target substrates of a putative SCF-Rca1 complex, a 4FLAG-Rca1 precipitate obtained from S2R+ cells was analyzed by mass spectrometry. Since Dap is a potential Rca1 interaction partner, a cell cycle inactive and stabilized version of Dap, 4XFLAG-Dap-dCDI-dPIPa, was precipitated and analyzed as well (see section 3.1.2). Furthermore, to find evidence for a functional SCF-Rca1 *in vivo*, the F-box dependent interaction between polyubiquitinated substrates and Rca1 was investigated (see section 3.1.3).

3.1.2 Rca1 is in complex with SCF components, Skp2, and Dap

To identify proteins that bind Rca1 *in vivo*, 4XFLAG-Rca1 was overexpressed in S2R+ cells and precipitated by using anti-FLAG antibodies. The 4XFLAG-Rca1 precipitate was then subjected to mass spectrometric analysis. Dap already represents an interesting candidate for interacting with Rca1 (see section 3.1). Therefore, a cell cycle inactive and stabilized version of Dap, 4XFLAG-Dap-dCDI-dPIPa (dCDI: deletion of CycE/Cdk2 binding motif, dPIPa: deletion of N-terminal PIP-box required for degradation by CRL4-Cdt2 during S-phase) was expressed and analyzed by mass spectrometry (MS) in parallel (see Figure 12A). Raw mass spectrometric data were searched against *Drosophila* proteins in the UniProtKB database. By this, a huge amount of different proteins was identified in the 4XFLAG-Rca1 (1294 proteins) and 4XFLAG-Dap-dCDI-dPIPa (928 proteins) precipitate. Since cell cycle control is the major function of both Rca1 and Dap, the obtained protein data sets were filtered against proteins that are known or assumed to be involved in cell cycle regulation. In the UniProtKB database, each protein is assigned to gene ontology (GO) terms that describe the identity of the protein (238). The annotation of GO terms occurs either manually based on experimental data or electronically by computational analyses. GO terms belong to three different domains, biological processes, molecular function and cellular component, each of which consists of a hierarchical ordered structure of interconnected GO terms. The GO term “cell cycle” (GO: 0007049) is part of the biological process domain and is connected to GO-terms describing cell cycle regulatory functions. Therefore, to restrict the identified proteins to proteins implicated in cell cycle regulation, the protein lists were additionally filtered against the GO-term “cell cycle” (GO: 0007049) using the QuickGO browser (239). This dramatically reduced the number of proteins (4XFLAG-Rca1: 176 proteins, 4XFLAG-Dap-dCDI-dPIPa: 123 proteins) and facilitated the analysis of physical interaction partners (see Table 39 and Table 40 in section 12).

A

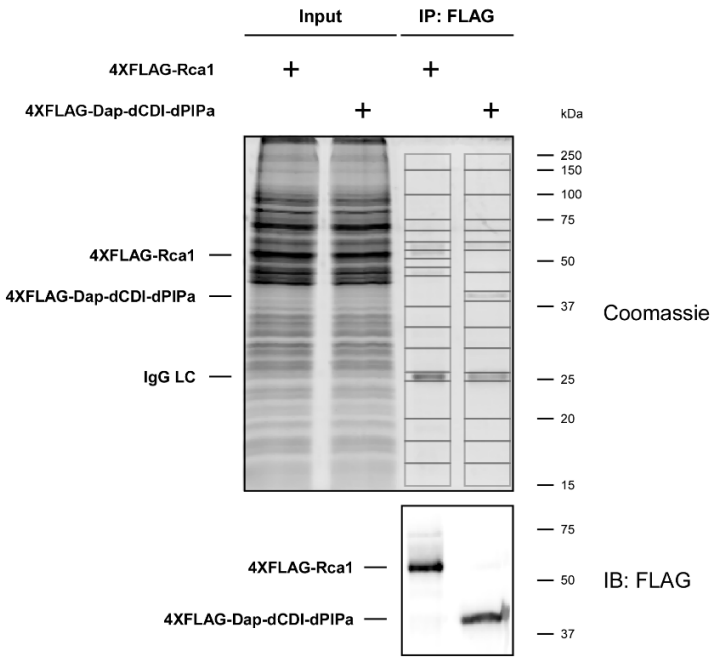

B

4XFLAG-Rca1 precipitate

Protein	Score	No. of peptides	Sequence coverage (%)
Rca1	1541.9	26	42.1
Skp2	1076.0	18	33.1
SkpA	776.1	10	72.2
Cul1	738.1	17	26.7
Cdk2	196.3	5	24.5
Cdc16	129.6	4	6.1
CycE	100.2	3	6.5
Dap	94.5	3	16.7
APC2	90.4	2	4.1

4XFLAG-Dap-dCDI-dPIPa precipitate

Protein	Score	No. of peptides	Sequence coverage (%)
Dap	1807.4	22	64.5
SkpA	211.8	4	25.9
Rca1	197.9	5	10.9

SCF component
F-box protein
Potential SCF-Rca1 target substrate
APC/C component
Other proteins

Figure 12 | Identification of Rca1 and Dap interaction partners by LC-MS/MS
Interaction partners of 4XFLAG-Rca1 and 4XFLAG-Dap-dCDI-dPIPa (stabilized and cell cycle inactive version of Dap) were identified by mass spectrometry. Both constructs were overexpressed in S2R+ cells, precipitated and analyzed by LC-MS/MS. **(A)** 4XFLAG-Rca1 and 4XFLAG-Dap-dCDI-dPIPa precipitates were separated by SDS-PAGE and stained with Coomassie Brilliant Blue. Gel pieces containing co-precipitated proteins were excised from the gel and subjected to LC-MS/MS analysis, as shown (grey boxes). Precipitation was verified by Western Blot using anti-FLAG antibodies. **(B)** Mass spectrometric identified components in the 4XFLAG-Rca1 and 4XFLAG-Dap-dCDI-dPIPa precipitate. Proteins were grouped according to their function, as seen in the legend. Protein lists show only a selection of detected proteins.

For both 4XFLAG-Rca1 and 4XFLAG-Dap-dCDI-dPIPa, only a selection of the most interesting proteins are shown and discussed here (see Figure 12B). Previous interaction studies have shown that Rca1 associates with the APC/C component Cdc27 and the APC/C co-activator subunit Fzr (230) suggesting that Rca1 directly binds APC/C-Fzr. In agreement with this, the APC/C components APC2/Mr and Cdc16 together with Fzr (see Table 39) were found in the 4XFLAG-Rca1 precipitate, even though Fzr was detected with a relative low Matrix Score (37.5). Surprisingly, Cdc27 was not detected. Furthermore, 4XFLAG-Rca1 was found in complex with the SCF components, SkpA and Cul1 suggesting that Rca1, as an F-box protein, functions in an SCF complex to label specific substrates for degradation. Notably, the SCF protein Rbx1 was not identified in this analysis. This was presumably due to its low molecular weight of 13 kDa, since proteins that were separated below 15 kDa were not subjected to MS analysis (see Figure 12A).

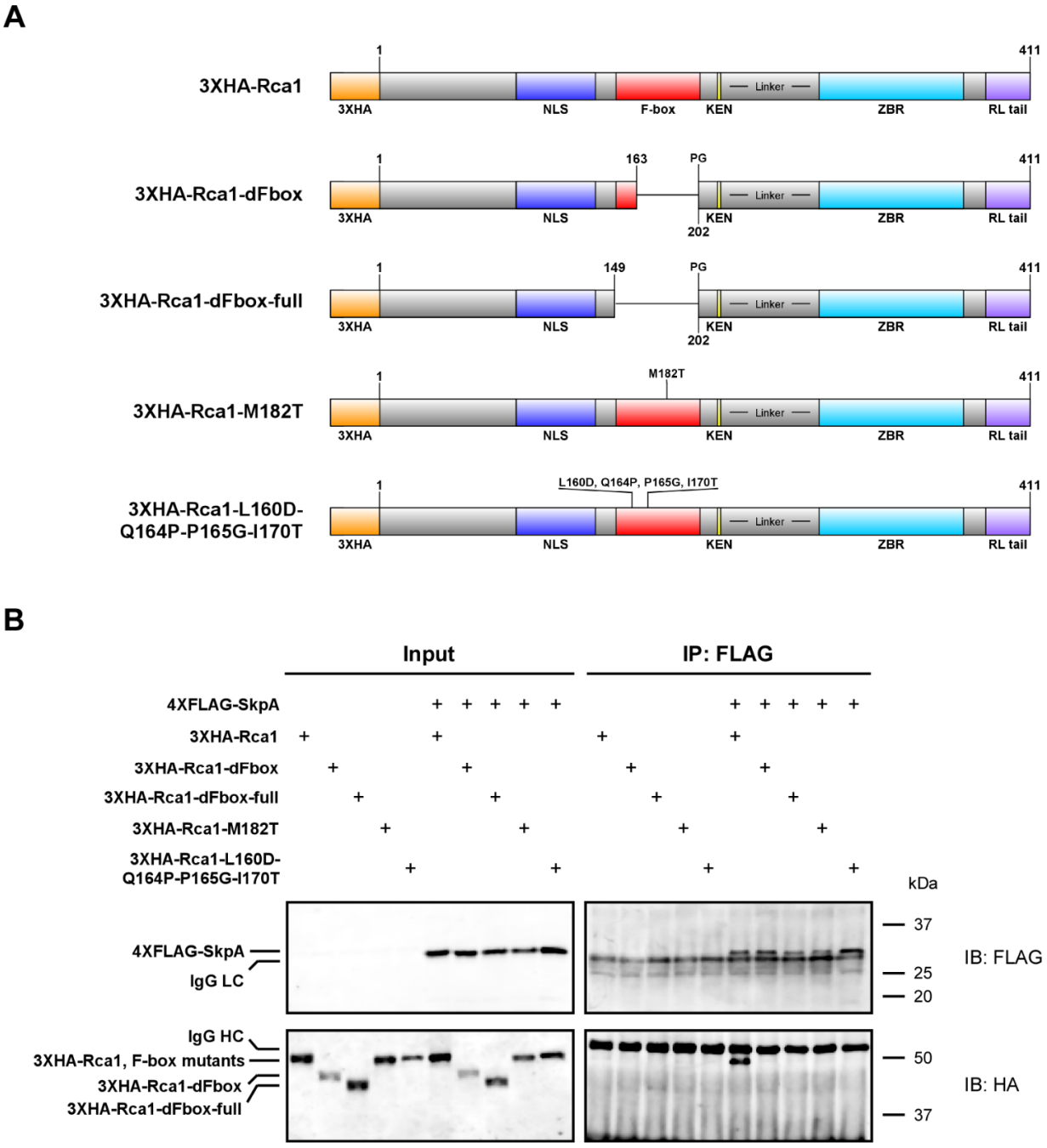

Figure 13 | Rca1 interacts with SkpA in an F-box dependent manner
F-box mutated Rca1 constructs were tested for 4XFLAG-SkpA binding by co-immunoprecipitations (co-IPs) using S2R+ lysates. **(A)** Schematic representation of the F-box mutated Rca1 variants used for interaction analysis. **(B)** Co-IP between 4XFLAG-SkpA and 3XHA-Rca1 constructs containing F-box mutations. All F-box mutations result in loss of 4XFLAG-SkpA binding.

F-box proteins associate with SkpA via their F-box (170). Therefore, to assess whether a functional F-box in Rca1 is required for SkpA binding, different 3XHA-tagged F-box mutants (see Figure 13A) were tested for their ability to bind 4XFLAG-SkpA in S2R+ lysates by co-immunoprecipitations (co-IPs) (see Figure 13B). Consistent with previous studies (231, 236), all Rca1 constructs harboring F-box mutations failed to interact

with SkpA. Thus, a functional F-box is required for SkpA binding . Moreover, considering the fact that the interaction between Rca1 and Cul1 is also F-box dependent (231), the co-IP studies demonstrate that the assembly of an SCF-Rca1 complex relies on a functional F-box. The MS analysis furthermore revealed the presence of Dap and CycE/Cdk2 in the 4XFLAG-Rca1 precipitate. The interaction to Dap was verified by co-IPs (see Figure 14A).

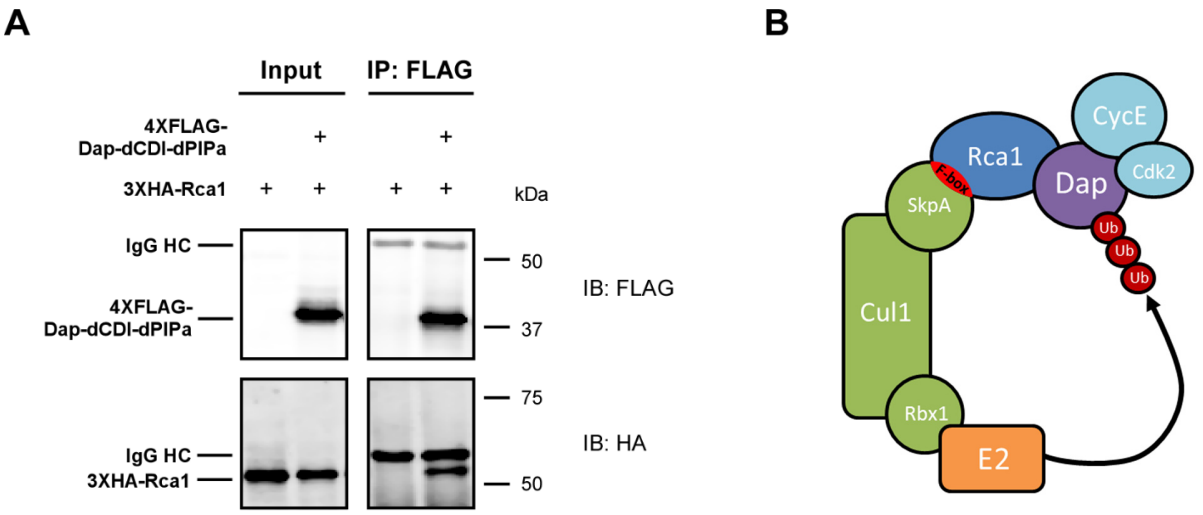

Figure 14 | Rca1 interacts with Dap providing a model for SCF-Rca1 mediated degradation of Dap
The mass spectrometric identified interaction between Rca1 and Dap was verified by co-IPs using S2R+ lysates. **(A)** Co-IP between 4XFLAG-Dap-dCDI-dPIPa and 3XHA-Rca1 demonstrating an interaction between Rca1 and Dap. **(B)** The mass spectrometric results, as shown in Figure 12B, provide a model, in which an SCF-Rca1 complex catalyzes polyubiquitination of Dap, thereby labeling it for degradation by the 26S proteasome. Rca1 (blue) interacts F-box (red) dependent with SCF components (green) and Dap (violet). Ubiquitin transfer is accomplished by a so far unknown E2 enzyme (orange). Binding of Dap does not impair its interaction with CycE/Cdk2 (cyan).

Dap is a CKI that specifically binds and inhibits CycE/Cdk2 (211, 212). The presence of CycE/Cdk2 in the 4XFLAG-Rca1 precipitate could therefore be the result of the interaction of Dap with CycE/Cdk2 and not necessarily caused by a direct interaction of 4XFLAG-Rca1 with CycE or Cdk2 or both. A more direct interaction between Rca1 and Dap is suggested by the presence of Rca1 in the 4XFLAG-Dap-dCDI-dPIPa precipitate (see Figure 12C). This Dap version can not bind to CycE/Cdk2 anymore indicating that the interaction between Rca1 and Dap occurs independently of CycE/Cdk2 binding. In addition, the precipitate also contained the SCF component SkpA. Taken together, the identified proteins in the precipitates provide a model, in which an SCF-Rca1 complex binds and labels substrates for degradation, with Dap being a potential target substrate (see Figure 14B). Interestingly, an additional protein, Skp2, was prominently present in the 4XFLAG-Rca1 precipitate. The interaction between Rca1 and Skp2 was confirmed by co-IP studies (see Figure 15). Skp2 is also an F-box protein that acts as substrate recognition subunit in an SCF complex. In mammals, SCF-Skp2 is implicated in the degradation of numerous cell cycle regulators (240). However, the functional relationship between the two F-Box proteins Rca1 and Skp2 remains to be analyzed and was not the main focus in this thesis.

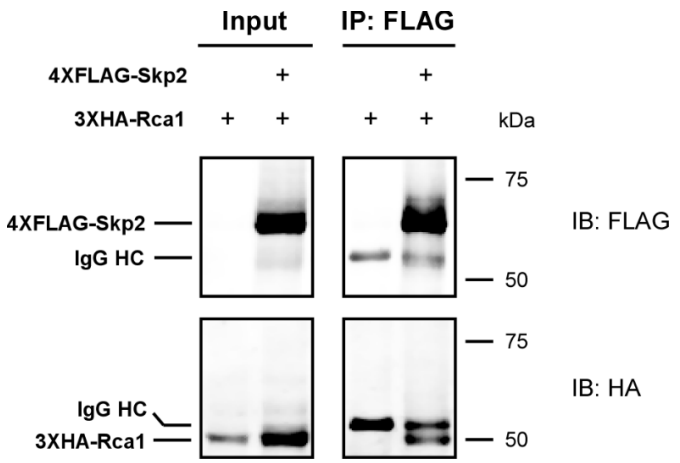

Figure 15 | Rca1 interacts with Skp2
The mass spectrometric identified interaction between Rca1 and Dap was verified by co-IPs using S2R+ lysates. Co-IP between 4XFLAG-Skp2 and 3XHA-Rca1 indicating that Rca1 binds to Skp2.

Beside this, many other proteins were identified in the 4XFLAG-Rca1 precipitate, of which the most are involved in regulation of mitosis, centrosome duplication, checkpoint control and spindle assembly (see Table 39). Although for most of the proteins, the purpose for the interaction to Rca1 is not clear, some can be explained by studies on the vertebrate homologue Emi1. For instance, CycB/Cdk1 and Plk1 (Polo kinase in *Drosophila*), which are known to bind Emi1 for its degradation (219, 222, 227) were also found in the 4XFLAG-Rca1 precipitate.

3.1.3 Rca1 interacts F-box dependent with polyubiquitinated substrates

SCF complexes are known to drive polyubiquitination of bound target substrates (241). *In vitro* interaction studies have indicated that the assembly of an SCF-Rca1 complex depends on the F-box domain of Rca1 (see section 3.1.2). To assess, whether SCF-Rca1 activity results in polyubiquitination of substrates *in vivo*, co-IPs in S2R+ lysates were used to analyze whether Rca1 binds polyubiquitinated substrates in an F-box dependent manner (see Figure 16). To precipitate proteins that were polyubiquitinated *in vivo*, a precursor protein consisting of a tandem repeat of a 4XFLAG-tagged version of Ubiquitin, 6XHIS-4XFLAG-Ub, was overexpressed. This mimics the situation of the polyubiquitin gene in *Drosophila* containing several tandem repeats of the Ubiquitin encoding gene (242). The translation product is a polyubiquitin precursor protein, which is processed by DUBs to release free Ubiquitin monomers (243). Previous experiments have shown that 6XHIS-4XFLAG-Ub derived from a tandem repeat precursor protein is efficiently incorporated into polyubiquitin chains (244). Consistent with this, upon precipitation of 6XHIS-4XFLAG-Ub, substrates from the middle to the high molecular weight region were detected indicating that polyubiquitinated substrates with 6XHIS-4XFLAG-Ub in their polyubiquitin chains were precipitated. Furthermore, single cleaved 6XHIS-4XFLAG-Ub was present as well. Precipitation of 6XHIS-4XFLAG-Ub conjugated substrates resulted in co-precipitation of 3XHA-tagged Rca1. In contrast, 3XHA-Rca1-dFbox-full that lacked the F-box was only slightly co-precipitated. However, this interaction was not specific, since 3XHA-Rca1-dFbox-full was also detected in the precipitate, which did not contain 6XHIS-4XFLAG-Ub. Thus, proteins labeled for degradation are found in complex with Rca1, but only when the F-box is present.

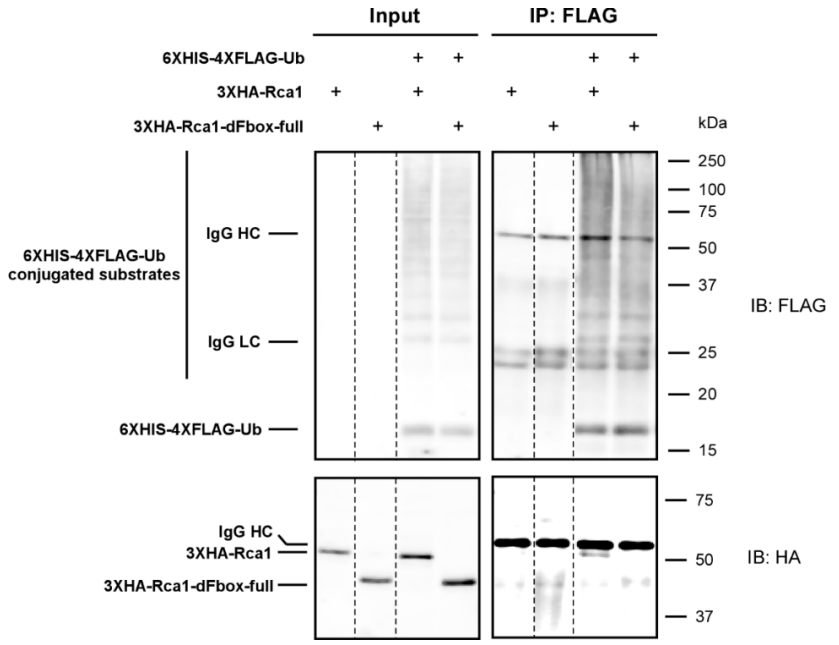

Figure 16 | Polyubiquitinated substrates bind Rca1 in an F-box dependent manner
4XFLAG tagged Ubiquitin (6XHIS-4XFLAG-Ub) and 3XHA-Rca1 were overexpressed in S2R+ cells. Precipitation of 6XHIS-4XFLAG-Ub conjugated substrates resulted in co-precipitation of 3XHA-Rca1, but not 3XHA-Rca1-dFbox-full lacking F-box (for illustration see Figure 13A). Dashed lines indicate omitted lanes.

Thus, assuming that deletion of the F-box does not interfere with substrate binding, these data suggest that active SCF-Rca1 stimulates polyubiquitination of bound target substrates.

3.2 Biochemical analysis of the interaction between Rca1 and Dap

3.2.1 Aim

Previous results have shown that Rca1 physically interacts with SCF components and Dap, implying that SCF-Rca1 binds Dap for degradation by the 26S proteasome (see section 3.1). To find more evidence for the existence of a functional SCF-Rca1 complex *in vivo*, Rca1 was fused to an ubiquitin-associated (UBA) domain binding K48-linked polyubiquitin chains with high affinity (245). Fusion of UBA domains to F-box proteins have been shown to increase their binding affinity to polyubiquitinated substrates, which allowed the identification of several target substrates of known F-box proteins (246). To see, whether this also accounts for Rca1, its ability to interact with polyubiquitinated Dap was investigated (see section 3.2.2). Direct substrate binding to the F-box protein does not depend on the structural integrity of the SCF complex (241). To evaluate, whether the interaction between Rca1 and Dap occurs independent of the SCF core complex, F-box mutated Rca1 constructs were tested for Dap binding (see section 3.2.3). Usually, phosphorylation is a prerequisite for recognition by the F-box protein (170). Therefore, to test, whether Dap represents a typical SCF target substrate for SCF-Rca1, the interaction between Rca1 and Dap was analyzed in a background of high kinase activity (see section 3.2.4). Several potential Cdk phosphorylation sites can be predicted in Dap. To assess, whether these sites contribute to Rca1 binding and to gain insight into the Rca1 interaction interface, N- and C-terminal truncated Dap constructs including Cdk site mutants were analyzed for their ability to interact with 3XHA-Rca1 (see section 3.2.5). Moreover, it was investigated whether the PIP-degron and the RXXL sequence in Dap, both potential degradation signals, are required for binding Rca1 (see section 3.2.7, 3.2.8). Finally, the region in Rca1 required to interact with Dap was characterized by different truncated Rca1 constructs (see section 3.2.9).

3.2.2 Fusion of UBA domains to Rca1 does not stimulate binding of polyubiquitinated Dap

Yeast Dsk2 and Rad23 belong to the family of proteins that harbor an UBA domain. These proteins recognize K48-linked polyubiquitin chains on proteins and target them to the 26S proteasome for degradation (247). Interaction studies with minimal UBA domains of the human homologues UQ1 (Dsk2) and hHR23A (Rad23) have shown that they bind polyubiquitin chains with high affinity (245). Fusion of the Dsk2/Rad23-UBA domain to F-box proteins of known SCF complexes specifically trapped their polyubiquitinated target substrates. This method, named "Ubiquitin Ligase Substrate Trapping", allowed the identification of several so far unreported SCF target substrates (246). Since Rca1 is believed to function as part of an SCF complex to label Dap for degradation (see section 3.1), it was assessed, whether Rca1 constructs fused to UBA domains from *Drosophila* Dsk2/Rad23 are capable of trapping polyubiquitinated Dap. The UBA domain of Dsk2 (codons 495 - 547) and the internal UBA domain of Rad23 (codons 154 – 200) were cloned using cDNA clones (Dsk2: LD38919, Rad23: LD10153) provided by the *Drosophila* Genomics Resource Center (248), and subsequently either N- or C-terminally linked to 4XFLAG-Rca1 (see Figure 17).

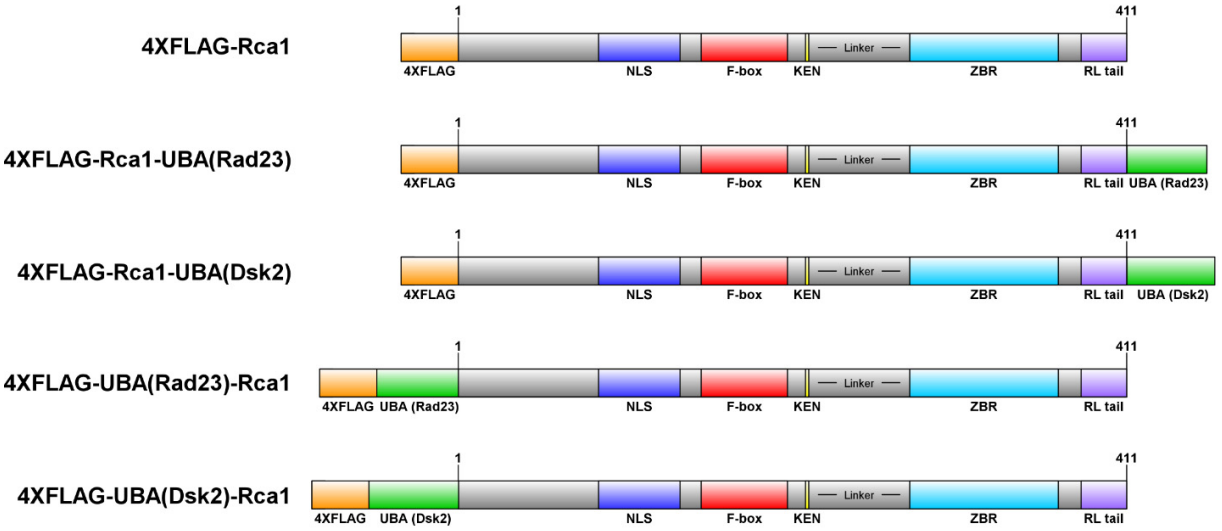

Figure 17 | UBA-fused Rca1 constructs that were analyzed for binding Dap polyubiquitin conjugates
Schematic illustration of the UBA-fused Rca1 constructs used for trapping of Dap polyubiquitin conjugates . 4XFLAG-Rca1 was either N- or C-terminally fused to an UBA domain derived from Rad23 or Dsk2, respectively.

The UBA-fused Rca1 constructs were analyzed for their ability to capture polyubiquitinated forms of HA-NLS-GFP-Dap-dCDI-dPIPa in SR2+ lysates by co-IPs (see Figure 18). Precipitation of 4XFLAG-Rca1 resulted in co-precipitation of HA-NLS-GFP-Dap-dCDI-dPIPa indicating that these two constructs interact with each other. The same was observed for the Rca1 constructs that are linked to an UBA domain. However, high molecular weight versions of the Dap construct were not detected suggesting that polyubiquitinated forms of HA-NLS-GFP-Dap-dCDI-dPIPa were not trapped.

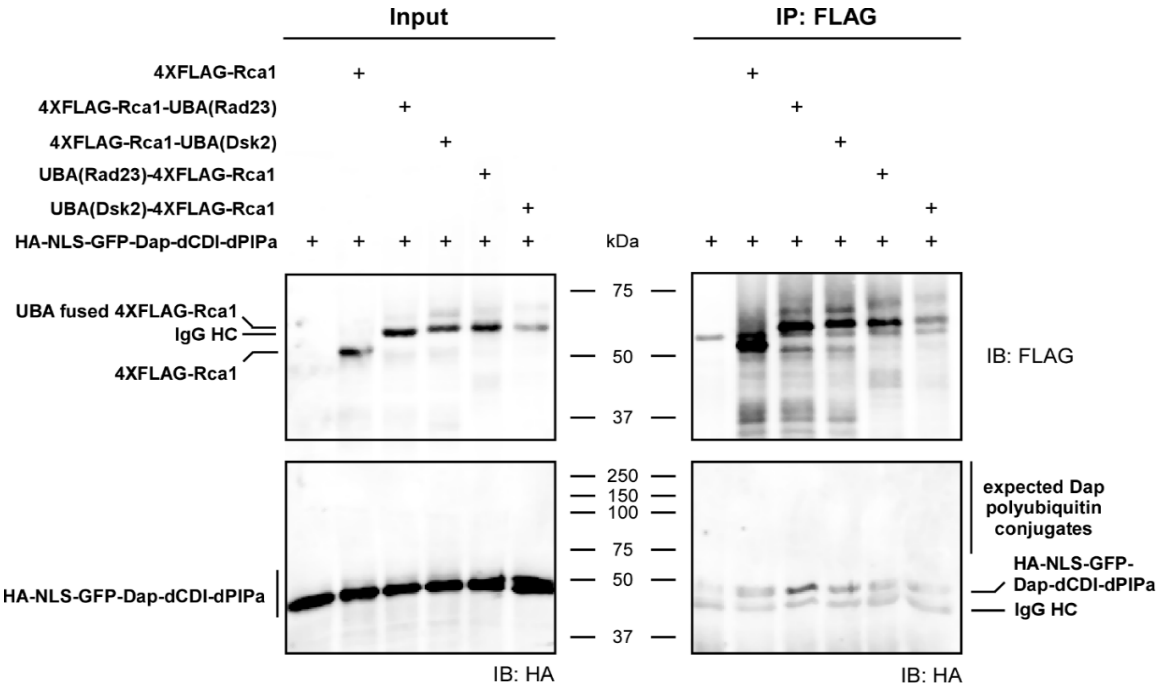

Figure 18 | Uba-fused Rca1 does not trap polyubiquitinated Dap
Co-IPs in S2R+ lysates were used to analyze, whether polyubiquitinated HA-NLS-GFP-Dap-dCDI-dPIPa is trapped by the UBA-fused Rca1 constructs (see Figure 15). All Rca1 constructs bound the Dap construct. However, polyubiquitin conjugated versions of HA-NLS-GFP-Dap-dCDI-dPIPa were not detected in the precipitates.

The absent of polyubiquitin conjugates in the precipitates contradicts the assumption that SCF-Rca1 stimulates the formation of polyubiquitin chains on Dap. However, several circumstances might be responsible for this negative result. Only low amounts of HA-NLS-GFP-Dap-dCDI-dPIPa were detected in the 4XFLAG-Rca1 precipitate making it likely impossible to identify a subset of polyubiquitinated proteins. Furthermore, it is not known whether the fused UBA domains are actually able to recognize and bind polyubiquitin chains. And even when this is the case, structural conditions might prevent the trapping process. Thus, albeit no direct evidence was found that demonstrates that Rca1 is in complex with polyubiquitinated Dap, the hypothesis of Dap being an SCF-Rca1 target substrate was not discarded.

3.2.3 SCF-Rca1 complex is not required for recruitment of Dap to Rca1

F-box proteins that function in SCF complexes usually interact simultaneously with two separate binding partners: 1) The SCF component SkpA through the F-box domain, and 2) the target substrate, which is recognized by another explicit domain (170, 241). Therefore, assuming that SCF-Rca1 binds Dap for degradation, the interaction between Rca1 and Dap should not be affected by a non-functional F-box. To test this hypothesis, Rca1 constructs carrying F-box mutations that fail to associate with SkpA (see Figure 13A,B) were analyzed for Dap binding in SR2+ lysates by co-IPs (see Figure 19).

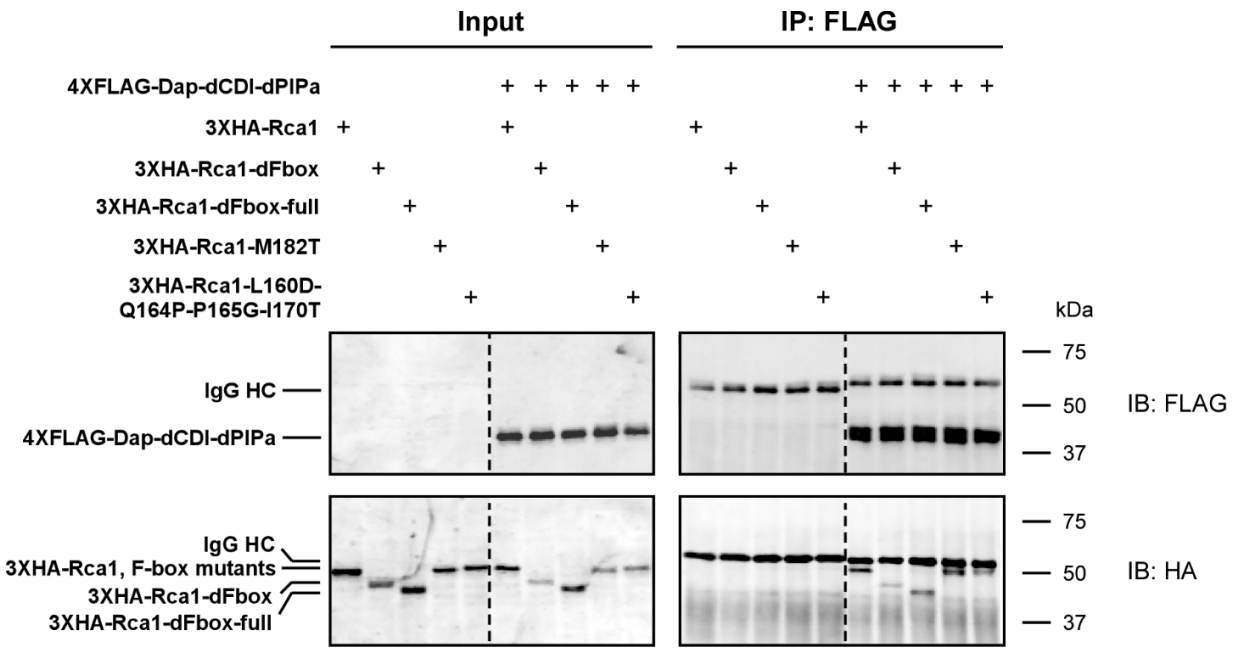

Figure 19 | A functional F-box in Rca1 is not required for Dap binding
An F-box dependent interaction between 3XHA-Rca1 constructs containing different F-box mutations (see Figure 13A) and 4XFLAG-Dap-dCDI-dPIPa was analyzed by co-IPs using S2R+ lysates. All F-box mutants interacted with the Dap construct. The amount of co-precipitated 3XHA-Rca1-dFbox-full was slightly reduced when compared to full-length 3XHA-Rca1. This also accounts for the F-box mutants 3XHA-Rca1-dFbox and 3XHA-Rca1-L160D-Q164P-P165G-I170T. However, these constructs were expressed at a lower level. 4XFLAG-Rca1-M182T expression was reduced as well, but co-precipitated with the same efficiency as wildtype 3XHA-Rca1. Dashed lines indicate omitted lanes.

Precipitation of 4XFLAG-Dap-dCDI-dPIPa resulted in co-precipitation of all tested 3XHA-tagged Rca1 F-box mutants, however with some different efficiencies. Both 3XHA-Rca1-dFbox and 3XHA-Rca1-L160D-Q164P-P165G-I170T were co-precipitated in lower amounts, when compared to full-length 3XHA-Rca1. Notably, the expression of these Rca1 constructs was reduced as well (see input), which let assume that this is the reason, why less of them was finally bound to the Dap construct. This does not account for 3XHA-Rca1-dFbox-full that lacks the complete F-box. Although this construct was expressed at the same level as full-length 3XHA-Rca1 (see input), its amount in the 4XFLAG-Dap-dCDI-dPIPa precipitate was slightly reduced indicating that the dFbox-full mutation impairs the interaction with Dap. Interestingly, although the expression of 3XHA-Rca1-M182T also occurred at a lower level (see input), this F-box mutant associated with the Dap construct with the same efficiency as the wildtype 3XHA-Rca1 construct suggesting that the F-box mutation M182T displays an hypermorphic mutation, which increases the interaction with Dap.

According to the result interpretation of the co-IP experiment shown above, the dFbox-full mutation affects Dap binding, whereas the dFbox mutation does not. However, the expression level of 3XHA-Rca1-dFbox and wildtype 3XHA-Rca1 were too different to make any clear conclusions. Thus, the influence of the dF-box mutation on Dap binding was repeated by using another co-IP approach, in which the experimental setup was slightly changed by linking the 4XFLAG-tag on Rca1/Rca1-dFbox. These Rca1 constructs were then analyzed for their ability to co-precipitate HA-NLS-GFP-Dap-dCDI-dPIPa (see Figure 20).

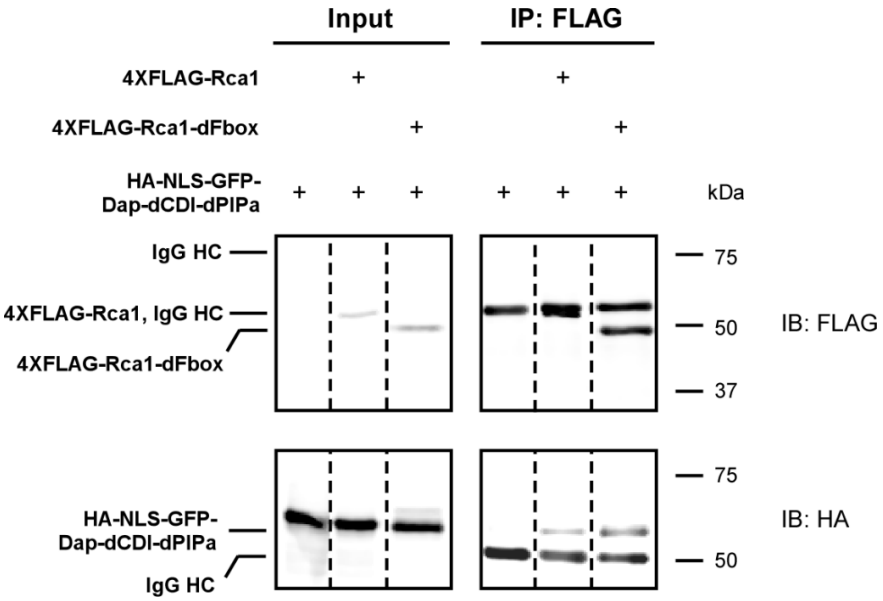

Figure 20 | F-box deletion in Rca1 does not affect interaction with Dap
The interaction between 4XFLAG-Rca1(-dFbox) and HA-NLS-GFP-Dap-dCDI-dPIPa was analyzed by co-IPs using S2R+ lysates. In comparison to 4XFLAG-Rca1, binding to HA-NLS-GFP-Dap-dCDI-dPIPa is not reduced when the F-box is broadly deleted, as in 4XFLAG-Rca1-dFbox (see Figure 13A). Dashed lines indicate omitted lanes.

Using this co-IP approach, the same amount of 4XFLAG-Rca1 and 4XFLAG-Rca1-dFbox was precipitated, while the amount of co-precipitated HA-NLS-GFP-Dap-dCDI-dPIPa was even slightly increased for 4XFLAG-Rca1-dFbox. Thus, the dFbox mutation does not interfere with Dap binding, confirming the interpretation of the previous co-IP study. It was assumed that the same accounts for the F-box mutation L160D-Q164P-P165G-I170T, which behaved in expression and binding like the dFbox mutation.

Taken together, with exception of the dFbox-full mutation that slightly affects the association with Dap, all F-box mutations allow binding to Dap with almost same efficiency. Thus, the interaction between Dap and Rca1 is achieved independent of a functional F-box domain, and therefore occurs independent of an SCF-Rca1 complex.

3.2.4 CycE/Cdk2 activity increases Rca1 binding to Dap

Substrate recognition by F-box proteins is usually regulated by phosphorylation. Once the target substrate is phosphorylated, it is recruited to the SCF complex for ubiquitination and subsequent degradation (170). In Dap, several potential Cdk phosphorylation sites could be predicted across the whole protein (see Figure 21A) by the kinase-specific phosphorylation site prediction tool KinasePhos 2.0 (249). CycE/Cdk2 is a good candidate to stimulate Dap phosphorylation, since the degradation of the mammalian homologues p21 and p27 is stimulated by phosphorylation by CycE/Cdk2 (182-184). To test, whether CycE/Cdk2 stimulates the binding of Rca1 to Dap, 4XFLAG-Rca1 and HA-NLS-GFP-Dap-dCDI-dPIPa were expressed in S2R+ cells when CycE/Cdk2 activity was increased by overexpression of HA-CycE. The interaction was analyzed in SR2+ lysates by co-IPs (see Figure 21B).

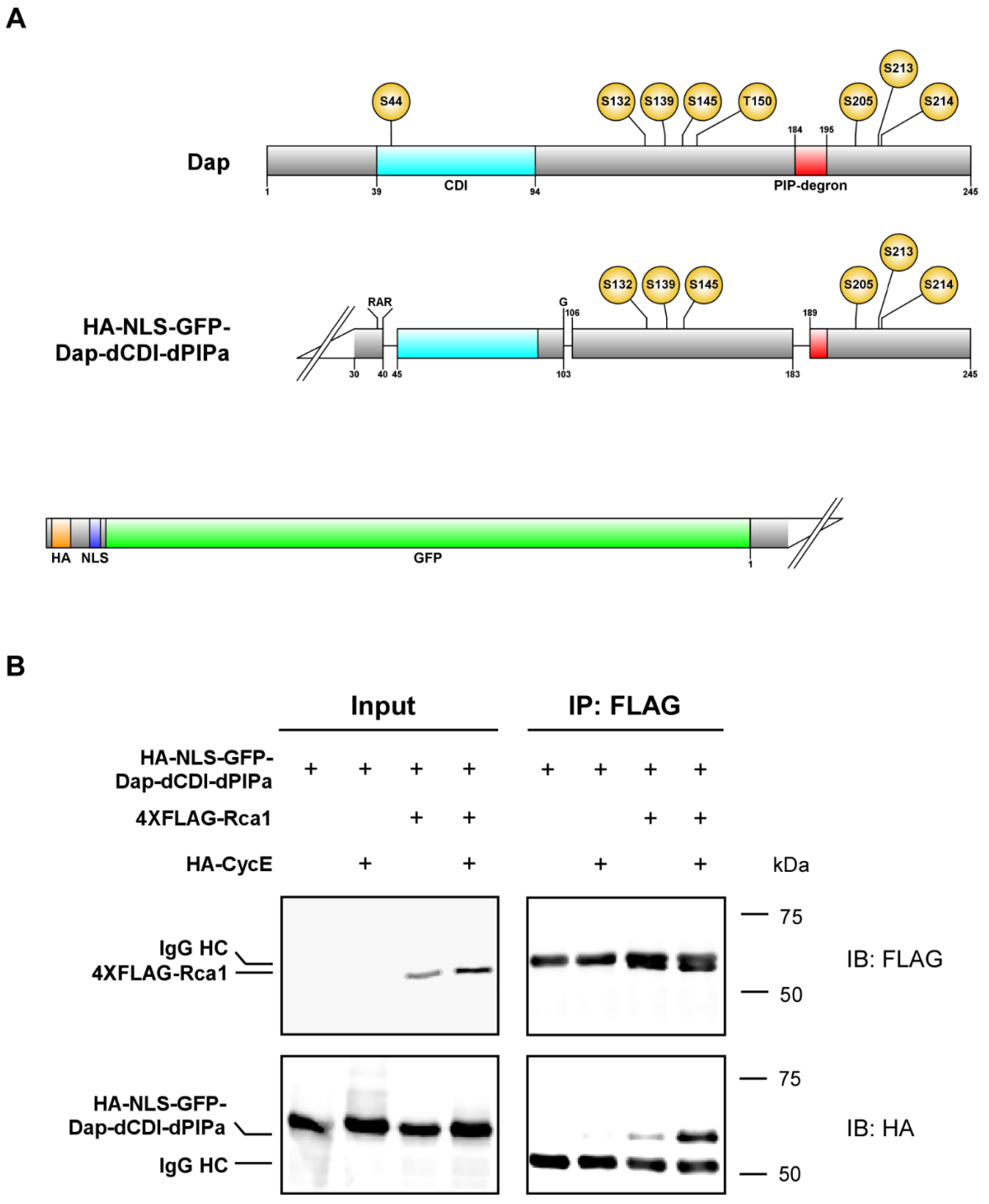

Figure 21 | CycE overexpression stimulates the interaction between Rca1 and Dap
The interaction between 4XFLAG-Rca1 and HA-NLS-GFP-Dap-dCDI-dPIPa was analyzed upon HA-CycE overexpression by co-IPs using S2R+ lysates. **(A)** Schematic presentation of wildtype Dap and GFP-Dap-dCDI-dPIPa showing potential Cdk phosphorylation sites (yellow circles). Mutations render the Dap construct cell cycle inactive (dCDI) and unable to be degraded during S-phase (dPIPa). Noteworthy, these mutations eliminate the potential Cdk sites S44 and T150. **(B)** Co-IP between 4XFLAG-Rca1 and HA-NLS-GFP-Dap-dCDI-dPIPa. HA-CycE overexpression increased co-precipitation of the Dap construct with 4XFLAG-Rca1. Here, it should be noted that equal amounts of 4XFLAG-Rca1 were present in the precipitate, while the lysate with overexpressed HA-CycE contained slightly more 4XFLAG-Rca1.

The amount of co-precipitated HA-NLS-GFP-Dap-dCDI-dPIPa upon precipitation of 4XFLAG-Rca1 was strongly increased when HA-CycE was overexpressed, suggesting that CycE/Cdk2 activity stimulates the interaction between Rca1 and Dap. These data support the assumption that CycE/Cdk2-mediated phosphorylation of Dap at one or several of the predicted Cdk sites is required for recognition by SCF-Rca1.

3.2.5 S/T-P Cdk phosphorylation sites in Dap (S205, S214) are not required for Rca1 binding

It was shown that CycE/Cdk2 promotes interaction between Rca1 and Dap, presumably by phosphorylating one or even several of the predicted Cdk phosphorylation sites present on Dap (see section 3.2.4). Sequence analysis indicate that only two of the predicted Cdk sites in the C-terminal region of Dap form the conventional consensus sequence S/T-P for Cdk phosphorylation (6). Both S205 (PKKL**S**PAKR) and S214 (MRTS**S**PSSS) are followed by proline, with S205 being in the optimal phosphorylation motif S/T-P-X-R/K. To analyze whether these S-P sites stimulate the interaction with Rca1, the binding of 3XHA-Rca1 to 4XFLAG-Dap-dCDI-dPIPa-S205A-S214A, which lacks both S-P sites by alanine mutations (see Figure 22) was investigated in S2R+ lysates by co-IPs (see Figure 23).

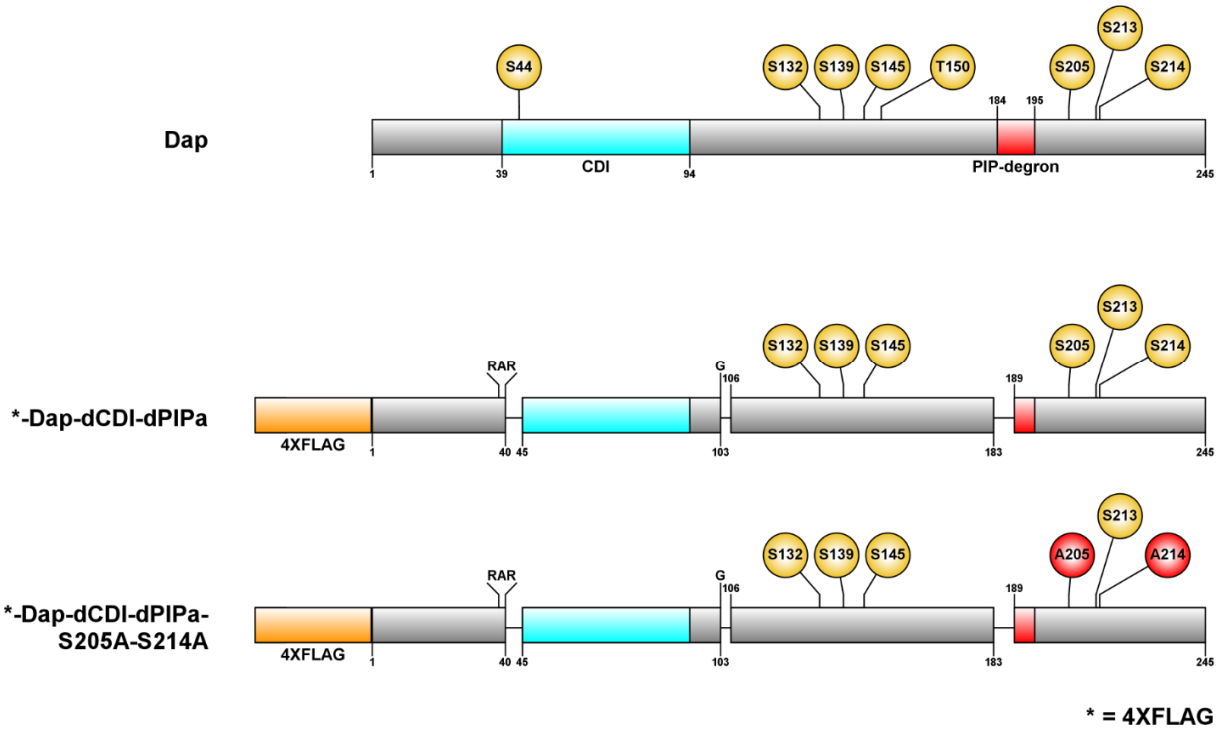

Figure 22 | Dap constructs used to analyze the requirement of the S-P sites for Rca1 binding
Schematic presentation of the 4XFLAG-tagged Dap constructs that were analyzed for their ability to interact with 3XHA-Rca1. In 4XFLAG-Dap-dCDI-dPIPa-S205A-S214A, serines in both S-P sites were mutated to alanine. Predicted (yellow circles) and mutated (red circles) Cdk phosphorylation sites are illustrated. The analyzed Dap constructs contain mutations that render them cell cycle inactive (dCDI) and unable to be degraded during S-phase (dPIPa). Top scheme indicates the wildtype version of Dap.

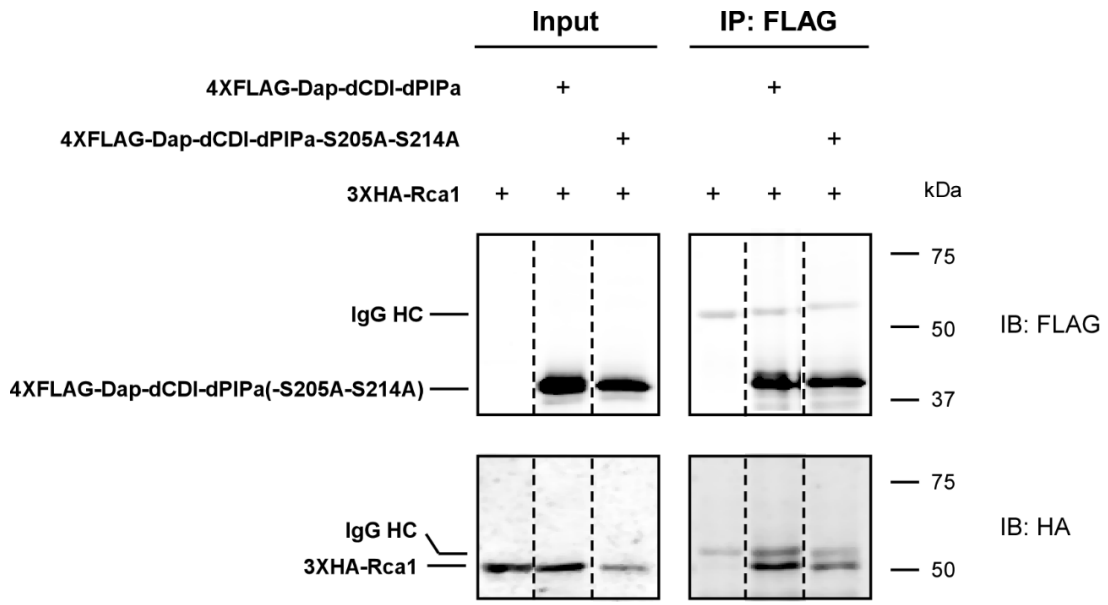

Figure 23 | Loss of the two S-P sites S205 and S214 in Dap does not impair interaction with Rca1
Co-IP between 4XFLAG-Dap-dCDI-dPIPa(-S205A-S214A) and 3XHA-Rca1. In comparison to 4XFLAG-Dap-dCDI-dPIPa, the amount of co-precipitated 3XHA-Rca1 in the 4XFLAG-Dap-dCDI-dPIPa-S205A-S214A precipitate was slightly reduced. However, this was likely caused by the lower amount of expressed 3XHA-Rca1 in the lysate (see input). Thus, binding to Rca1 is not affected by the S205A-S214A double mutation. Dashed lines indicate omitted lanes.

Loss of both conventional S-P Cdk phosphorylation sites in 4XFLAG-Dap-dCDI-dPIPa did not affect the interaction with 3XHA-Rca1 indicating that phosphorylations at these sites are not essential for Rca1 recruitment. This was unexpected, since overexpression of CycE/Cdk2 has been shown to stimulate the binding between Rca1 and Dap (see Figure 21B). Furthermore, S205 is localized in an optimal Cdk phosphorylation motif. One explanation for the interaction between 3XHA-Rca1 and 4XFLAG-Dap-dCDI-dPIPa-S205A-S214A might be that the S-P sites contribute only to a minor part to the interaction interface. In this context, it was hypothesized that the requirement of the S-P sites might become visible when the interaction to Rca1 occurs in a more relaxed manner. 4XFLAG-Dap-Del-1-53-dCDI-dPIPa, which lacks the N-terminal region of Dap, was shown to exhibit a greatly reduced binding strength to 3XHA-Rca1 (see following section 3.2.6). Therefore, it was assumed that this Dap construct provides a better opportunity to analyze the importance of the S-P sites in 3XHA-Rca1 binding (see Figure 24). Compared to full-length 4XFLAG-Dap-dCDI-dPIPa, the amount of 3XHA-Rca1 was reduced in the 4XFLAG-Dap-Del-1-53-dCDI-dPIPa precipitate. The same protein level of 3XHA-Rca1 was detected in the 4XFLAG-Dap-Del-1-53-dCDI-dPIPa-S205A-S214A precipitate. Thus, even in the presence of a low binding strength to 3XHA-Rca1, elimination of the S-P sites did not affect the weak interaction, further supporting their non-relevance for Rca1 recruitment.

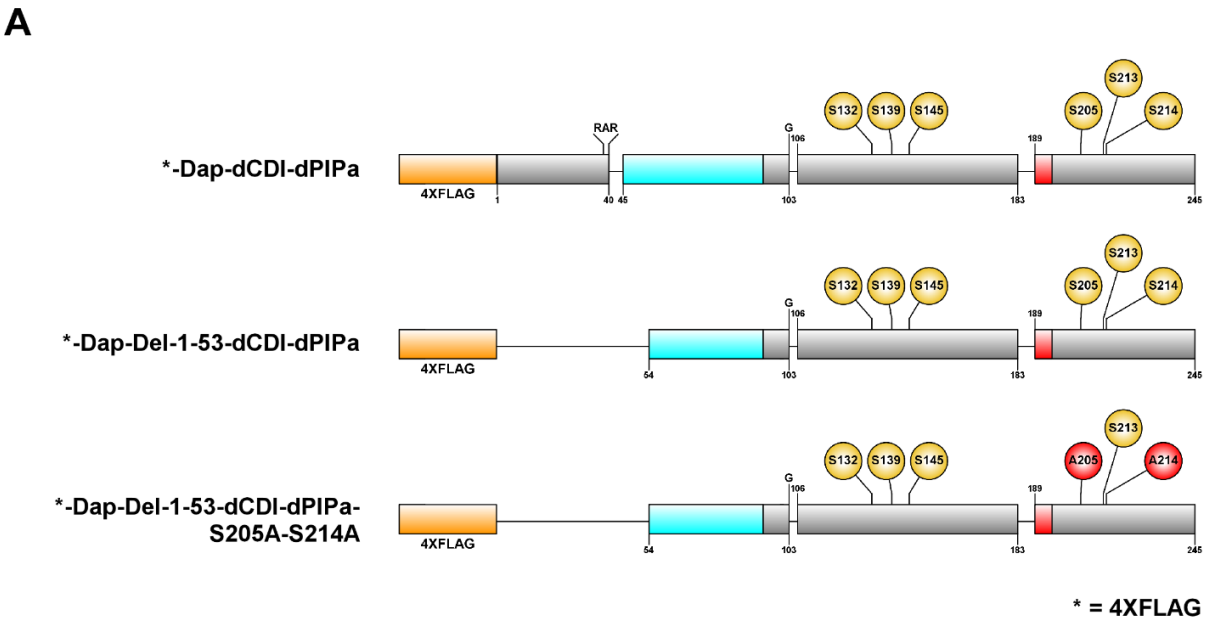

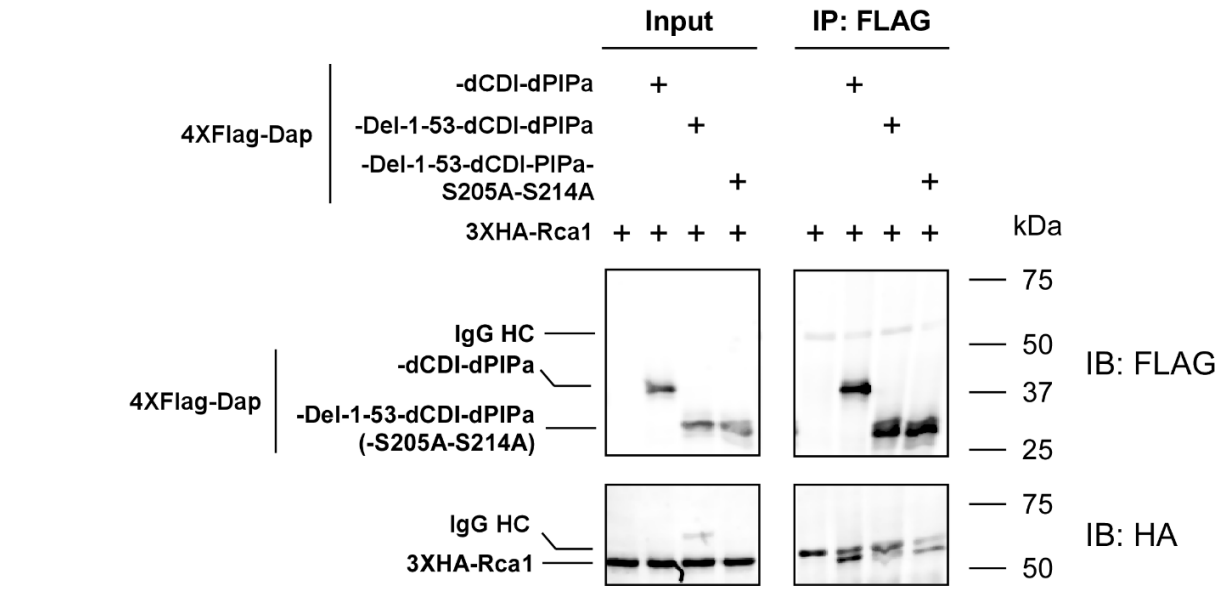

Figure 24 | Low Rca1 binding strength to Dap lacking the N-terminal region is not further reduced by the two S-P Cdk phosphorylation sites S205 and S214

The requirement of the S-P Cdk phosphorylation sites in Dap for Rca1 interaction was analyzed under weak binding conditions in S2R+ lysates by co-IPs. **(A)** Schematic presentation of the 4XFLAG-tagged Dap constructs that were used to analyze the interaction with 3XHA-Rca1. Several mutations render the Dap constructs cell cycle inactive (dCDI) and unable to be degraded during S-phase (dPIPa). Predicted (yellow circles) and mutated Cdk sites (red circles) are indicated. **(B)** Co-IP between 4XFLAG-tagged Dap constructs and 3XHA-Rca1, as indicated in (A). N-terminal deletion of the first 53 residues, as in 4XFLAG-Dap-Del-1-53-dCDI-dPIPa, strongly reduced its binding efficiency to 3XHA-Rca1. Additional loss of the two S-P Cdk phosphorylation sites S205 and S214 by alanine mutations, as in 4XFLAG-Dap-Del-1-53-dCDI-dPIPa-S205A-S214A, did not alter the interaction with 3XHA-Rca1.

3.2.6 N-terminal half of Dap is required but not sufficient to mediate interaction with Rca1

In order to get a general idea what regions are required to allow association with Rca1, N- and C-terminal truncated 4XFLAG-tagged Dap constructs were characterized for their ability to interact with 3XHA-Rca1 (see Figure 25).

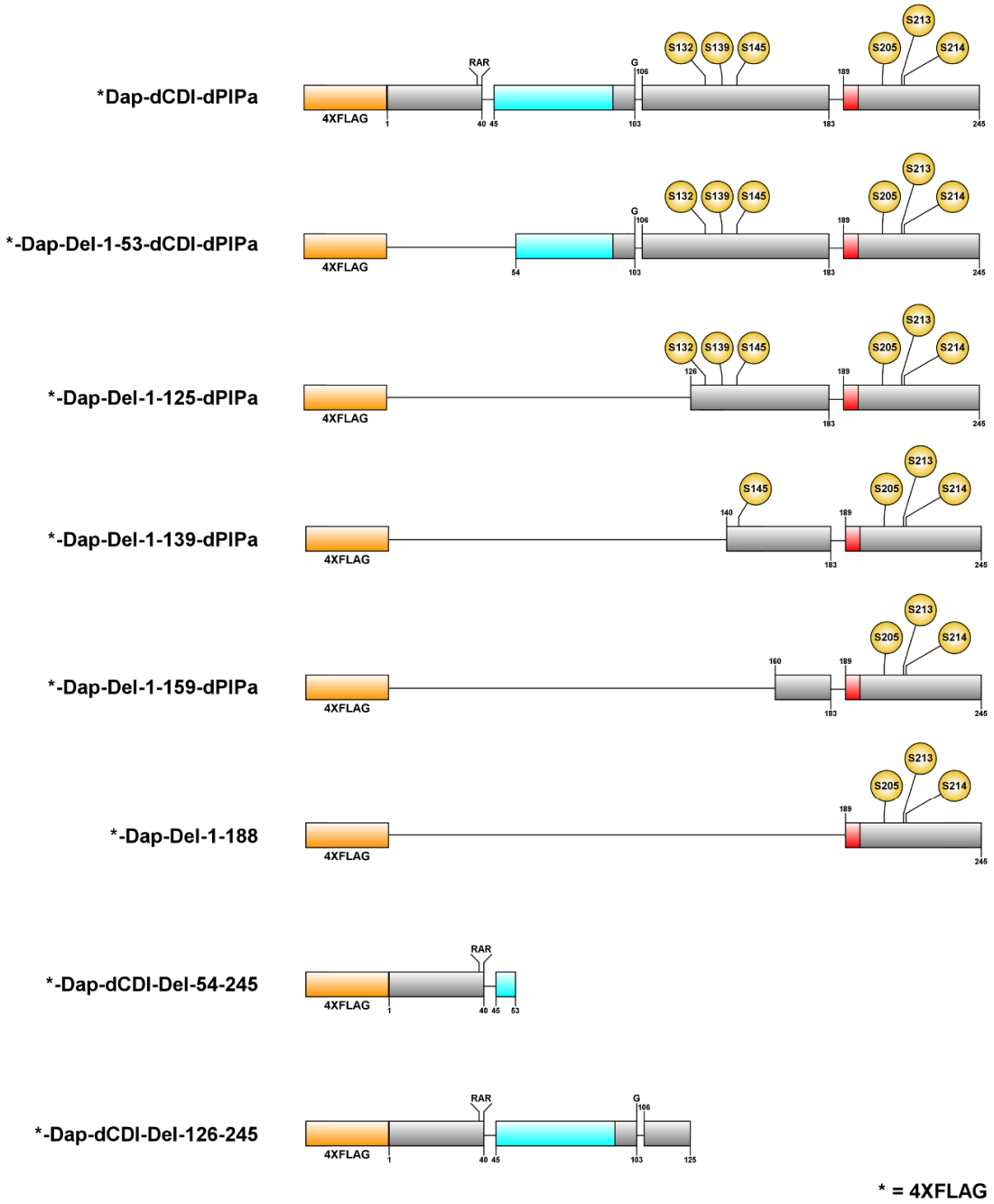

Figure 25 | 4XFLAG-tagged truncated Dap constructs tested for their ability to bind 3XHA-Rca1
Schematic presentation of 4XFLAG-tagged Dap constructs used to analyze the interaction with 3XHA-Rca1. All Dap constructs contain mutations that render them cell cycle inactive (dCDI) and unable to be degraded during S-phase (dPIPa). Predicted Cdk sites are indicated (yellow circles).

Interaction analyses were performed in S2R+ cell lysates by co-IPs (see Figure 26A). Precipitation of 4XFLAG-Dap-Del-1-53-dCDI-dPIPa that lacks the first 53 residues resulted in lower amounts of co-precipitated 3XHA-Rca1, when compared to full length 4XFLAG-Dap-dCDI-dPIPa. Further deletion of the N-terminus up to 125 residues, as in 4XFLAG-Dap-Del-1-125-dPIPa, completely eliminated binding to 3XHA-Rca1 indicating that the N-terminal half in Dap is required for Rca1 recruitment (see Figure 26B).

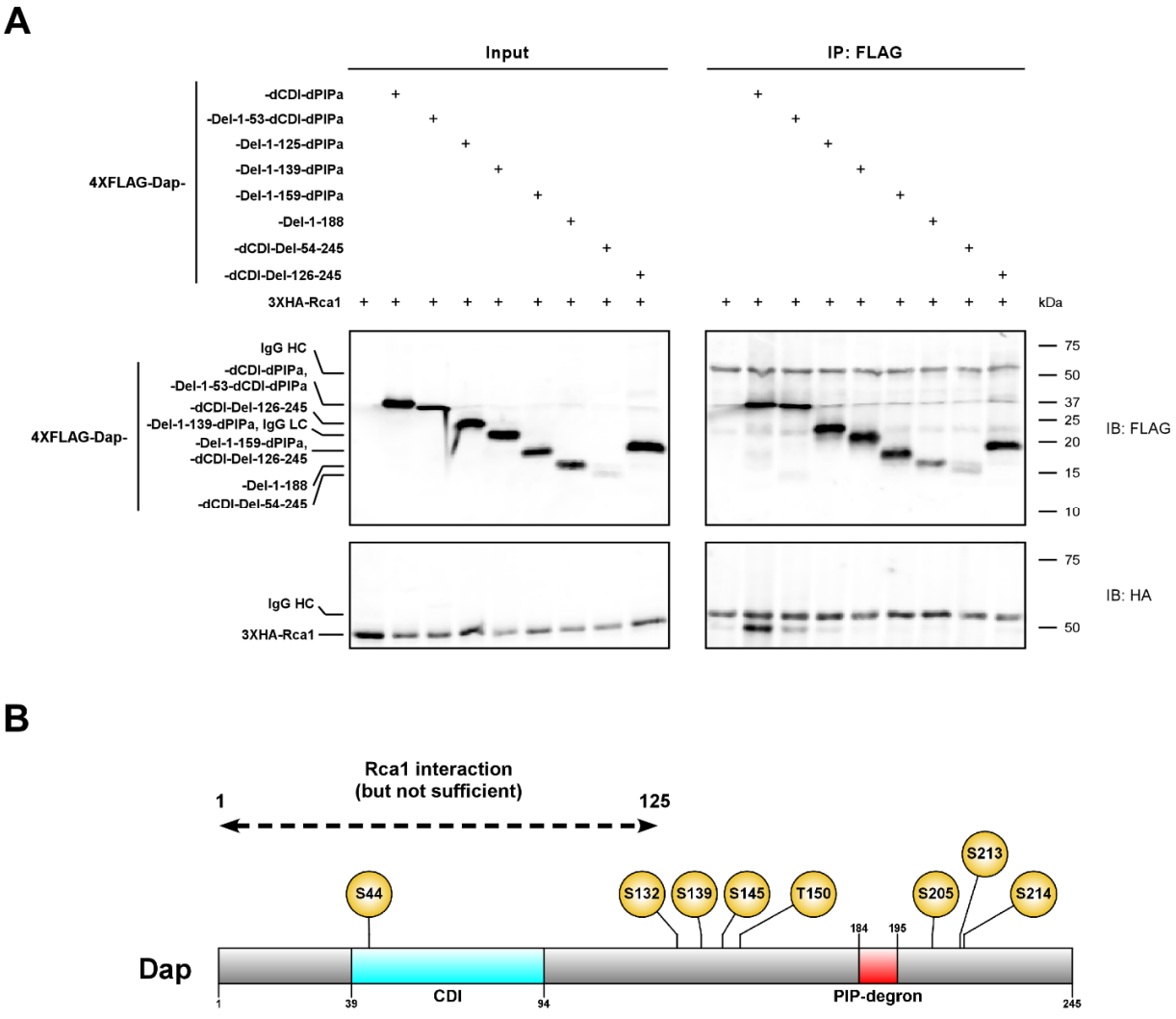

Figure 26 | N-terminal region in Dap (residues 1 – 125) is required but not sufficient for interaction with Rca1
Several N- and C-terminal truncated Dap constructs (see Figure 25) were tested for binding 3XHA-Rca1 in S2R+ lysates by co-IPs. **(A)** Co-IP between 4XFLAG-tagged Dap constructs and 3XHA-Rca1. N-terminal deletion of the first 53 residues, as in 4XFLAG-Dap-Del-1-53-dCDI-dPIPa, strongly reduced the binding strength to 3XHA-Rca1. Further reduction of the N-terminus (125 residues), as in 4XFLAG-Dap-Del-1-125-dPIPa, completely abolished the interaction with 3XHA-Rca1 suggesting that the N-terminal half in Dap is important for Rca1 binding. However, the N-terminal half alone, 4XFLAG-Dap-dCDI-Del-126-245, was not sufficient to interact with 3XHA-Rca1. **(B)** Schematic presentation of Dap showing the N-terminal region required for Rca1 binding (dashed double arrow). Predicted Cdk sites are indicated (yellow circles).

Noteworthy, the N-terminal half alone, 4XFLAG-Dap-dCDI-Del-126-245, did not interact with 3XHA-Rca1. This could be caused by a failure of this fragment to fold correctly or could indicate that residues in the C-

terminal half such as potential Cdk phosphorylation sites (Figure 21A) are also required for efficient Rca1 binding. Taken together, the interaction studies could reveal that the N-terminal half of Dap is essential, but not sufficient to stimulate the interaction with Rca1.

3.2.7 PIP-degron in Dap is not required for interaction with Rca1

Dap belongs to the family of PIP-degron containing proteins (analyzed in detail in section 3.4.3) that are labeled for degradation by CRL4-Cdt2 during S-phase (207, 250). The PIP-degron interacts with chromatin-bound PCNA during DNA replication, thereby creating a combined interaction interface for recruitment of Cdt2, a substrate recognition subunit of the CRL4 E3 ligase (207, 208, 250). Several Dap constructs lacking the N-terminal part of the PIP-degron (dPIPa mutation) were able to interact with 3XHA-Rca1 (see co-IP studies in this thesis) suggesting that Cdt2 and Rca1 bind to different interaction interfaces in Dap. To support this, HA-NLS-GFP-Dap-dCDI-dPIP, which is characterized by deletion of the entire PIP-degron was analyzed for binding 4XFLAG-Rca1 (see Figure 27).

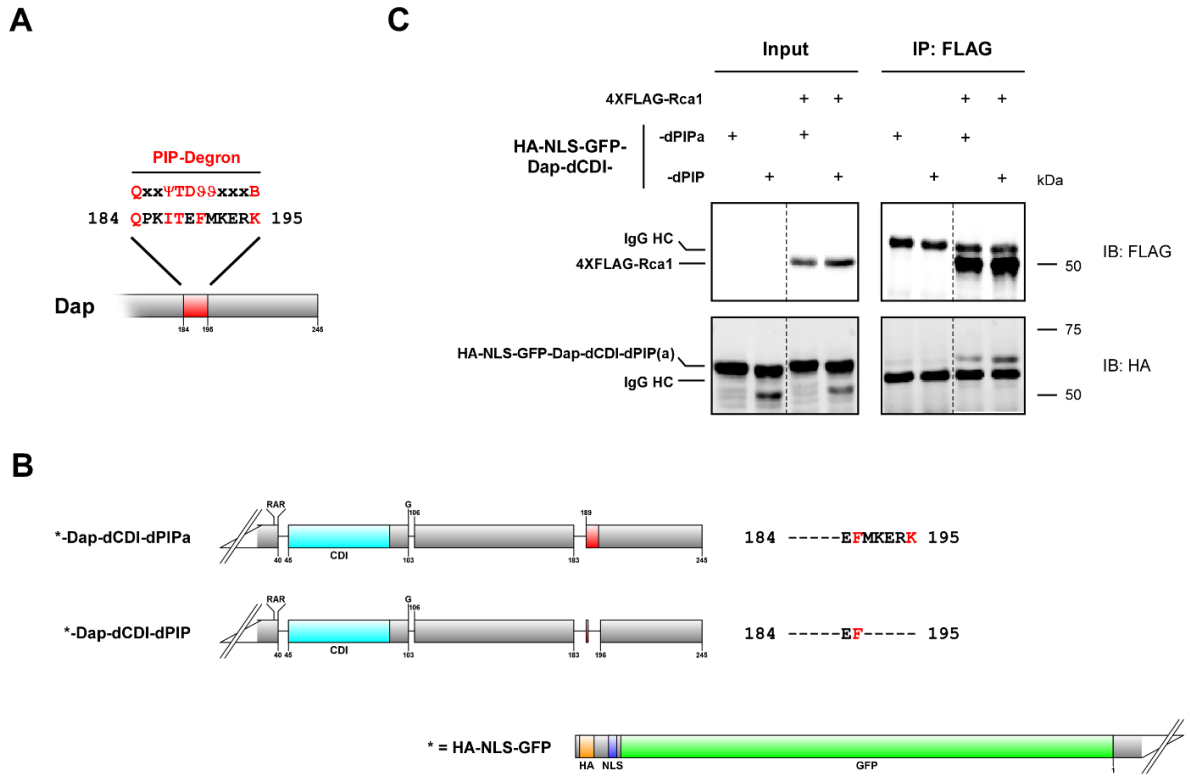

Figure 27 | Entire loss of the PIP-degron in Dap does not affect Rca1 binding
HA-NLS-GFP-tagged Dap constructs harboring different PIP-degron mutations were studied for association with 4XFLAG-Rca1 in S2R+ lysates by co-IPs. **(A)** Schematic illustration of the N-terminal part of Dap that contains the PIP-degron. The PIP-degron recruits CRL4-Cdt2 during S-phase. Residues that match the PIP-degron consensus sequence (Q-x-x-Ψ-T-D-ϑ-ϑ-x-x-x-B, Ψ = I/L/M/V, ϑ = Y/F, B = K/R) are highlighted (red). **(B)** Schematic illustration of the Dap constructs that were analyzed for 4XFLAG-Rca1 binding. In HA-NLS-GFP-Dap-dCDI-dPIPa, the N-terminal part of the PIP-degron is deleted. HA-NLS-GFP-Dap-dCDI-dPIP almost lacks the complete PIP-degron. Mutations render the constructs cell cycle inactive (dCDI). **(C)** Co-IP between 4XFLAG-Rca1 and HA-NLS-GFP-Dap-dCDI harboring PIP-degron mutations, as indicated in (B). Both HA-NLS-GFP-Dap-dCDI-dPIPa and HA-NLS-GFP-Dap-dCDI-dPIP were able to associate with 4XFLAG-Rca1 with the same efficiency. An additional band is present below the HA-NLS-GFP-Dap-dCDI-PIP band in the input lanes. Since proteins within this molecular weight range were not co-precipitated, these bands were ignored in this study. Dashed lines indicate omitted lanes.

The interaction with 4XFLAG-Rca1 was not reduced upon deletion of the entire PIP-degron indicating that the complete PIP-degron in Dap is not required for binding Rca1. Thus, Cdt2 and Rca1 associate with Dap on different regions, suggesting that their binding occurs independent from each other.

3.2.8 The RXXL sequence in Dap is not a degron motif but mutations in this sequence reduces Rca1 binding

Recognition of APC/C target substrates occurs via specific degrons in these substrates. The most common degrons are the D-box, which consists of the minimal consensus sequence R-X-X-L, and the KEN-box with consensus of K-E-N (251). These degrons are recognized by specific binding sites on the surface of the APC/C co-activators Cdh1/Fzr and Cdc20/Fzy (126, 128, 252). Dap carries an RXXL sequence (RKRL) suggesting that Dap is able to interact with both co-activators (see Figure 28).

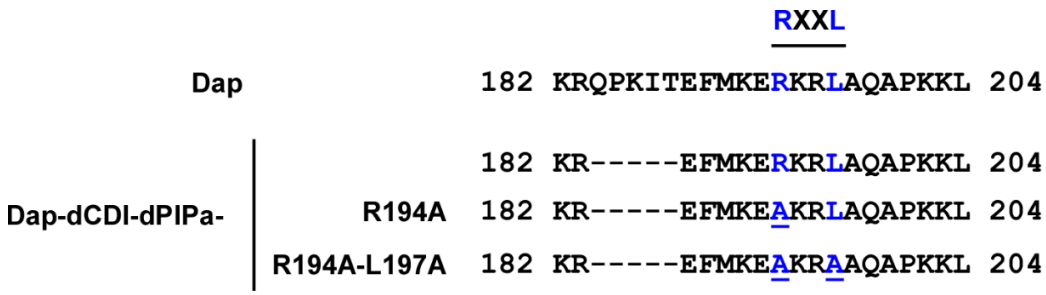

Figure 28 | Dap carries a RXXL sequence
Sequence of Dap showing the RXXL sequence (RKRL) in alignment with the Dap constructs used for Rca1 interaction analysis (see Figure 29). Mutations render the Dap construct cell cycle inactive (dCDI) and unable to be degraded during S-phase (dPIPa). The RXXL sequence was either mutated by AXXL or AXXA (underlined residues). Essential residues in the RXXL sequence are highlighted (blue).

Interestingly, Rca1 possesses a KEN-box, and therefore should be able to interact with the co-activators Fzy and Fzr as well, but on a different region. Thus, both Rca1 and Dap are potentially able to associate with either Fzy or Fzr at the same time, promoting the idea that they might function as co-adaptor proteins that bring Dap and Rca1 together. To test this hypothesis, Dap constructs carrying a mutated RXXL sequence were analyzed for their ability to bind Rca1 constructs in S2R+ lysates by co-IPs (see Figure 29). HA-NLS-GFP-Dap-dCDI-dPIPa-R194A in which the arginine of the RXXL sequence is mutated to alanine (AXXL) co-precipitated with 4XFLAG-Rca1 in the same manner as HA-NLS-GFP-Dap-dCDI-dPIPa (see Figure 29A). Thus, the RXXL sequence is not required for Rca1 binding. To support this finding, both essential residues of the RXXL sequence were mutated to alanine (AXXA). This time, 4XFLAG-tagged Dap constructs and 3XHA-Rca1 were used for co-IP studies (see Figure 29C). Unexpectedly, only a low amount of 3XHA-Rca1 was co-precipitated with the AXXA double mutant 4XFLAG-Dap-dCDI-dPIPa-R194-L197A. Assuming that the use of different tags did not affect the interaction analysis, these data suggest that L197 alone or in combination with R194 plays an important role for Rca1 recruitment. In this regard, further single and double mutation analyses of the RXXL sequence that rely on the same co-IP setup are necessary to reveal the importance of these residues in binding Rca1.

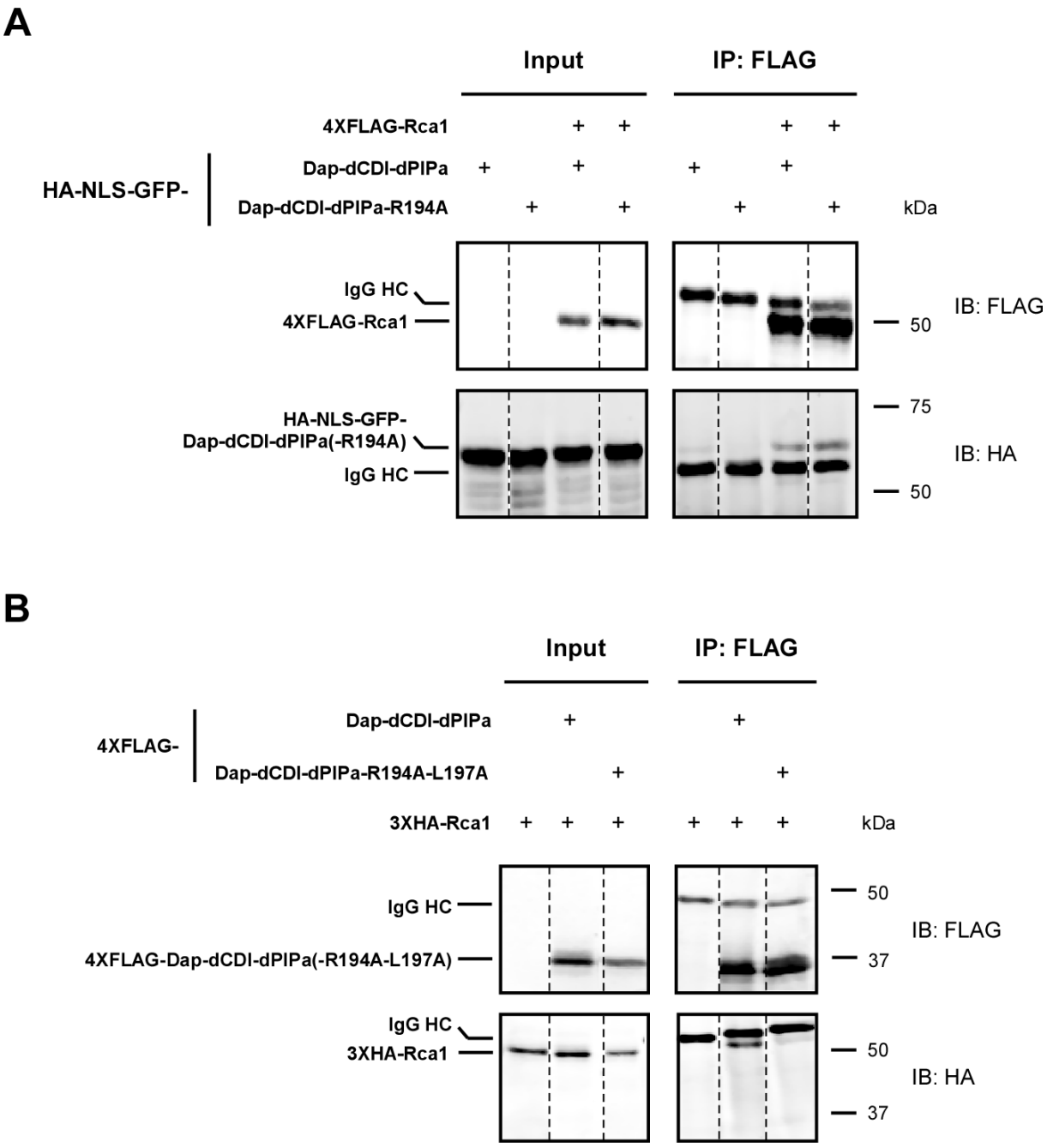

Figure 29 | RXXL sequence mutation R194A-L197A in Dap affects binding to Rca1
Dap constructs harboring RXXL mutations were studied for binding Rca1 constructs in S2R+ lysates by co-IPs. **(A)** Co-IP between 4XFLAG-Rca1 and HA-NLS-GFP-Dap-dCDI-dPIPa(-R194A). Both HA-NLS-GFP-Dap-dCDI-dPIPa and HA-NLS-GFP-Dap-dCDI-dPIPa-R194A were equally co-precipitated with 4XFLAG-Rca1. **(B)** Co-IP between 4XFLAG-Dap-dCDI-dPIPa(-R194A-L197A) and 3XHA-Rca1. The interaction between 3XHA-Rca1 and 4XFLAG-Dap-dCDI-dPIPa-R194A-L197A was strongly reduced when compared to 4XFLAG-Dap-dCDI-dPIPa. Dashed lines indicate omitted lanes.

Even though different co-IP approaches were used, it was concluded that the AXXA double mutation impairs the interaction with Rca1, while the single mutation AXXL does not. Since the AXXL mutation already represents a loss of the RXXL sequence that is present in D-boxes to mediate binding to the APC/C

co-activators Cdc20/Fzy and Cdh1/Fzr, Fzy and Fzr are likely not required to stimulate the interaction between Rca1 and Dap.

3.2.9 Central region in Rca1 is required for Dap binding

Dap has been shown to interact with Rca1. To identify the region required for Dap binding, N- and C-terminal truncated 3XHA-tagged Rca1 constructs (see Figure 30) were tested for their ability to associate with 4XFLAG-Dap-dCDI-dPIPa.

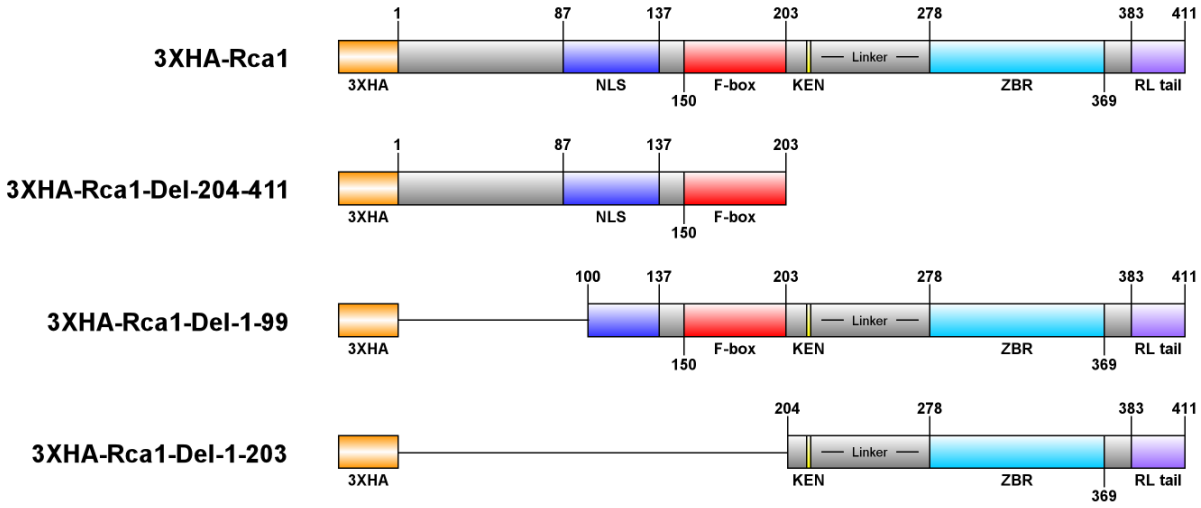

Figure 30 | 3XHA-tagged truncated Rca1 constructs tested for their ability to bind 4XFLAG-Dap-dCDI-dPIPa
Schematic presentation of 3XHA-tagged Rca1 constructs used to analyze the interaction with 4XFLAG-Dap-dCDI-dPIPa (see Figure 31).

The interaction was analyzed in SR2+ lysates by co-IPs (see Figure 31A). The interaction to 4XFLAG-Dap-dCDI-dPIPa was not impaired when the N- or C-terminal part of 3XHA-Rca1 was missing, as in 3XHA-Rca1-Del-1-99 or 3XHA-Rca1-Del-204-411. The interaction was even increased for the latter Rca1 construct. Thus, neither the N-terminal part (residues 1 – 99) nor the C-terminal part (residues 204 – 411) of Rca1 is required for the association with Dap. In contrast, only a weak interaction with the Dap construct was observed, when additional to the N-terminal part the central region of Rca1 was eliminated, as in 3XHA-Rca1-Del-1-203. This great loss in interaction suggests that the central region (residues 100 – 203) is important for binding Dap (see Figure 31B). An association with 4XFLAG-Dap-dCDI-dPIPa was still possible to a slight extent indicating that residues in the C-terminal half of Rca1 also contributes to Dap binding.

Taken together, the interaction studies demonstrate that the central region in Rca1 including part of the NLS sequence and the F-box is required for the interaction with Dap. Residues within the C-terminal part also associates with Dap, but these interactions play only a minor role. Further truncations are necessary to narrow down the region implicated in Dap recruitment.

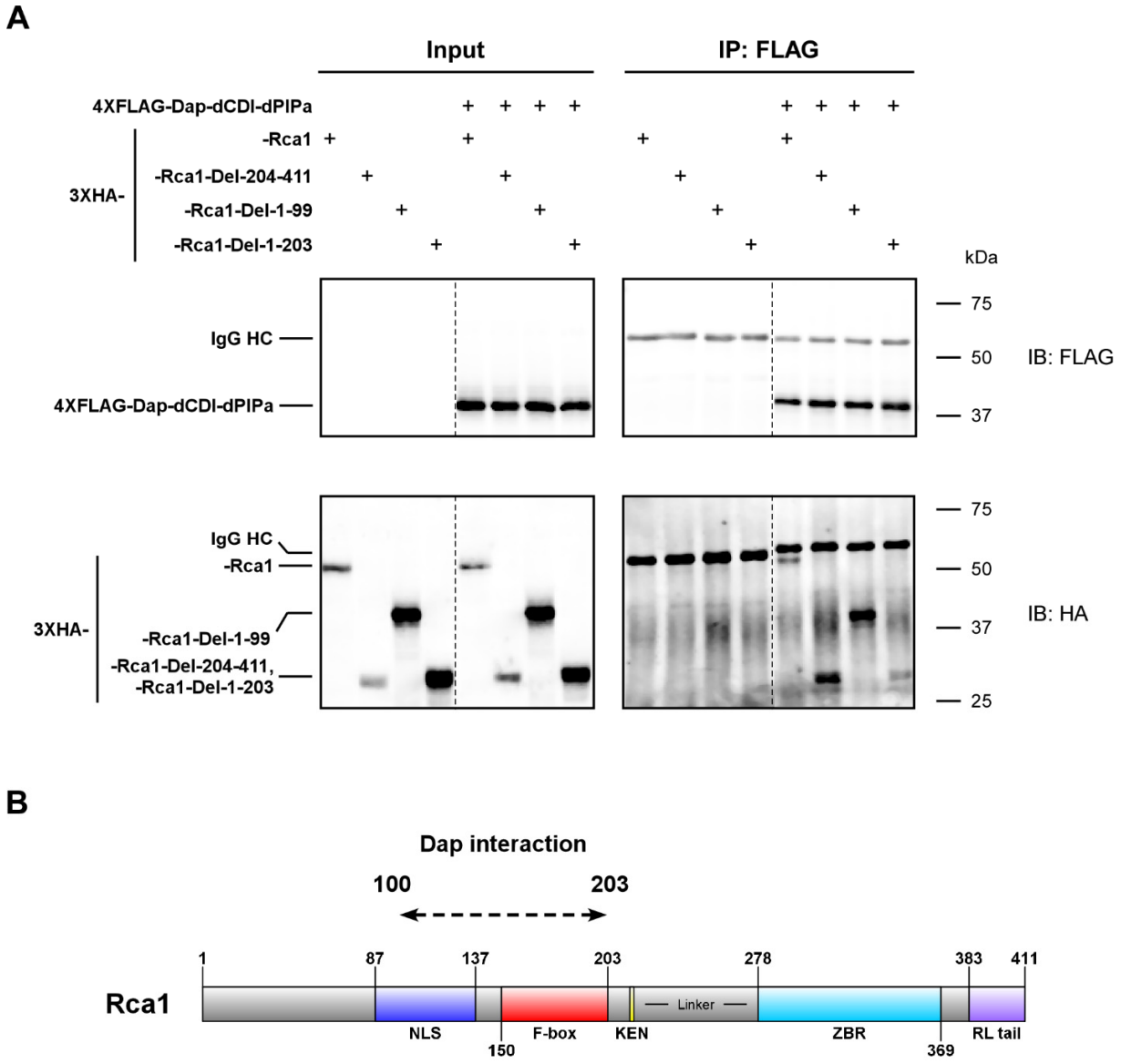

Figure 31 | Central region in Rca1 (100 – 203) is required for the interaction with Dap
N- and C-terminal truncated 3XHA-tagaged Rca1 constructs (see Figure 30) were analyzed for binding 4XFLAG-Dap-dCDI-dPIPa in S2R+ lysates by co-IPs. **(A)** Co-IP between 4XFLAG-Dap-dCDI-dPIPa and truncated 3XHA-Rca1 constructs. Upon precipitation of 4XFLAG-Dap-dCDI-dPIPa, the amount of co-precipitated 3XHA-Rca1-Del-204-411 was increased in comparison to full-length 3XHA-Rca1. These constructs were equally expressed (see input). The protein level of 3XHA-Rca1-Del-1-99 was strongly increased in the 4XFLAG-Dap-dCDI-dPIPa precipitate, likely caused by the strong expression of this construct (see input). In contrast, 3XHA-Rca1-Del-1-203 was hardly co-precipitated despite its strong expression (see input). **(B)** Schematic presentation of Rca1 showing the central region required for Dap binding (dashed double arrow).

3.3 *In vivo* analysis of APC/C-Fzr activity regulation by Rca1 and Dap

3.3.1 Aim

Direct inhibition of APC/C-Fzr by Rca1 depends on a functional ZBR (see section 2.12). *In vitro* interaction studies described above (see section 3.2) suggest that Rca1 requires its F-box to function in an SCF complex

by targeting substrates for degradation. Since Rca1 associates with the CycE/Cdk2 inhibitor Dap, Dap is a potential target substrate for SCF-Rca1. Rca1 mediated degradation of Dap might contribute to APC/C-Fzr inhibition, since CycE/Cdk2 activity is known to drive APC/C-Fzr inhibition (230). Thus, a hypothetical model can be established, in which Rca1 downregulates APC/C-Fzr activity by two independent inhibitory pathways. APC/C-Fzr inhibition occurs either directly by Rca1 based on its ZBR, or indirectly by SCF-Rca1 that stimulates activation of CycE/Cdk2 by targeting its inhibitor Dap for degradation (see Figure 32).

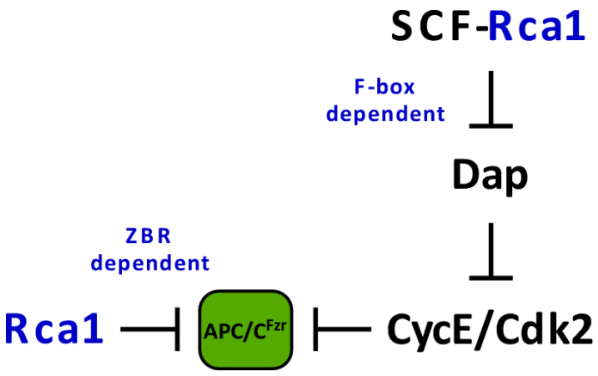

Figure 32 | Hypothetical model for dual APC/C-Fzr inhibition by Rca1
Rca1 (blue) inhibits APC/C-Fzr activity 1) directly ZBR dependent, and 2) indirectly F-box dependent as part of an SCF complex (SCF-Rca1) by targeting Dap for degradation, thereby releasing CycE/Cdk2 activity for APC/C-Fzr inhibition.

To test, whether Dap activity is negatively regulated by Rca1 in an F-box dependent manner, an *in vivo* APC/C activity assay based on *rca1* knock-down S2R+ cells was performed (see section 3.3.2). Different Rca1 constructs were analyzed for their ability to drive APC/C-Fzr inhibition in G2-phase (see section 3.3.3). Subsequently, the fold change of APC/C-Fzr inhibition was analyzed, when Dap activity was prevented by RNA interference (see section 3.3.4).

3.3.2 APC/C-Fzr activity is inhibited by Rca1 and does not depend on Dap

In vivo APC/C-Fzr activity assays were used to validate the hypothetical model, in which SCF-Rca1 stimulates APC/C-Fzr inhibition by targeting the CycE/Cdk2 inhibitor Dap for degradation (see Figure 32). This assay is based on the co-expression of a cell cycle inactive CycB construct that consists of the N-terminal part of CycB tagged with HA-NLS and followed by 2XGFP, HA-NLS-CycB-N285-2XGFP (CycB-N285-2XGFP), and a Cherry containing construct, HA-NLS-3XCherry (3XCherry). Both constructs are overexpressed in S2R+ cells by transient transfection. Overexpression of CycB-N285-2XGFP does not affect cell cycle progression, but is still recognized by APC/C for degradation. Thus, CycB-N285-2XGFP functions as sensor for APC/C activity and gets degraded during the cell cycle, when the APC/C is active. In contrast, 3XCherry is stable throughout the cell cycle and therefore serves as reference. Thus, cells positive for both GFP and Cherry possess an inactive APC/C, while cells only positive for Cherry, contain an active APC/C. By transient transfection, cells with different expression levels of the fluorescent constructs are produced. Consequently, APC/C activity can be quantified by the ratio GFP&Cherry / Cherry cells. Hence, the ratio and the level of APC/C activity are indirectly proportional to each other. This means, the higher the ratio, the lowe

r the level of APC/C activity, or the other way around, the lower the ratio, the higher the level of APC/C activity. The amount of GFP and Cherry positive cells is analyzed by flow cytometry. Furthermore, the DNA content, and by this the cell cycle stage, is determined by additional treatment of the cells with the DNA fluorophore Hoechst 33342.

Rca1 functions as inhibitor of APC/C-Fzr activity in G2-phase (230). To see, whether this can be detected in the APC/C activity assay, Rca1 expression was downregulated by using dsRNA that is complement against both the 5'- and 3'UTR region of *rca1* (*rca1-UTR*). In addition, to assess, whether APC/C-Fzr activity is influenced by Dap, Dap expression was downregulated as well, using dsRNA against the coding region of *dap* (*dap-CDS*). APC/C-Fzr activity in G2-phase was quantified by restricting the analysis to cells in G2-phase (see Figure 33A).

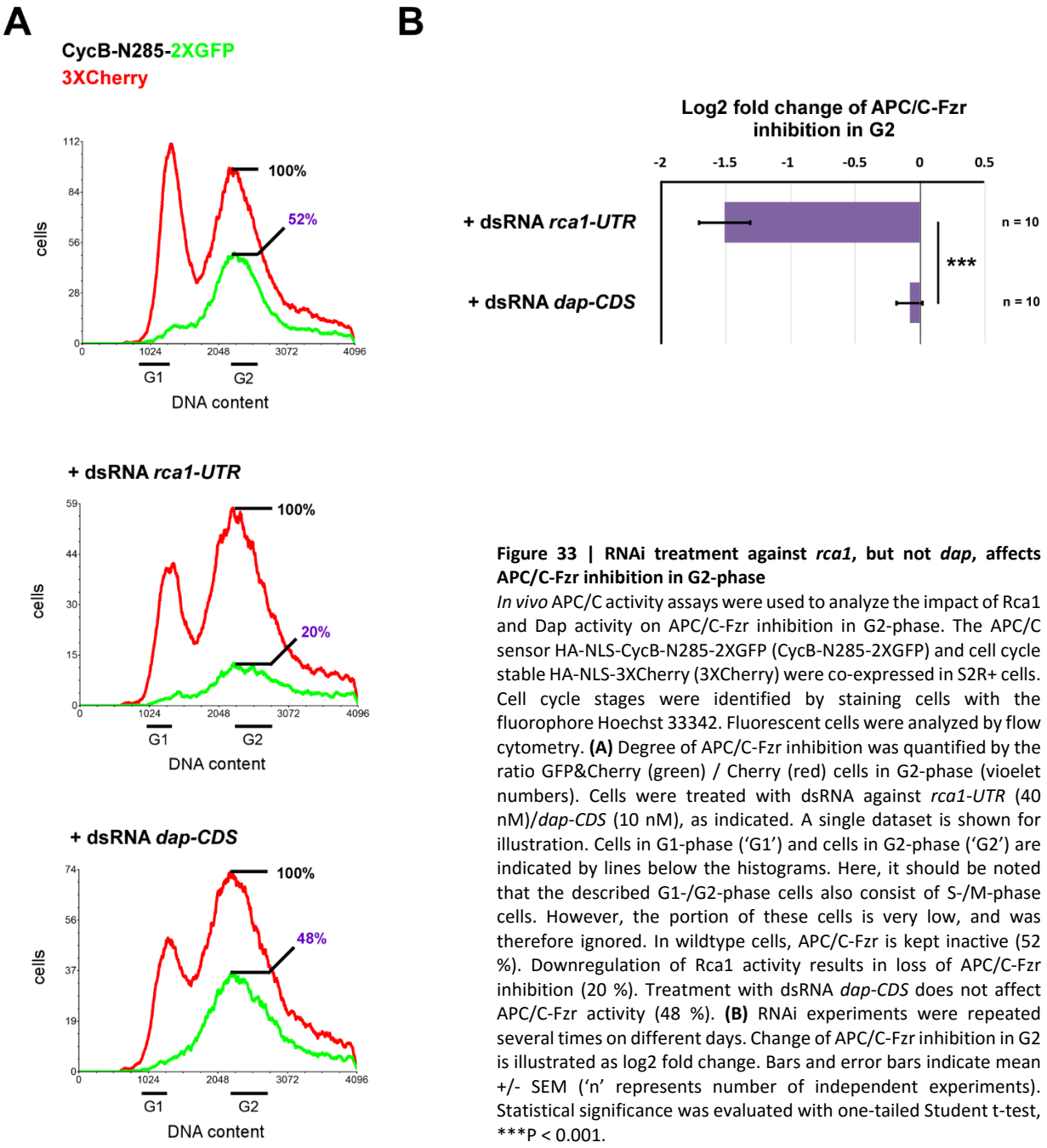

Figure 33 | RNAi treatment against *rca1*, but not *dap*, affects APC/C-Fzr inhibition in G2-phase

In vivo APC/C activity assays were used to analyze the impact of Rca1 and Dap activity on APC/C-Fzr inhibition in G2-phase. The APC/C sensor HA-NLS-CycB-N285-2XGFP (CycB-N285-2XGFP) and cell cycle stable HA-NLS-3XCherry (3XCherry) were co-expressed in S2R+ cells. Cell cycle stages were identified by staining cells with the fluorophore Hoechst 33342. Fluorescent cells were analyzed by flow cytometry. **(A)** Degree of APC/C-Fzr inhibition was quantified by the ratio GFP&Cherry (green) / Cherry (red) cells in G2-phase (vioelet numbers). Cells were treated with dsRNA against *rca1-UTR* (40 nM)/*dap-CDS* (10 nM), as indicated. A single dataset is shown for illustration. Cells in G1-phase ('G1') and cells in G2-phase ('G2') are indicated by lines below the histograms. Here, it should be noted that the described G1-/G2-phase cells also consist of S-/M-phase cells. However, the portion of these cells is very low, and was therefore ignored. In wildtype cells, APC/C-Fzr is kept inactive (52 %). Downregulation of Rca1 activity results in loss of APC/C-Fzr inhibition (20 %). Treatment with dsRNA *dap-CDS* does not affect APC/C-Fzr activity (48 %). **(B)** RNAi experiments were repeated several times on different days. Change of APC/C-Fzr inhibition in G2 is illustrated as log2 fold change. Bars and error bars indicate mean +/- SEM ('n' represents number of independent experiments). Statistical significance was evaluated with one-tailed Student t-test, ***P < 0.001.

Without dsRNA treatment, a high number of GFP-positive cells was present in G2-phase demonstrating that APC/C-Fzr was inactive during this cell cycle stage. This allowed the accumulation of CycB-N285-2XGFP. In contrast, during G1-phase, almost all cells were GFP-negative indicating that CycB-N285-2XGFP was targeted for degradation by active APC/C-Fzr. 3XCherry was not degraded, as seen by the presence of Cherry-positive cells during the whole cell cycle. Notably, the ratio of GFP&Cherry / Cherry cells in G2-phase was only 52 %, giving the expression that only half of the transfected cells was able to express the GFP-tagged CycB construct. However, technical issues prevented the detection of all GFP-positive cells, since Hoechst background signals that interfere with the GFP channel did not allow the identification of cells with low GFP fluorescence. Nevertheless, the assays showed the expected results, in which APC/C-Fzr is active during G1-phase and inhibited during G2-phase. Rca1 downregulation by *rca1-UTR* greatly reduced the ratio GFP&Cherry / Cherry cells (violet number) in G2-phase (from 52 % to 20 %) indicating that APC/C-Fzr activity was increased. In contrast, treatment with dsRNA against *dap-CDS* did not affect APC/C-Fzr inhibition (from 52 % to 48 %). Furthermore, both *rca1-UTR* and *dap-CDS* caused a cell cycle shift in G2-phase. This agrees previous *in vivo* studies, that have shown that Rca1 is essential for mitotic entry (230), while Dap is required to arrest cells in G1-phase (211, 212).

To check these findings for significance, the experiments were repeated several times on separate days (see Figure 33B). Here, it was important that each dataset contained a negative control, in which cells were only co-transfected with CycB-N285-2XGFP and 3XCherry. The fold change of APC/C-Fzr inhibition was calculated by dividing the ratio of treated GFP&Cherry / Cherry cells in G2-phase by the ratio of GFP&Cherry / Cherry cells in G2-phase of the negative control. The results were averaged and displayed as log2 values. Negative values mean a decrease, “0” no change, and positive values an increase in APC/C-Fzr inhibition. Several repetitions of the dsRNA experiments revealed the same result as observed for the single dataset. APC/C-Fzr inhibition was greatly lost upon *rca1-UTR*, whereas APC/C-Fzr activity was not changed, when cells were treated with dsRNA *dap-CDS*. The difference of the log2 fold change of APC/C-Fzr inhibition between these treatments was significant. This method for illustration of APC/C-Fzr inhibition was also used in following APC/C assays in this thesis.

Taken together, the APC/C activity assay was able to confirm the role of Rca1 as APC/C-Fzr inhibitor. When Rca1 expression was downregulated by dsRNA, APC/C-Fzr was in an active state. Interestingly, treating cells with dsRNA against *dap* did not influence APC/C-Fzr activity. This is in agreement with the idea that Dap is targeted for degradation by SCF-Rca1 during G2-phase to drive APC/C-Fzr inhibition (see Figure 32).

3.3.3 Rca1 requires both ZBR and F-box for efficient APC/C-Fzr inhibition

The ZBR region in Rca1 is absolutely required for APC/C-Fzr inhibition in G2-phase to allow entry into mitosis (230, 231, 235). *rca1* mutants that lack the F-box were not able to enter mitosis 16 (235, 236) suggesting that the F-box in Rca1 is also implicated in APC/C-Fzr inhibition. To elucidate the efficiency of the ZBR and F-box to drive APC/C-Fzr, Rca1 constructs mutated for the ZBR and/or F-box were overexpressed in S2R+ cells and tested for their ability to inhibit APC/C-Fzr activity (see Figure 34). To avoid background effects derived from endogenous Rca1, its expression was silenced by using dsRNA *rca1-UTR* that binds to the UTR regions in the *rca1* transcript. The protein level of the Rca1 constructs was not affected by this dsRNA, since their expression did not rely on *rca1-UTR* regions. The efficiency of these Rca1 constructs to stimulate APC/C-Fzr inhibition was assessed by *in vivo* APC/C activity assays.

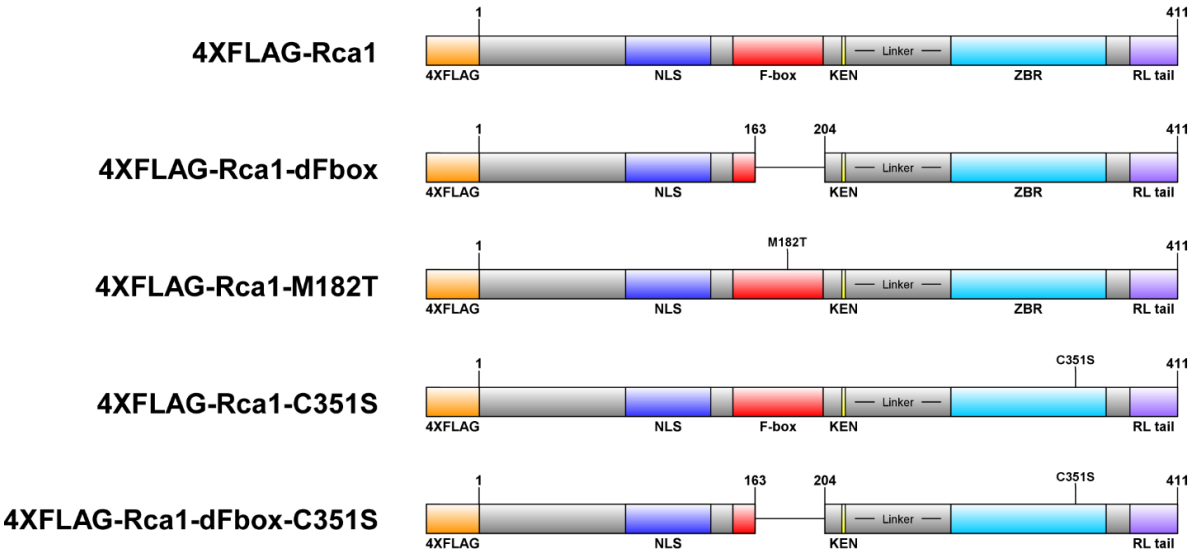

Figure 34 | 4XFLAG-tagged Rca1 constructs tested for their ability to inhibit APC/C-Fzr
Schematic presentation of 4XFLAG-tagged Rca1 constructs that were used to analyze their ability to drive APC/C-Fzr inhibition. F-box was either deleted (dFbox) or mutated by M182T. ZBR was disrupted by the internal single mutation C351S.

First, the requirement of the F-box was analyzed for APC/C-Fzr inhibition (see Figure 35). As already shown before (see Figure 33), downregulation of Rca1 activity by dsRNA *rca1-UTR* resulted in ectopically active APC/C-Fzr in G2-phase indicated by the low ratio of GFP&Cherry / Cherry cells at this cell cycle stage (12 %). Overexpression of 4XFLAG-Rca1 reduced APC/C-Fzr activity to a great extend (from 12 % to 47 %). The same level of APC/C-Fzr activity was detected in untreated cells (see Figure 33). Thus, full-length 4XFLAG-Rca1 could fully restore APC/C-Fzr inhibition in *rca1* mutant cells. In contrast, 4XFLAG-Rca1-dFbox lacking the F-box was only partially able to inhibit APC/C-Fzr activity (from 12 % to 28 %).

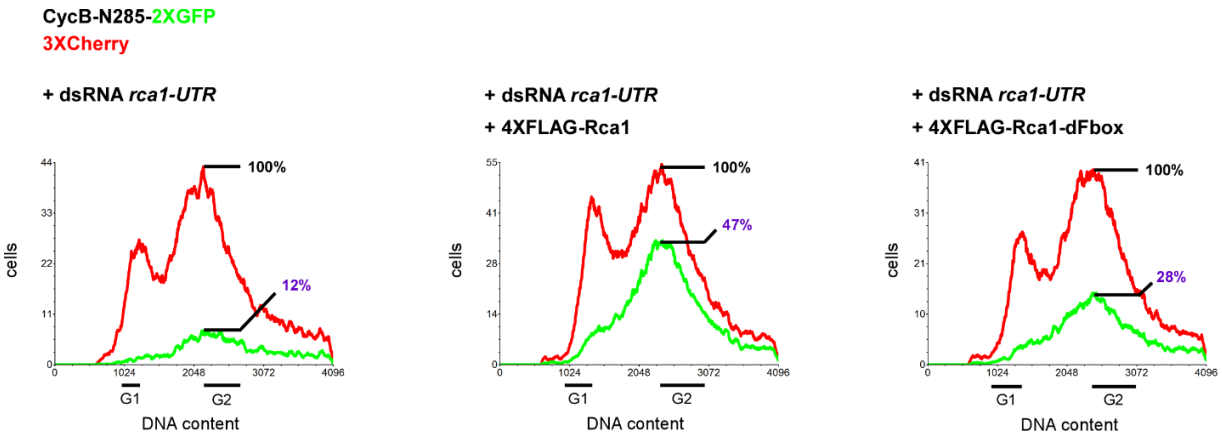

Figure 35 | F-box in Rca1 is required for efficient inhibition of APC/C-Fzr
In vivo APC/C activity assays were performed to analyze the function of the F-box in APC/C-Fzr inhibition in G2-phase. A single dataset for 4XFLAG-Rca1 and 4XFLAG-Rca1-dFbox is shown (see Figure 34). Endogenous Rca1 expression was downregulated by RNAi using dsRNA against *rca1-UTR* (40 nM). Cells in G1-phase ('G1') and cells in G2-phase ('G2') are indicated by lines below the histograms. Loss of APC/C-Fzr inhibition upon downregulation of endogenous Rca1 (12 %) can be restored by overexpression of 4XFLAG-Rca1 (47 %). In contrast, 4XFLAG-Rca1-dFbox that lacks the F-box was only partially able to complement the *rca1* mutant phenotype (28 %).

The remaining Rca1 constructs were subsequently analyzed for APC/C-Fzr inhibition. *In vivo* APC/C activity assays were repeated several times on different days to test the results for significance (see Figure 36).

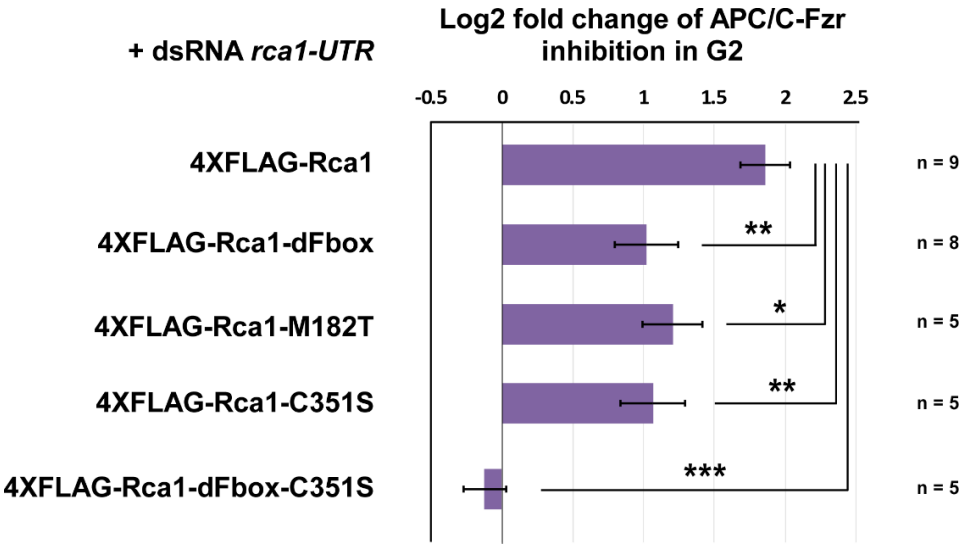

Figure 36 | Both F-box and ZBR in Rca1 contribute to APC/C-Fzr inhibition
In vivo APC/C activity assays were used to analyze several Rca1 constructs (see Figure 34) for APC/C-Fzr inhibition. Assays were performed as described in Figure 35. Experiments were repeated several times on different days. Change in APC/C-Fzr inhibition in G2 is illustrated as log2 fold change. 4XFLAG-Rca1-dFbox with an inactive F-box showed a reduced ability in APC/C-Fzr inhibition, compared to full-length 4XFLAG-Rca1. The same was observed for 4XFLAG-M182T, which carries a point mutation inside the F-box domain. Disruption of the ZBR by C351S in 4XFLAG-Rca1-C351S also exhibited only partial APC/C-Fzr inhibition. 4XFLAG-Rca1-dFbox-C351S that lacks both a ZBR and F-box completely failed to inhibit APC/C-Fzr activity. Thus, Rca1 requires both ZBR and F-box to mediate full APC/C-Fzr inhibition in G2-phase. Bars and error bars indicate mean +/- SEM ('n' represents number of independent experiments). Statistical significance was evaluated with one-tailed Student t-test, ***P < 0.001, **P < 0.01, *P < 0.05.

Loss of the F-box significantly reduced APC/C-Fzr inhibition in G2-phase when compared to full-length 4XFLAG-Rca1, which was almost twice as efficient in inhibiting APC/C-Fzr activity. The same was observed for 4XFLAG-Rca1-M182T that contains a point mutation inside the F-box region. Disruption of the ZBR by C351S in 4XFLAG-Rca1-C351S also reduced the ability to inhibit APC/C-Fzr activity. F-box and ZBR mutations failed to drive APC/C-Fzr inhibition to the same extend. Loss of both ZBR and F-box in 4XFLAG-Rca1-dFbox-C351S completely abolished the ability to inhibit APC/C-Fzr.

To exclude that different expression levels of the tested Rca1 constructs were responsible for the differences in APC/C-Fzr inhibition, expression plasmids encoding these constructs were transiently transfected into S2R+ cells. The gene for 3XCherry expression was additionally present on the same plasmid and served as reference. Upon expression, the constructs were analyzed for their stability by Western Blot (see Figure 37). Each 4XFLAG-tagged Rca1 construct was expressed. Using anti-Cherry antibodies a specific band could be detected in the transfected cells, but this band did not correspond to the size of 3XCherry (81 kDa). Instead, it more resembled the size of 2XCherry (54 kDa), which might have emerged by homologous recombination between the repeated cherry sequences in the *3Xcherry* gene. Nevertheless, since the band was specifically present in all transfected cells, but not in non-transfected cells, the protein level of this putative Cherry construct was used as reference. The integrated density (the product of area and mean gray value) was used to identify the amount of protein for the respective band.

To allow comparison of the expression level of the different Rca1 constructs, the protein level of each Rca1 construct was divided by the protein level of the co-expressed Cherry construct. The result was a value that described how much more of the Rca1 construct was expressed in comparison to the Cherry construct. Different values were obtained for some Rca1 constructs indicating that they do not obtain the same stability. Thus, the mutations have an impact on Rca1 stability. 4XFLAG-Rca1 (2.1) and 4XFLAG-Rca1-dFbox (2.6) were almost equally expressed. The remaining Rca1 constructs, 4XFLAG-Rca1-M182T (1.2), 4XFLAG-Rca1-C351S (1.5) and 4XFLAG-Rca1-dFbox-C351S (1.1) were equally expressed as well, but at a lower level. The APC/C activity assays have shown that Rca1 constructs that lack the F-box possess a reduced capability to inhibit APC/C-Fzr. Since the construct pairs 4XFLAG-Rca1/4XFLAG-Rca1-dFbox and 4xFLAG-Rca1-C3531S/4XFLAG-Rca1-dFbox-C351S did exhibit the same protein stability, it was concluded that their differences in driving APC/C-Fzr inhibition were due to the dFbox mutation and not caused by their different expression levels. However, the protein levels of 4XFLAG-Rca1-M182T and 4XFLAG-Rca1-C351S were too different from 4XFLAG-Rca1 to make the same conclusions for the mutations M182T and C351S. However, these constructs did still show good expression levels, which let assume that their mutations, and not their reduced expression, were the reason for the observed reduction in APC/C-Fzr inhibition. This is supported by the fact that overexpression of full-length 4XFLAG-Rca1 did not increase the level of APC/C-Fzr inhibition that was achieved by endogenous expressed Rca1 (compare Figure 35 with Figure 33). Thus, efficient APC/C-Fzr inhibition does not require huge amount of Rca1 protein levels, rather APC/C-Fzr inhibition depends on the functional domains in Rca1 such as F-box and ZBR.

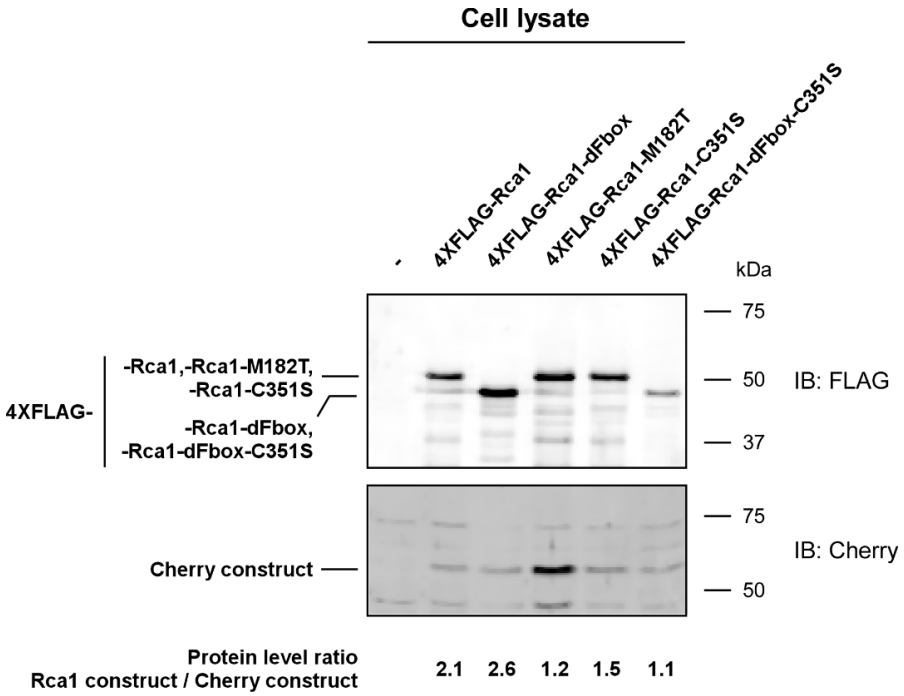

Figure 37 | Rca1 constructs tested for APC/C-Fzr inhibition differ in their expression levels
The Rca1 constructs that were employed for *in vivo* APC/C activity assays were co-expressed with 3XCherry in S2R+ cells. Each Rca1 construct was expressed. Notably, expression of 3XCherry (81 kDa) was not detected by using anti-Cherry antibodies. Instead, another Cherry construct which corresponds to the size of 2XCherry (54 kDa) was identified. The expression level of this Cherry construct was used as reference. The protein level of each construct was determined by the integrated density (the product of area and mean gray value) of the respective band. A protein level ratio was calculated by dividing the protein level of the Rca1 construct by the protein level of the co-expressed Cherry construct. The different protein level ratios indicate that the Rca1 constructs are differentially expressed. '-' represents non-transfected cells.

Summarized, the APC/C activity assays with the different Rca1 constructs have revealed that both ZBR and F-box contribute to efficient APC/C-Fzr inhibition in G2-phase. Functional loss of either of these domains dramatically reduces the ability of Rca1 to inhibit APC/C-Fzr.

3.3.4 Loss in APC/C-Fzr inhibition by F-box deficient Rca1 is restored by downregulation of Dap activity

According to the hypothetical model, the F-box functions as indirect APC/C-Fzr inhibitor by stimulating degradation of the CycE/Cdk2 inhibitor Dap (see Figure 32). Thus, the presence of Dap makes the F-box indispensable for efficient APC/C-Fzr inhibition. 4XFLAG-Rca1-dFbox lacking the F-box was only partially able to inhibit APC/C-Fzr activity, compared to full-length 4XFLAG-Rca1 (see Figure 35). To test, whether partial loss of APC/C-Fzr inhibition by 4XFLAG-Rca1-dFbox is due to failure to downregulate Dap activity, cells were treated with dsRNA *dap-CDS*. The change of APC/C-Fzr inhibition was subsequently analyzed by *in vivo* APC/C-Fzr activity assays. To exclude effects from endogenous Rca1, its expression was silenced by dsRNA *rca1-UTR*. APC/C-Fzr inhibition was not affected by dsRNA *dap-CDS*, when 4XFLAG-Rca1 was overexpressed (see Figure 38, from 47 % to 49 %).

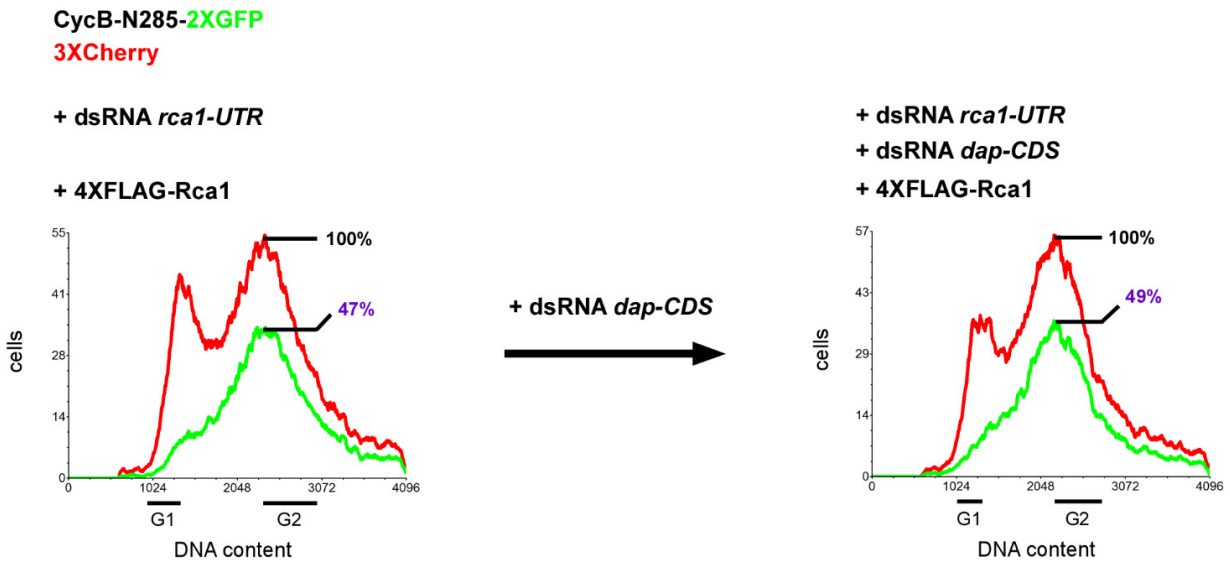

Figure 38 | Treatment with dsRNA against *dap* does not affect APC/C-Fzr inhibition by full-length Rca1
In vivo APC/C activity assays were performed to analyze, whether APC/C-Fzr inhibition by Rca1 is influenced by RNAi treatment against *dap*. Endogenous Rca1 expression was downregulated by RNAi using dsRNA against *rca1-UTR* (40 nM). As indicated, cells were treated with dsRNA against the coding region of *dap*, dsRNA *dap-CDS* (10 nM). Cells in G1-phase ('G1') and cells in G2-phase ('G2') are indicated by lines below the histograms. A single dataset is shown for illustration. APC/C-Fzr activity was not changed by dsRNA *dap-CDS*, when full-length 4XFLAG-Rca1 was overexpressed (without dsRNA *dap-CDS*: 47 %, after dsRNA *dap-CDS*: 49 %).

This was expected, since overexpression of 4XFLAG-Rca1 should allow the formation of active SCF-Rca1 complexes that stimulate Dap degradation during G2-phase, explaining why dsRNA *dap-CDS* did not show any effect. However, this was not expected for 4XFLAG-Rca1-dFbox that lacks the F-box, and therefore does not enable assembly of SCF-Rca1 complexes. When the F-box mediates APC/C-Fzr inhibition by downregulating Dap protein levels, it was assumed that APC/C-Fzr inhibition by 4XFLAG-Rca1-dFbox

should be increased by dsRNA *dap-CDS*. Indeed, APC/C-Fzr activity was reduced upon dsRNA *dap-CDS* treatment (see Figure 39, from 28 % to 35 %) indicating that the partial loss of APC/C-Fzr inhibition by lack of the F-box was rescued by downregulation of Dap activity.

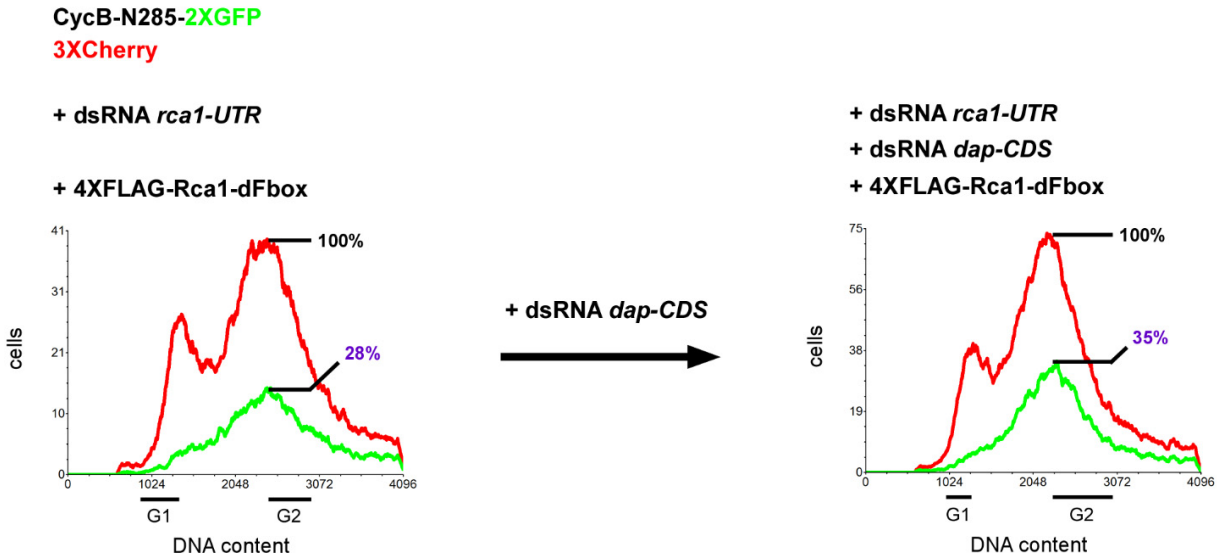

Figure 39 | Rca1 inhibits APC/C-Fzr activity by F-box dependent downregulation of Dap activity
In vivo APC/C activity assays were performed to analyze the functional F-box dependent interaction between *rca1* and *dap*. Endogenous Rca1 expression was downregulated by RNAi using dsRNA against *rca1-UTR* (40 nM). As indicated, cells were treated with dsRNA against the coding region of *dap*, dsRNA *dap-CDS* (10 nM). Cells in G1-phase ('G1') and cells in G2-phase ('G2') are indicated by lines below the histograms. Single datasets are shown for illustration. When 4XFLAG-Rca1-dFbox lacking the F-box was overexpressed, treatment with dsRNA *dap-CDS* increased APC/C-Fzr inhibition (without dsRNA *dap-CDS*: 28 %, after dsRNA *dap-CDS*: 35 %).

To confirm these results and the hypothetical model that F-box mediated degradation of Dap drives APC/C-Fzr inhibition, the same APC/C assays were conducted for all Rca1 mutants that showed deficits in APC/C-Fzr inhibition (see Figure 36). Repetition of the experiments confirmed the previous results that have shown that the F-box downregulates Dap activity to stimulate APC/C-Fzr inhibition (see Figure 40). When Rca1 constructs with an intact F-box were overexpressed, such as 4XFLAG-Rca1 and 4XFLAG-Rca1-C351S, APC/C-Fzr inhibition was not increased by dsRNA *dap-CDS*. However, when the F-box was deleted, an increase in APC/C-Fzr inhibition was observed. This was significant for 4XFLAG-Rca1/4XFLAG-Rca1-dFbox but not 4XFLAG-Rca1-C351S/4XFLAG-Rca1-dFbox-C351S. Here, it should be noted that the C351S mutated constructs displayed a high variation of the mean levels, which prevented a significant statement about their difference. The reason for this high variation is unclear, but seems to correlate with dsRNA *dap-CDS* treatment, since the variation by these constructs was reduced when dsRNA *dap-CDS* was not present (see Figure 36). Surprisingly, no change in APC/C-Fzr was detected for 4XFLAG-Rca1-M182T, which carries the single point mutation M182T within the F-box domain.

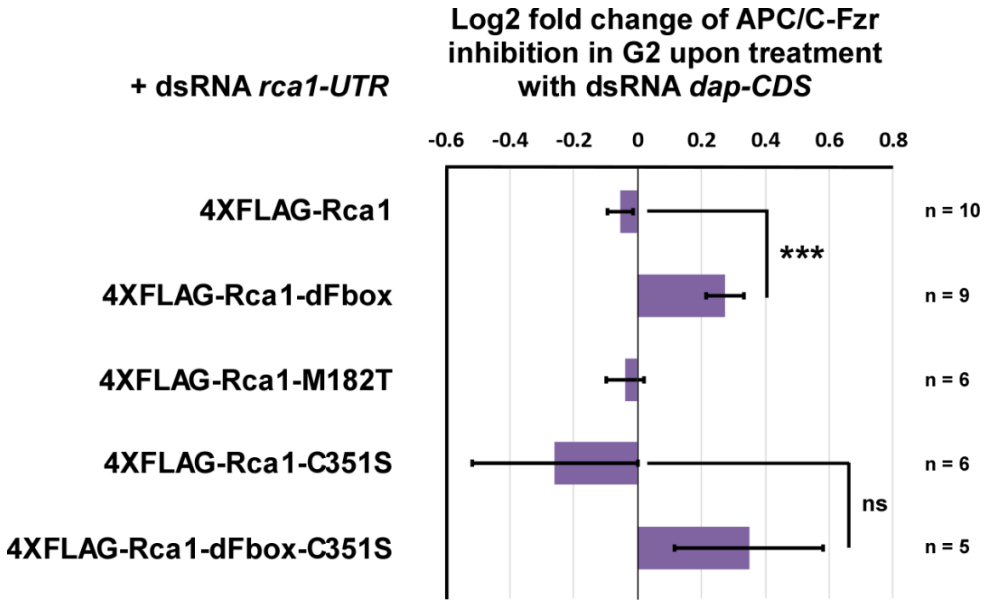

Figure 40 | F-box but not ZBR mediates APC/C-Fzr inhibition by downregulating Dap activity
In vivo APC/C activity assays were used to assess, which Rca1 constructs (see Figure 34) are rescued for APC/C-Fzr inhibition by RNAi treatment against *dap*. Assays were performed as described in Figure 39. Experiments were repeated several times on different days. Change of APC/C-Fzr inhibition in G2-phase upon dsRNA *dap-CDS* is illustrated as log2 fold change. dsRNA *dap-CDS* did not affect APC/C-Fzr inhibition, when full-length 4XFLAG-Rca1 was overexpressed. However, APC/C-Fzr inhibition was significantly increased when the F-box was eliminated (4XFLAG-Rca1-dFbox). Thus, the F-box downregulates Dap activity to stimulate APC/C-Fzr inhibition. APC/C-Fzr inhibition was not increased, when the ZBR region was disrupted by the point mutation C351S (4XFLAG-Rca1-C351S). Additional deletion of the F-box again increased APC/C-Fzr inhibition (4XFLAG-Rca1-dFbox-C351S), but here, the difference was not significant. Notably, APC/C-Fzr was not affected in presence of 4XFLAG-Rca1-M182T harboring a point mutation inside the F-box region. Bars and error bars indicate mean +/- SEM ('n' represents number of independent experiments). Statistical significance was evaluated with one-tailed Student t-test, ns: not significant, ***P < 0.001.

Summarized, the studies have revealed an F-box dependent genetic interaction between *rca1* and *dap*. The F-box mediates APC/C-Fzr inhibition by downregulating Dap activity. This fits the model, in which SCF-Rca1 indirectly inhibits APC/C-Fzr activity in G2-phase by targeting Dap for degradation (see Figure 32).

3.4 Protein stability analyses of potential SCF-Rca1 target substrates by flow cytometry

3.4.1 Aim

Mass spectrometric analyses have revealed that Rca1 is in complex with SCF components suggesting that Rca1 functions as part of an SCF complex to label specific substrates for degradation. In this context, the cell cycle regulators Dap and Skp2 were identified as potential target substrates for SCF-Rca1 (see section 3.1.2). To find more evidence for this, a flow cytometric method for the analysis of protein stability in S2R+ cells at distinct cell cycle stages was developed (see section 3.4.2). Using this method, cell cycle inactive GFP fluorescent Dap constructs were expressed and analyzed for their stability during cell cycle progression. A slight variation of the PIP-degron consensus sequence as well as a RXXL sequence were identified in Dap. The PIP-degron stimulates degradation during S-phase by CRL4-Cdt2 (207, 250), while the RXXL sequence is present in D-boxes that recruit substrates to APC/C for their destruction (126, 128, 252). The impact of these two sequence elements on Dap stability was assessed by deletions or mutations

of essential residues (see sections 3.4.3.1, 3.4.3.2 and 3.4.3.3). Next, it was analyzed whether Rca1 activity drives Dap degradation and whether this requires the F-box (see section 3.4.3.4). SCF target substrates are often recognized upon phosphorylation (170). Several Cdk phosphorylation sites are present in Dap. Therefore, the protein stability of Dap constructs was investigated when CycE/Cdk2 activity was increased (see section 3.4.3.5). A Dap mutant construct that lacks typical Cdk phosphorylation sites was analyzed as well (see section 3.4.3.7). The N-terminal region in Dap has been shown to be important for the interaction with Rca1 (see section 3.2.6). To analyze whether Rca1 binding is linked to Dap degradation, N-terminal truncated Dap constructs were analyzed for their stability (see section 3.4.3.8). Finally, degradation of Skp2 was assessed using GFP-labeled Skp2 (GFP-Skp2). Subsequently, the impact of CycE/Cdk2 and SCF-Rca1 activity on GFP-Skp2 stability was investigated (see section 3.4.4).

3.4.2 Method for analysis of protein stability by flow cytometry

In order to analyze the stabilities of proteins during the cell cycle, proteins were N-terminally fused with HA-NLS-GFP (GFP). Next, S2R+ cells were transiently transfected with an expression plasmid that encodes for the GFP-tagged construct to be analyzed. In addition, 3XCherry was expressed from the same plasmid. 3XCherry is stable throughout the cell cycle, and therefore served as reference for protein stability analyses. Cells were additionally treated with the DNA fluorophore Hoechst 33342 to analyze their DNA content, which gives information about their cell cycle stage. Fluorescent cells were analyzed by flow cytometry. The method applied for evaluation of protein stabilities including the preparation of the flow cytometric data is described in detail in this section. In general, the analysis of GFP-tagged constructs required cells expressing GFP alone and 3XCherry. (see Figure 41).

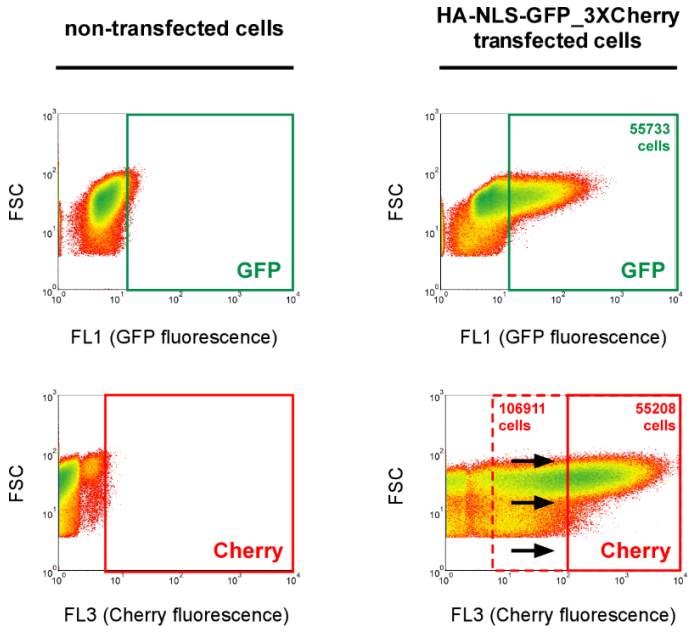

Figure 41 | Definition of fluorescent cells suitable for protein stability analyses in S2R+ cells
S2R+ cells were transiently transfected with an expression plasmid (HA-NLS-GFP_3XCherry) encoding for both HA-NLS-GFP (GFP) alone and 3XCherry. These cells were required to define the subpools of fluorescent cells that are suitable for protein stability analyses of GFP-tagged constructs. Flowcytometric data were evaluated using FCS Express (De Novo Software). Bivariate density plots (FCS versus FL1/FL3) for the GFP (FL1) and Cherry channel (FL3) are shown, respectively. The GFP gate (green rectangle) enables detection of cells expressing GFP. Background GFP signals, as seen in non-transfected cells, are excluded. The same accounts for the Cherry gate (red rectangle). Low Cherry signals were discarded by shrinking the gate (arrows) until the amount of Cherry cells was equally to the amount of GFP cells. Based on this setup of gates, protein stability of any GFP construct was analyzed. Number of gated GFP/Cherry cells are indicated in the gate. FCS: forward scatter.

These cells were necessary to define the pool of cells suitable for protein stability analyses. Non-transfected cells were used to identify GFP and Cherry positive cells. By this, more Cherry cells (106911) than GFP cells (55733) were detected. This was caused by the Hoechst fluorescence signals that interfere with the GFP channel during flow cytometry, and thereby prevented the identification of cells with low

GFP expression. It was assumed that low GFP expression correlates with low 3XCherry expression. Therefore, cells with low Cherry signals were ignored for analysis resulting in a pool of Cherry positive cells (55208) that contained the same number of cells as the pool of identified GFP positive cells. By restricting the analysis to these subpopulations of fluorescent cells, the amount of GFP and Cherry positive cells was equal during the whole cell cycle indicating that GFP alone possesses the same stability as 3XCherry (Figure 42A, first histogram).

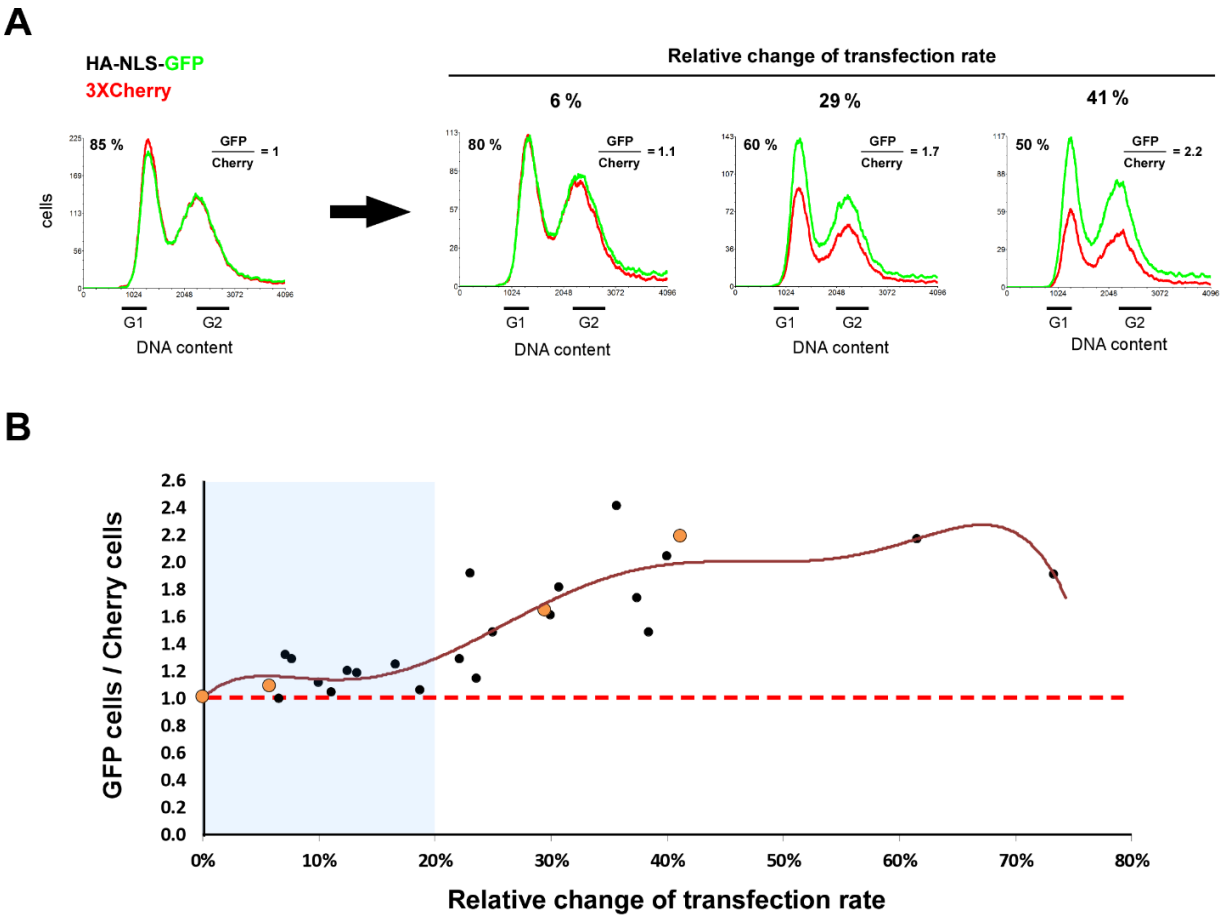

Figure 42 | Larger transfection rate differences influence protein stability analyses
The protein stability of HA-NLS-GFP (GFP) alone was calculated in S2R+ cells that differ in their transfection rates (TR). Different TRs were established by transiently transfecting cells with different amounts of the expression plasmid HA-NLS-GFP_3XCherry. **(A)** Histograms of transfected cells (GFP cells: green, Cherry cells: red) with different TRs (upper left corner) are illustrated. TRs were calculated by the ratio of Cherry cells / all cells. A single dataset is shown as example. Cells transfected with a TR of 85 % were used to define the subpopulation of fluorescent cells used for protein stability analyses (see Figure 41). Using 85 % as starting transfection rate, the calculated protein stability value increased with reduction of the TR (6 %: "1.1", 29 %: "1.7", 41 %: "2.2"). **(B)** Stability analyses of GFP alone in dependence of the TR, as described in (A), were repeated several times by using starting transfection rates between 85 % and 40 %. The relative change of the TR is plotted against the calculated protein stability value defined by the ratio GFP cells / Cherry cells (black points). Data points showing the result from (A) are highlighted (orange points). Protein stability values with the same relative change of the TR were averaged. When protein stability values do not rely on TRs, the protein stability value "1" is expected (red dashed line). Data were fitted to a polynomial regression function of order 6 with $R^2 = 0.753$ (dark red curve). When the relative change of the TR was reduced less than 20 % (blue region), GFP stability remained stable with little variation around "1.0". Reduction of the TR more than 20 % (white region) caused a high distribution of the calculated protein stability.

The protein stability was calculated by the ratio of GFP positive to Cherry positive cells, giving in the case of GFP alone the so called protein stability value “1”. The analysis of GFP-tagged constructs was based on transient transfection. Thus, cells with different expression levels were produced (cells obtain different amounts of plasmid DNA). Therefore, the amount of GFP positive cells was dependent on the stability of the GFP-tagged construct during cell cycle progression, and the protein stability value was interpreted as follows: The lower the value, the lower the stability of the GFP-tagged protein.

Transfection efficiencies can greatly vary depending on the expression plasmid. Thus, it was assessed, whether different transfection efficiencies may influence the analysis of protein stabilities. Cells were transfected with different amounts of the expression plasmid that encodes for GFP alone and 3XCherry. This resulted in a set of cells with different transfection rates (see Figure 42A). The transfection rate was calculated by the ratio of Cherry positive cells to all measured cells. In this dataset, cells with the highest transfection rate (85 %) were used to define the subpopulation of GFP and Cherry positive cells, as described in Figure 41. This gave the same amount of GFP and Cherry positive cells during the whole cell cycle, and therefore the protein stability value “1”. Next, the protein stability was calculated for the cells with lower transfection rates without redefinition of the cell subpopulations. While a low relative change of the transfection rate (6 %) did hardly change the calculated protein stability (“1.1”), a relative high relative change of the transfection rate (29 % and 41 %) resulted in a strong increase of the protein stability value (“1.7” and “2.2”). These analyses indicate that the calculated protein stability of GFP alone varies with great changes in the transfection rate making protein stability analyses not reliable when transfection rates are too different.

In order to reveal the range of transfection rates that still gives reliable results according to protein stabilities, several datasets including cells expressing GFP alone and 3XCherry with different transfection rates were analyzed (see Figure 42B). A relative change of the transfection rate up to 20 % did not greatly affect the protein stability. Most of the values of the calculated protein stabilities of GFP alone were between “1.0” and “1.2”. However, a relative change of the transfection rate of more than 20 % resulted in a strong distortion of the protein stability with reaching values of more than “2”. Generally, the more the transfection rate did differ, the higher the protein stability value did become. This analysis demonstrate that protein stabilities can not be analyzed and compared when the relative change of the transfection rate is more than 20 %.

Cells expressing GFP alone were used as reference for the analysis of the different GFP-tagged constructs in this thesis. To produce reliable results, the protein stability of a GFP-tagged construct was only calculated when the relative change of the transfection rate of the cells expressing the GFP-tagged construct and the cells expressing GFP alone was not greater than 20 %. To avoid discarding experiments due to their inapplicable transfection rate, cells that express GFP alone at different transfection rates were prepared in parallel. The GFP expressing cells with the slightest variation in the transfection rate were used as reference for the GFP construct to be analyzed.

For illustration, the protein stability of Dap was assessed by using the Dap construct GFP-Dap-dCDI (see Figure 44). The CDI domain was inactivated by mutations in and near the CDI domain (dCDI), which abolish the ability of the Dap construct to bind and inhibit CycE/Cdk2. Thus, overexpression of the Dap construct does not interfere with the cell cycle. As described above, cells expressing GFP alone with different transfection rates were prepared in parallel (not shown). Cells that were transfected with GFP alone with a transfection rate of 45 % (see Figure 43A, left histogram) were chosen as reference for the analysis of GFP-Dap-dCDI, whose transfection rate was 52 % (see Figure 43A, right histogram). This corresponds to a

relative transfection change of 13 %. Thus, the difference of the transfection rates between GFP alone and GFP-Dap-dCDI were in the acceptable range. Compared to GFP alone, the relative amount of GFP-Dap-dCDI expressing cells to Cherry expressing cells is strongly reduced throughout the cell cycle resulting in the protein stability value "0.3". Hence, Dap is destabilized during cell cycle progression. To make this result more reliable, the stability analysis of the Dap construct was repeated several times on different days (see Figure 43B). In general, the protein stability of the GFP-tagged constructs analyzed in this thesis were always compared to GFP alone. The fold change of protein stability was calculated for each dataset by dividing the protein stability value of the GFP construct by the protein stability value of GFP alone under the same condition. Different conditions were caused by overexpression of additional constructs such as HA-CycE and different versions of Rca1 or by treatment with dsRNA molecules. The calculated fold changes were averaged and displayed as log2 values. Negative values mean destabilization of the GFP construct, "0" means no change and positive values mean stabilization of the GFP construct (relative to GFP alone under the same condition). Notably, in case of protein stability analyses in which special conditions were not present, as with the protein stability analysis of GFP-Dap-dCDI (see Figure 43A, right histogram), the GFP reference, whose protein stability value is "1" (see Figure 43A, left histogram) was used for the calculation of the fold change. Thus, in such cases, the fold change equals the calculated protein stability value of the analyzed GFP construct. Repetition of the protein stability analysis of GFP-Dap-dCDI (see Figure 43B) confirmed the previous observation that this construct is greatly destabilized during the cell cycle. The Dap construct is even less than half as stable as GFP alone.

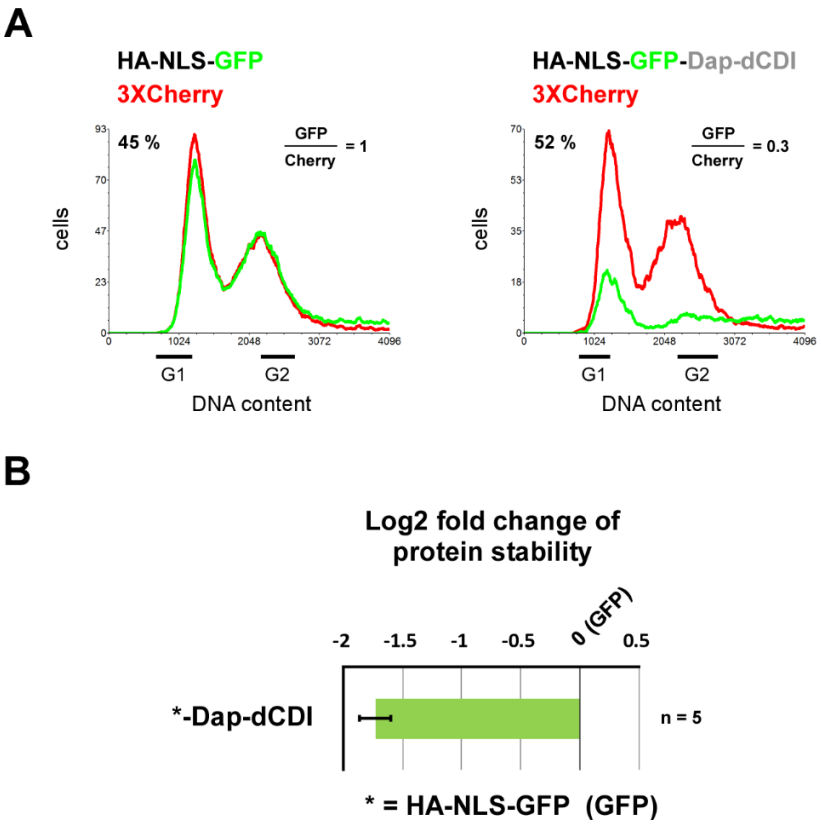

Figure 43 | Dap is unstable during the cell cycle
The protein stability of Dap was analyzed in S2R+ cells by using the cell cycle inactive Dap construct HA-NLS-GFP-Dap-dCDI (dCDI: deletion of the CycE/Cdk2 binding motif). **(A)** The pool of GFP and Cherry fluorescent cells used for analysis was defined by cells expressing HA-NLS-GFP (GFP) alone and 3XCherry, as described in Figure 41. For GFP-Dap-dCDI, the protein stability value was strongly reduced (0.3) indicating that Dap is unstable during cell cycle progression. **(B)** Stability analysis of GFP-Dap-dCDI was repeated several times on different days. Protein stability is presented as log2 fold change compared to GFP alone. Bars and error bars indicate mean +/- SEM ('n' represents number of independent experiments).

In summary, it can be stated that a method allowing the analysis of protein stabilities during the cell cycle was successfully established. Using this method, it was shown that Dap is extremely unstable during the

cell cycle suggesting that one or more efficient degradation pathways act on Dap. In the following sections, different potential degradation motifs in Dap were investigated in detail to reveal the mechanisms that drive downregulation of Dap stability. Furthermore, the established method was also used to find more evidence that Dap is a target substrate of an SCF-Rca1 complex.

3.4.3 Analysis of Dap stability

3.4.3.1 PIP-degron mutations result in Dap stabilization

The protein stability analysis of GFP-Dap-dCDI has shown that Dap is unstable during the whole cell cycle (see Figure 43A). Strikingly, destabilization of Dap occurs especially after G1-phase suggesting that Dap is degraded during the upcoming cell cycle stages including S- and G2-phase. Indeed, Dap contains a PIP-degron that is known to promote degradation during S-phase. Proteins containing a PIP-degron are CRL4-Cdt2 target substrates (207, 250). These substrates bind chromatin-bound PCNA during S-phase via their PIP-degron with high affinity, thereby creating a combined interaction interface for recruitment of CRL4-Cdt2 (207, 208, 250). PIP-degrons share the consensus sequence Q-x-x-Ψ-T-D-ϑ-ϑ-x-x-x-B, in which Ψ stands for a hydrophobic residue (I/L/M/V), ϑ stands for an aromatic residue (Y/F) and B is a basic residue (K/R). The basic residue at the end of the PIP-degron is essential for recognition by CRL4-Cdt2 (207, 250). Such a PIP degron sequence can be found in Dap with minor changes (see Figure 27A): Q-P-K-I-T-**E**-F-**M**-K-E-R-K (residues in bold do not fit the consensus sequence). To test, whether this sequence functions as PIP-degron that is responsible for Dap instability, GFP-tagged Dap constructs harboring different PIP-degron mutations (see Figure 44) were analyzed for stability in S2R+ cells by flow cytometry.

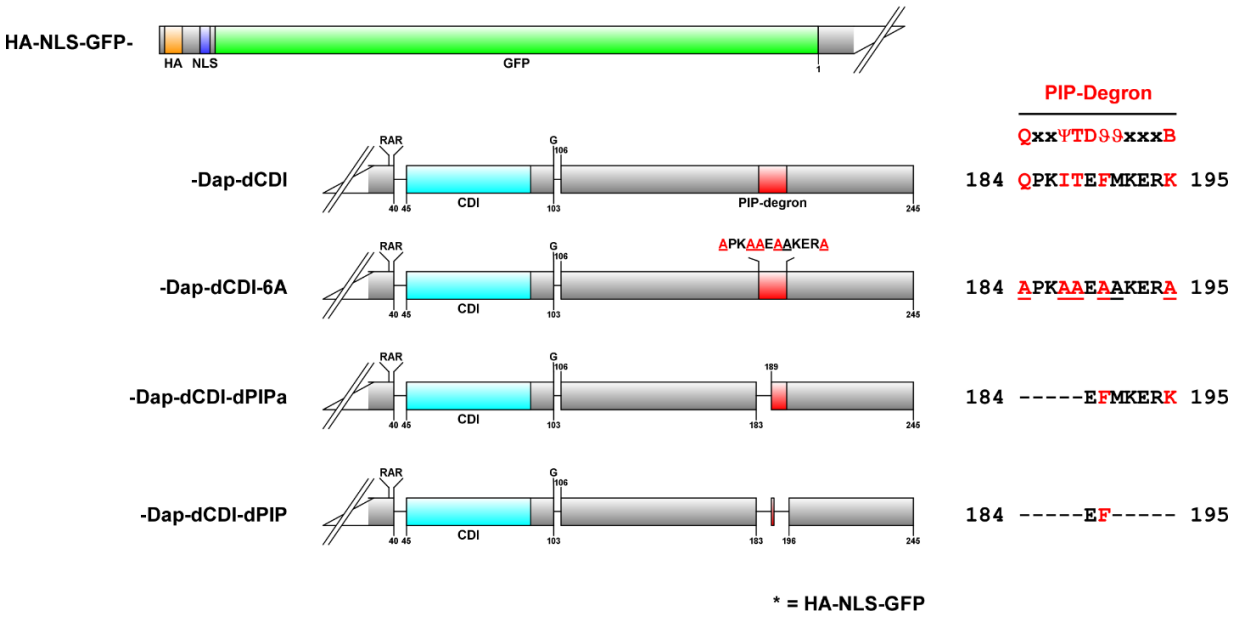

Figure 44 | PIP-degron mutated Dap constructs used for protein stability analyses
Schematic presentation of PIP-degron mutated GFP-tagged Dap constructs that were analyzed for their protein stability in S2R+ cells (see Figure 45, Figure 46). All constructs harbor deletions inside and near the CDI domain (dCDI), which prevents binding and inhibition of CycE/Cdk2. Essential residues in the PIP-degron consensus sequence (Q-x-x-Ψ-T-D-ϑ-ϑ-x-x-x-B, Ψ = I/L/M/V, ϑ = Y/F, B = K/R) are highlighted (red residues). In GFP-Dap-dCDI-6A, essential residues in the PIP-degron are mutated to alanine (underlined residues). In GFP-Dap-dCDI-dPIPa, the N-terminal part of the PIP-degron is missing, whereas GFP-Dap-dCDI-dPIP additionally lacks the C-terminal part. The deletions made for GFP-Dap-dCDI-dPIP are regarded as complete loss of the PIP-degron.

As illustration, the protein stability analysis of GFP-Dap-dCDI-dPIPa that lacks the N-terminal part of the PIP-degron is shown in more detail (see Figure 45).

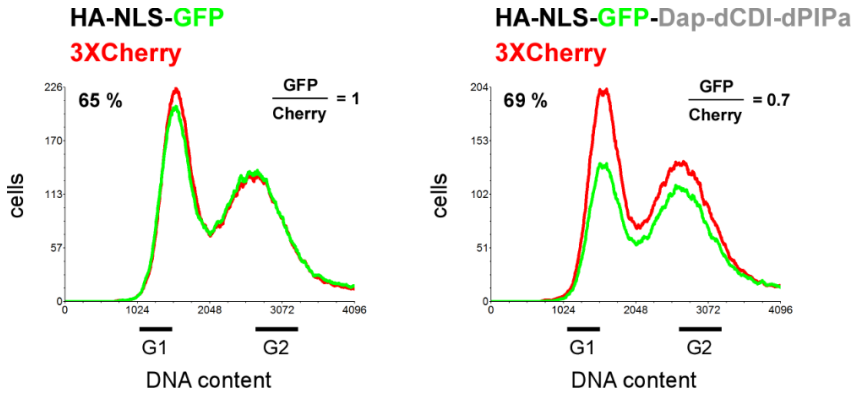

Figure 45 | Protein stability analysis of GFP-Dap-dCDI-dPIPa
As an example, a single dataset for the protein stability analysis of GFP-Dap-dCDI-dPIPa is shown. Histogram illustrates GFP (green) and Cherry (red) fluorescent cells. Compared to GFP alone, GFP-Dap-dCDI-dPIPa was more destabilized during the cell cycle. The protein stability value was decreased from "1" to "0.7".

GFP-Dap-dCDI-dPIPa was measured with the protein stability value "0.7". In contrast, GFP-Dap-dCDI that contains the PIP-degron was much more unstable, as indicated by the protein stability value "0.3" (see Figure 43A). Thus, N-terminal deletion of the PIP-degron stabilizes Dap, but does not completely abolish Dap instability during the cell cycle. The difference between the protein stability of GFP-Dap-dCDI-dPIPa and GFP-Dap-dCDI is significant, as revealed by repeated analyses (see Figure 46A). The same was observed for GFP-Dap-dCDI-6A, in which essential PIP-degron residues are mutated to alanine. Strikingly, deletion of the complete PIP-degron, as in GFP-Dap-dCDI-dPIP, resulted in full stabilization indicating that the C-terminal part of the PIP-degron contributes to Dap degradation. Compared to GFP-Dap-dCDI-dPIPa, this stabilization was significant. To analyze, whether the calculated protein stabilities by flow cytometry are reliable, a dataset of the different Dap constructs was additionally analyzed by Western Blot (Figure 46B). The Western Blot confirmed the flow cytometric results. GFP-Dap-dCDI is more unstable than GFP-Dap-dCDI-dPIPa, which is in turn more unstable than GFP-Dap-dCDI-dPIP.

Altogether, the stabilization of the Dap constructs by different PIP-degron mutations indicate that Dap carries a functional PIP-degron, although it does not completely fit the consensus sequence. PIP-degron containing proteins are known to recruit the E3 ligase CRL4-Cdt2 for degradation during S-phase. Deletion of the N-terminal part of the PIP-degron, as well as mutations of essential residues of the PIP-degron consensus sequence greatly stabilized Dap. Thus, the protein stability analyses demonstrate that CRL4-Cdt2 targets Dap for degradation during S-phase. However, the fact that deletion of the complete PIP-degron completely stabilized the Dap construct let suggest that either part of the PIP-degron is still functional or, more likely, that CRL4-Cdt2 is not the only E3 ligase that mediates Dap degradation.

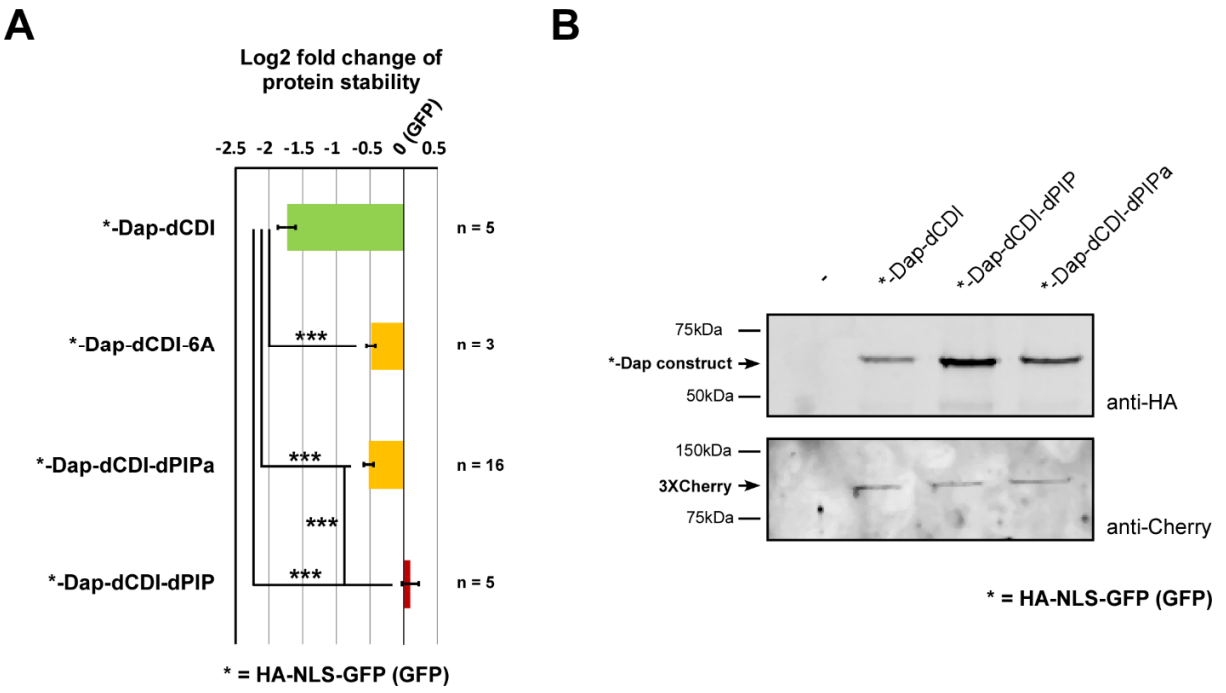

Figure 46 | PIP-degron mutations stabilize Dap
The protein stability of different GFP-tagged Dap constructs harboring PIP-degron mutations (see Figure 44) was studied in S2R+ cells. **(A)** The protein stability of the PIP-degron mutant Dap constructs was analyzed several times. GFP-Dap-dCDI showed strong destabilization. Compared to GFP-Dap-dCDI, both GFP-Dap-dCDI-6A and GFP-Dap-dCDI-dPIPa were significantly destabilized and still revealed some instability. Ultimate stabilization was reached by complete deletion of the PIP-degron, as in GFP-Dap-dCDI-dPIP. Color represent relative protein stability: very unstable (green), unstable (yellow) and stable (red). Bars and error bars indicate mean +/- SEM ('n' represents number of independent experiments). Statistical significance was evaluated with one-tailed Student t-test, ***P < 0.001. **(B)** Protein stability results from (A) were verified by Western Blot. Each lane contains whole cell extracts. Protein levels of HA-NLS-GFP-tagged Dap constructs and 3XCherry were detected by anti-HA or anti-Cherry antibodies, as indicated. 3XCherry served as reference. As described in (A), following order of stabilization was detected: GFP-Dap-dCDI-dPIP > GFP-Dap-dCDI-dPIPa > GFP-Dap-dCDI.

3.4.3.2 N-terminal PIP-degron deletion (dPIPa) is sufficient for inactivation of the PIP-degron

N-terminal deletion of the PIP-degron resulted in great stabilization of GFP-Dap-dCDI. Full stabilization was achieved when the PIP-degron was completely deleted (see Figure 46). This lead to the question, whether the C-terminal part of the PIP-degron is still able to function as a weak PIP-degron, or whether another degradation mechanism requires the C-terminal PIP-degron to drive Dap degradation. PIP-degron proteins recruit CRL4-Cdt2 for degradation during S-phase (207, 250). Thus, loss of CRL4-Cdt2 activity should stabilize Dap. To test this assumption, the stability of GFP-Dap-dCDI possessing a functional PIP-degron was analyzed in S2R+ cells upon downregulation of CRL4-Cdt2 activity (see Figure 47A). This was achieved by decreasing protein levels of the CRL4-Cdt2 scaffold protein Cul4 by using dsRNA against exon 10 in *cul4* (*cul4-Ex10*).

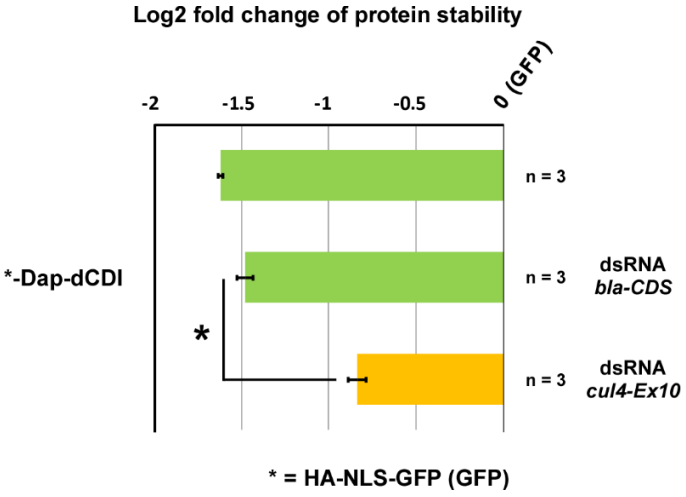

Figure 47 | Dap is stabilized upon downregulation of CRL4-Cdt2 activity
Protein stability of GFP-Dap-dCDI (see Figure 44) was analyzed upon downregulation of CRL4-Cdt2 activity, which was achieved by treatment with dsRNA dsRNA *cul4-Ex10* (40 nM). As control, *bla-CDS* (40 nM) was used. Addition of dsRNA *bla-CDS* did not show any effect, whereas dsRNA *cul4-Ex10* significantly stabilized GFP-Dap-dCDI. Color represent relative protein stability: very unstable (green) and unstable (yellow). Bars and error bars indicate mean +/- SEM ('n' represents number of independent experiments). Statistical significance was evaluated with one-tailed Student t-test, *P < 0.05.

As expected, GFP-Dap-dCDI levels were increased when cells were treated with dsRNA *cul4-Ex10*. This was not the case upon treatment with dsRNA against the coding sequence of the *beta-lactamase* gene, which was used as negative control. Thus, Dap is destabilized by CRL4-Cdt2. Next, GFP-Dap-dCDI-dPIPa lacking the N-terminal part of the PIP-degron was analyzed upon downregulation of CRL4-Cdt2 activity (see Figure 48). Here, no stabilization was observed, in contrast, protein levels were even further reduced. Treating cells with dsRNA *bla-CDS* did not affect the stability of GFP-Dap-dCDI-dPIPa. Since recognition by CRL4-Cdt2 requires a functional PIP-degron, this experiment indicates that N-terminal deletion of the PIP-degron is sufficient for its inactivation.

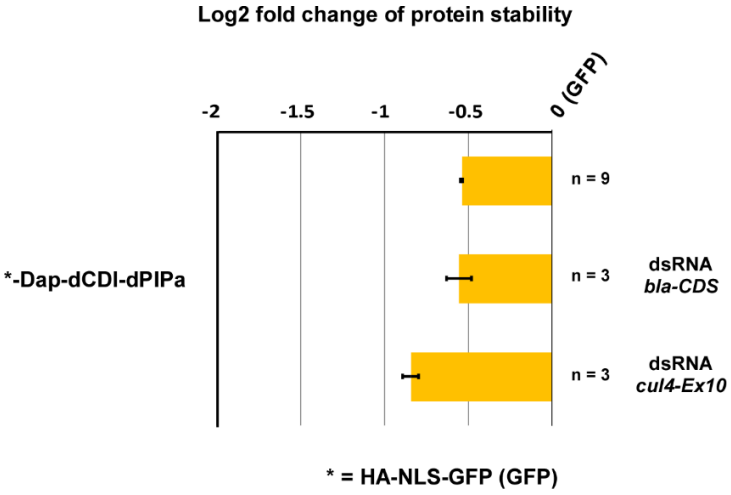

Figure 48 | N-terminal deletion of the PIP-degron in Dap eliminates CRL4-Cdt2 mediated degradation
As described in Figure 47, the same was performed for GFP-Dap-dCDI-dPIPa that lacks the N-terminal part of the PIP-degron (see Figure 44). The protein stability of GFP-Dap-dCDI-dPIPa was not increased upon treatment with dsRNA *cul4-Ex10* and not affected by dsRNA *bla-CDS*. Bars and error bars indicate mean +/- SEM ('n' represents number of independent experiments).

Taken together, these data demonstrate that full stabilization of GFP-Dap-dCDI-dPIP that lacks the complete PIP-degron (see Figure 46) was not caused by further inactivation of CRL4-Cdt2. Rather this was likely due to loss of another degradation mechanism that acts on Dap.

3.4.3.3 Mutation of the RXXL sequence stabilizes Dap

The RXXL sequence is a core sequence within the D-box that is often found in APC/C substrates (126). Crystallographic structural studies have shown that the RXXL sequence interacts with specific sides on the

APC/C co-activator Cdc20/Fzy and Cdh1/Fzr to recruit target substrates for ubiquitination and subsequent degradation (126, 128, 252). A RXXL sequence that overlaps with the C-terminal part of the PIP-degron is present in Dap with the sequence RKRL. Thus, Dap might be targeted for degradation by APC/C-Fzy or APC-Fzr during cell cycle progression. To test this assumption, GFP-tagged Dap mutants that carry a mutated RXXL sequence were analyzed for their stability in S2R+ cells by flow cytometry (Figure 49A).

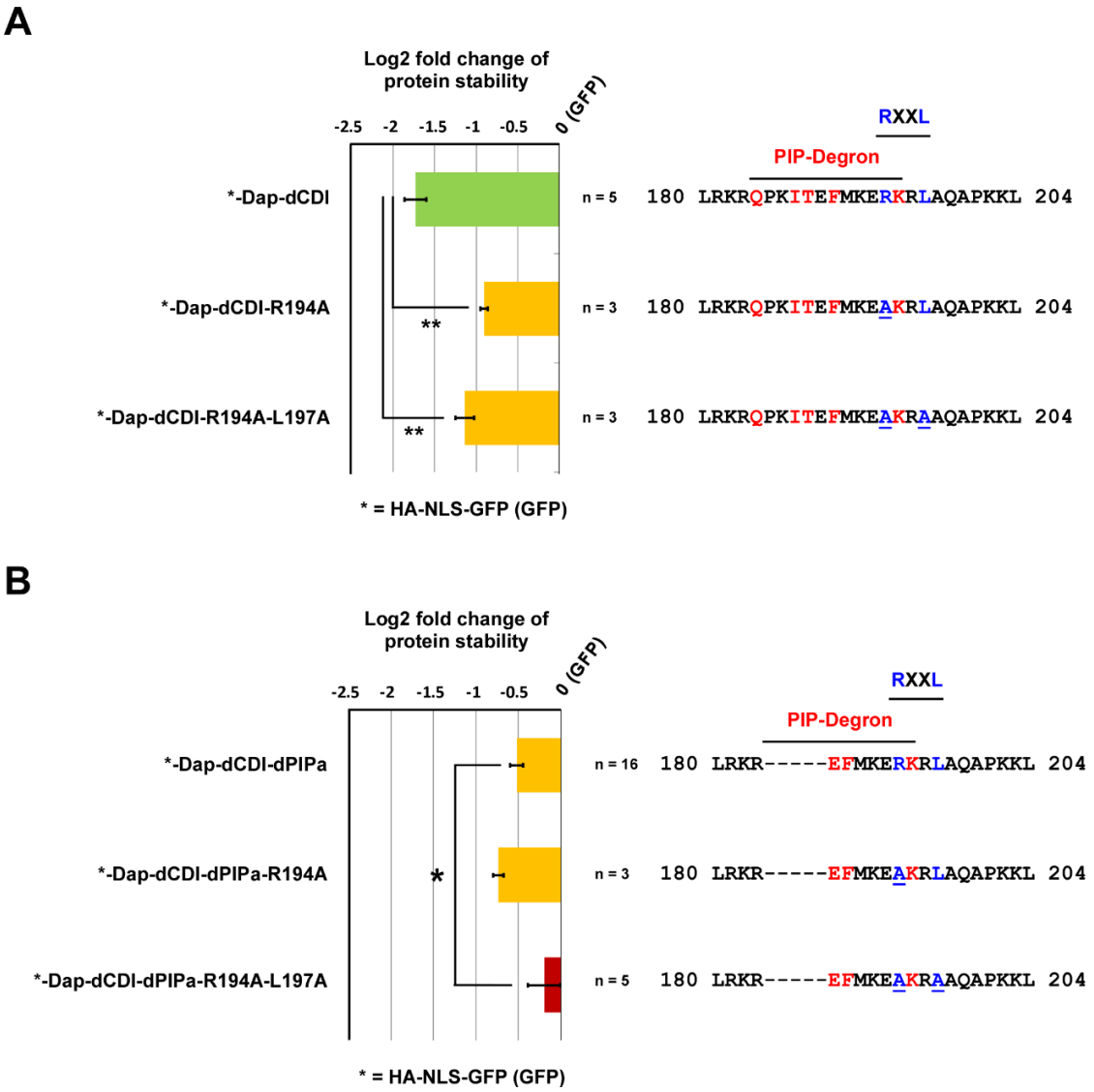

Figure 49 | The RXXL sequence in Dap does not mediate instability as part of a D-box
RXXL mutated Dap constructs were analyzed for their stability in S2R+ cells. A RXXL sequence overlaps with the C-terminal part of the PIP-degron. Essential residues are highlighted (PIP-degron: red, RXXL sequence: blue). The RXXL sequence was either mutated by AXXL (R194A) or AXXA (R194A-L197A), as indicated (underlined residues). **(A)** The protein stability of GFP-Dap-dCDI-R194A and GFP-Dap-dCDI-R194A-L197A was analyzed. Both mutations significantly stabilized the Dap construct. **(B)** The same RXXL mutations were analyzed for GFP-Dap-dCDI-dPIPa that lacks S-phase dependent degradation due to N-terminal deletion of the PIP-degron (see section 3.4.3.2). Here, only the double mutation R194A-L197A was able to significantly stabilize the Dap construct, but not the single mutation R194A. Color represent relative protein stability: very unstable (green), unstable (yellow) and stable (red). Bars and error bars indicate mean +/- SEM ('n' represents number of independent experiments). Statistical significance was evaluated with one-tailed Student t-test, **P < 0.01, *P < 0.05.

The RXXL sequence was either mutated by changing arginine to alanine (AKRL), or by replacing both essential residues, arginine and leucine to alanine (AKRA). Both GFP-Dap-dCDI-R194A and GFP-Dap-dCDI-R194A-L197A revealed a significant stabilization, when compared to GFP-Dap-dCDI suggesting that the RXXL sequence functions as a degradation signal. However, since the RXXL sequence overlaps with the PIP-degron, it was uncertain whether the RXXL mutations result in a non-functional PIP-degron, albeit essential residues of the PIP-degron consensus are not affected. Therefore, the RXXL mutations were additionally analyzed for GFP-Dap-dCDI-dPIPa (see Figure 49B), which harbors a non-functional PIP-degron due to deletion of its N-terminal part (Figure 44). This Dap construct is not destabilized by CRL4-Cdt2 during S-phase, and thus, it is more qualified for the analysis of alternative degradation pathways. When the RXXL sequence confers instability, it was expected that both RXXL mutations result in stabilization of the Dap construct. Interestingly, the double mutant GFP-Dap-dCDI-dPIPa-R194A-L197A, but not the single mutant GFP-Dap-dCDI-dPIPa-R194A was stabilized. Since the R194A mutation stabilized GFP-Dap-dCDI harboring a functional PIP-degron and since R194 is within the PIP-degron, it was concluded that the residue R194 is important to promote ubiquitination by CRL4-Cdt2, even though the nature of the residue at this position is not strictly prescribed in the PIP-degron consensus sequence. Thus, the RXXL sequence in Dap does not function as part of a D-box that stimulates degradation by recruiting substrates to co-activator bound APC/C complexes. To find further evidence that the RXXL sequence does not promote APC/C mediated degradation, the protein stability of GFP-Dap-dCDI-dPIPa was investigated, when APC/C-Fzr activity was increased by overexpression of 4XFLAG-Fzr (Figure 50). This did not affect the stability of the Dap construct indicating that Dap is not an APC/C-Fzr target substrate. Since Cdh1 recognize the same substrates as Cdc20 (115, 251), it was assumed that Dap is also not a target substrate of APC/C-Fzy.

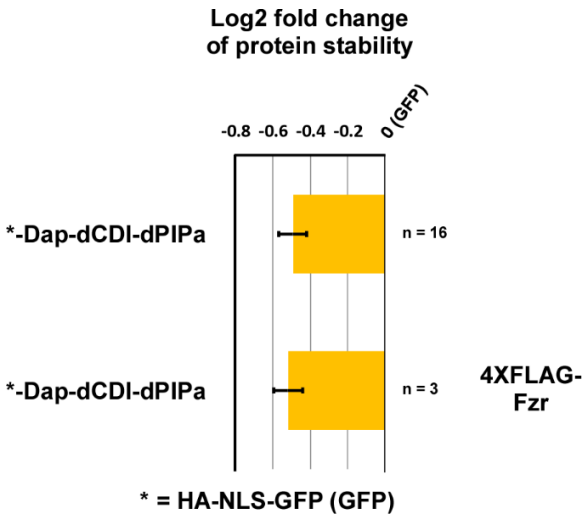

Figure 50 | APC/C-Fzr activity does not stimulate Dap degradation
Protein stability of Dap-dCDI-dPIPa was analyzed in S2R+ cells under increased APC/C-Fzr activity by overexpression of 4XFLAG-Fzr. Dap-dCDI-dPIPa protein levels were not affected by 4XFLAG-Fzr indicating that Dap is not an APC/C-Fzr target substrate. Bars and error bars indicate mean +/- SEM ('n' represents number of independent experiments).

Summarized, the protein stability analyses of the different RXXL mutated Dap constructs have shown that the RXXL sequence does not mediate degradation as part of a D-box. The single mutation of the arginine residue in the RXXL sequence stabilized the Dap construct, however, this was likely caused by elimination of the PIP-degron because of following facts. First, the arginine residue is part of the PIP-degron sequence and second, its mutation to alanine did not affect the stability of the Dap construct, when the N-terminal part of the PIP-degron, which is essential for the functionality of the PIP-degron, was deleted. The fact that both mutations together, R194A and L197A, resulted in stabilization of GFP-Dap-dCDI-dPIPa suggests that

L197 is required to stimulate degradation by a pathway that does not involve the E3 ligase CRL4-Cdt2. Single mutations of this residue are required to analyze this assumption in more detail.

3.4.3.4 Dap is destabilized by Rca1 in an F-box dependent manner

Several interactions studies give evidence that Rca1 is an F-box protein that functions as part of an SCF complex to target Dap for degradation (see section 3.1 and 3.2). To test, whether the protein level of Dap is controlled by Rca1, the stability of GFP-Dap-dCDI was analyzed in S2R+ cells by flow cytometry when Rca1 activity was increased by overexpression of 4XFLAG-Rca1 (see Figure 51A). GFP-Dap-dCDI was destabilized in presence of overexpressed 4XFLAG-Rca1. This was not the case when the F-box was deleted, as in 4XFLAG-Rca1-dFbox or 4XFLAG-Rca1-dFbox-full (see Figure 34 for illustration of the Rca1 constructs). The same was observed when GFP-Dap-dCDI-dPIPa was used for analysis instead (see Figure 51B). This Dap construct lacks the N-terminal part of the PIP-degron, and therefore is not targeted for degradation by CRL4-Cdt2 (see section 3.4.3.2).

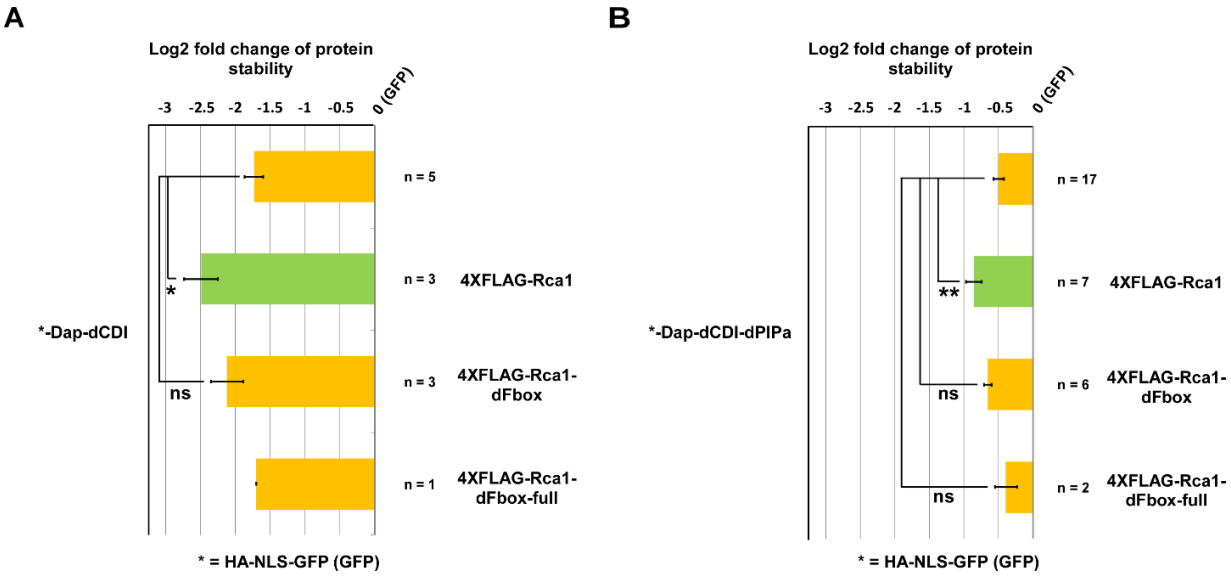

Figure 51 | In addition to CRL4-Cdt2, Rca1 downregulates Dap protein levels in an F-box dependent manner
The protein stability of GFP-tagged Dap constructs was studied in S2R+ cells upon down- or upregulation of Rca1 activity. Rca1 activity was increased by overexpression of 4XFLAG-Rca1. **(A)** GFP-Dap-dCDI was significantly destabilized by overexpression of 4XFLAG-Rca1. In contrast, overexpression of 4XFLAG-Rca1-dFbox and 4XFLAG-Rca1-dFbox-full, both lacking the F-box (for illustration see Figure 34) did not affect protein stability. **(B)** The same, as described in (A) was observed for GFP-Dap-dCDI-dPIPa that carries a non-functional PIP-degron, and therefore is not targeted for degradation by CRL4-Cdt2. Thus, Rca1 downregulates Dap protein levels independent of CRL4-Cdt2. Color represent relative protein stability: very unstable (green) and unstable (yellow). Bars and error bars indicate mean +/- SEM ('n' represents number of independent experiments). Statistical significance was evaluated with one-tailed Student t-test, *P < 0.05, ns: not significant.

Next, the Rca1 protein level was downregulated by treating cells with dsRNA either against the UTR regions of *rca1*, using dsRNA *rca1-UTR*, or against its coding region, using dsRNA *rca1-CDS* (see Figure 52).

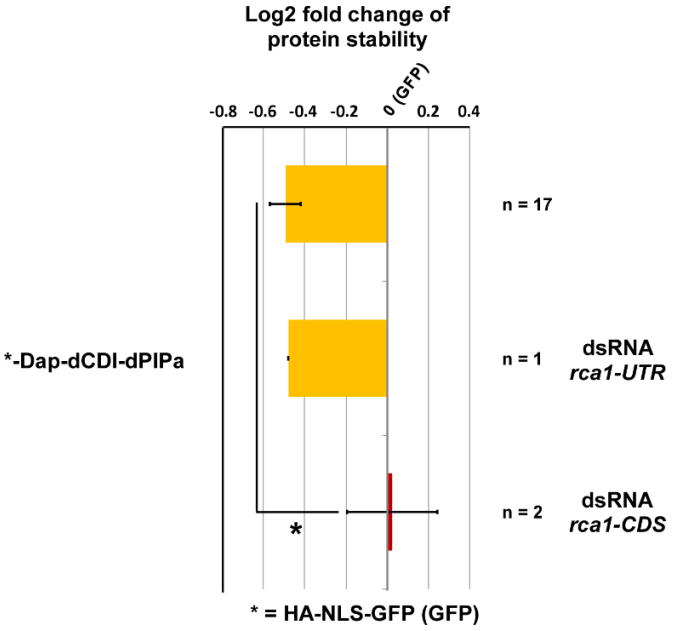

Figure 52 | Downregulation of Rca1 activity stabilizes Dap
The protein stability of GFP-Dap-dPIPa was analyzed upon downregulation of Rca1 activity. This was achieved by treating cells with dsRNA either against the UTR region of *rca1* (*rca1-UTR*, 40 nM) or against its coding region (*rca1-CDS*, 5 nM). Dap protein levels were not affected by dsRNA *rca1-UTR*. However, addition of dsRNA *rca1-CDS* resulted in great stabilization of GFP-Dap-dPIPa indicating that Rca1 stimulates destabilization of Dap. Color represent relative protein stability: unstable (yellow) and stable (red). Bars and error bars indicate mean +/- SEM ('n' represents number of independent experiments). Statistical significance was evaluated with one-tailed Student t-test, *P < 0.05.

The protein stability of GFP-Dap-dCDI-dPIPa was not affected by dsRNA *rca1-UTR*. However, treatment with dsRNA *rca1-CDS* resulted in significant stabilization of GFP-Dap-dCDI-dPIPa. Apparently, the RNA interference induced by dsRNA *rca1-UTR* was not efficient enough to reveal any effect, at least not by determining protein levels with the method used in this thesis (see section 3.4.2).

Altogether, these results demonstrate that Rca1 drives degradation of Dap in an F-box dependent manner giving more evidence for Dap being a SCF-Rca1 target substrate. Furthermore, the fact that downregulation of Dap stability by Rca1 does not require the PIP-degron indicates that SCF-Rca1 and CRL4-Cdt2 mediate Dap degradation independent from each other in separate degradation pathways.

3.4.3.5 CycE/Cdk2 and Rca1 function synergistically to drive Dap degradation

Several experiments described above suggest that Rca1 functions as F-box protein in an SCF complex to target Dap for degradation (see sections 3.2, 3.2.8 and 3.4.3.4). Often, recognition of SCF target substrates require their phosphorylation (170). Indeed, the interaction between 4XFLAG-Rca1 and GFP-Dap-dCDI-dPIPa was enhanced by upregulation of CycE/Cdk2 activity (see Figure 21). Thus, CycE/Cdk2 might phosphorylate Dap to stimulate its recognition by SCF-Rca1. To analyze, whether Dap is also destabilized when CycE/Cdk2 activity is increased, the protein stability of GFP-Dap-dCDI-dPIPa was analyzed in S2R+ cells upon overexpression of HA-CycE (see Figure 53). HA-CycE overexpression significantly destabilized GFP-Dap-dCDI-dPIPa indicating that CycE/Cdk2 drives degradation of Dap. This supports the assumption that CycE/Cdk2 phosphorylates Dap to stimulate its recognition by SCF-Rca1.

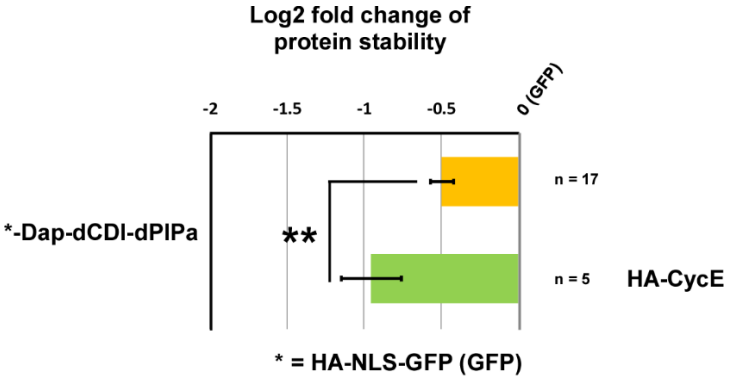

Figure 53 | CycE/Cdk2 stimulates Dap instability
The protein stability of GFP-Dap-dCDI-dPIPa was analyzed in S2R+ cells upon overexpression of HA-CycE. HA-CycE overexpression significantly destabilized GFP-Dap-dCDI-dPIPa. Bars and error bars indicate mean +/- SEM ('n' represents number of independent experiments). Color represent relative protein stability: very unstable (green) and unstable (yellow). Statistical significance was evaluated with one-tailed Student t-test. **P < 0.01.

To analyze, whether Rca1 and CycE synergize to stimulate Dap degradation, the protein stability of GFP-Dap-dCDI-dPIPa was investigated upon overexpression of both 4XFLAG-Rca1 and HA-CycE (see Figure 54). Additional overexpression of HA-CycE further significantly downregulated the stability of GFP-Dap-dCDI-dPIPa in presence of overexpressed 4XFLAG-Rca1. As expected, the protein level of GFP-Dap-dCDI-dPIPa was significantly increased when 4XFLAG-Rca1 was replaced with 4XFLAG-Rca1-dFbox that lacks the F-box, which is unable to function in an SCF complex.

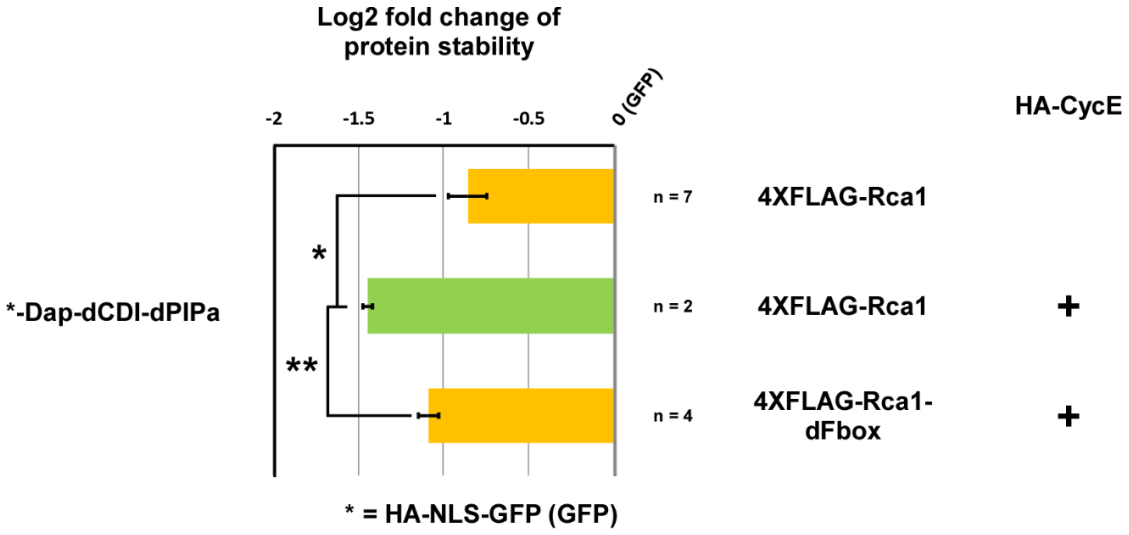

Figure 54 | CycE/Cdk2 and SCF-Rca1 synergize to stimulate Dap degradation
The protein level of GFP-Dap-dCDI-dPIPa was analyzed in S2R+ cells upon overexpression of both HA-CycE and 4XFLAG-Rca1(-dFbox) (see Figure 34 for illustration of the Rca1 constructs). Destabilization of GFP-Dap-dCDI-dPIPa by 4XFLAG-Rca1 was significantly enhanced by additional overexpression of HA-CycE. This was not the case for 4XFLAG-Rca1-dFbox lacking the F-box demonstrating that both CycE/Cdk2 and SCF-Rca1 contribute to Dap degradation. Bars and error bars indicate mean +/- SEM ('n' represents number of independent experiments). Color represent relative protein stability: very unstable (green) and unstable (yellow). Statistical significance was evaluated with one-tailed Student t-test, *P < 0.05, **P < 0.01.

Summarized, these data, in combination with previous findings suggest that SCF-Rca1 and CycE/Cdk2 act in concert to stimulate Dap degradation in following order: First, CycE/Cdk2 catalyzes phosphorylation of Dap. Next, phosphorylated Dap is recognized by SCF-Rca1, which labels bound Dap for proteasomal destruction.

3.4.3.6 A functional ZBR is required for stimulated Dap destabilization by CycE/Cdk2

In vivo APC/C activity assays have shown that the ZBR in Rca1 does not play a role in the downregulation of Dap activity to achieve efficient APC/C-Fzr inhibition (see Figure 40). Furthermore, the ZBR is neither required for the interaction with SkpA (231) nor for the interaction with Dap (see Figure 31). Together, these results suggest that the ZBR does not contribute to the assembly of a functional SCF-Rca1 complex that mediates degradation of Dap. To test this, the effect on the protein stability of GFP-Dap-dCDI-dPIPa was analyzed in S2R+ cells upon overexpression of 4XFLAG-Rca1-C351S which harbors a disrupted ZBR due to the point mutation C351S (see Figure 55). Destabilization of GFP-Dap-dCDI-dPIPa by 4XFLAG-Rca1 was enhanced by additional overexpression of HA-CycE (see also Figure 54). Surprisingly, destabilization of GFP-Dap-dCDI-dPIPa by HA-CycE was obscured when 4XFLAG-Rca1-C351S was overexpressed. To assess, whether loss of the ZBR impaired SCF-Rca1 activity, 4XFLAG-Rca1-dFbox-C351S lacking both the F-box and ZBR was overexpressed. Compared to 4XFLAG-Rca1-C351S, 4XFLAG-Rca1-dFbox-C351S further significantly stabilized GFP-Dap-dCDI-dPIPa suggesting that loss of the ZBR did not impair the ability of SCF-Rca1 to target Dap for degradation. One explanation for the ZBR-dependent effect on GFP-Dap-dCDI-dPIPa stability upon HA-CycE overexpression might be that the ZBR is required to allow destabilization of Dap by CycE/Cdk2. However, this hypothesis requires more evidence. Thus, further experiments including GFP-Dap-dCDI-dPIPa protein stability analyses without HA-CycE overexpression, in combination with analyses of the expression levels of the Rca1 mutant constructs are necessary to elucidate the reasons for the observed results in more detail.

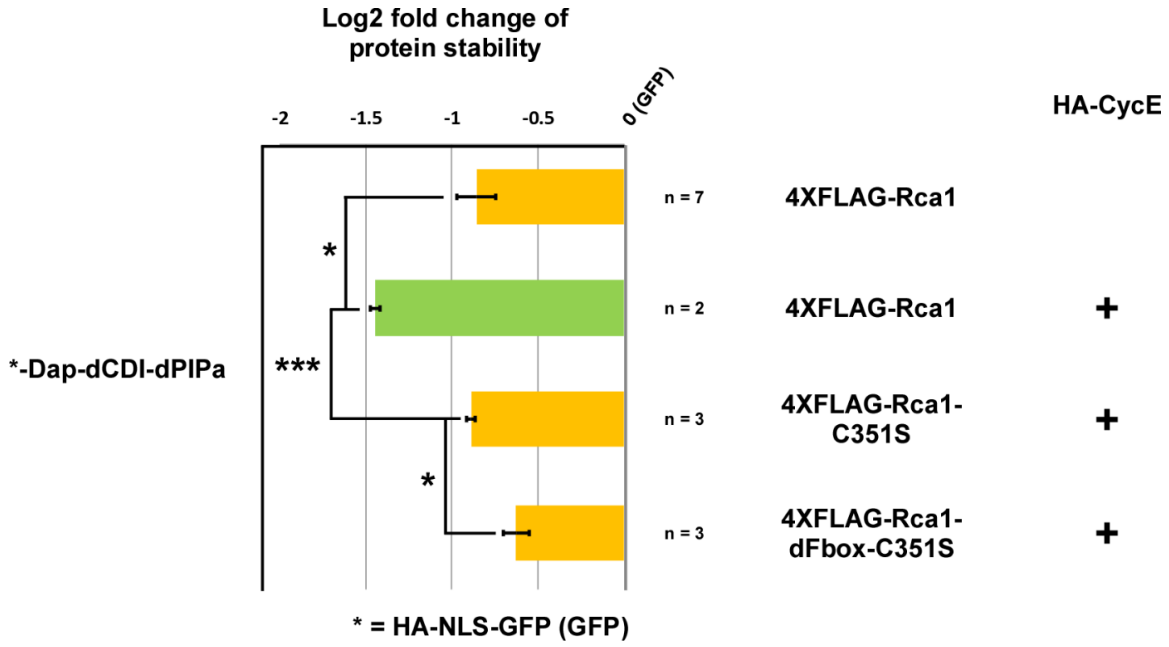

Figure 55 | Dap destabilization by CycE/Cdk2 depends on ZBR in Rca1
The protein stability of GFP-Dap-dCDI-dPIPa was analyzed in S2R+ cells upon overexpression of HA-CycE and F-box/ZBR mutated Rca1 constructs (see Figure 34 for illustration of the Rca1 constructs). Destabilization of GFP-Dap-dCDI-dPIPa by 4XFLAG-Rca1 was further increased by HA-CycE overexpression. However, HA-CycE dependent destabilization of GFP-Dap-dCDI-dPIPa was lost upon overexpression of 4XFLAG-Rca1-C351S that contains a non-functional ZBR. GFP-Dap-dCDI-dPIPa was further significantly stabilized by overexpression of 4XFLAG-Rca1-dFbox-C351S that lacks both F-box and ZBR. Bars and error bars indicate mean +/- SEM ('n' represents number of independent experiments). Color represent relative protein stability: very unstable (green) and unstable (yellow). Statistical significance was evaluated with one-tailed Student t-test, *P < 0.05, ***P < 0.001.

3.4.3.7 S/T-P Cdk phosphorylation sites in Dap (S205, S214) are not required for its degradation

Interaction studies have demonstrated that the minimal Cdk phosphorylation sites in Dap, S205 and S214 (both followed by proline) do not stimulate Rca1 binding (see section 3.2.5) implying that these sites do not contribute to the recruitment of Dap to SCF-Rca1. To confirm this, S2R+ cells were used to analyze the protein stability of Dap constructs harboring mutations in these Cdk sites (see Figure 56A). In GFP-Dap-dCDI-S205A-S214A, both Cdk sites were mutated to alanine, whereas in GFP-Dap-dCDI-S205E-S214E both sites were replaced with glutamic acid to mimic the phosphorylated state. When phosphorylation at these sites is important for degradation, it was expected that GFP-Dap-dCDI-S205A-S214A should be stabilized, while the GFP-Dap-dCDI-S205E-S214E mutant should exhibit higher instability, when compared to GFP-Dap-dCDI. However, the protein stability of the Cdk site mutated Dap constructs did not differ from the non-mutated version indicating that the Cdk sites, S205 and S214, do not confer Dap instability. The effect of the double mutation S205A-S214A was repeated for GFP-Dap-dCDI-dPIPa (see Figure 56B) that is not destabilized during S-phase by CRL4-Cdt2 (see section 3.4.3.2). By this, alternative degradation pathways of Dap become more focused.

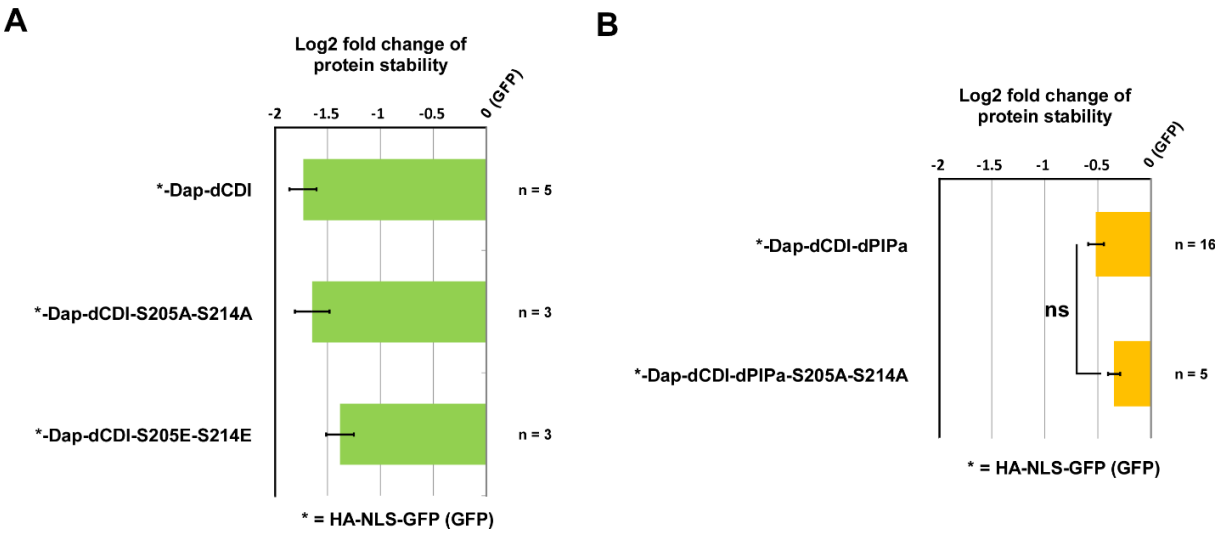

Figure 56 | The Cdk phosphorylation sites S205 and S214 do not mediate Dap degradation
GFP-tagged Dap constructs carrying mutations of the Cdk sites S205 and S214 were studied for their stability in S2R+ cells. **(A)** The protein stability of GFP-Dap-dCDI-S205A-S214A and GFP-Dap-dCDI-S205E-S214E was compared with GFP-Dap-dCDI. The double mutation S205A-S214A removes the Cdk sites, whereas S205E-S214E mimics a permanent phosphorylation state. None of these mutations revealed any effect on the stability of GFP-Dap-dCDI. **(B)** The S205A-S214A double mutation was analyzed for GFP-Dap-dCDI-dPIPa that is not targeted for degradation by CRL4-Cdt2 due to loss of the N-terminal part of the PIP-degron. GFP-Dap-dCDI-dPIPa-S205A-S214A protein levels did not differ significantly in comparison to GFP-Dap-dCDI-dPIPa. Thus, the Cdk sites S205 and S214 are not required for Dap degradation. Bars and error bars indicate mean +/- SEM ('n' represents number of independent experiments). Statistical significance was evaluated with one-tailed Student t-test, ns: not significant.

A slight increase of the protein stability was observed for GFP-Dap-dCDI-dPIPa-S205A-S214A. However, the difference was not significant to GFP-Dap-dCDI-dPIPa. Thus, it was concluded that the Cdk sites S205 and S214 do not contribute to Dap degradation.

3.4.3.8 N-terminal region in Dap is required for its degradation

In vitro studies have revealed that the N-terminal half of Dap is essential for binding Rca1 (see section 3.2.6). Furthermore, stability analyses suggest that Dap is a target substrate of SCF-Rca1 (see Figure 51). Therefore, it was expected that elimination of the region in Dap required to associate with Rca1 should turn off SCF-Rca1 mediated degradation, resulting in stabilization of Dap. To test this, GFP-tagged Dap constructs with N-terminal truncations that were already used for Rca1 interaction studies (see Figure 25) were analyzed for their stability in S2R+ cells (see Figure 57). CRL4-Cdt2 dependent degradation during S-phase was inactivated by N-terminal deletion of the PIP-degron. This ensures that changes of protein stability are not influenced by CRL4-Cdt2.

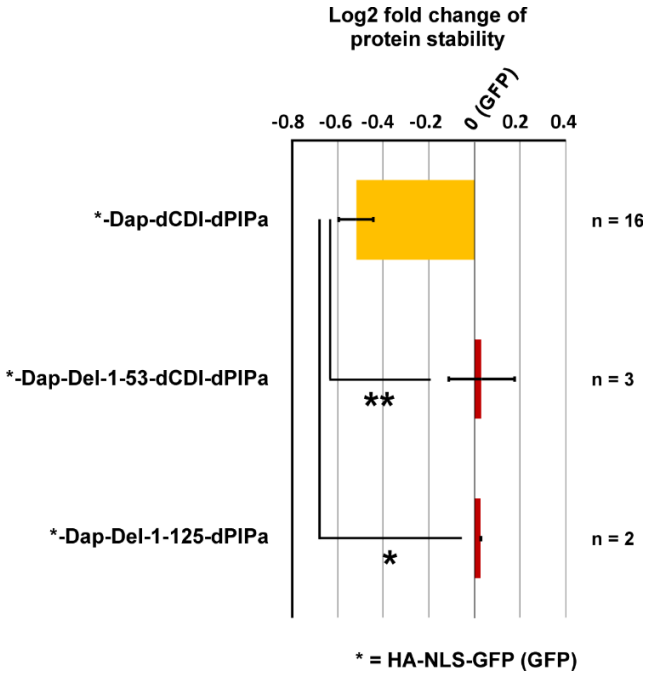

Figure 57 | The first 53 residues in Dap mediate Dap degradation
N-terminal truncated GFP-tagged Dap constructs were studied for their stability in S2R+ cells (for illustration of the Dap constructs see Figure 25). The protein stability of GFP-Dap-Del-1-53-dCDI-dPIPa and GFP-Dap-Del-1-125-dPIPa lacking the first 53 or 125 residues, respectively, was compared with full-length GFP-Dap-dCDI-dPIPa. Complete stabilization was already achieved by deletion of the first 53 residues. Bars and error bars indicate mean +/- SEM ('n' represents number of independent experiments). Color represent relative protein stability: unstable (yellow) and stable (red). Statistical significance was evaluated with one-tailed Student t-test, *P < 0.05, **P < 0.01.

While full-length GFP-Dap-dCDI-dPIPa was unstable, deletion of the first 53 residues completely stabilized the Dap construct (GFP-Dap-Del-1-53-dCDI-dPIPa) indicating that the N-terminal region of Dap is important for degradation. As expected, the same was observed when the first 125 residues were deleted (GFP-Dap-Del-1-125-dPIPa). Since the first 53 residues in Dap play a major role in binding Rca1 (see section 3.2.6), the performed stability analyses support the idea that an SCF-Rca1 complex recruits Dap for degradation.

3.4.4 Analysis of Skp2 stability

3.4.4.1 CycE/Cdk2 stimulates degradation of Skp2

Rca1 was found in complex with SCF components and Skp2 suggesting that SCF-Rca1 targets Skp2 for degradation (see section 3.1.2). Recognition of SCF target substrates is usually regulated by phosphorylation (170). Several Cdk phosphorylation sites could be predicted in Skp2 (data not shown). To test, whether kinase activity stimulates Skp2 degradation, the protein stability of GFP-Skp2 was analyzed when CycE/Cdk2 activity was increased by overexpression of HA-CycE (see Figure 58).

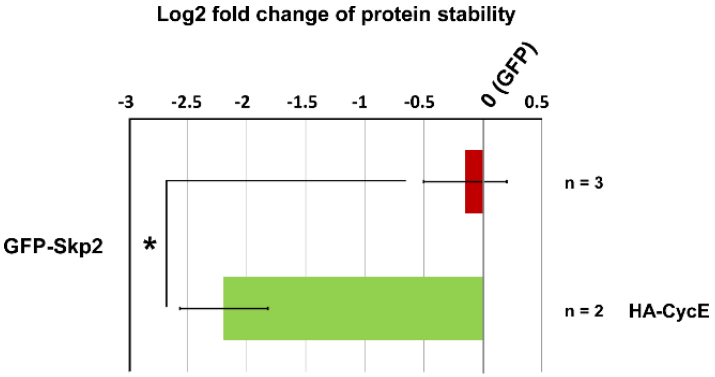

Figure 58 | CycE/Cdk2 activity downregulates Skp2 protein levels
The protein stability of GFP-Skp2 was analyzed upon overexpression of HA-CycE. The protein level of GFP-Skp2 was significantly decreased when HA-CycE was overexpressed indicating that CycE/Cdk2 activity destabilizes Skp2. Bars and error bars indicate mean +/- SEM ('n' represents number of independent experiments). Color represent relative protein stability: very unstable (green) and stable (red). Statistical significance was evaluated with one-tailed Student t-test, *P < 0.05.

GFP-Skp2 was greatly destabilized when HA-CycE was overexpressed demonstrating that CycE/Cdk2 activity promotes Skp2 degradation. These data suggest that Skp2 is another SCF target substrate.

3.4.4.2 Skp2 stability does not depend on Rca1

Since CycE/Cdk2 activity downregulates Skp2 (see section 3.4.4.1), Skp2 might be a typical SCF target substrate. The fact that Skp2 was identified as interaction partner of Rca1 suggests that SCF-Rca1 targets Skp2 for degradation. To test this assumption, GFP-Skp2 protein stability was measured upon overexpression of 4XFLAG-Rca1 (see Figure 59).

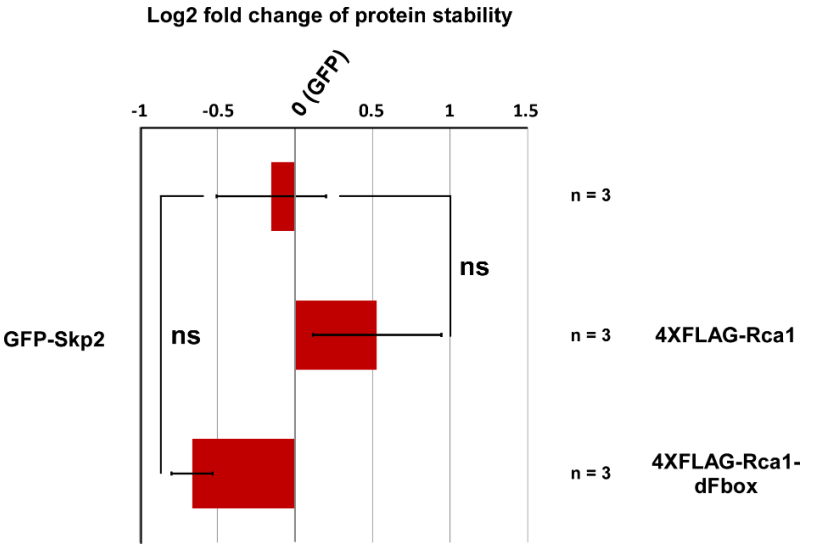

Figure 59 | Rca1 activity does not stimulate Skp2 degradation
The protein stability of GFP-Skp2 was analyzed upon overexpression of 4XFLAG-Rca1 or 4XFLAG-Rca1-dFbox that lacks the F-box domain (for illustration see Figure 35). The GFP-Skp2 protein level was not affected by the Rca1 constructs. Bars and error bars indicate mean +/- SEM ('n' represents number of independent experiments).

Overexpression of 4XFLAG-Rca1 did not change the protein level of GFP-Skp2. The same was observed when 4XFLAG-Rca1-dFbox lacking the F-box was overexpressed. To assess, whether an Rca1 dependent effect can be seen in presence of high CycE/Cdk2 activity, HA-CycE was additionally overexpressed (see Figure 60).

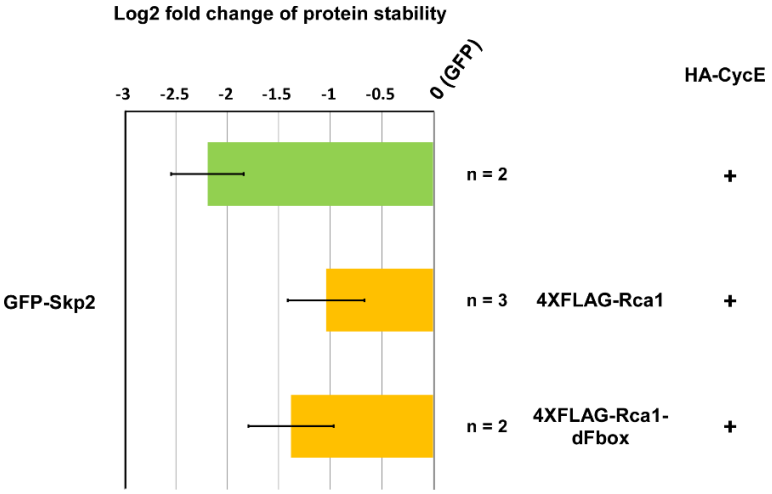

Figure 60 | Rca1 does not stimulate Skp2 degradation in presence of high CycE/Cdk2 activity
The protein stability of GFP-Skp2 was analyzed upon overexpression of 4XFLAG-Rca1 or 4XFLAG-Rca1-dFbox in presence of high CycE/Cdk2 activity, which was achieved by overexpression of HA-CycE. GFP-Skp2 protein levels were not downregulated by the Rca1 constructs. Bars and error bars indicate mean +/- SEM ('n' represents number of independent experiments). Color represent relative protein stability: very unstable (green) and unstable (yellow).

GFP-Skp2 was not further destabilized by 4XFLAG-Rca1 in presence of overexpressed HA-CycE. In contrast, GFP-Skp2 was even more stabilized. Thus, Skp2 is not a target substrate of SCF-Rca1. Interestingly, Skp2 also harbors an F-box domain and is known to recognize several cell cycle regulators for degradation in mammals (240). It is therefore possible that Rca1 is another target substrate of SCF-Skp2. Protein stability studies of Rca1 are necessary to analyze this hypothesis.

3.5 Establishment of an *in vitro* APC/C-Fzr activity assay

3.5.1 Aim

To understand what domains are required for direct APC/C-Fzr inhibition in more detail, great efforts were made to develop a biochemical assay system that allows the analysis of APC/C-Fzr inhibition by Rca1 *in vitro*. So far, the establishment of an ubiquitination assay that imitates *in vitro* ubiquitination of *Drosophila* proteins by APC/C-Fzr was only partly completed (253). Active components of the ubiquitin proteasome pathway were successfully purified including the E1 enzyme (6XHIS-Uba1), the E2 enzyme (Effete-6XHIS) and a FLAG-tagged version of Ubiquitin for detection of polyubiquitin conjugates (6XHIS-4XFLAG-Ubiquitin). Rabbit reticulocyte lysate that was supplemented with these components stimulated polyubiquitination of the purified APC/C-Fzr target substrate Geminin-10XHA-6XHIS. Next, multiple attempts were made to purify active *Drosophila* APC/C-Fzr for functional Rca1 analyses. However, GFP-Cdc16 precipitate obtained from transgenic *Drosophila* embryos did not release any ubiquitination activity in the rabbit reticulocyte lysate, whose internal ligase activity was suppressed by NEM/DTT treatment. Ligation activity was also not stimulated by addition of *in vitro* translated 4XFLAG-Fzr suggesting that the precipitate did not contain a functional APC/C complex. Therefore, further approaches resulting in purification of active APC/C-Fzr were tried in this thesis. Transgenic S2R+ cell line expressing Cdc16-MYC-TEV-GFP (Cdc16-GFP) or GFP alone as negative control were established. Subsequently, these GFP precipitates were applied for *in vitro* ubiquitination assays that were performed in an ATP-containing ubiquitination buffer (see section 3.5.3). In addition, ligase activity was analyzed when GFP precipitates were incubated with *in vitro* translated 4XFLAG-Fzr or baculovirus-expressed 6XHIS-TEV-FLAG-Fzr (see section 3.5.2), respectively.

3.5.2 Purification of 6XHIS-TEV-FLAG-Fzr by baculovirus-infected SF21 cells

APC/C activity requires association with one of the two activator subunits, Fzy or Fzr (251). *In vitro* ubiquitination assays were used to analyze vertebrate APC/C activity *in vitro* (131, 254). In these assays, antibodies against the APC/C subunit Cdc27 were used for APC/C precipitation. However, Cdc27 precipitates exhibited only weak ubiquitination activity. Only additional pre-incubation with the *in vitro* translated activator subunits, Cdc20/Fzy or Cdh1/Fzr, stimulated the formation of ubiquitin conjugates. Thus, it seems that the physical interaction between APC/C and its co-activator subunit is relatively weak, or that only a small fraction of APC/C are associated with activator subunits. Therefore, expression and purification of Fzr is an important key step for the establishment of an ubiquitination assay system that is based on *Drosophila* APC/C-Fzr. Since Fzr requires chaperones for proper folding (255), *E. coli* is not suitable as expression system. In such cases, the baculoviral expression system has emerged as an efficient and relatively simple method for the production of eukaryotic proteins in SF21 insect cells. Recombinant baculovirus expressing 6XHIS-TEV-FLAG-Fzr were generated by the MultiBac system developed by Berger et al. (256-258). After the production of the first generation of recombinant baculovirus, the solubility of expressed 6XHIS-TEV-FLAG-Fzr was analyzed (Figure 61A).

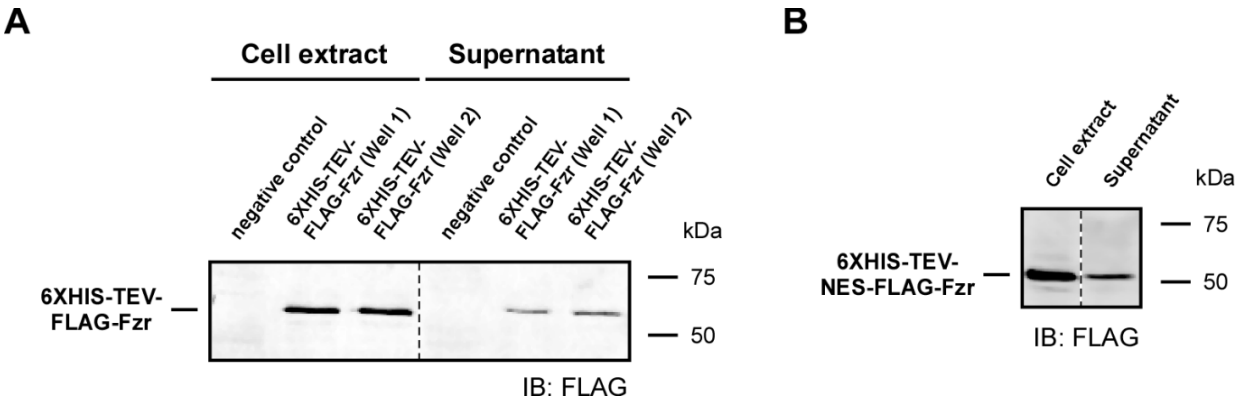

Figure 61 | Expression of 6XHIS-TEV-FLAG-Fzr in baculovirus-infected SF21 cells
SF21 insect cells were infected with recombinant baculovirus expressing 6XHIS-TEV-FLAG-Fzr or 6XHIS-TEV-NES-FLAG-Fzr, respectively (V0 generation). **(A)** Transfection of recombinant baculovirus DNA encoding for 6XHIS-TEV-FLAG-Fzr was carried out twice in a 6-well plate format (Well1, Well2). Non-transfected SF21 cells were used as negative control. Extract and supernatant samples were subjected to SDS-PAGE and analyzed by Western Blot using anti-FLAG antibodies. **(B)** As described in (A), the same was performed for 6XHIS-TEV-NES-FLAG-Fzr. Here, only one well was transfected. Dashed lines indicate omitted lanes.

Only a small portion 6XHIS-TEV-FLAG-Fzr was found in the supernatant as soluble protein. It was assumed that this was because of difficulties to isolate 6XHIS-TEV-FLAG-Fzr from the nucleus. Therefore, the Fzr construct was fused to the nuclear export sequence G-S-L-A-L-K-L-A-G-L-D-I (NES) to stimulate export from the nucleus into the cytoplasm. Next, the Fzr construct, 6XHIS-TEV-NES-FLAG-Fzr was expressed from baculovirus-infected SF21 insect cells and tested for solubility (Figure 61B). The integrated density (the product of area and mean gray value) was used to determine the portion of soluble protein (data not shown). For both, 6XHIS-TEV-FLAG-Fzr and 6XHIS-TEV-NES-FLAG-Fzr, the same relative soluble portion of 35 % was calculated indicating that the NES-tag did not improve the extraction of the Fzr construct. Nevertheless, the relative amount of soluble 6XHIS-TEV-FLAG-Fzr was regarded as sufficient to perform a large scale expression. Upon expression, 6XHIS-TEV-FLAG-Fzr was purified by Ni-NTA affinity chromatography (see Figure 62A).

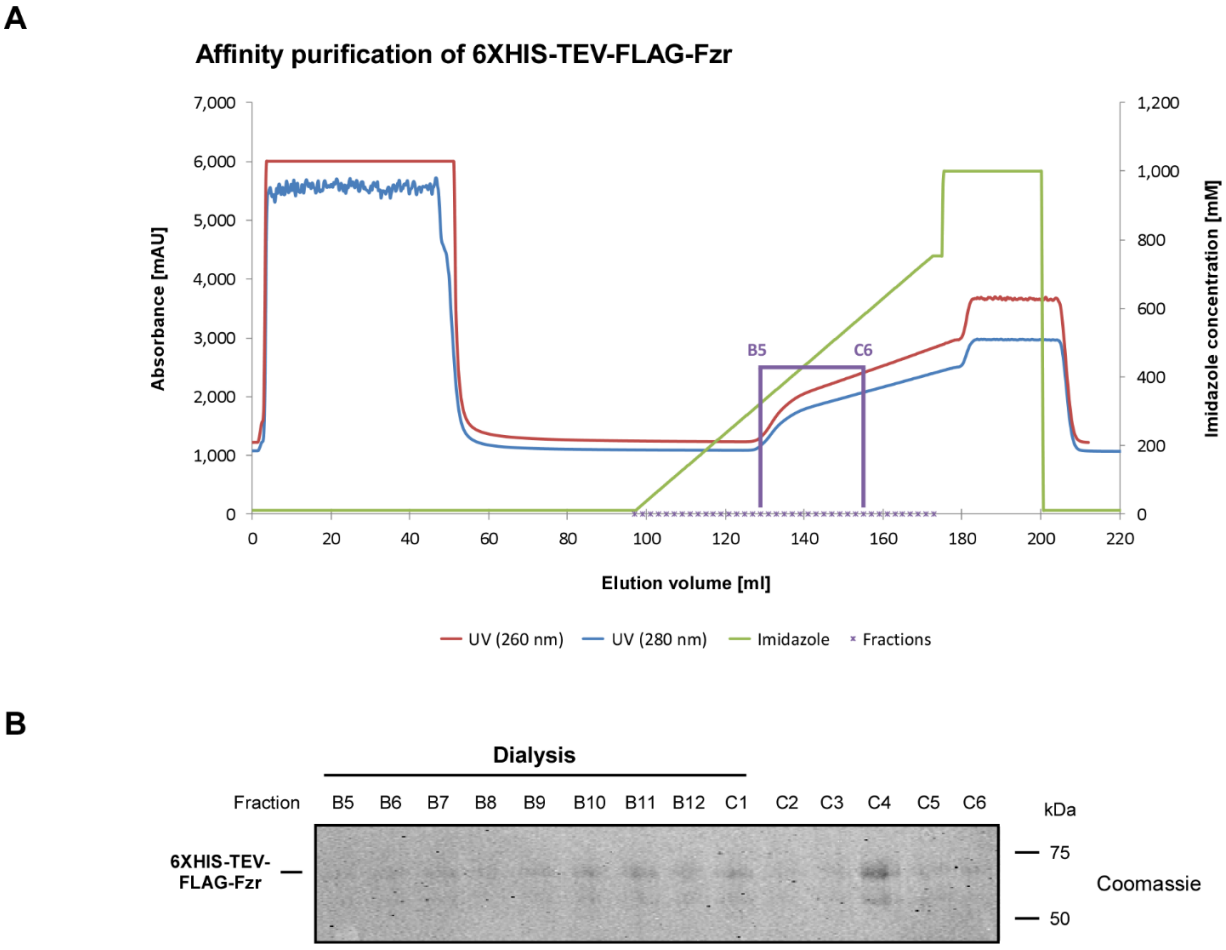

Figure 62 | Purification of 6XHIS-TEV-FLAG-Fzr from baculovirus-infected SF21 cells
6XHIS-TEV-FLAG-Fzr was purified via Ni-NTA affinity chromatography. **(A)** Purification profile of 6XHIS-TEV-FLAG-Fzr is shown. Purification was performed by affinity chromatography using a Ni-NTA affinity column. Elution was carried out with an imidazole gradient from 10 mM to 750 mM imidazole (green). The UV absorbance at 260 nm (red) and 280 nm (blue) is demonstrated. 6XHIS-TEV-FLAG-Fzr was eluted between 200 mM and 300 mM imidazole. Eluted fractions (purple asterisks) that were analyzed by SDS-PAGE are indicated (purple rectangular box). Running buffer: 20 mM HEPES, 500 mM NaCl, pH 7.7. Elution buffer: 20 mM HEPES, 100 mM NaCl, pH 7.7. **(B)** Fractions containing purified 6XHIS-TEV-FLAG-Fzr were separated by SDS-PAGE and stained with Coomassie Blue. Fractions that were combined and used for dialysis (dialysis buffer: 20 mM HEPES, 500 mM NaCl, pH 7.7) are indicated.

Quantitative analysis of the eluted fractions revealed a very low concentration of purified 6XHIS-TEV-FLAG-Fzr (see Figure 62B). Eluates containing the protein were dialyzed and subsequently concentrated using the Amcion Ultra 10k device resulting in a 60-fold concentration (data not shown). Concentrated 6XHIS-FLAG-Fzr was stored in aliquots at -20 °C and -80 °C until being used for ubiquitination assays.

3.5.3 Cdc16 precipitate from a stable S2R+ cell line provides APC/C-Fzr activity when supplemented with *in vitro* translated 4XFLAG-Fzr

Cdc16 is a subunit of the APC/C complex (251) suggesting that APC/C can be co-precipitated by precipitation of an expressed Cdc16 construct. Therefore, Cdc16-MYC-TEV-GFP (Cdc16-GFP) that carries a GFP tag at the C-terminus was cloned. A TEV cleavage site was inserted upstream of GFP to allow isolation

of APC/C complexes upon precipitation. Furthermore, a MYC tag upstream of the TEV site was introduced to enable detection of the cleaved Cdc16 construct. To isolate active APC/C from S2R+ cells, a transgenic S2R+ cell line expressing Cdc16-GFP was established, and as control, a cell line that expresses GFP alone. Both GFP constructs were expressed from the polyubiquitin promoter. Using these cell lines, GFP precipitates were obtained using anti-GFP antibodies. It was assumed that precipitation of Cdc16-GFP, but not GFP results in co-precipitation of functional APC/C. Precipitates were incubated with *in vitro* translated 4XFLAG-Fzr (see Figure 63A) or baculovirus-expressed 6XHIS-FLAG-Fzr (see Figure 63B) to stimulate formation of active APC/C-Fzr complexes.

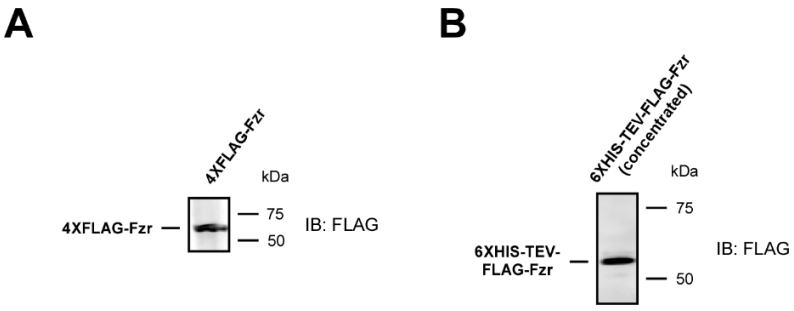

Figure 63 | Expression of 4XFLAG-Fzr and 6XHIS-TEV-FLAG-Fzr
FLAG-tagged versions of Fzr were either expressed in reticulocyte lysate or SF21 cells. **(A)** 4XFLAG-Fzr was *in vitro* translated in rabbit reticulocyte lysate. **(B)** 6XHIS-TEV-FLAG-Fzr purified from baculovirus-infected SF21 cells. Fzr constructs were subjected to SDS-PAGE and analyzed by Western Blot using anti-FLAG antibodies.

Subsequently, the GFP and Cdc16-GFP precipitates were subjected to ubiquitination assays (see Figure 64). Rabbit reticulocyte lysate that provides ligase activity capable of driving ubiquitination of Geminin-10XHA-6XHIS was used as positive control for the ubiquitination system. Ubiquitinated forms of Geminin-10XHA-6XHIS were not detected, when the GFP precipitate was used. The same was observed for the Cdc16-GFP precipitate that was not pre-incubated with either of the expressed Fzr constructs. However, pre-incubation with baculovirus-expressed 6XHIS-TEV-FLAG-Fzr revealed weak ubiquitination activity, and a relatively high amount of ubiquitin conjugates of Geminin-10XHA-6XHIS was detected with *in vitro* translated 4XFLAG-Fzr.

The fact that the Cdc16-GFP precipitate stimulated strong ubiquitination of the Geminin construct when pre-incubated with *in vitro* translated 4XFLAG-Fzr demonstrates that functional APC/C complexes co-precipitated with Cdc16-GFP. Thus, the established Cdc16-GFP transgenic cell line can be used for the isolation of *Drosophila* APC/C, which provides the opportunity to analyze APC/C-Fzr inhibition by Rca1 in more detail.

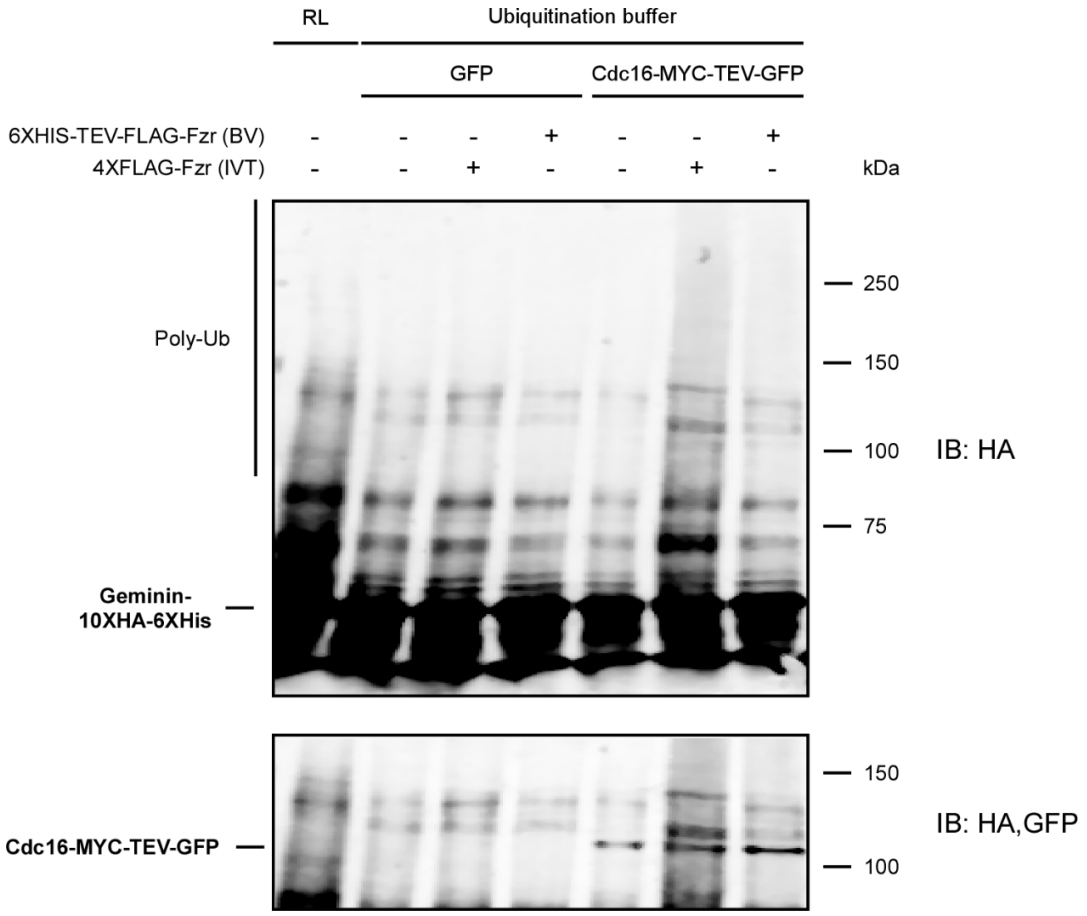

Figure 64 | Ubiquitination assay using Cdc16-TEV-MYC-GFP precipitate from S2R+ cells
Ubiquitination assays were performed with GFP precipitate (negative control) or Cdc16-MYC-TEV-GFP (Cdc16-GFP) precipitate in ubiquitination buffer, as indicated. Precipitates were obtained from transgenic S2R+ cell lines. Precipitates were either pre-incubated with *in vitro* translated 4XFLAG-Fzr or baculovirus-expressed 6XHIS-TEV-FLAG-Fzr, as shown. The amount of the Fzr construct used for incubation corresponds to the amount of protein detected in **Error! Reference source not found.**A and B. Ubiquitination activity was quantified by the APC/C target substrate Geminin-10XHA-6XHIS. Ubiquitin conjugates were detected by anti-HA antibodies. Presence of Cdc16-GFP was verified by additional staining with anti-GFP antibodies. Ligase activity provided by rabbit reticulocyte lysate was used as control for ubiquitination of Geminin-10XHA-6XHIS. Ubiquitin conjugates were not detected when the GFP precipitate was used. The Cdc16-GFP precipitate revealed a strong ubiquitination activity when it was pre-incubated with 4XFLAG-Fzr, and only a weak activity with 6XHIS-TEV-FLAG-Fzr. Ubiquitination buffer: 50 mM Tris (ph 7.5), 2 mM ATP, 5 mM MgCl2 and 2 mM DTT. RL: rabbit reticulocyte lysate. BV: baculovirus-expressed. IVT: *in vitro* translated.

4 Discussion

4.1 Establishment of a method for protein stability analyses during cell cycle progression

A wide range of biochemical processes interact with each other to keep a proper balance between the rate of protein synthesis and degradation. Variations in protein expression might have dramatic effects on biological functions, and in the worst case might lead to the cell's death. Cell division is one prominent example that requires a strict regulation of protein metabolism. Proper cell cycle progression relies on the synthesis and degradation of cell cycle regulators at specific stages of the cell cycle (1). Therefore, it is of great interest to understand the mechanisms that mediate the timely ordered degradation of proteins involved in cell cycle regulation. To asses this, a method should be established that facilitates the analysis of protein stabilities during cell cycle progression (see section 3.4). Since our workgroup is focused on *Drosophila* as model organism, S2R+ *Drosophila* culture cells were chosen to analyze the stability of *Drosophila* cell cycle proteins. Flow cytometric measurements allow efficient high-throughput analyses of whole cell populations in a very short time. Thus, proteins of interest were fluorescently labeled with HA-NLS-GFP (GFP) and transiently co-expressed with 3XCherry in S2R+ cells. 3XCherry is not degraded during any stage of the cell cycle, and therefore useful as reference for the protein stability analyses of GFP-tagged cell cycle regulated proteins. In addition, cells were stained with Hoechst to determine their cell cycle stage. This information can be used to specifically analyze the stability of proteins at specific cell cycle stages. Cell cycle profiles were used to confirm the efficiency of down- and upregulation of specific proteins that control cell cycle progression and whose misexpression result in an altered distribution of the cell cycle phases. For instance, knockdown of *rca1* results in an increase of the G2-phase population, while the G1-phase population is decreased (see Figure 33A). The overall protein stability of GFP-tagged proteins was determined by the flow cytometric quantification of GFP- and Cherry-fluorescent cells. Transient transfection produces cells with different expression levels of the fluorescent proteins. Thus, the amount of GFP-fluorescent cells strongly depends on the stability of the GFP-labeled protein. The less the stability of the GFP-labeled protein, the less is the number of GFP-positive cells. To determine the degree of protein stability, the ratio of GFP- to Cherry-fluorescent cells was calculated resulting in a value between "0" (totally unstable) and "1" (totally stable). First, the stability of GFP alone was analyzed. Due to technical limitations of the detection, low GFP expression cells could not be analyzed as they are present in the background caused by Hoechst staining of the cells. To circumvent this issue, low Cherry signal intensities were ignored and the analysis of Cherry positive cells was restricted to cells with Cherry signal intensities going from medium to high (see Figure 41). This resulted in an overlapping cell cycle profile of GFP- and Cherry-positive cells and a protein stability value of "1" indicating that both proteins share the same stability. Next, it was tested whether transfection efficiencies might influence the calculated protein stability (see Figure 42). This was an important question since an equal transfection efficiency can not be guaranteed for each GFP-tagged construct. Cells expressing GFP alone with a high transfection rate were used to adjust the threshold for Cherry signals. The same setting was used for cells harboring lower transfection rates. And indeed, transfection rates with a relative change of reduction of more than 20 % resulted in a strong distortion of the calculated protein stability of GFP alone. Below a relative change of 20 %, a slight increase of the protein stability value was observed, but in average the values were close to the expected value of "1". However, the higher the relative change of the transfection rate, the higher the protein stability value did become, with reaching values more than "2". The cell cycle profiles of GFP- and

Cherry-positive cells showed that this was caused be the relative reduction of analyzed Cherry-positive cells. The reason for this might be differences in the expression efficiencies of the GFP-tagged protein and 3XCherry. Although both proteins are expressed from the same plasmid, their expression is controlled by different promoters. While expression of the GFP-tagged protein is under control of the metallothionein promoter, expression of 3XCherry is driven by the actin promoter. It is assumed that a reduction of the transfection rate is accompanied by a decrease of the number of transfected expression plasmids in individual cells. Therefore, it is possible that the metallothionein promoter is able to compensate for the reduction of expression plasmids to some extent, whereas the actin promoter is not that efficient and more sensitive to the presence of transfected plasmids. Anyway, this result demonstrated that the calculated protein stability value depends on the transfection rate, which makes the analysis of protein stabilities of GFP-tagged proteins unreliable when the transfection rates differ too much. To circumvent this issue, cell expressing GFP alone with different transfection efficiencies were prepared and individually used for the stability analyses of GFP-tagged proteins. Only cells expressing GFP alone that did not show a relative change of transfection rate of more than 20 % to the cells expressing the GFP-tagged protein of interest were used to adjust the threshold setting for the Cherry fluorescent signals. By this, the calculated protein stability values were kept in a reliable range. All protein stability analyses of GFP-tagged cell cycle proteins in this thesis were performed by this method and western blot analyses of an experimental setup confirmed the obtained results (see Figure 46). To uncouple the stability analyses of different proteins, their stability was presented relative to the stability of GFP alone. In general, independent repetitions of the same experiments showed clear results about the protein stabilities and this with low fluctuations supporting the reliability of these results. However, some comparisons of protein stabilities showed low significance values in the performed Student t-tests. Therefore, it would be interesting to know, whether the reliability of protein stability analyses can be further improved by reducing their fluctuations. This might be achieved by using the same promoter for the expression of the GFP-tagged protein and 3XCherry, or by expressing these proteins from a common pre-cursor transcript by using the T2A expression system (259). Beside this, it is questionable, whether the qualitative analysis of fluorescent signals might be a better way to analyze protein stabilities, instead of quantitatively counting fluorescent cells. The quantification of GFP-positive cells gives only an “on” or “off” information, meaning that only significant degradation of the GFP-tagged protein is registered. This prevents the analysis of slight protein stability differences and the detection of partial degradation. Qualitative measurements would therefore give a more detailed information about the degradation behavior of specific proteins. This problematic was not analyzed in this thesis, but is already under investigation. Anyway, using the method described in this thesis, protein stabilities for different cell cycle proteins could be determined under different conditions, thereby giving more insight into the mechanisms that allow proper cell cycle progression.

4.2 CRL4-Cdt2 targets Dap for degradation

In *Drosophila*, Dap is the only CKI that is homologue to the mammalian CKI proteins p21, p27 and p57 (211). The stability of p21 has been shown to be regulated by the E3 ligase CRL4-Cdt2 (205-209). This depends on a PIP-degron motif that interacts with chromatin-bound PCNA during DNA replication. Both the PCNA protein and the PIP-degron generate a surface for the recruitment of CRL4-Cdt2. By this, CRL4-Cdt2 promotes polyubiquitination of PIP-degron containing substrates during S-phase. Alignment of the PIP-degron consensus sequence (Q-x-x-Ψ-T-D-ϑ-ϑ-x-x-x-B, Ψ = I/L/M/V, ϑ = Y/F, B = K/R) with the coding sequence of Dap revealed a potential PIP-degron in the C-terminal part of Dap (see section 3.4.3.1). However, this potential PIP-degron does not fit all essential residues of the consensus sequence (Q-P-K-I-

T-E-F-M-K-E-R-K, underlined residues do not fit the consensus sequence). The T-D motif that promotes tight binding to PCNA (207) is lost due to replacement of the aspartic acid with glutamic acid. Since these amino acids are almost equal in structure and share the same chemical properties (acidic), it is assumed that this difference does not dramatically influence the functionality of the T-D motif. Furthermore, Cdt1 is targeted for degradation by CRL4-Cdt2 although it completely lacks the T-D motif in its PIP-degron (207). Thus, despite the strong conservation of the T-D motif among known PIP-degron proteins, this motif seems not to be strictly required to activate the CRL4-Cdt2 dependent degradation pathway. The second difference between the Dap PIP-degron and its consensus sequence is an exchange of an aromatic residue for methionine. Also here, both amino acids are similar in their chemical properties (non-polar), and therefore the PIP-degron was not assumed to be affected by this mutation. This assumption is supported by the CRL4-Cdt2 target substrate CKI1 from *C. elegans*, which contains the same replacement (207). Taken together, the presence of PIP-degron proteins harboring the same changes in the consensus sequence suggested that Dap contains a functional PIP-degron. This hypothesis was first supported by flow cytemtric analysis of GFP-Dap-dCDI stability in S-phase cells (see Figure 43A). S-phase cells are characterized by a DNA content between that of G1- and G2-phase cells. The ratio of GFP- to Cherry-postive cells with such a S-phase DNA content was strongly reduced when compared to cells expressing GFP alone, demonstrating that Dap is efficiently degraded during S-phase. To assess the functionality of the PIP-degron in more detail, GFP-Dap-dCDI constructs with different PIP-degron mutations were analyzed for their overall stability (see section 3.4.3.1). Deletion of the N-terminal part of the PIP-degron (dPIPa) greatly stabilized GFP-Dap-dCDI. Interestingly, complete deletion of the PIP-degron (dPIP) led to complete stabilization of GFP-Dap-dCDI. This raised the question whether N-terminal deletion of the PIP-degron is sufficient to inactivate the PIP-degron, or whether the C-terminal part of the PIP-degron still possesses some rest activity. Downregulation of CRL4-Cdt2 activity by RNAi did not further decrease the protein levels of GFP-Dap-dCDI-dPIPa indicating that the dPIPa mutation results in a non-functional PIP-degron (see section 3.4.3.2). This is also supported by the observation that mutations of essential residues to alanine (6A) stabilized GFP-Dap-dCDI in the same manner as dPIPa (see Figure 46A). Thus, it is still questionable why additional deletion of the C-terminal PIP-degron results in further stabilization of Dap. One possiblity might be that beside CRL4-Cdt2, another E3 ligase functions on Dap, which requires the C-terminal part of the PIP-degron. Indeed, SCF-Rca1, an E3 ligase that contains the F-box protein Rca1 for substrate recruitment has been shown to drive degradation of Dap (see section 3.4.3.4). This is further discussed in section 4.3. One interesting finding was made, when the function of the RXXL sequence in Dap was investigated (see section 3.4.3.3). The RXXL sequence is found as a minimal consensus sequence in the D-box degron that recruits target substrates to the APC/C complex for degradation (126, 128, 252). This gave rise to the possibility of Dap being an APC/C target substrate. This assumption was first tested by mutating the arginine residue in the RXXL sequence (R194A). This resulted in stabilization of Dap-dCDI. However, the R194 overlaps with the C-terminal part of the PIP-degron suggesting that the function of the PIP-degron was affected by the R194A mutation. Thus, the same mutation was analyzed in Dap-dCDI-dPIPa, which carries a non-functional PIP-degron. If R194 is part of a functional D-box, the R194A mutation should also stabilize this Dap construct. However, Dap-dCDI-dPIPa-R194A did not exhibit reduced stability in comparison to Dap-dCDI-dPIPa. Thus, stabilization by R194A in GFP-Dap-dCDI was not caused by the mutation of the putative D-box, instead this mutation impaired only the functionality of the PIP-degron. In general, PIP-degrons depend on two essential elements: the PIP-box promoting PCNA binding during DNA replication and a basic amino acid four residues downstream of the PIP-box. The basic residue is essential for recruitment of CRL4-Cdt2 and mutation of this residue to alanine results in great or even complete stabilization of the PIP-degron substrate (207, 250). In the case of Dap, the basic residue is a lysine (K+4, number describes position relative to the PIP-box). The arginine of the

RXXL sequence is located only one residue downstream of the lysine residue (R+3). Both lysine and arginine belong to the class of basic residues. Therefore, it is possible that both residues contribute to the interaction with CRL4-Cdt2. Notably, Dap-dCDI-R194A was more unstable than Dap-dCDI-dPIPa indicating that the destabilizing function of the PIP-degron was not completely lost by the R194A mutation (see Figure 49). Anyway, although the residue at position +3 has not been described as a consensus PIP-degron residue, a basic residue at this position might also contribute to the complete functionality of the PIP-degron in special cases, with Dap being one of them. Taken together, the protein stability analyses of different PIP-degron Dap mutants have shown that Dap contains a functional PIP-degron, which mediates instability during S-phase. These observations were confirmed by a recent publication from Duronio's workgroup, who has demonstrated that the PIP-degron drives downregulation of Dap protein levels in both mitotic cycles and endocycles (214). In cells of both cell cycle types, the PIP-degron mediated destabilization of Dap during S-phase. Interestingly, expression of a S-phase stabilized version of Dap did not affect cell proliferation in mitotically dividing tissues. In contrast, endocycle progression was blocked in several endocycling tissues (midgut, ovarian follicle cells and salivary glands) indicating that the PIP-degron plays an essential role in the generation of polyploid cells.

4.3 SCF-Rca1 targets Dap for degradation

Rca1 belongs to the family of F-box proteins as it harbors an F-box domain in its central region (see section 2.11). Usually, F-box proteins are part of SCF ubiquitin ligases that recruit specific substrates for polyubiquitination, thereby labeling them for degradation by the 26S proteasome (170). SCF complexes consist of Skp1, Cul1, Rbx1, and an exchangeable F-box protein that interacts via its F-box with Skp1 and recognizes the target substrate. Several studies including co-immunoprecipitation experiments and yeast two hybrid screens have revealed that Rca1 interacts with SkpA and Cul1 in an F-box dependent manner (231, 236). These data gave rise to the existence of an SCF-Rca1 complex that mediates degradation of target substrates during cell cycle progression. Although Emi1, the vertebrate homologue of Rca1, was initially identified in a yeast two-hybrid screen for F-box proteins by using Skp1 as bait protein (219), no studies are present that deal with the biological relevance of the F-box. Therefore, to get more insight into the function of the F-box in Rca1, Rca1 interacting proteins were identified by mass spectrometric analysis of a Rca1 precipitate derived from S2R+ cells (see section 3.1). The presence of SkpA and Cul1 confirmed the fact that Rca1 is in complex with SCF components. In addition, CycE/Cdk2 and its inhibitor Dap were also found to interact with Rca1. Since some experiments point to Dap as SCF-Rca1 target substrate (discussed in detail below), a Dap-dCDI-dPIPa precipitate was additionally analyzed. Dap-dCDI-dPIPa lacks degradation during S-phase due to inactivation of the PIP-degron (dPIPa). Moreover, deletions of essential residues within and near the CDI domain (dCDI) eliminate CycE/Cdk2 inhibition. This becomes visible by flow cytometric cell cycle analysis. While overexpression of Dap caused a cell cycle arrest in G1-phase, cell cycle progression was not affected by Dap-dCDI (236). Surprisingly, CycE and Cdk2 were identified in the Dap-dCDI-dPIPa precipitate by mass spectrometry. However, only 1 – 2 peptides of these proteins were detected with a very low Matrix score (see Table 39). Assuming that CycE/Cdk2 was specifically precipitated, the interaction of Dap-dCDI-dPIPa with CycE/Cdk2 is therefore either weak or indirect. Importantly, Rca1 and SkpA were identified in the Dap-dCDI-dPIPa precipitate, confirming the interaction between Rca1, SCF-components and Dap. Cul1 was also identified, but only with one peptide and a low Matrix score (see Table 40). The fact that CycE/Cdk2 was found with significant scores in the Rca1 but not in the Dap-dCDI-dPIPa precipitate might indicate that Rca1 can bind to Dap that is associated with CycE/Cdk2. Dap represents a potential SCF-Rca1 target substrate, since several previous *in vivo* studies

suggest that Dap activity is negatively regulated by Rca1 in an F-box dependent manner. Firstly, Rca1 overexpression resulted in an F-box dependent rough eye phenotype due to the induction of ectopic S-phases in cells of the developing eye imaginal disc (231). Dap is required for the establishment of a stable G1-phase by inhibiting CycE/Cdk2 activity stimulating S-phase entry (211, 212). The observed acceleration of the G1/S transition might be explained by ectopic SCF-Rca1 activity causing Dap degradation that results in premature release of active CycE/Cdk2. Here, it should be noted that overexpression of Rca1 was not accompanied by the downregulation of Dap protein levels. However, a more detailed analysis of the performed antibody stainings of the eye imaginal disc revealed an expression pattern of Dap that did not always fit the expression pattern of CycA. Posterior to the morphogenetic furrow, cells expressing both the S-phase initiator CycA and the S-phase inhibitor Dap were detected. Thus, it is doubtful whether the anti-Dap staining was based on specific interactions. Another evidence for Dap being a SCF-Rca1 substrate comes from *in vivo* studies with *Drosophila* mutant embryos that revealed a genetic interaction between *rca1* and *dap* in an F-box dependent manner (236). $rca1^{2}$ dap^{6} double mutants that express Rca1 whose F-box is still intact executed an additional round of cell division at the end of embryogenesis. This corresponds to the dap^{6} mutant phenotype, which is caused by loss of CycE/Cdk2 inhibition in G1-phase (211, 212, 236). In contrast, $rca1^{C1474}$ dap^{6} double mutants carrying an F-box mutation in Rca1 display the typical *rca1* mutant phenotype, which is characterized by an G2-phase arrest in cell cycle 16 (230). This arrest might be caused by residual maternal amounts of Dap that could not been targeted for degradation by SCF-Rca1 prior mitosis. As CycE/Cdk2 functions as negative regulator of APC/C-Fzr activity (162, 163, 230), it is likely that inhibition of CycE/Cdk2 by residual Dap resulted in a G2-phase arrest due to ectopic APC/C-Fzr activity. Taken together, the studies mentioned so far suggest a functional relationship between Rca1 and Dap in a way that the F-box is required for the assembly of an SCF-Rca1 complex to downregulate Dap activity. This hypothesis was supported by several protein analyses and interaction studies performed in this thesis. The presence of a functional SCF-Rca1 complex *in vivo* was given by the fact that polyubiquitinated substrates were only found in complex with Rca1, but not when the F-box was deleted (see Figure 16). Next, it was assessed, whether SCF-Rca1 recruits Dap for polyubiquitination. Here, a previously described method allowing the capture of SCF target substrates upon their polyubiquitination was applied (246). In this method, F-box proteins are fused to UBA domains that possess a high affinity to polyubiquitin chains. This modification allowed the detection of polyubiquitinated target substrates in precipitates of UBA-fused F-box proteins. It was thought, that this might also work for SCF-Rca1 and its potential target substrate Dap. However, fusion of UBA domains to Rca1 derived from the UBA-containing proteins Rad23 or Dsk2 did not trap polyubiquitinated forms of Dap-dCDI-dPIPa (see section 3.2.2). However, this negative result was not regarded as evidence that Dap is not targeted for degradation by SCF-Rca1. In general, it is not clear, whether the cloned UBA domains are even functional. Moreover, structural conditions might prevent the capturing process. This was also observed by studies from Toczysk's workgroup that have established the method for SCF substrate trapping to identify so far unknown substrates. The identification of SCF target substrates was generally dependent on the position of the UBA-fusion, and in some cases, they failed to identify known substrates (246). Thus, this method does not allow the capture of all recruited target substrates, and this might also account for SCF-Rca1 and Dap. Thus, further studies were made to test, if Dap behaves like a typical SCF substrate, which is targeted for degradation by SCF-Rca1. A large variety of experiments in this thesis supported this idea, and are summarized here:

1) F-box proteins do not require their F-box domain to bind their substrates (241). Rca1 constructs that lost their interaction with SkpA due to F-box mutations were still able to interact with Dap-dCDI-dPIPa

(see section 3.2.3). Thus, SCF components are not involved in binding Dap supporting the requirement of Rca1 for Dap recruitment.

2) Usually, the target substrate binds near to the F-box domain, likely to bring the substrate in close proximity to the SCF complex and E2 enzyme for polyubiquitination (172). Interaction studies with N- and C-terminal truncated Rca1 constructs restricted the interaction interface to a region (residues 100 – 203) containing the F-box and around 50 residues upstream of the F-box (see section 3.2.9). Assuming that the F-box is not involved in Dap recruitment, interaction with Dap occurs presumably N-terminal close to the F-box domain. This is also in line with the identified binding sites in mammalian F-box proteins. Interaction with the target substrate is often found close to the F-box domain (172).

3) SCF target substrates are usually phosphorylated before they are recognized by the F-box protein (170). In this context, it was questioned which kinase might stimulate phosphorylation of Dap. Interestingly, Dap was phosphorylated by human CycE/Cdk2 *in vitro* (211). In mammals, phosphorylation of the Dap homologues p21 (S130) and p27 (T187) by CycE/Cdk2 complexes stimulated recruitment to the SCF-Skp2 complex (182-184). It is likely that SCF-Rca1 might replace the function of the SCF-Skp2 complex in *Drosophila* in terms of Dap degradation (SCF-Skp2 discussed in section 4.7). Upregulation of CycE/Cdk2 activity by overexpression of CycE enhanced the interaction between Rca1 and Dap-dCDI-dPIPa, presumably by phosphorylation of Dap (see section 3.2.4). Unfortunately, no associated mobility shift in Dap-dCDI-dPIPa due to phosphorylation was detected after CycE overexpression. Since addition of one phosphate group does not add much weight to the protein, it might be that only a single site is phosphorylated, like in the human system (182-184) and/or phosphorylation might not lead to a detectable shift in electrophoretic mobility in the applied gel system. Anyway, these data support the assumption that CycE/Cdk2 mediated phosphorylation of Dap is required for recognition by SCF-Rca1 to drive ubiquitination and subsequent degradation. Several Cdk phosphorylation sites were predicted in Dap-dCDI-dPIPa (see Figure 21). In this context, two S-P sites were found in the C-terminal region of Dap, S205 and S214, with S205 being part of the canonical Cdk motif S-P-X-K/R. Surprisingly, mutation of both Cdk sites to alanine did not reduce the interaction with Rca1 (see section 3.2.5). An effect was also net seen, when a N-terminal truncated Rca1 construct with low binding strength to Dap-dCDI-dPIPa was used. When the S-P sites do not contribute to SCF-Rca1 recruitment, it was expected that the protein levels of Dap are not affected by loss of the two S-P sites. Consistent with this expectation, the double mutations S205A-S214A and S205E-S214E did not influence the stability of GFP-Dap-dCDI (see section 3.4.3.7). This is supported by de Nooij et al., who did not observe any change in the expression level of a *dap* transgene lacking the Cdk site S205 *in vivo* (213). Thus, it is likely that one or several of the other Cdk sites (center: S132, S139, S145 and C-terminal: S213) mediate association with Rca1 upon phosphorylation, although these sites are not part of the typical S-P consensus. Therefore, further analyses with Cdk site mutants are necessary to identify the Cdk sites relevant for Rca1 binding. However, it is still possible that it is not Dap, but Rca1 that gets phosphorylated to stimulate the interaction with Dap. Accordingly, in Rca1, two Cdk phosphorylation sites, S112 and S196 were predicted within the Dap interacting region by using the tool KinasePhos 2.0 (data not shown). Finally, it can not be excluded that CycE/Cdk2 mediates the interaction between Rca1 and Dap indirectly.

4) F-box proteins function as substrate recognition subunits and recruit the substrate to the SCF complex for ubiquitination and subsequent degradation (170). Interaction studies combined with protein stability analyses have shown that the stability of Dap depends on its ability to bind Rca1. Several truncated Dap constructs were analyzed for binding Rca1. Deletion of the first 53 residues of Dap strongly reduced the interaction with Rca1 and was completely lost when the deletion was extended to 125 residues (see section 3.2.6). Consistent with the idea of Dap functioning as SCF-Rca1 target substrate, deletion of the first 53 residues resulted in full stabilization of Dap-dCDI-dPIPa (see section

3.4.3.8). Interestingly, the first 125 residues were not sufficient to detect an interaction with Rca1 suggesting that residues in the remaining part of Dap are additionally required for the association with Rca1 (see section 3.2.6). In this context, interesting results were obtained by the investigation of the RXXL sequence in the C-terminal part of Dap. RXXL sequences are found in D-box degrons of APC/C substrates (126). However, this is not the case for Dap, since overexpression of the APC/C activator subunit Fzr did not affect Dap-dCDI-dPIPa stability and the AXXL mutation did not stabilize Dap-dCDI-dPIPa (see section 3.4.3.3). Intriguingly, the RXXL sequence was found to be important for the recruitment to SCF-Rca1. Mutation of both arginine (R194) and leucine (L197) to alanine abolished the interaction with Rca1 and stabilized Dap-dCDI-dPIPa (see sections 3.2.8, 3.4.3.3). This indicates that either both residues or only leucine alone in the RXXL sequence stimulates both destabilization and binding to Rca1. The analysis of a single leucine mutation should bring more insight into this issue. Summarized, the interaction studies gave more evidence for Dap being a SCF-Rca1 target substrate. Whenever the interaction between Rca1 and Dap was disturbed by different mutations, this was accompanied by the stabilization of Dap. However, one exception was observed. Although complete loss of the PIP-degron in Dap-dCDI-dPIP did not interrupt the interaction with Rca1 (see section 3.2.7), Dap-dCDI-dPIP was completely stabilized (see section 3.4.3.1). Two lysine residues (K192 and K195) are present in the C-terminal part of the PIP-degron giving the idea that these lysines might function as ubiquitin acceptor lysine residues for the formation of polyubiquitin chains by SCF-Rca1. In the Dap-dCDI-6A mutant, K195 is already mutated to alanine and this mutation did not cause complete stabilization suggesting that K192 is essential for polyubiquitination by SCF-Rca1. The importance of specific lysine residues for ubiquitination is supported by studies of the APC/C-Cdh1 inhibitor Acm1 in yeast (260). Like Rca1/Emi1, Acm1 directly binds and inhibits APC/C-Cdh1. Mutation of specific residues to lysine (N83K-N84K) promoted APC/C-Cdh1-mediated ubiquitination of Acm1 *in vitro*. A similar observation was made for the SCF-Hos/βTrCP target substrate LMP1-95-8, a variant of the latent membrane protein of the Epstein-Barr virus (261). Replacing specific residues with lysine residues (L339K-M340K) stimulated LMP1-95-8 destabilization by SCF-Hos/βTrCP. Thus, the positioning of lysine residues within E3-ligase substrates can play an important role for the formation of polyubiquitin chains to promote their degradation. Interestingly, the lysine substitutions that transformed Acm1 and LMP1-95-8 into target substrates were close to binding sites for Cdh1 and Hos/βTrCP, respectively. This suggests that ubiquitin acceptor lysine residues have to be placed close to residues required for the interaction with the E3-ligase to allow ubiquitination. In Dap, K192 is close to L197 that has been shown to be essential for recognition by Rca1 (see above), underlining the importance of K192 as ubiquitin acceptor lysine. Further detailed mutational analyses within and near the PIP-degron will provide more details on Dap degradation in the future.

5) If Dap is indeed an SCF-Rca1 target substrate, it was expected that Rca1 influences the stability of Dap in an F-box dependent manner. This is supported by overexpression experiments in which Rca1 or Rca1 lacking a functional F-box was overexpressed alone or in conjunction with CycE/Cdk2 (see sections 3.4.3.4 and 3.4.3.5). Enhanced destabilization of Dap-dCDI-dPIPa by Rca1 was dependent on the F-box domain suggesting that SCF-Rca1 stimulates Dap degradation.

Taken all studies together, many lines of evidence argue for the presence of an SCF-Rca1 complex that binds and polyubiquitinates Dap to initiate its degradation. It should be noted, that all protein stability analyses of Dap were performed using a version of Dap (Dap-dCDI-dPIPa) that is uncoupled from destabilization by CRL4-Cdt2 during S-phase. Thus, side effects from this degradation pathway can be excluded, meaning that SCF-Rca1 and CRL4-Cdt2 promote degradation of Dap independent from each other.

4.4 SCF-Rca1 contributes to APC/C-Fzr inhibition in G2-phase

Both Rca1 and its vertebrate homologue Emi1 have been shown to be essential for APC/C-Fzr/Cdh1 inhibition in G2-phase (see sections 2.11, 2.12). A large variety of studies were made for Emi1 and could reveal the mechanisms that allow direct downregulation of APC/C-Cdh1 activity. Several domains in the C-terminal part of Emi1 bind the APC/C complex on different sites and thereby synergistically inhibit APC/C-Cdh1 activity (see Figure 10). It is assumed that Rca1 blocks APC/C-Fzr activity in a similar manner, since both Rca1 and Emi1 share the same order of functional domains in their C-terminal part (see Figure 11). This becomes visible for studies that focused on the ZBR. Loss of the ZBR function in Emi1 eliminates its ability to drive APC/C-Cdh1 inhibition (117, 223). The same was observed for Rca1. *Drosophila* embryos carrying the *rca1[2]* allele leading to the point mutation A344T inside the ZBR failed to enter mitosis 16 due to ectopic APC/C-Fzr activity in G2-phase (230, 235). Consistent with that, *rca1[2]* mutants were rescued by overexpression of a full length Rca1 construct, but not when the ZBR was disrupted by the point mutation C351S (231). However, previous studies suggest that not only the C-terminal part of Rca1 is essential to inhibit APC/C-Fzr activity, but also the central localized F-box. The *rca1[C1474]* allele contains the point mutation M182T within the F-box and mutants carrying this allele did not execute mitosis 16 (235, 236). The same was observed for *rca1[2]* mutant embryos expressing a *rca1* transgene lacking the F-box under the control of the endogenous *rca1* promoter (236). Thus, an intact F-box is additionally required to inhibit APC/C-Fzr activity. The question therefore arose by which mechanism the F-box provides this function. Interaction studies and protein stability measurements in this thesis demonstrated that the F-box is required for the assembly of an SCF-Rca1 complex that targets the CycE/Cdk2 inhibitor Dap for degradation. Cdk activity has been shown to inhibit the assembly of APC/C-Cdh1 by phosphorylation of Cdh1 (131, 262). In *Drosophila*, CycE/Cdk2 is able to inhibit APC/C-Fzr activity suggesting that CycE/Cdk2 mediates phosphorylation of the Cdh1 homologue Fzr (163, 230). This led to the proposal of a model in which SCF-Rca1 contributes to APC/C-Fzr inhibition by targeting Dap for degradation (see Figure 32). *In vivo* APC/C activity assays were used to analyze this hypothesis. Rca1 constructs with F-box and/or ZBR mutations were overexpressed and assessed for their ability to stimulate APC/C-Fzr inhibition in G2-phase in *rca1* mutant cells (see section 3.3.3). Wildtype Rca1 fully restored APC/C-Fzr inhibition (see Figure 33, Figure 35). Mutation of the F-box by M182T (Rca1-M182T) or its deletion (Rca1-dFbox) reduced APC/C-Fzr inhibition, and a similar phenotype was observed for the ZBR mutation C351S (Rca1-C351S). Each mutation failed to reduce APC/C-Fzr activity to the same extent indicating that the F-box and ZBR contribute equally to APC/C-Fzr inhibition. To see, whether these domains act in separate inhibitory pathways, both domains were mutated. Functional loss of both F-box and ZBR (Rca1-dFbox-C351S) resulted in a total loss of APC/C-Fzr inhibition (see Figure 36). Thus, both F-box and ZBR function together to fully inactivate APC/C-Fzr. Many of the different mutant Rca1 constructs tested in this assay were expressed at lower levels than wildtype Rca1 raising the possibility that deficits in APC/C-Fzr inhibition were caused by their reduced protein levels. The Rca1 constructs were expressed by the metallothionein promoter, which results in much higher protein levels than the endogenous Rca1 promoter (data not shown). Thus, all Rca1 mutant constructs were expressed at (or above) normal protein levels that are sufficient for complete APC/C-Fzr inhibition. Therefore, the observed loss of APC/C-Fzr inhibition is caused by the different mutations in the Rca1 coding sequence. Next, it was tested, whether RNAi treatment against *dap* rescues the deficiency of the Rca1 mutants to inhibit APC/C-Fzr. According to the assumption made in the model, the F-box downregulates Dap protein levels to allow APC/C-Fzr inhibition by CycE/Cdk2 (see Figure 32). Consistently, upon RNAi treatment against *dap*, APC/C-Fzr inhibition was increased for Rca1 lacking the F-box (see Figure 40), but not for full-length Rca1 and Rca1

carrying the C351S mutation. These Rca1 constructs contained a functional F-box, and therefore were able to function as SCF-Rca1 complexes to remove Dap proteins. Surprisingly, a change of APC/C-inhibition was not present for the Rca1 construct with the F-box mutation M182T. This was unexpected due to several reasons. First, the M182T mutation abolished the interaction with the SCF component SkpA in co-IP experiments (see Figure 13). Second, APC/C-Fzr inhibition was impaired by M182T (see Figure 36), and third, *rca1[C1474]* embryo mutants that encode for Rca1-M182T failed to enter the final mitosis (235). Co-IP experiments can be very stringent resulting in the loss of weak interactions. The M182T mutation might not completely abolish the interaction between Rca1 and SkpA in the cell and might provide residual F-box function that is sufficient to eliminate Dap protein during G2-phase, when Rca1-M182T is overexpressed. However, even when the F-box is still partially functional, it is surprising that this mutation failed to stimulate efficient APC/C-Fzr inhibition. One reason might be that critical protein and RNA transcript levels of Dap can change the outcome of the experiment and that the RNAi treatment failed to downregulate Dap sufficiently. The M182T mutations requires more attention in the future to understand the different behavior in the APC/C assay, and also to understand the *rca1[C1474]* mutant. The mutant phenotype of the *rca1[C1474]* allele shows the same phenotype as other *rca1* alleles and the only mutation in the coding region is the M182T mutation (235). However, due to lack of antibodies that can detect endogenous levels of Rca1, it is difficult to ascertain if the M182T mutation express normal levels of (mutant) Rca1 protein. Quantitative analyses of *rca1[C1474]* transcripts by real-time PCR and comparing the protein stability of wildtype and Rca1-M182T should bring some light into this issue. Beside this, interesting and sometimes unexplainable observations were obtained with the C351S mutation that inactivates the ZBR region required for APC/C inhibition (see section 3.3.3). In comparison to wildtype Rca1, Rca1-C351S failed to fully inhibit APC/C-Fzr activity (see Figure 36). Surprisingly, additional RNAi treatment against *dap* further reduced the ability of Rca1-C351S to stimulate APC/C-Fzr inhibition (see Figure 40). Interestingly, protein stability analyses of Dap-dCDI-dPIPa revealed a functional interaction between the ZBR and CycE/Cdk2 activity (see section 3.4.3.6). Destabilization of Dap-dCDI-dPIPa by Rca1 was pushed by upregulation of CycE/Cdk2 activity. However, the CycE/Cdk2 destabilizing effect was lost when the ZBR in Rca1 was mutated by C351S. Thus, the ZBR might be required to stimulate CycE/Cdk2 activity. However, further experiments (e.g. detailed protein expression analysis) will be required to uncover the reasons behind these phenotypes. This might provide us with further insights about the regulatory network controlling Rca1 activity and its ability to inhibit APC/C-Fzr activity. Taken together, the APC/C activity assays have shown that Rca1 mediates downregulation of APC/C-Fzr activity via its F-box. APC/C-Fzr inhibition requires inhibition of Dap activity and this is achieved by a functional F-box. This further supports the idea that SCF-Rca1 inhibits APC/C-Fzr activity by mediating degradation of the CycE/Cdk2 inhibitor Dap.

4.5 Dual regulation of APC/C-Fzr inhibition by Rca1

Structural analyses in combination with several different *in vivo* and *in vitro* studies have demonstrated that the C-terminal part of Emi1 is required to directly block APC/C-Cdh1 activity (see section 2.11). In *Drosophila*, APC/C-Fzr inhibition is achieved by Rca1 (see section 2.12). Both Rca1 and Emi1 share the same functional domains in the C-terminal part (only the D-box is replaced by a KEN-box), and therefore it is likely that Rca1 directly inhibits APC/C-Fzr activity in the same manner (see Figure 11). In this context, the C-terminal located ZBR has been shown to be essential for APC/C-Fzr inhibition (see Figure 36). However, the analysis of different *rca1* alleles have suggested that the central localized F-box is also involved in the downregulation of APC/C-Fzr activity (235). F-box proteins are well known as substrate recognition subunits of SCF complexes (170). Several studies in this thesis were performed to elucidate the APC/C-Fzr

inhibitory function of the F-box. Physical and genetic interaction analyses in combination with protein stability measurements propose a so far unknown indirect mechanism of APC/C-Fzr inhibition: As part of an SCF-complex, Rca1 mediates degradation of the CycE/Cdk2 inhibitor Dap. Free CycE/Cdk2 stimulates phosphorylation of Fzr, which renders Fzr unable to bind and activate the APC/C complex.

In conclusion, Rca1 has established two different mechanisms to downregulate APC/C-Fzr activity, and importantly both mechanisms are required to allow efficient APC/C-Fzr inhibition. The C-terminal part of Rca1 likely binds and inhibits pre-assembled APC/C-Fzr complexes, while SCF-Rca1 activity might be required to indirectly inhibit the activation of APC/C by preventing its association with Fzr. Rca1 binds Dap N-terminal next to the F-box, whereas the C-terminal part binds regions of APC/C-Fzr. Thus, Rca1 is likely in complex with two E3 ligases at the same time, however with different consequences. While the ligase activity of APC/C-Fzr is inhibited, Rca1 promotes the assembly of another ligase, SCF-Rca1, to stimulate further APC/C-Fzr inhibition (see Figure 65).

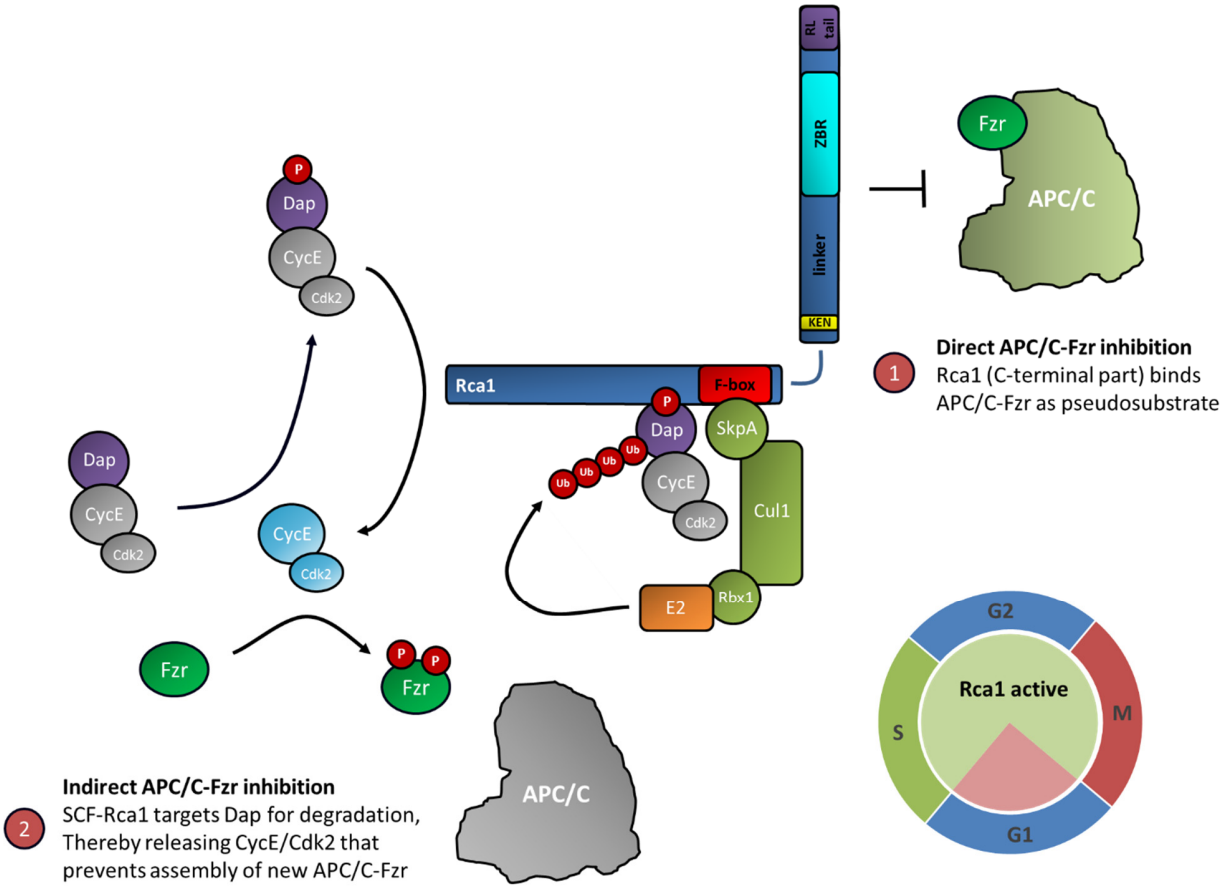

Figure 65: Model for dual regulation of APC/C-Fzr inhibition by Rca1
Rca1 is thought to be active during S-, G2- and M-phase to stimulate APC/C-Fzr inhibition by two independent mechanisms. APC/C-Fzr activity is blocked 1) directly by domains in the C-terminal part of Rca1, and 2) indirectly by Rca1 as part of an SCF complex. Indirect APC/C-Fzr inhibition is initiated by an increase in CycE/Cdk2 activity at the G1/S transition. Phosphorylation of the CycE/Cdk2 inhibitor Dap mediates its recruitment to SCF-Rca1, which catalyzes the polyubiquitination of Dap resulting in its degradation. By this, high CycE/Cdk2 activity is released, promoting phosphorylation of the APC/C activator subunit Fzr. Phosphorylated Fzr is unable to bind and activate the APC/C. Both inhibitory mechanisms allow efficient APC/C-Fzr inhibition to facilitate entry into mitosis. Inactive enzymes are shown in grey.

According to the model, both APC/C-Fzr inhibitory mechanisms differ in their mode of inhibition. Direct APC/C-Fzr inhibition by Rca1 occurs stoichiometrically. The inhibition of a single APC/C-Fzr complex requires the binding of a single Rca1 protein that functions as pseudosubstrate to block APC/C-Fzr activity. In contrast, indirect APC/C-Fzr inhibition by SCF-Rca1 occurs catalytically. The assembly of several APC/C-Fzr complexes can be prevented by a single SCF-Rca1 complex. SCF-Rca1 catalyzes the polyubiquitination of several Dap proteins, which releases several CycE/Cdk2 complexes that in turn catalyze the phosphorylation of several Fzr proteins. Thus, these catalytic steps allow a single SCF-Rca1 complex to prevent the formation of many APC/C-Fzr complexes. Yamano mentioned that the concentration of APC/C-Cdc20 is more than ten-fold higher than that of the meiotic Emi1 homologue Emi2 in *Xenopus* egg extracts (224). When this also accounts for Rca1 and APC/C-Fzr, the amount of Rca1 proteins is not able to block all APC/C-Fzr complexes in a direct manner to allow entry into mitosis, and would explain the requirement of a catalytic inhibitory mechanism for full APC/C-Fzr inhibition. Nevertheless, both inhibitory mechanisms are essential for efficient APC/C-Fzr inhibition and loss of one of the two mechanisms significantly impairs APC/C-Fzr inhibition, as shown by *in vivo* APC/C-Fzr activity assays. Endogenous expression of wildtype Rca1 is sufficient to mediate efficient APC/C-Fzr inhibition and the degree of APC/C-Fzr inhibition is not increased, when Rca1 is overexpressed (see Figure 33A and Figure 35). However, overexpression of Rca1 lacking the F-box as well as Rca1 carrying a mutated ZBR failed to mediate full APC/C-Fzr inhibition (see Figure 36). The importance of both inhibitory mechanisms can be also observed in rescue experiments of the *rca1[2]* mutant phenotype. The *rca1[2]* allele encodes for a Rca1 protein that contains the point mutation A344T inside the ZBR (235) suggesting that the failure to enter mitosis 16 in *rca1[2]* mutant embryos is caused by a non-functional ZBR. Additional overexpression of Rca1 lacking the F-box, but harboring a functional ZBR restored entry into mitosis. However, this was not observed for Rca1 containing a disrupted ZBR due to the point mutation C351S (231) suggesting that both direct and indirect APC/C-Fzr inhibition mediated by the two domains ZBR and F-box, respectively, are required for entry into mitosis. This might be explained by the fact that pre-assembled APC/C-Fzr complexes require direct Rca1 binding for inhibition, whereas low amounts of Rca1 make the catalytic SCF-Rca1-dependent inhibitory pathway essential for counteracting the assembly of new APC/C-Fzr complexes, whose amount would exceed the amount of available Rca1 proteins.

Interestingly, SCF-Rca1 is not the only ligase that mediates degradation of Dap. During S-phase, CRL4-Cdt2 is active and stimulates the destruction of Dap (214). Degradation analyses have shown that CRL4-Cdt2 efficiently downregulates Dap protein levels (see section 3.4.3.2), raising the question why the action of an additional ligase is important. CRL4-Cdt2-dependent degradation of Dap can only occur during S-phase. SCF-Rca1 might help at the end of G1 and after S-phase completion to downregulate Dap protein levels. Furthermore, polyubiquitination of Dap by CRL4-Cdt2 is tightly coupled to the recruitment of Dap to PCNA. Any non-chromatin associated Dap would remain stable and SCF-Rca1 might be required to remove this pool of Dap. Another opportunity might be that CRL4-Cdt2 is only able to target free Dap for degradation. Dap bound to CycE/Cdk2 might be protected for degradation by CRL4-Cdt2, but not by SCF-Rca1. In the mammalian system, the interaction of the CKI proteins p21, p27 and p57 with CycE/Cdk2 is even a prerequisite for their recognition by SCF-Skp2 (183). The same might account for SCF-Rca1 that is only able to recognize Dap in complex with CycE/Cdk2, explaining why SCF-Rca1 plays such an important role for APC/C-Fzr inhibition. Degradation of Dap releases CycE/Cdk2 activity to stimulate efficient APC/C-Fzr inhibition for entry into mitosis. The importance of Dap downregulation during interphase have been shown in *cycA* mutants overexpressing Dap (263). *cycA* single mutants failed to enter mitosis 16. Additional overexpression of Dap in *cycA* mutants already prevented entry into mitosis 15. This was accompanied by

loss of CycB accumulation indicating that APC/C-Fzr was ectopically active prior mitosis 15. These studies suggest that downregulation of Dap activity is important to allow CycE/Cdk2 activity to stimulate APC/C-Fzr inhibition.

An F-box is also present in the vertebrate homologue Emi1 at a relative same position (see Figure 11), suggesting that Emi1 proteins might also target substrates for degradation. Among all CKIs in Emi1, p21 is most similar to Dap, making p21 a potential target substrate of SCF-Emi1 (211). The degree of conservation of APC/C inhibition between *Drosophila* and vertebrates is therefore an interesting question of future research.

4.6 Establishment of an *in vitro* APC/C assay

Rca1 functions as APC/C-Fzr inhibitor and several domains in the C-terminal part and the F-box are thought to be involved in APC/C-Fzr inhibition. To analyze downregulation of APC/C-Fzr activity by Rca1 in more detail, attempts were made to establish an ubiquitination assay that allows the analysis of APC/C-Fzr activity *in vitro* (253). Such an assay mimics the *in vivo* ubiquitination of substrates, and therefore requires the purification of all components of the ubiquitination pathway. So far, 6XHIS-Uba1 (E1 enzyme), Effete-6XHIS (E2 enzyme), 6XHIS-4XFLAG-Ubiquitin (Ubiquitin) and Geminin-10XHA-6XHIS (Geminin), an APC/C target substrate, were successfully expressed in *E. coli* and purified. Adding these components to reticulocyte lysate resulted in the formation of Geminin Ubiquitin conjugates. To specifically analyze *Drosophila* APC/C-Fzr activity, several attempts were made to isolate active APC/C-Fzr from *Drosophila* embryos. Transgene embryos expressing the APC/C subunit Cdc16 tagged to GFP were used for purification. However, ubiquitination assays supplemented with GFP-Cdc16 precipitate and *in vitro* translated 4XFLAG-Fzr did not result in ubiquitination of Geminin (253). It was hypothesized that either GFP-Cdc16 is not incorporated in the APC/C complex or that the N-terminal fusion of GFP impairs APC/C-Fzr activity. Furthermore, it is also possible that *Drosophila* embryos do not provide enough material to isolate high amounts of APC/C-Fzr complexes that allow the detection of good ubiquitination activity. To circumvent these problems, a stable S2R+ cell line expressing a C-terminal GFP-tagged version of Cdc16, Cdc16-MYC-TEV-GFP (Cdc16-GFP), was established during this thesis. A transgenic S2R+ cell line expressing GFP alone was additionally generated as negative control. *In vitro* assays from different systems have shown that APC/C co-activators (Cdh1 or Cdc20) are not present in precipitates of APC/C subunits (131, 254). This is likely due to the weak interaction between the APC/C and the co-activator subunit. Therefore, Fzr was additionally purified using different expression systems. Fzr was either expressed in reticulocyte lysate (4XFLAG-Fzr), or expressed in baculovirus-infected SF21 cells (6XHIS-TEV-FLAG-Fzr). Only a small portion of soluble protein was obtained from SF21 cells. This was not due to difficulties to extract 6XHIS-TEV-FLAG-Fzr from the nucleus since addition of a NES sequence did not increase the isolation of soluble protein (see section 3.5.2). Thus, 6XHIS-TEV-FLAG-Fzr generally possesses only weak solubility or only a small fraction of soluble protein is produced in SF21 cells. However, it can not be ruled out that the used NES sequence was not functional active. Because of the low solubility, only a low yield of 6XHIS-TEV-FLAG-Fzr was obtained upon purification by NI-NTA affinity chromatography (see Figure 62). Using a protein concentration column, the concentration of 6XHIS-TEV-FLAG-Fzr was greatly increased and concentrated Fzr protein was used for ubiquitination assays. Cdc16-GFP precipitate was either pre-incubated with *in vitro* translated 4XFLAG-Fzr or baculovirus-expressed 6XHIS-TEV-FLAG-Fzr (see Figure 64). While the use of 4XFLAG-Fzr resulted in the efficient formation of Geminin conjugates, only slight ubiquitination activity was seen for 6XHIS-TEV-FLAG-Fzr. However, the difference to the negative control (GFP precipitate) was

too weak to exclude background effects suggesting that 6XHIS-TEV-FLAG-Fzr was not active. It is possible that the concentration procedure denatured the protein. Using more SF21 cells for expression could help to yield a higher concentration of protein upon purification without the need of its subsequent concentration. Furthermore, finding ways to increase the solubility of 6XHIS-TEV-FLAG-Fzr expression would be also very helpful. Nevertheless, 4XFLAG-Fzr expressed in reticulocyte lysate was able to stimulate ubiquitination activity of the Cdc16-GFP precipitate, which was not present without incubation of 4XFLAG-Fzr. Thus, it can be concluded that functional APC/C was obtained by precipitation of Cdc16-GFP, which is activated by *in vitro* translated 4XFLAG-Fzr. Surprisingly, the ubiquitination of Geminin using Cdc16-GFP precipitate and 4XFLAG-Fzr was not constantly reproducible. Often, assays failed to form Geminin Ubiquitin conjugates. The same was observed when other tagged components of the APC/C complex were used for its purification from *Drosophila* embryos (D. Bergér, personal communication). Since the transgene embryos and cell lines still expressed the endogenous APC/C component, it is conceivable that the endogenous untagged component is preferentially integrated into the APC/C complex, thereby reducing the chance for the assembly of recombinant APC/C. Thus, mostly, cells used for APC/C purification did not contain enough active recombinant APC/C, which would explain why only a few precipitates did provide ubiquitination activity. To circumvent this issue, endogenous expressing APC/C components should be tagged for purification. By this, the formation of recombinant APC/C is guaranteed since cells are not livable without a functional APC/C. In this regard, the CRISPR/Cas system provides a relatively easy opportunity to modify endogenous gene products.

4.7 Rca1 interacts with Skp2 and a broad range of further cell cycle proteins

Surprisingly, the mass spectrometric analysis of the Rca1 precipitate has revealed more than 1,000 different proteins (see section 3.1.2). Precipitation of Rca1 was performed by agarose beads. Since agarose beads are very porous, most of the identified proteins were likely bound unspecifically. This is supported by the analysis of the Dap-dCDI-dPIPa precipitate, in which almost 1,000 different interaction partners were identified. Rca1 plays an essential role in cell cycle regulation, and therefore, it was assumed that Rca1 mediates its cell cycle regulatory function by the interaction and modification of other cell cycle proteins. Restricting the analysis of Rca1 binding partners to proteins that are involved in cell cycle regulation strongly reduced the number of identified proteins to around 150 (see Table 39). These proteins cover a lot of different processes of cell cycle regulation, such as mitotic regulation, centrosome duplication and checkpoint control. Despite the possibility of unspecific interactions, the huge amount of Rca1 interacting cell cycle proteins suggest that Rca1 is involved in a lot of different cell cycle regulatory functions. Rca1 has been shown to be essential for entry into mitosis by stimulating the inhibition of APC/C-Fzr activity during interphase (see section 2.12). Structural studies of the vertebrate homologue Emi1 have demonstrated that Emi1 directly binds on different regions of APC/C-Cdh1 (see section 2.11). Consistent with this, the APC/C-Fzr components APC2/Mr, Cdc16 and Fzr were found in the Rca1 precipitate. Furthermore, Rca1 was also identified as part of an SCF complex by the interaction with the SCF components SkpA and Cul1. CycE/Cdk2 and its inhibitor Dap were also present in the Rca1 precipitate and Dap has been shown to be targeted for degradation by SCF-Rca1 (see section 3.4.3.4). Interestingly, Skp2 was also in complex with Rca1. However, in contrast to Dap, protein stability analyses showed that Skp2 does not function as SCF-Rca1 target substrate (see section 3.4.4.2). Skp2 is another F-box protein and in mammals, SCF-Skp2 is known to target many different cell cycle regulators for destruction (240). Dui et al. demonstrated in the *Drosophila* system that Skp2 stimulates polyubiquitination of Dap *in vivo* (215). This and several other *in vivo* experiments indicating that Skp2 downregulates Dap protein levels suggest that

SCF-Skp2 also targets Dap for degradation in *Drosophila*. However, some experiments argue against this hypothesis. Ghorbani et al. did not detect any increase of Dap protein levels in *skp2* mutant larvae (216). This was confirmed by protein stability analyses of GFP-Dap-dCDI-dPIPa in our lab that have shown that Skp2 protein levels do not affect Dap protein levels (T. Rössler, personal communication, June 27, 2016). Thus, SCF-Skp2 might function in *Drosophila* to target other substrates for degradation. One of these substrates might be Rca1. However, this would be contradictory, since Rca1 activity is required when Skp2 protein levels are present. In the mammalian system, Skp2 is stabilized at the G1/S transition and mediates the degradation of cell cycle regulatory proteins until mid-mitosis (183). During interphase, Rca1 activity is important to stimulate APC/C-Fzr inhibition to allow accumulation of mitotic cyclins and entry into mitosis (230). Thus, Rca1 is not a plausible SCF-Skp2 target substrate during interphase. However, it is possible that SCF-Skp2 stimulates degradation of Rca1, when its activity is not required anymore, which would be the case when the cells have entered mitosis. APC/C-Fzr activity is necessary to promote exit from mitosis (115) and this might be delayed or even inhibited when Rca1 would be still present as APC/C-Fzr inhibitor. Degradation studies suggest that Rca1 is converted from an APC/C-Fzr inhibitor to an APC/C-Fzr substrate during mitosis (232). This might be facilitated by initial downregulation of Rca1 protein levels by SCF-Skp2. However, live cell imaging analyses did not detect any degradation of Rca1 during mitosis (232). Thus, further investigations are necessary to analyze whether protein levels of Rca1 and/or other proteins are regulated by Skp2. In addition to the proteins mentioned so far, several more cell cycle regulators are physically associated with Rca1. Interesting candidates might be components of the minichromosome maintenance (MCM2–7) helicase complex and Geminin, both proteins involved in the formation of pre-replicative complexes (161) suggesting that Rca1 is directly involved in the regulation of DNA replication. Emi1 indirectly blocks rereplication by inhibiting the APC/C mediated degradation of the rereplication inhibitors CycA and Geminin (167). Consistently, depletion of Rca1 results in rereplication in S2R+ cells (data not shown) and large nuclei in imaginal discs (229, 230). Thus, Rca1 ensures that replication occurs only once per cell cycle and it is possible that Rca1 has emerged direct and indirect mechanisms to achieve this. Beside this, the two kinases CycB/Cdk1 and the polo kinase were also identified as Rca1 interaction partner. Consistently, these kinases have been implicated in the regulation of Emi1 stability in the vertebrate system (219, 222, 227). This might also account for Rca1, even when timing and mechanisms regulating Rca1 degradation differ from that of Emi1 (232). Ban et al. described a so called END (Emi1/NuMA/dynein-dynactin) network that mediates APC/C inhibition at spindle poles to allow accumulation of spindle pole-associated CycB (136). High CycB/Cdk1 activity is required at the spindle poles to facilitate proper formation of the mitotic spindle. In this network, Emi1 is associated with the NuMA/dynein-dynactin complex. Mud (NuMA), and components of the dynein-dynactin complex such as Arp1, Dlic and GI (264) were also found in the Rca1 precipitate (see Table 39). Thus, a similar mode of spatial APC/C regulation might also exist in *Drosophila*.

Summarized, many proteins that are associated with Rca1 are also known to be in complex with Emi1, thereby regulating several different cell cycle dependent processes. Thus, the biological function between Rca1 and Emi1 seems to be conserved, suggesting that findings for Emi1 are applicable to Rca1 and also the other way around. Nevertheless, regarding the large variety of Rca1 binding partners, several more intensive studies are required to elucidate all the cell cycle regulatory functions that involve Rca1 in the *Drosophila* system.

5 Material

5.1 Chemicals

Table 1: Chemicals

Chemical	Distributor
1 kb Gene Ruler DNA Mix (DNA ladder)	ThermoScientific
Acetic acid (CH_3COOH, HAc)	Merck KGaA
AcN (acetonitrile)	AG Deutzmann (University of Regensburg)
Acrylamide 30%/bisacrylamide	Carl Roth GmbH
Agarose ultra	Invitrogen GmbH
Ampicillin	Carl Roth GmbH
APS (ammonium persulfate)	Merck KGaA
ATP (100 mM)	New England Biolabs
Bacto Pepton	Becton
Bacto Trypton	Becton
Bacto Yeast Extract	Becton
Beta-Mercaptoethanol	Fluka
Bromophenol blue	SERVA Electrophoresis
CH_3COOK (potassium acetate)	Merck KGaA
Chloramphenicol	Sigma-Aldrich Chemie GmbH
Coomassie Brilliant Blue	Sigma-Aldrich Chemie GmbH
CTP (100 mM)	New England Biolabs
$CuSO_4$ (copper sulfate)	AppliChem GmbH
DMSO (Dimethyl sulfoxide)	Merck KGaA, Sigma-Aldrich Chemie GmbH
dNTP mix (dATP, dCTP, dGTP, dTTP)	New England Biolabs
DTT (1,4-dithiothreitol)	AppliChem GmbH
EDTA (ethylenediaminetetraacetic acid)	Fluka
EGTA (ethylene glycol tetraacetic acid)	Sigma-Aldrich Chemie GmbH
Ethanol	Carl Roth GmbH
Ethidiumbromide	SERVA Electrophoresis
Euroagar	Becton
FuGENE HD	Promega Corporation
Gentamycine	Unknown
Glucose	Merck KGaA
Glycerol	Carl Roth GmbH
Glycine	AppliChem GmbH
GTP (100 mM)	New England Biolabs
HCl (hydrochloric acid)	Merck KGaA
HEPES (2-[4-(2-hydroxyethyl)piperazin-1-yl]ethanesulfonic acid)	AppliChem GmbH
Hoechst 33342	Sigma-Aldrich Chemie GmbH
Hygromycin B Gold	InvivoGen
Imidazole	AppliChem GmbH
IPTG (Isopropyl β-D-1-thiogalactopyranoside)	AppliChem GmbH
Kanamycin	AppliChem GmbH
KH_2PO_4 (potassium dihydrogen phosphate)	Sigma-Aldrich Chemie GmbH
Liquid nitrogen	AG Schneuwly (University of Regensburg)
Methanol	Carl Roth GmbH
$MgCl_2$	Merck

Chemical	Distributor
Na_2HPO_4 (sodium hydrogen phosphate)	Fluka
NaCl (Sodium chloride)	Carl Roth GmbH, Merck
NaF (sodium fluoride)	Fluka
NaH_2PO_4 (sodium dihydrogen phosphate)	Fluka
NaN_3 (Sodium azide)	Sigma-Aldrich Chemie GmbH
NaOH (sodiumhydroxide)	Gerbu Trading GmbH
NH_4HCO_3 (ammonium bicarbonate)	AG Deutzmann (University of Regensburg)
Penicillin 100X	Invitrogen GmbH
Phusion GC buffer	Thermo Scientific
Phusion HF buffer	Thermo Scientific
Precision Plus Protein Standard	Bio-Rad Laboratories
Protease inhibitor mix	Bimake
Rabbit reticulocyte lysate	Promega (Rabbit Reticulocyte Lysate System)
Restriction buffers 10X	New England Biolabs
Schneider`s *Drosophila* medium	Invitrogen, PAN Biotech
SDS (sodium dodecyl sulfate)	Carl Roth GmbH, SERVA Electrophoresis
Skim milk powder Gloria	Nestle
Spermidine	Sigma-Aldrich Chemie GmbH
Streptomycin 100X	Invitrogen GmbH
T4 ligase Buffer 10X	New England Biolabs
TEMED (tetramethylethylenediamine)	Fluka
Tetracycline	Sigma-Aldrich Chemie GmbH
Tris (tris(hydroxymethyl)aminomethane)	Carl Roth GmbH
Triton X-100	Fluka
Trypan Blue	Sigma-Aldrich Chemie GmbH
Tween20	Carl Roth GmbH
UTP (100 mM)	New England Biolabs
X-gal	AppliChem GmbH
Xylene cyanol	SERVA Electrophoresis

5.2 Kits

Table 2: Kits

Kit	Distributor
Bac-to-Bac HT Vector Kit	Invitrogen
FLAG Tagged Immunoprecipitation Kit	SIGMA
Invisorb Spin DNA Extraction Kit	STRATEC Molecular GmbH
MSB Spin PCRapace Kit	STRATEC Molecular GmbH
PureYield Plasmid Midiprep system	Promega
Rabbit Reticulocyte Lysate System	Promega

5.3 Proteins/Enzymes

Table 3: Proteins/Enzymes

Protein	Distributor
6XHis-4XFLAG-Ubiquitin	Own production (253)
6XHis-Effete	Own production (253)
6XHis-Uba1	Own production (253)
BSA (bovine serum albumin)	Sigma-Aldrich Chemie GmbH
Geminin-10XHA-6XHis	Own production (253)
Lysozyme	Boehringer Mannheim, Fluka, Sigma-Aldrich Chemie GmbH
Phusion DNA polymerase	AG Thomm
Restriction endonucleases	New England Biolabs
RNase A	AppliChem GmbH
RNase Inhibitor	AG Medenbach
Shrimp Alkaline Phosphatase (rSAP)	New England Biolabs
SP6 RNA Polymerase	Thermo Scientific
T4 DNA Ligase	New England Biolabs
T4 DNA polymerase	New England Biolabs
T7 RNA polymerase	Thermo Scientific

5.4 Oligonucleotides

Oligonucleotides used for molecular cloning are not listed, but can be accessed from the internal AG Sprenger database.

Table 4: Oligonucleotides

Oligonucleotide	Purpose	Sequence
CO_002	Amplification of DNA for *in vitro* transcription	CCTTTTGCTCACATGTTCTTTCC
CO_045	Amplification of DNA for *in vitro* transcription	GGGGCCTGCCACCATACCCACGCC
SPO_288	Amplification of DNA for dsRNA production	TAGGCCTTAATACGACTCACTATAGGG

5.5 cDNA clones

All cDNA clones were provided by the *Drosophila* Genomics Resource Center (248).

Table 5: cDNA clones

cDNA clone	Gene
LD10153	Rad23
LD38919	Dsk2

5.6 Plasmids

Protein mutations were described as suggested by Dunnen and Antonarakis (265).

Table 6: Plasmids

Plasmid	Insert	Promoter	3'-UTR	Alternative name	Purpose
pFSR-0092	LacZ	LacPro	-	-	9)
pFSR-0207	HA-NLS-CycB-S286_K530del-2XGFP	MtPro	-	CycB-N285-2XGFP	*1)*
pFSR-0251	4XFLAG-Rca1	MtPro	SV40UTR	-	3), 6)
pFSR-0255	Rca1	T7	-	-	2)
pFSR-0372	4XFLAG-Rca1-Q164_L203delinsPG	MtPro	SV40UTR	4XFLAG-Rca1-dFbox	3)
pFSR-0419	HA-CycE	MtPro	CycE-3'UTR	-	3), 4)
pFSR-0440	6XHIS-TEV-FLAG-Fzr	PhPro	SV40UTR	-	10)
pFSR-0456	4XFLAG-Rca1	SP6	GloACUTR	-	*5)*
pFSR-0512	3XCherry	ActPro	SV40UTR	-	*1)*
pFSR-0574	3XCherry 4XFLAG-Rca1	ActPro MtPro	- SV40UTR	-	*1)*
pFSR-0594	3XCherry 4XFLAG-Rca1-Q164_L203delinsPG	ActPro MtPro	- SV40UTR	3XCherry_4XFLAG-Rca1-dFbox	*1)*
pFSR-0595	3XCherry 4XFLAG-Rca1-M182T	ActPro MtPro	- SV40UTR	3XCherry_4XFLAG-Rca1-M182T	*1)*
pFSR-0596	3XCherry 4XFLAG-Rca1-C351S	ActPro MtPro	- SV40UTR	3XCherry_4XFLAG-Rca1-C351S	*1)*
pFSR-0597	3XCherry 4xFLAG-Rca1-A344T	ActPro MtPro	- SV40UTR	3XCherry_4xFLAG-Rca1-A344T	*1)*
pFSR-0598	3XCherry 4XFLAG-Rca1-Q164_L203delinsPG-C351S	ActPro MtPro	- SV40UTR	3XCherry_4XFLAG-Rca1-dFbox-C351S	*1)*
pFSR-0599	4XFLAG-Fzr	SP6	GloACUTR	-	*5)*
pFSR-0659	4XFLAG-SkpA	MtPro	-	-	7)
pFSR-0665	Dap	T7	-	-	2)
pFSR-0696	*rca1*-5'UTR-*rca1*-3'UTR	T7	-	-	2)
pFSR-0705	3XCherry HA-NLS-GFP	ActPro MtPro	rca1UTR SV40UTR	3XCherry_GFP	3)
pFSR-0723	4XFLAG-Rca1-C351S	MtPro	SV40UTR	-	3)
pFSR-0725	4XFLAG-Rca1-Q164_L203delinsPG-C351S	MtPro	SV40UTR	4XFLAG-Rca1-dFbox-C351S	3)
pFSR-0753	3XCherry HA-NLS-GFP-Dap-K38_S44delinsRAR-E103_Y105delinsG-S205A-S214A	ActPro MtPro	rca1UTR SV40UTR	3XCherry_GFP-Dap-dCDI-S205A-S214A	3)

Plasmid	Insert	Promoter	3'-UTR	Alternative name	Purpose
pFSR-0754	3XCherry HA-NLS-GFP-Dap-K38_S44delinsRAR-E103_Y105delinsG-S205E-S214E	ActPro MtPro	rca1UTR SV40UTR	3XCherry_GFP-Dap-dCDI-S205E-S214E	3)
pFSR-0755	3XCherry HA-NLS-GFP-Dap-K38_S44delinsRAR-E103_Y105delinsG	ActPro MtPro	rca1UTR SV40UTR	3XCherry_GFP-Dap-dCDI	3)
pFSR-0778	3XCherry HA-NLS-GFP-Dap-K38_S44delinsRAR-E103_Y105delinsG-Q184_T188del	ActPro MtPro	rca1UTR SV40UTR	3XCherry_GFP-Dap-dCDI-dPIPa	3)
pFSR-0781	3XCherry HA-NLS-GFP-Dap-K38_S44delinsRAR-E103_Y105delinsG-Q184_T188del-M191_K195del-Q184A-I187A-T188A-F190A-M191A-K195A	ActPro MtPro	rca1UTR SV40UTR	3XCherry_GFP-Dap-dCDI-6A	3)
pFSR-0790	3XCherry HA-NLS-GFP-Dap-K38_S44delinsRAR-E103_Y105delinsG-Q184_T188del-M191_K195del	ActPro MtPro	rca1UTR SV40UTR	3XCherry_GFP-Dap-dCDI-dPIP	3)
pFSR-0799	3XCherry HA-NLS-GFP-Dap-K38_S44delinsRAR-E103_Y105delinsG-Q184_T188del-S205A-S214A	ActPro MtPro	rca1UTR SV40UTR	3XCherry_GFP-Dap-dCDI-dPIPa-S205A-S214A	3)
pFSR-0800	6XHis-TEV-FLAG-NES-Fzr	PhPro	SV40UTR	-	10)
pFSR-0832	HA-NLS-GFP-Dap-K38_S44delinsRAR-E103_Y105delinsG-Q184_T188del	MtPro	SV40UTR	GFP-Dap-dCDI-dPIPa	4)
pFSR-0837	4XFLAG-Rca1	PubPro	ryUTR	-	4)
pFSR-0843	4XFLAG-Rca1-UBA(Dsk2)	PubPro	ryUTR	-	4)
pFSR-0846	4XFLAG-Dap-K38_S44delinsRAR-E103_Y105delinsG-Q184_T188del	MtPro	SV40UTR	4XFLAG-Dap-dCDI-dPIPa	6)
pFSR-0848	UBA(Rad23)-4XFLAG-Rca1	PubPro	ryUTR	-	4)

Plasmid	Insert	Promoter	3'-UTR	Alternative name	Purpose
pFSR-0849	UBA(Dsk2)-4XFLAG-Rca1	PubPro	ryUTR	-	4)
pFSR-0850	4XFLAG-Rca1-UBA(Rad23)	PubPro	ryUTR	-	4)
pFSR-0856	Cul4	T7	-	-	2)
pFSR-0859	Beta-lactamase	T7	-	-	2)
pFSR-0876	3XCherry 4xFLAG-Rca1-L160D-Q164P-P165G-I170T	ActPro MtPro	- SV40UTR	3XCherry_4xFLAG-Rca1-L160D-I170T	*1)*
pFSR-0899	3XCherry HA-NLS-GFP-Dap-M1_D125del-Q184_T188del	ActPro MtPro	rca1UTR SV40UTR	3XCherry_GFP-Dap-Del-1-125-dPIPa	3)
pFSR-0900	3XCherry HA-NLS-GFP-Dap-M1_N53del-Q184_T188del	ActPro MtPro	rca1UTR SV40UTR	3XCherry_GFP-Dap-Del-1-53-dCDI-dPIPa	3)
pFSR-0929	GFP Hpt	PubPro CopPro	- SV40UTR	GFP_stable-cell-line	
pFSR-0934	(6XHIS-4XFLAG-Ubiquitin)X2	PubPro	ryUTR	6XHIS-4XFLAG-Ub	8)
pFSR-0952	4XFLAG-Skp2	PubPro	ryUTR	-	11)
pFSR-0955	3XHA-Rca1	PubPro	ryUTR	-	4), 7), 8)
pFSR-0977	3XHA-Rca1-Q164_L203delinsPG	PubPro	ryUTR	3XHA-Rca1-dFbox	4), 7)
pFSR-1001	HA-NLS-GFP-Dap-K38_S44delinsRAR-E103_Y105delinsG-Q184_T188del	PubPro	ryUTR	HA-NLS-GFP-Dap-dCDI-dPIPa	4)
pFSR-1020	Cdc16-MYC-TEV-GFP Hpt	PubPro CopPro	- SV40UTR	Cdc16-GFP_stable-cell-line	12)
pFSR-1027	3XCherry HA-NLS-GFP-Dap-K38_S44delinsRAR-E103_Y105delinsG-Q184_T188del-R194A	ActPro MtPro	rca1UTR SV40UTR	3XCherry_GFP-Dap-dCDI-dPIPa-R194A	3)
pFSR-1046	4XFLAG-Dap-M1_D125del-Q184_T188del	PubPro	ryUTR	4XFLAG-Dap-Del-1-125-dPIPa	4)
pFSR-1047	4XFLAG-Dap-M1_N53del-K38_S44delinsRAR-E103_Y105delinsG-Q184_T188del	PubPro	ryUTR	4XFLAG-Dap-Del-1-53-dCDI-dPIPa	4)
pFSR-1050	3XCherry HA-NLS-GFP-Dap-K38_S44delinsRAR-E103_Y105delinsG-R194A	ActPro MtPro	rca1UTR SV40UTR	3XCherry_GFP-Dap-dCDI-R194A	3)

Plasmid	Insert	Promoter	3'-UTR	Alternative name	Purpose
pFSR-1051	3XCherry HA-NLS-GFP-Dap-K38_S44delinsRAR-E103_Y105delinsG-Q184_T188del-R194A-S205A-S214A	ActPro MtPro	rca1UTR SV40UTR	3XCherry_GFP-Dap-dCDI-dPIPa-R194A-S205A-S214A	3)
pFSR-1085	4XFLAG-Dap-M1_S139del-Q184_T188del	PubPro	ryUTR	4XFLAG-Dap-Del-1-139dPIPa	4)
pFSR-1086	4XFLAG-Dap-M1_Q159del-Q184_T188del	PubPro	ryUTR	4XFLAG-Dap-Del-1-159-dPIPa	4)
pFSR-1088	4XFLAG-Dap-M1_T188del	PubPro	ryUTR	4XFLAG-Dap-Del-1-188	4)
pFSR-1113	4XFLAG-Rca1-G150_L203delinsPG	MtPro	SV40UTR	4XFLAG-Rca1-dFbox-full	3)
pFSR-1114	3XHA-Rca1-M1_E99del	PubPro	ryUTR	3XHA-Rca1-Del-1-99	8)
pFSR-1115	3XCherry HA-NLS-GFP-Dap-K38_S44delinsRAR-E103_Y105delinsG-Q184_T188del-R194A-L197A	ActPro MtPro	rca1UTR SV40UTR	3XCherry_GFP-Dap-dCDI-dPIPa-R194A-L197A	3)
pFSR-1138	3XHA-Rca1-G150_L203delinsPG	PubPro	ryUTR	3XHA-Rca1-dFbox-full	4), 7), 8)
pFSR-1139	3XHA-Rca1-M1_L203del	PubPro	ryUTR	3XHA-Rca1-Del-1-203	4)
pFSR-1140	4XFLAG-Dap-K38_S44delinsRAR-E103_Y105delinsG-Q184_T188del-R194A-L197A	PubPro	ryUTR	4XFLAG-Dap-dPIPa-R194A-L197A	4)
pFSR-1148	3XCherry HA-NLS-GFP-Dap-K38_S44delinsRAR-E103_Y105delinsG-R194A-L197A	ActPro MtPro	rca1UTR SV40UTR	3XCherry_GFP-Dap-dCDI-R194A-L197A	3)
pFSR-1155	3XHA-Rca1-M182T	PubPro	ryUTR	-	4), 7)
pFSR-1156	3XHA- Rca1-L160D-Q164P-P165G-I170T	PubPro	ryUTR	3XHA-Rca1-L160D-I170T	4), 7)
pFSR-1157	4XFLAG-Dap-K38_S44delinsRAR-E103_Y105delinsG-Q184_T188del-M191_K195del	PubPro	ryUTR	4XFLAG-Dap-dCDI-dPIP	4)
pFSR-1158	3XHA-Rca1-Q204_F411del	PubPro	ryUTR	3XHA-Rca1-Del-204-411	4)

Plasmid	Insert	Promoter	3'-UTR	Alternative name	Purpose
pFSR-1162	4XFLAG-Dap-K38_S44delinsRAR-K54_N245del	PubPro	ryUTR	4XFLAG-Dap-dCDI-Del-54-245	4)
pFSR-1163	4XFLAG-Dap -K38_S44delinsRAR-E103_Y105delinsG-I126_N245del	PubPro	ryUTR	4XFLAG-Dap-dCDI-Del-126-245	4)
pFSR-1190	4XFLAG-Dap-K38_S44delinsRAR-E103_Y105delinsG-Q184_T188del-S205A-S214A	PubPro	ryUTR	4XFLAG-Dap-dCDI-dPIPa-S205A-S214A	4)

1) *In vivo* APC/C-Fzr activity assay
2) Production of dsRNA for RNA interference
3) Analysis of Dap stability by flow cytometry
4) Interaction studies between Rca1 and Dap
5) *In vitro* translation
6) Analysis of interaction partners by mass spectrometry
7) Interaction studies between Rca1 and SkpA
8) Interaction studies between Rca1 and Ubiquitin
9) Empty DNA for transfection
10) Purification
11) Interaction studies between Rca1 and Skp2
12) Production of stable S2R+ cell line

5.7 Bacterial strains

Table 7: Bacterial strains

Strain	Genotype	Distributor
DH10EmBacY (chemically competent)	F⁻*mcr*A Δ(*mrr*-hsdRMS-*mcr*BC) Φ80*lac*ZΔM15 Δ*lac*X74 *rec*A1 *end*A1 *ara*D139 Δ(*ara*, *leu*)7697 *gal*U *gal*K λ⁻*rps*L *nup*G/EMBacY/pMON7124	AG Längst
DH5 alpha (electrocompetent)	F⁻ *endA1 glnV44 thi-1 recA1 relA1 gyrA96 deoR nupG purB20* ϕ80d*lacZ*ΔM15 Δ(*lacZYA-argF*)U169, hsdR17($r_K^- m_K^+$), λ⁻	AG Sprenger

5.8 Eukaryotic cell lines

Table 8: Cell lines

Strain	Transgenic element	Distributor
Cdc16-MYC-TEV-GFP	pUbPro-Cdc16-MYC-TEV-GFP_CopPro-Hph	Own production
GFP	pUbPro-GFP_CopPro-Hph	Own production
S2R+	-	AG Sprenger
SF21	-	AG Längst

5.9 Antibodies

5.9.1 Primary antibodies

Table 9: Primary antibodies used for western blot analysis

Antigen	Number	Source	Western Blot	Co-IP	Distributor
Cherry	362	Rabbit	1:2000	-	Unknown
FLAG	374	Mouse	1:5000	1:500	Sigma
GFP	387	Mouse	1:2000	1:250	Roche
HA	373	Mouse	1:2000	-	Cavance

5.9.2 Secondary antibodies

Table 10: Secondary antibodies used for the detection of proteins in the Odyssey system

Antigen	Number	Source	Fluorochrome	Dilution	Distributor
Mouse	381	Goat	IRDye 680LT	1:5000	Li-Cor
Rabbit	366	Goat	IRDye 680	1:5000	Li-Cor

5.10 Solutions and buffers

Table 11: Solutions and buffers

Solution/buffer	Components	Concentration
Ampicillin stock solution	Ampicillin In 50 % glycerol	50 mg/ml
APS solution 10 %	APS In H_2O	10 % (w/v)
Cell Lysis Solution (from PureYield Plasmid Midiprep system)	NaOH SDS In H_2O	0.2 M 1 % (v/v)
Cell Resuspension Solution (from PureYield Plasmid Midiprep system)	Tris, pH 7.5 EDTA RNase A In H_2O	50 mM 10 mM 100 µg/ml

Solution/buffer	Components	Concentration
Chromatography elution buffer	HEPES, pH 7.7 NaCl Imidazole Beta-Mercaptoethanol In H_2O	20 mM 100 mM 1 M 10 mM
Chromatography running buffer	HEPES, pH 7.7 NaCl Imidazole Beta-Mercaptoethanol In H_2O	20 mM 500 mM 10 mM 10 mM
Column Wash Solution	Tris, pH 7.5 Potassium acetate EDTA, pH 8.0 For use dilute 2:5 in 99 % EtOH	22.6 mM 162.8 mM 0.109 mM
Coomassie destaining solution	Acetic acid Ethanol In H_2O	10 % (v/v) 40 % (v/v)
Coomassie staining solution	Coomassie Brilliant Blue Acetic acid Ethanol In H_2O	0.1 % (w/v) 10 % (v/v) 40 % (v/v)
Dialysis buffer	HEPES, pH 7.7 NaCl Beta-Mercaptoethanol In H_2O	20 mM 500 mM 10 mM
DNA/RNA Loading buffer 10X	Bromphenol blue Xylene cyanol EDTA, pH 8.0 Tris, pH 7.8 Glycerol In H_2O For analysis of DNA bands with low molecular weight DNA loading buffer without Bromphenol blue was used.	0.25% (w/v) 0.25% (w/v) 1 mM 10 mM 50% (v/v)

Solution/buffer	Components	Concentration
dNTP mix (2 mM each)	dNTP mix In H_2O	2 mM
EasyPrep buffer	Tris, pH 8.0 EDTA, pH 8.0 Sucrose Lysozym RNase A BSA In H_2O	10 mM 1 mM 150 mg/ml 2 mg/ml 0.2 mg/ml 0.1 mg/ml
IP Lysis buffer	HEPES, pH 7.5 NaCl EGTA NaF Triton X-100 Glycerol In H_2O For use Protease inhibitor mix is freshly added.	50 mM 150 mM 1 mM 10 mM 1 % (v/v) 10 % (v/v)
IP Washing buffer	HEPES, pH 7.5 NaCl Triton X-100 Glycerol In H_2O	50 mM 150 mM 1 % (v/v) 10 % (v/v)
Kanamycin stock solution	Kanamycin In H_2O	50 mg/ml
LSB 2X	Tris, pH 6.8 SDS Glycerol Bromphenol blue Beta-Mercaptoethanol In H_2O	120 mM 4 % (w/v) 20 % (v/v) 0.04 % (w/v) 10 % (v/v)
LSB, non-reducing 2X	Tris, pH 6.8 SDS Glycerol Bromphenol blue In H_2O	120 mM 4 % (w/v) 20 % (v/v) 0.04 % (w/v)

Solution/buffer	Components	Concentration
Milk powder solution	Skim milk powder Sodium azide In PBS	5 % (m/v) 0.01 % (m/v)
MS Lysis buffer (from FLAG Tagged Protein Immunoprecipitation Kit)	Tris, pH 7.4 NaCl EDTA Triton X-100 In H_2O For use Protease inhibitor mix is freshly added.	50 mM 150 mM 1 mM 1 % (v/v)
MS Trypsin Solution	Trypsin Gold, Mass Spectrometry Grade In 50 mM NH_4HCO_3	30 % (v/v)
MS Washing buffer (from FLAG Tagged Protein Immunoprecipitation Kit)	HEPES, pH 7.4 NaCl In H_2O	50 mM 150 mM
MS Washing Solution I	AcN In 50 mM NH_4HCO_3	25 % (v/v)
MS Washing Solution II	AcN In 50 mM NH_4HCO_3	50 % (v/v)
Neutralization Solution (from PureYield Plasmid Midiprep system)	Guanidine hydrochloride, pH 4.2 Potassium acetate Glacial acetic acid In H_2O	4.09 M 759 mM 2.12 M
NTP mix (25 mM each)	ATP CTP GTP UTP	25 mM 25 mM 25 mM 25 mM
PBS	NaCl Na_2HPO_4 NaH_2PO_4 pH In H_2O	130 mM 7 mM 3 mM 7.2

<table>
<tr><th>Solution/buffer</th><th>Components</th><th>Concentration</th></tr>
<tr><td>PBT</td><td>Tween 20

In PBS</td><td>0.1 % (v/v)</td></tr>
<tr><td>Resolving gel (SDS PAGE)</td><td colspan="2"><u>For 10 ml resolving gel:</u>
<table>
<tr><th>Gel</th><th>H_2O (ml)</th><th>Acrylamide 30%/ Bisacrylamide (µl)</th><th>1.5 M Tris/HCl pH 8.8 (µl)</th><th>10 % SDS (µl)</th><th>10 % APS (µl)</th><th>TEMED (µl)</th></tr>
<tr><td>6%</td><td>5.4</td><td>2.0</td><td>2.5</td><td>0.1</td><td>100</td><td>10</td></tr>
<tr><td>7%</td><td>5.1</td><td>2.3</td><td>2.5</td><td>0.1</td><td>100</td><td>10</td></tr>
<tr><td>8%</td><td>4.7</td><td>2.7</td><td>2.5</td><td>0.1</td><td>100</td><td>10</td></tr>
<tr><td>9%</td><td>4.4</td><td>3.0</td><td>2.5</td><td>0.1</td><td>100</td><td>10</td></tr>
<tr><td>10%</td><td>4.1</td><td>3.3</td><td>2.5</td><td>0.1</td><td>100</td><td>10</td></tr>
<tr><td>11%</td><td>3.7</td><td>3.7</td><td>2.5</td><td>0.1</td><td>100</td><td>10</td></tr>
<tr><td>12%</td><td>3.4</td><td>4.0</td><td>2.5</td><td>0.1</td><td>100</td><td>10</td></tr>
<tr><td>13%</td><td>3.1</td><td>4.3</td><td>2.5</td><td>0.1</td><td>100</td><td>10</td></tr>
<tr><td>14%</td><td>2.7</td><td>4.7</td><td>2.5</td><td>0.1</td><td>100</td><td>10</td></tr>
<tr><td>15%</td><td>2.4</td><td>5.0</td><td>2.5</td><td>0.1</td><td>100</td><td>10</td></tr>
</table>
Resolving gels were stored as 50 ml stock solutions without APS and TEMED.</td></tr>
<tr><td>SDS solution 10 %</td><td>SDS

In H_2O</td><td>10 % (w/v)</td></tr>
<tr><td>Stacking gel (SDS PAGE)</td><td colspan="2"><u>For 10 ml stacking gel:</u>
<table>
<tr><th>Gel</th><th>H_2O (ml)</th><th>Acrylamide 30%/ Bisacrylamide (µl)</th><th>1.5 M Tris/HCl pH 6.8 (µl)</th><th>10 % SDS (µl)</th><th>10 % APS (µl)</th><th>TEMED (µl)</th></tr>
<tr><td>4%</td><td>6.1</td><td>1.3</td><td>2.5</td><td>0.1</td><td>100</td><td>10</td></tr>
</table>
Stacking gel was stored as 50 ml stock solution without APS and TEMED.</td></tr>
<tr><td>TAE buffer</td><td>Tris, pH 8.0
EDTA

In H_2O</td><td>40 mM
10 mM</td></tr>
</table>

Solution/buffer	Components	Concentration
Transcription buffer 5X (SP6, T7)	HEPES, pH 7.5 Spermidine DTT NTPs (ATP, CTP, GTP, UTP) $MgCl_2$ In H_2O	80 mM 2 mM 10 mM 3 mM 12 mM
Transfer buffer 3 (Western blot)	Methanol Tris, pH 7.5 EDTA, pH 8.0 Sodium acetate SDS In H_2O	20 % (v/v) 40 mM 2 mM 20 mM 0.05 % (v/v)
Turbo Laemmli running buffer 10X	Tris Glycin SDS In H_2O	250 mM 9,46 M 10 g/l
Ubiquitination buffer 10X	Tris, pH 7.5 ATP $MgCl_2$ DTT In H_2O	500 mM 20 mM 50 mM 20 mM

5.11 Media and agar plates

Antibiotics and Reagents were used in following concentrations: ampicillin 50 µg/ml; kanamycin 50 µg/ml; tetracycline 10 µg/ml; gentamycin 10 µg/ml; IPTG 1 mM, X-gal 200 µg/ml.

Table 12: Media and agar plates

Medium/Agar plate	Components	Concentration
Drosophila freezing medium	Schneider's *Drosophila* complete medium (conditioned) Schneider's *Drosophila* complete medium DMSO	45 % (v/v) 45 % (v/v) 10 % (v/v)
LB agar plate	Euroagar In LB medium (autoclaved) Solution is boiled for casting plates. Before adding any antibiotic, the solution is first cooled down to 50 °C.	1.7 % (w/v)
LB medium (autoclaved)	BactoTrypton Bacto Yeast Extract NaCl pH In H_2O	10 g/l 5 g/l 10 g/l 7.2
Schneider's *Drosophila* complete medium	GIBCO FBS Penicillin Streptomycin In Schneider's *Drosophila* Medium	10 % (v/v)
Schneider's *Drosophila* hygromycin medium	Hygromycin B Gold In Schneider's *Drosophila* complete Medium	100 µg/ml
SOC Medium (sterile filtrated)	BactoTrypton Bacto Yeast Extract NaCl KCl $MgCl_2$ Glucose In H_2O	20 g/l 5 g/l 10 mM 2.5 mM 10 mM 20 mM

Medium/Agar plate	Components	Concentration
TY medium 2X	BactoTrypton Bacto Yeast Extract NaCl In H_2O	1.6 % 1 % 0.5 %
TYE agar plate	BactoTrypton Bacto Yeast Extract NaCl Euroagar In H_2O Solution is boiled for casting plates. Before adding any antibiotic/reagents, the solution is first cooled down to 50 °C.	1 % (w/v) 0.5 % (w/v) 0.8 % (w/v) 1.5 % (w/v)

5.12 Consumable material

Table 13: Consumable material

Equipment	Manufacturer
12-well plate	Cellstar
6-well plate	Sarstedt
Amicon Ultra 10K device (MWCO: 10,000)	Merck
Axygen 200 µl Maxymum Recovery Pipet Tips (for MS)	Axygen Scientific
Cell culture flask, 250 ml, 75 cm²	Cellstar
Cell scraper	Sarstedt
Cryo vial	Greiner Bio-One
Cups (0.5 ml, for MS)	Axygen Scientific
Cups (1.5 ml, 2 ml)	Eppendorf, Sarstedt
Electroporation cuvettes	Peqlab
Falcons 15 ml, 50 ml	Sarstedt
Filter pipette tips 10 µl, 20 µl, 200 µl	Axygen Scientific, VWR
GIBCO FBS (fetal bovine serum)	Invitrogen GmbH
GIBCO Sf-900 II SFM	Invitrogen GmbH
Glass pasteur pipettes 150 mm	BRAND
Latex gloves	Roth
Nitrile gloves	VWR
Nitrocellulose membrane	Schleicher & Schuell BioScience
Paper towel Waschfix	Fripa
Parafilm “M” Laboratory Film	Pechiney
PCR-Cups 200 µl	Sarstedt
Petri dishes 92 X 16 mm	Sarstedt
Pipet tips 10 µl, 200 µl, 1000 µl	Sarstedt
ProteinG agarose beads	Santa Cruz Biotechnology
Serological pipettes 10 ml	Cellstar

Equipment	Manufacturer
Spectra/Por Dialysis Membrane (MWCO: 6-8,000)	Spectrum
Syringe filter 0.45 µm	Millipore
Trypsin Gold, Mass Spectrometry Grade	Promega
Trypsin/EDTA solution	PAN Biotech
Tube 3.5 ml	Sarstedt
Whatman paper	Whatman International Ltd

5.13 Software

DELL Optiplex 755 computers installed with following programs were used for the analysis and presentation of results:

Table 14: Used software

Software	Developer
Canvas 11	ACD Systems International Inc.
Compass 1.7	Bruker Daltonics
Data Analysis 4.2	Bruker Daltonics
Endnote X7.5	Thomson Reuters Corp.
FCS Express 4.07	De Novo Software
Filemaker Pro 15	Filemaker Inc.
GSP-ARM: Predictor for APC/C Recognition Motif 1.0	The CUCKOO Workgroup
IBS: Illustrator for Biological Sequences	The CUCKOO Workgroup
ImageJ 1.50i	NIH
KinasePhos 2.0	Wong et al. (249)
Mascot 2.5.1	Matrix Science
Microsoft Office Professional Plus 2016	Microsoft Corp.
NLS Mapper	Kosugi et al. (234, 266, 267)
Protein Scape 3.1.3	Bruker Daltonics
Vektor NTI Advance 11	Invitrogen

5.14 Equipment

Table 15: Used equipments in the various laboratories

Equipment	Manufacturer
Acclaim Pepmap100 C18 nano column (75 µm i.d. × 150 mm)	Thermo Fisher
Acrylamide gel apparatus	Bio-Rad Laboratories
Agarose gel electrophoresis apparatus HE33	Hoefer
Beaker 250 ml, 500 ml, 5 L	Schott, VITLAB, VWR
C18 Acclaim Pepmap100 preconcentration column (100µm i.D.x20mm)	Thermo Fisher
Caps with holes for 0.5 ml Axygen Cups	Own production
Caps with holes for 1.5 ml Cups	Own production
CaptiveSpray nanoflow electrospray source	Bruker Daltonics
Cell culture incubator	Hereaus
Cellculture roller TC-7	New Brunswick Scientific

Equipment	Manufacturer
Centrifuge 5418	Eppendorf
Centrifuge Heraeus Multifuge 1S	Thermo Scientific
Centrifuge RC-5b	Sorvall
Centrifuge Sorvall RC 2B, 5C plus	Du Pont Instruments
Clean bench	Ceag Schirp Reinraumtechnik
Clean bench Mars Safety Class 2	SCANLAF
Culture roller drum TC-7	New Brunswick Scientific
Electrophoresis power supply EPS 200/600	Pharmacia Biotech
Electroporation apparatus Easyject Prima	Equibio
Erlenmeyer flask	DURAN Group GmbH
FastPette V2 Pipette Controller	Labnet
Flow cytometer CyFlow space	Partec
FPLC System ÄKTA purifier 10	GE Healthcare
Freezer	AEG, Bosch, Siemens
Freezer C760	New Brunswick Scientific
Fuchs-Rosenthal Counting chamber (16 mm^2, 0.2 mm cell depth)	Hausser Scientific
Glass bottle 250 ml, 500 ml, 1 L	Schott
Glass pipettes 1 ml, 5 ml, 10 ml, 25 ml	Hirschmann
Glass tube	Schuett-biotec
Gyrotory Water Bath shaker G76	New Brunswick Scientific
Heating block (Digital Dry Bath, dual position)	Benchmark Scientific
HisTrap FF Crude 5 ml (affinity column)	GE Healthcare
Ice Bucket	Unknown
Ice maker MF22	Scotsman
Incubator Heraeus B 5050 E	Heraeus
Incubator Sanyo MIR-153	Sanyo
Incubator WB120K (equipped with culture roller drum TC-7)	Mytron
Inverted microscope CKX41 (equipped with Reflected Fluorescence System with Light Source X-Cite 120Q)	Olympus
Magnetic stirrer	Heidolph
Marienfeld Superior counting chamber	Marienfeld
MaXis plus UHR-QTOF System	Bruker Daltonics
Measuring cylinder	VITLAB
Microliter syringe 705	Hamilton
Microwave	Vestel
Odyssey Infrared Imaging system	LI-COR
PerfectBlue Semi-Dry Electro Blotter	Peqlab
PH meter 766 Caltimatic	Knick
Plastic boxes 11 cm x 7 cm x 4 cm(Coomassie/Antibody staining)	Unknown
Portable light table	Unknown
RED Imaging System	Biozym
Reflected Fluorescence System	Olympus
Refrigerator	AEG, Bosch
Rocking Shaker ST 5	Ingenieurbüro CAT M. Zipperer GmbH
Scale Kern EW6200-2NM	Kern & Sohn GmbH
Scale MC1	Sartorius
Scale Mettler AE50	Mettler Toledo Intl. Inc.
Scalpel	Bayka
Sieve (2 cm^2 diameter)	Own production
Sonifier Branson 250D	Heinemann

Equipment	Manufacturer
Spectrophotometer / Fluorometer DS-11 FX+	DeNovix
Syringe Omnifix 60 ml	Braun Biotech
Table centrifuge ROTOFIX 32 A	Hettich
Test-Tube-Rotator 34528	Snijders Scientific
Thermocycler GTC96S	Cleaver Scientific Ltd
Thermocycler UNO II	Biometra
ThermoMixer F1.5	Eppendorf
UltiMate 3000 RSLCnano UHPLC System	Thermo Fisher
UV Crosslinker	Stratalinker
UV table TF-20 M	VilbertLourmat
Vacuum Blotting Pump, 2016 Vacugene	LKB Bromma
Vacuum gas pump VP86	VWR
Vacuum manifold	Promega
Vortex-Genie	WINN
Water purification system	ELGA
Wide-Field Fluorescence Microscope Excitation Light Source X-Cite 120Q	Excelitas Technologies

6 Methods

6.1 DNA/RNA methods

6.1.1 Molecular cloning

The generation of recombinant DNA (molecular cloning) was first simulated by using the software Vector NTI Advance 11. After that, cloning steps were performed as follows (see Table 16):

Table 16: Timetable for molecular cloning

Time	Protocol	Result
Day 1	1) When necessary, amplification of Insert DNA by PCR (see section 6.1.2). 2) Restriction enzyme digestion of plasmid DNA carrying Vector/Insert and/or amplified PCR DNA, respectively (see section 6.1.9). 3) Isolation of Insert and Vector DNA by gel electrophoresis (see section 6.1.3) and subsequent DNA isolation (see section 6.1.7.3, 6.1.7.4). 4) Quantification of isolated Vector and Insert DNA (see section 6.1.8.2). 5) When necessary, DNA modification of Vector: Dephosphorylation (see section 6.1.10), Blunting (see section 6.1.11). 6) Ligation of Vector and Insert DNA (see section 6.1.12).	Digested Vector DNA and Insert DNA.
Day 2	Transformation of ligation mix (see section 6.1.4).	LB agar plates coated with transformed *E. coli*.
Day 3	Picking of several clones for preparation of pre-cultures (see section 6.1.6).	Pre-cultures for screening.
Day 4	1) Mini scale plasmid DNA isolation from pre-cultures (see section 6.1.7.1). 2) Identification of recombinant clones by test digestion of isolated plasmid DNA (see section 6.1.9). 3) Preparation of main-culture with positive pre-culture (see section 6.1.6).	Main-culture of recombinant clone.
Day 5	1) Midi scale plasmid DNA isolation from main-culture (see section 6.1.7.2). 2) Analysis of yield and purity of isolated recombinant plasmid DNA (see section 6.1.8.1). 3) When Plasmid DNA is required for transfection, DNA is additionally quantified by gel analysis (see section 6.1.8.2).	Recombinant plasmid DNA.

6.1.2 DNA amplification by PCR

Polymerase chain reaction (PCR) was applied as method for the amplification of DNA fragments according to Mullis et al. (268). PCR reactions were catalyzed by a *Pyrococcus*-like enzyme fused with a processivity-enhancing domain (Phusion) in following reaction mixes (see Table 17):

Table 17: PCR reaction mix

Component	Amount
Phusion	0.5 µl
5X Phusion HF/GC buffer	10 µl
(Phusion GC buffer for GC rich templates)	
dNTP mix (2 mM each dNTP)	5 µl
Forward primer	1 µl
Reverse primer	1 µl
DNA (template)	100 ng
H_2O	Ad 50 µl
Total reaction volume	**50 µl**

The amplification of DNA was performed with following PCR program (see Table 18):

Table 18: PCR program

Step	Temperature	Duration	Cycles
1: Initial denaturation	96 °C	30 sec	
2: Denaturation	96 °C	10 sec	30
3: Primer annealing	62° C	20 sec	
4: Elongation	72 °C	40 sec/1 kb	
5: Final elongation	72 °C	5 min	
6: Hold	4 °C	∞	

Amplified PCR DNA was purified using the MSB Spin PCRapace Kit according to the manufacturer's instructions. Elution was carried out in 30 µl.

6.1.3 Agarose gel electrophoresis

The separation of DNA fragments was carried out by agarose gel electrophoresis. 0.4 g agarose was boiled up in 40 ml TAE buffer (1 % agarose) and additionally mixed with 10 mg/ml ethidium bromide. After the gel has cooled down, DNA samples were mixed with 10X loading buffer and loaded on gel. Additionally, the 1 kb Gene Ruler Mix was loaded on gel. Gels were run for 45 minutes at 90 volts. For analytical purposes, separated DNA bands were visualized in a Red Imaging System, in which the gel was exposed to UV light at 365 nm. The result was saved digitally for further processing.

6.1.4 Transformation of electrocompetent cells

Plasmid DNA was transformed in *E. coli* cells (DH5α) by electroporation by following protocol:

1) A 100 µl aliquot of electrocompetent cells is thawed and mixed with 100 µl H_2O.
2) 100 µl of the diluted cells are transferred into an electroporation cuvette.
3) 1 µl plasmid DNA are added to the cell suspension.
4) Electroporation with following electroporater settings: voltage 2.5 kV, capacitance 25 µF and resistance 200 ohms.
5) Cell suspension is transferred into 1 ml SOC medium for regeneration.
6) When an antibiotic other than ampicillin was used, cell suspension is rotated for 90 min at 37 °C.
7) 100 µl of the cell suspension are plated on a LB plate containing the appropriate antibiotic. The plate is incubated overnight at 37 °C.

6.1.5 Transformation of chemically competent cells

Chemically competent *E. coli* cells were transformed as follows:

1) A 100 µl aliquot of chemically competent cells is thawed on ice.
2) Around 100 ng of plasmid DNA are added to the cell suspension.
3) The cells are kept on ice for 20 min.
4) The cells are heat shocked at 40 °C for 30 sec and subsequently kept on ice for 2 min.
5) The cells are transferred in 900 µl SOC medium.
6) When an antibiotic other than ampicillin was used, cell suspension is rotated for 90 min at 37 °C.
7) 100 µl of the cell suspension are plated on an agar plate containing the appropriate antibiotic. The plate was incubated overnight at 37 °C.

6.1.6 Preparation of *E. coli* cultures

E. coli cultures were prepared by inoculating LB liquid medium with a picked single colony grown on a LB agar plate. Depending on the purpose, either 3 ml (test tube, pre-culture) or 50 ml (Erlenmeyer flask, main-culture) LB liquid medium containing the appropriate antibiotic were used for inoculation. The cell suspension was rotated overnight at 37 °C.

6.1.7 Isolation of DNA

6.1.7.1 Mini scale isolation of plasmid DNA

For the analysis of recombinant clones, low amounts of plasmid DNA were isolated according to Berghammer and Auer (269) by following protocol:

1) 2 ml cells of a 3 ml overnight pre-culture are centrifuged in a 2 ml cup for 1 min at 14,000 rpm.
2) The supernatant is discarded and the pellet is resuspended in 40 µl EasyPrep buffer.
3) The bacterial suspension is boiled for 1 min.
4) The bacterial suspension is cooled down for 2 min on ice.
5) Cell material is centrifuged off for 2 min at 14,000 rpm.

6.1.7.2 Midi scale isolation of plasmid DNA

The isolation of large amount of plasmid DNA was based on the alkaline lysis procedure developed by Birnboim and Doly (270). Plasmid DNA was isolated using the Promega PureYield Plasmid Midiprep system according to the manufacturer's instructions:

1) 50 ml of a main culture are centrifuged in a 50 ml Falcon at 4,500 rpm for 10 minutes. Supernatant is discarded.
2) Cell pellet is resuspended in 3 ml Cell Resuspension Solution.
3) 3 ml Cell Lysis Solution are added to the cell suspension. Cell suspension is mixed gently by inverting the tube 3 – 5 times. The suspension is incubated for 3 minutes at room temperature.
4) 5 ml Neutralization Solution are added to the lysed cells. Solution is mixed by inverting the tube 3 – 5 times.
5) Protein precipitate is centrifuged off at 4,500 rpm for 25 minutes.
6) The PureYield Binding Column is placed onto the vacuum manifold.
7) The centrifuged lysate is poured through a sieve into the PureYield Binding Column (sieves are treated by UV light in an UV Crosslinker before use).
8) Vacuum is applied. Vacuum is continued until all the liquid has passed through the column.
9) 20 ml Column Wash Solution are added to the column. Vacuum is continued until the solution is drawn completely through the column.
10) The membrane is dried by applying a vacuum for 10 minutes.
11) The PureYield Binding Column is removed from the vacuum manifold. Excess ethanol is removed by tapping the tip of the column on a paper towel. The column is placed into a new 50 ml Falcon tube.
12) 700 µl sterile H_2O are added to the DNA binding membrane in the PureYield Binding Column.
13) The PureYield Binding Column is centrifuged at 1,500 rpm for 2 minutes.

After isolation, the DNA concentration was measured photometrically and the recovered plasmid DNA was stored at -20 °C.

6.1.7.3 Preparative isolation of DNA fragments from agarose gels

After separating DNA fragments in an agarose gel, the corresponding bands were cut out by a sterile scalpel on an UV table that emits UV light at 312 nm. The purification of the DNA from the excised agarose pieces was carried out by using the Invisorb Spin DNA Extraction Kit according to the manufacturer's instructions.

6.1.7.4 Isolation of DNA fragments after PCR

DNA fragments obtained by PCR were purified by the MSB Spin PCRapace Kit according to the manufacturer's instructions.

6.1.8 Quantification of DNA

6.1.8.1 Photometric quantification of purified DNA

Subsequent to DNA isolation, yield and purity of DNA was quantified spectrophotometrically, based on the absorbance at 260 nm and 280 nm. For this, 1 µl DNA was used for analyses.

6.1.8.2 Quantification of DNA/RNA by gel analysis

The amount of *in vitro* transcribed RNA as well as the concentration of plasmid DNA used for cell transfection was estimated by gel analysis. Depending on the DNA/RNA, different preparations were made (see Table 19):

Table 19: Preparation for quantification of DNA/RNA by gel analysis

DNA/RNA	Preparation	Loaded on gel
In vitro transcribed dsRNA	1:14 dilution in DNA/RNA loading buffer	4 µl
In vitro transcribed RNA	-	1 µl
Plasmid DNA for transfection	Restriction digestion that results in a linear fragment of around 1000 bps and around 100 ng (usually by BglI)	complete
Purified DNA fragments	-	3 µl

After gel electrophoresis (see section 6.1.3), the amounts of the loaded DNA/RNA fragments were determined by their band intensities. For the calculation of the DNA/RNA concentration, the intensities of the ladder bands that represent a distinct amount of DNA were used as reference. The quantification of DNA/RNA bands was performed by ImageJ.

6.1.9 Restriction digestion of DNA

Digestion of DNA was performed using restriction endonucleases in buffers and at temperatures recommended by the enzyme manufacturers. DNA was cut for 2 h. Depending on the purpose of the digestion, following reaction mix was prepared (see Table 20):

Table 20: Various reaction mixes for different types of restriction digestions

Component	Amount			
	Preparative digestion of plasmid DNA for cloning	**Digestion of purified PCR DNA**	**Test digestion of mini prep DNA**	**Test digestion of midi prep DNA**
DNA	5000 ng	30 µl	5 µl	500 ng
10X restriction buffer	4 µl	4 µl	1 µl	2 µl
Restriction enzyme	1 µl each	1 µl each	0.5 µl each	0.5 µl each
H_2O	Ad 40 µl	Ad 40 µl	Ad 10 µl	Ad 20 µl
Total volume	**40 µl**	**40 µl**	**10 µl**	**20 µl**

6.1.10 Dephosphorylation of DNA-ends

Dephosphorylation of DNA-ends was necessary when performing molecular cloning with vector DNA cut with only one restriction enzyme in order to prevent self-ligation. Dephosphorylation was catalyzed by the Shrimp Alkaline Phosphatase (rSAP) in following reaction mix (see Table 21):

Table 21: Reaction mix for dephosphorylation of vector DNA

Component	Amount
Digested vector DNA (preperative digestion)	20 µl
rSAP	1 µl
Total volume	**21 µl**

The reaction mix was incubated for 1 h at 37 °C and subsequently for 5 min at 65 °C to inactivate the phosphatase and to remove the phosphate molecules from the DNA-ends.

6.1.11 Blunting of DNA-ends

For ligation of incompatible 3’ or 5’ DNA overhangs, DNA-ends were blunted by T4-DNA-Polymerase filling in 5’ overhangs or removing 3’ overhangs, respectively. Blunting was performed in following reaction mix (see Table 22):

Table 22: Reaction mix for blunting of DNA

Component	Amount
Purified DNA	30 µl
NEBuffer 2.1	4 µl
dNTP mix (2 mM each dNTP)	2 µl
T4-DNA-Polymerase	2 µl
H2O	2 µl
Total volume	**40 µl**

The reaction mix was incubated for 15 min at 12 °C. After that, reaction was stopped by incubation for 20 min at 75 °C in presence of 10 mM EDTA. For ligation, the blunted DNA was purified using the MSB Spin PCRapace Kit according to the manufacturer's instructions.

6.1.12 Ligation of DNA fragments

For the ligation of DNA fragments, a molar ratio of vector to insert of 1:3 (sticky end ligation) or 1:6 (blunt end ligation) was chosen. The required amount of vector and insert DNA was estimated by gel analysis (see section 6.1.8.2). The ligation reaction mix consisted of the following components (see Table 23).

Table 23: Ligation reaction mix

Component	Amount
Vector DNA	50 ng
Insert DNA	x ng
10X T4 ligase buffer	2 µl
T4 DNA ligase	1 µl
H_2O	Ad 20 µl
Total volume	**20 µl**

In addition to this, a ligation reaction mix without insert DNA was performed as negative control to identify the background of vector self-ligation. The ligation mix was incubated overnight at room temperature.

6.1.13 Production of dsRNA for RNA interference

RNA mediated interference (RNAi) was applied as a simple and rapid method for the silencing of specific genes in S2R+ Schneider cells (271). RNAi was initiated by double stranded RNA constructs (dsRNAs) that were introduced into Drosophila S2R+ cells. DsRNA fragments were produced *in vitro* using plasmids that contain a part of the gene to be silenced flanked by two T7 promoters. Using this plasmid as template for T7 RNA polymerase, single stranded RNA molecules, in sense and antisense direction, are transcribed resulting in the formation of dsRNAs when annealed. To get an adequate amount of DNA template, the region with the flanking T7 promoters was first amplified by PCR (see section 6.1.2, Primer: SPO_288). *In vitro* transcription was performed according to Gurevich et al. (272) by following reaction mix (see Table 24).

Table 24: Reaction mix for the *in vitro* production of dsRNA

Component	Amount
5X transcription buffer	10 µl
PCR DNA (purified)	10 µl
T7 RNA polymerase	1.5 µl
NTP mix (25 mM each)	5 µl
RNase inhibitor	0.5 µl
H_2O	Ad 50 µl
Total volume	**50 µl**

The *in vitro* transcription mix was incubated overnight at 37 °C. Concentration of the produced dsRNA was determined by gel analysis. The dsRNA mix was stored at -20 °C until being used for RNAi experiments.

6.2 Protein methods

6.2.1 Analysis of interaction partners

6.2.1.1 Identification of protein interaction partners by mass spectrometry

Mass spectrometry was applied as an analytical technique for the identification of *in vivo* interaction partners of a protein of interest (bait protein) in S2R+ culture cells. The bait protein was terminally fused to a FLAG epitope, overexpressed and subjected to anti-FLAG immunoprecipitation. Co-precipitated proteins were separated by SDS-PAGE, stained with Coomassie, excised and in-gel trypsin digested. Tryptic peptides were sent to the MS facility (AG Deutzmann) for tandem mass spectrometric analysis (LC-MS/MS). LC-MS/MS analyses were performed with following components (A. Bruckmann, personal communication, November 18, 2016): Separation of peptides by reversed-phase chromatography was carried out on an UltiMate 3000 RSLCnano System which was equipped with a C18 Acclaim Pepmap100 preconcentration column (100µm i.D.x20mm) in front of an Acclaim Pepmap100 C18 nano column (75 µm i.d. × 150 mm). A linear gradient of 4% to 40% acetonitrile in 0.1% formic acid over 90 min was used to separate peptides at a flow rate of 300 nl/min. The LC-system was coupled on-line to a maXis plus UHR-QTOF System via a CaptiveSpray nanoflow electrospray source. Data-dependent acquisition of MS/MS spectra by CID fragmentation was performed at a resolution of minimum 60000 for MS and MS/MS scans. The MS spectra rate of the precursor scan was 2 Hz processing a mass range between m/z 175 and m/z 2000. Via the Compass 1.7 acquisition and processing software a dynamic method with a fixed cycle time of 3 s and an m/z dependent collision energy adjustment between 34 and 55 eV was applied. Raw data processing was performed in Data Analysis 4.2, and Protein Scape 3.1.3 in connection with Mascot 2.5.1 facilitated database searching of the UniProt *Drosophila* database (2015 April). Search parameters were as follows: enzyme specificity trypsin with 1 missed cleavage allowed, precursor tolerance 5 ppm, MS/MS tolerance 0.04 Da, carbamidomethylation or propionamide modification of cysteine, oxidation of methionine, deamidation of asparagine and glutamine were set as variable modifications. Mascot peptide ion-score cut-off was set 25. Search conditions were adjusted to provide a false discovery rate of less than 1%. Protein list compilation was done using the Protein Extractor function of Protein Scape. Samples for MS analyses were prepared as follows (see Table 25):

Table 25: Protocol for mass spectrometric analysis of protein interaction partners

Time	Protocol
Day 1	S2R+ cells are seeded in a 6-well plate (two wells per MS analysis, see section 6.2.12.6).
Day 2	Two S2R+ wells are transfected with the plasmid expressing the bait protein (see section 7.3.5).
Day 4	1) Cell culture medium in the wells is removed. 2) Adherent cells are scratched off the dish in 500 µl PBS using a cell scraper. 3) Cells are pooled in a 2 ml cup (from now on samples are kept at 4 °C). 4) Samples are centrifuged at 2,000 rpm for 10 min at 4 °C. 5) Cells are resuspended in 1 ml cold MS lysis buffer (containing protease inhibitors) and incubated for 20 min at 4 °C. 6) Samples are centrifuged at 12,000 rpm for 15 min at 4 °C. 7) 50 µl of supernatant are transferred in a 1.5 ml cup and stored at 4 °C (input sample). 8) 850 µl of supernatant are transferred in a 1.5 ml cup (IP sample). 9) Immunoprecipitation of the bait protein was performed using the FLAG Tagged Protein Immunoprecipitation Kit according to the manufacturer's instructions. 40 µl anti-FLAG-M2-agarose resin is washed twice with 1 ml MS washing buffer by centrifuging at 1,000 rpm for 1 min. Supernatant is removed using a Hamilton syringe and beads are resuspended in 40 µl MS washing buffer. 10) The IP sample is incubated with 40 µl pre-washed anti-FLAG-M2-agarose resin for 2 h at 4 °C under gentle rotation. 11) Beads in IP samples are washed three times with 1 ml MS washing buffer by centrifuging at 1,000 rpm for 1 min. Supernatant is discarded using the Hamilton syringe and beads are resuspended and boiled in 20 µl non-reducing 2X LSB for 5 min. 12) Supernatant is transferred in a 1.5 ml cup, mixed with 20 µl 2X LSB. Input sample is mixed with 50 µl 2X LSB. 13) All samples are boiled for 5 min. 14) Samples are centrifuged at 12,000 rpm for 1 min. **Break possible:** Sample can be stored at -20 °C. 15) Samples are separated by SDS-PAGE (see section 6.2.2): 20 µl of the input sample and 10 µl of the IP sample are loaded twice on two separate gels. One gel is used for evaluation of the precipitation using anti-FLAG antibodies (see section 6.2.4). The other gel is stained with Coomassie Brilliant Blue by shaking for 1 h in Coomassie staining solution. Destaining is carried out overnight in 7 % HAc. **Break possible:** Destained gel can be stored in H_2O at -4 °C.

Time	Protocol
Day 5	1) Coomassie stained proteins in the gel are detected at 700 nm using the Odyssey Infrared Imaging System. A picture of the lane showing the separated proteins of the IP sample is printed. 2) Using a portable light table, the lane of the gel is cut in several pieces with a sharp scalpel as follows: Visible protein bands are cut separately, whereas the rest of the lane is divided into gel pieces according to the ladder (region between two bands is usually divided into three gel pieces). Excised gel slices are further divided into small pieces and placed together in separate 2 ml Eppendorf Cups. Excised regions are marked and numbered on the printed picture, same numbering is used for the 2 ml Eppendorf Cups. **Break possible:** Gel pieces can be stored in liquid nitrogen and stored at -20 °C.
Day 6	1) Gel pieces are washed by shaking in 1 ml 50 mM NH_4HCO_3, 1 ml MS Washing Solution I and 1 ml MS Washing Solution II for 30 min each using a thermomixer. 2) Gel pieces are washed in 200 µl AcN by shaking them for another 10 min (gel pieces become smaller and get an opaque white color). 3) AcN is discarded, cups containing gel pieces are closed with caps containing holes and frozen in liquid nitrogen. 4) Gel pieces are lyophilized for 1 h. **Break possible:** Lyophilized gel pieces can be frozen in liquid nitrogen and stored at -20 °C. 1) Gel pieces are transferred into Axxygen 0.5 ml Cups. 2) Proteins are subjected to *in gel* tryptic digest as follows: 15 µl MS Trypsin Solution are added to the gel pieces and incubated for 15 min at room temperature. This is repeated until all gel pieces are filled completely with MS Trypsin Solution (gel pieces will become transparent). For digestion, gel pieces are coated with 50 µl NH_4HCO_3 and incubated overnight at 37 °C.
Day 7	1) Peptides are eluted as follows: Supernatants of the digested samples are transferred into 0.5 ml Axxygen cups using low binding tips (samples are kept at 4 °C). Remaining gel pieces are washed twice in 100 µl 100 mM NH_4HCO_3 at 37°C for 2h in a thermomixer. The last washing step is carried out in 100 µl MS Washing Solution II at 24 °C for 20 min. After each step, the supernatant is combined with the previous supernatant of the corresponding sample. 2) Combined eluates are closed with caps containing holes and frozen in liquid nitrogen. 3) Eluates are lyophilized overnight using … following the manufacturer's instructions.
Day 8	Dry-Samples are stored at -20 °C at the MS facility (AG Deutzmann) until MS analysis.

6.2.1.2 Analysis of protein interaction partners by Co-Immunoprecipitation

Co-immunoprecipitation was used as a technique for protein-protein interaction analyses *in vivo* in S2R+ culture cells. For this, a protein of interest (bait protein) was terminally tagged with a FLAG epitope, whereas the suspected interaction protein (prey protein) was terminally fused to an HA tag. The interaction analysis between bait and prey protein was performed as follows (see Table 26):

Table 26: Timetable for analysis of protein interaction by Co-immunoprecipitation.

Time	Protocol
Day 1	S2R+ cells are seeded in a 6-well plate (four wells per Co-IP experiment, see section 6.2.12.6).
Day 2	Two S2R+ wells are transfected with the plasmid expressing the prey protein (negative control), whereas the remaining 2 wells are additionally co-transfected with the plasmid expressing the bait protein (see section 6.2.12.8).
Day 4	1) Adherent cells are scratched off the dish in 500 µl PBS using a cell scraper. 2) Cells that were equally transfected (2 wells) are pooled in a 2 ml cup (from now on samples are kept at 4 °C). 3) Samples are centrifuged at 2,000 rpm for 10 min at 4 °C. 4) Cells are resuspended in 1 ml cold IP lysis buffer (containing protease inhibitors) and incubated for 20 min at 4 °C. 5) Samples are centrifuged at 12,000 rpm for 15 min at 4 °C. 6) 50 µl of supernatant are transferred in a 1.5 ml cup and stored at 4 °C (input samples). 7) 850 µl of supernatant are transferred in a 1.5 ml cup (IP samples). 8) Co-IP samples are incubated with 1.7 µl anti-FLAG antibodies (#374, 1:500) for 30 min at 4 °C under rotation. 9) PrG-agarose beads are prepared by washing beads twice with 1 ml IP washing buffer in a 1.5 ml cup by centrifugation at 1,000 rpm for 1 min (25 µl beads per IP sample). Supernatant is removed using a Hamilton syringe and beads are resuspended in 25 µl IP washing buffer. 10) IP samples are incubated with with 25 µl washed agarose beads overnight at 4 °C under gentle rotation.
Day 5	1) Beads in IP samples are washed three times with 1 ml IP washing buffer by centrifuging at 1,000 rpm for 1 min. After that, supernatant is discarded using the Hamilton syringe and Beads are resuspended in 40 µl 2X LSB. 2) Input samples are mixed with 50 µl 2X LSB. 3) All samples are boiled for 5 min. 4) Samples are centrifuged at 12,000 rpm for 1 min. **Break possible:** Samples can be stored at -20 °C. 5) Samples are separated by SDS-PAGE (see section 6.2.1): 20 µl of input samples and 10 µl of IP samples are loaded twice on different gels. 6) Interaction between bait and prey protein are analyzed by Western Blot. Gels are stained either with anti-FLAG or anti-HA antibodies (see section 6.2.4).

6.2.2 SDS-PAGE

Discontinuous sodium dodecyl sulfate polyacrylamide gel electrophoresis (SDS-PAGE) developed by Laemmli was applied as a technique to separate proteins only according to their molecular weight (273). An acrylamide gel system (BioRad) was used for preparation of polyacrylamide gels (7 ml resolving gel, 3 ml stacking gel) and electrophoresis in Turbo Laemmli running buffer. A protein ladder was additionally loaded on gel as reference. Gels were run at a constant current of 200 V for 65 min.

6.2.3 Coomassie staining of polyacrylamide gels

Proteins separated by SDS-PAGE were visualized by staining with Coomassie Brilliant Blue as follows:

1) The gel is shaked for 1 h in Coomassie staining solution.
2) The gel is shaked for 30 min in Coomassie destaining solution for destaining.
3) The gel is shaked overnight in water.

For analysis, stained proteins were detected at 700 nm using the Odyssey Infrared Imaging System.

6.2.4 Western blotting

For the immunological detection of specific proteins after SDS-PAGE (see section 6.2.2), proteins were transferred electrophoretically onto a nitrocellulose membrane using a semi-dry blotting system. Two whatman papers and a nitrocellulose membrane were soaked in transfer buffer 3 and used for the assembly of a blotting stack with following order from cathode to anode: Whatman paper, gel, nitrocellulose membrane, whatman paper. The blotting procedure was carried out at a constant current of 70 mA per gel for 90 min.

6.2.5 Antibody staining of Western blots

Proteins blotted on nitrocellulose membranes were detected by a combination of primary and secondary antibodies. Primary antibodies bind the target protein, whereas fluorophore-conjugated secondary antibodies recognize the primary antibodies allowing detection and quantification of the target protein. Antibody staining was performed as follows:

1) The nitrocellulose membrane is shaken in a plastic box filled with milk powder solution for 5 min.
2) The membrane is washed twice with PBT.
3) The membrane is incubated with 5 ml primary antibody solution (antibody diluted in PBT) and shaken overnight at 4 °C.
4) The membrane is washed twice with PBT.
5) The membrane is incubated with 5 ml secondary antibody solution (antibody diluted in PBT) and shaken for 90 min at room temperature in darkness.
6) The membrane is washed twice with PBT.
7) The membrane is shaken in PBT for 15 min.

Following antibody staining, target proteins were detected by using the Odyssey Infrared Imaging System according to the manufacturer's instructions.

6.2.6 *In vitro* synthesis of proteins

The gene encoding for the protein was first transcribed *in vitro* using the SP6 promoter. Usually, the coding sequence was followed by a 3'-UTR region of the Xenopus β-globolin gene to achieve a high translation rate. To get an adequate amount of DNA template for transcription, the gene including the regulatory elements (SP6 promoter, Xenopus β-globolin 3'-UTR) was first amplified by PCR (see section 7.1.2, Primer:

CO_045, CO_002). *In vitro* transcription was performed according to Gurevich et al. (272) and carried out in following reaction mix (see Table 27):

Table 27: *In vitro* transcription reaction mix

Component	Amount
5X transcription buffer	4 µl
PCR DNA (purified)	10 µl
SP6 RNA polymerase	1 µl
NTPs (25 mM each)	2 µl
RNase inhibitor	0.5 µl
H_2O (RNase free)	Ad 20 µl
Total volume	**20 µl**

The *in vitro* transcription mix was incubated overnight at 37 °C. Transcription of RNA was verified by gel electrophoresis (see section 6.1.3). Transcribed RNA was stored at -20 °C until being used as template for *in vitro* translation. The *in vitro* translation of proteins was performed in a rabbit reticulocyte lysate system according to the manufacturer's instructions. Following reaction mix was prepared (see Table 28):

Table 28: *In vitro* translation reaction mix

Component	Amount
In vitro transcribed RNA	4.5 µl
Reticulocyte lysate	14 µl
Amino acid mix minus cysteine (1 mM)	0.5µl
Amino acid mix minus methionine (1 mM)	0.5 µl
RNase inhibitor	0.5 µl
Total volume	**20 µl**

The reaction mix was incubated for 90 min at 30 °C. Translation was checked by SDS-PAGE (see section 6.2.2).

6.2.7 Purification of heterologous expressed proteins by affinity chromatography

Heterologously expressed proteins fused to a polyhistidine epitope were purified by affinity chromatography on an ÄKTAdesign fast potein liquid chromatography (FPLC) system equipped with a HisTrap HP 5 ml column. Protein samples for purification were prepared as follows:

1) Cells used for expression of the target protein are resuspended in 50 ml pre-cooled chromatography running buffer.
2) Cell lysate is prepared by sonication for 8 min using 50 % duty cycle (pulse on: 10 sec, pulse off: 10 sec) and 40 % pulse intensity (Sonifier Branson 250D).
3) The cell lysate is cleared of cell debris by centrifugation twice for 45 min at 14,000 rpm at 4 °C.
4) The supernatant is filtered by using filter papers containing pores with a diameter of 0.45 µm.

The filtered sample was applied to the ÄKTAdesign FPLC system. The handling of the device as well as the column was carried out according to the manufacturer's instructions. Purification by affinity chromatography was performed by following method settings (see Table 29):

Table 29: FPLC method settings for affinity chromatography

Step	Setting
1: Equilibration	3 CV chromatography running buffer
2: Sample loading	50 ml protein sample
3: Washing	8 CV chromatography running buffer
4: Elution	15 CV linear gradient of 10 – 1000 mM imidazole (chromatography elution buffer), eluate was collected in 2 ml fractions
5: Column cleaning	10 CV chromatography elution buffer
6: Equlibration	5 CV chromatography running buffer
7: Washing and column storage	5 CV H_2O, 3 CV 20 % ethanol

(The purification was performed at a constant flow rate of 5 ml/min)

Eluted fractions were analyzed by SDS-PAGE (see section 6.2.2). 10 µl of the corresponding fractions were mixed with 10 µl 2X LSB (samples: fractions). After boiling, 10 µl of each sample were loaded on gel. Purity of the eluted fractions was analyzed by Coomassie staining (see section 6.2.3), or when higher detection sensitivity was necessary by Western Blot (see section 6.2.4). Depending on the degree of purity, several fractions were combined and further used for dialysis (see section 6.2.8).

6.2.8 Dialysis of purified proteins

The purified protein was placed inside a dialysis bag consisting of a semi-permeable membrane with pores small enough to retain the proteins in the bag. Preparation and filling of the dialysis bag was performed according to the manufacturer's instructions. The filled bag was stirred in 5 l dialysis buffer overnight at 4 °C allowing substitution of the buffer solution by diffusion.

6.2.9 Concentration of protein samples

Protein samples were concentrated by the Amcion Ultra 10k device according to the manufacturer's instructions. Concentration was carried out in a centrifuge with a swinging-bucket rotor at 4 °C.

6.2.10 Storage of purified proteins

For short term storage (up to a week), protein preparataions were stored at -4 °C. For long term storage (several months), protein samples were supplemented with 50 % glycerol and kept in small aliquots at -20°C. For even longer periods of storage (months to years) aliquots were rapidly frozen using liquid nitrogen and stored at -80 °C.

6.2.11 *In vitro* ubiquitination assay

In vitro ubiquitination assays were used to analyze ubiquitination activity *in vitro*. Ubiquitination reactions were performed in following reaction mix (see Table 30):

Table 30: Reaction mix for *in vitro* ubiquitination assay

Component	Amount
H_2O/rabbit reticulocyte lysate	5 µl
10X Ubiquitination buffer	1 µl
6XHIS-4XFLAG-Ubiquitin	1 µl
6XHIS-Uba1	1 µl
Effete-6XHIS	1 µl
Geminin-10XHA-6XHIS	1 µl
APC/C beads	20 µl
Total volume	**30 µl**

Following incubation for 1 h at 30 °C, reaction was stopped by boiling in 2X LSB for 5 min. 5 µl were applied to SDS-PAGE (see section 6.2.2). Ubiquitination was detected by Western Blot (see section 6.2.4) using primary anti-HA antibodies against the APC/C-Fzr target substrate Geminin-10XHA-6XHIS (#373, 1:2000). To verify the presence of precipitated Cdc16-GFP, primary anti-GFP antibodies (#387, 1:2000) were used for staining.

APC/C was obtained by precipitation of the potential APC/C subunit Cdc16-MYC-TEV-GFP (Cdc16-GFP) from a transgenic *Drosophila* S2R+ cell line continuously overexpressing Cdc16-GFP. Precipitation was performed as follows:

1) Harvested cells from a confluent T25 cell culture flask (see section 6.2.12.9) are lysed by incubation in 1 ml cold IP lysis buffer containing protease inhibitors for 20 min at 4 °C.
2) Cell lysate is cleared of cell debris by centrifugation at 12,000 rpm for 15 min at 4 °C.
3) 900 µl supernatant are transferred in a 1.5 ml cup and incubated with 4 µl anti-GFP antibodies (#387, 1:250) for 30 min at 4 °C under rotation.
4) 50 µl PrG-agarose beads are prepared by washing beads twice with 1 ml IP washing buffer in a 1.5 ml cup by centrifugation at 1,000 rpm for 1 min. Supernatant is removed using a Hamilton syringe and beads are resuspended in 50 µl IP washing buffer. Washed PrG-agarose beads are added to the cell lysate.
5) Cell lysate is incubated for 90 min at 4 °C under rotation.
6) APC/C-Beads are washed twice with 1 ml IP washing buffer by centrifugation at 1,000 rpm for 1 min at 4 °C, resuspended in 50 µl IP washing buffer and transferred into a PCR cup.

Activation of precipitated APC/C by its activator subunit Fzr was achieved by incubation with *in vitro* translated 4XFLAG-Fzr or baculovirus-expressed 6XHIS-TEV-FLAG-Fzr as follows:

1) <u>*In vitro* translated 4XFLAG-Fzr</u>
   20 µl APC/C beads are incubated with 20 µl rabbit reticulocyte lysate containing *in vitro* translated 4XFLAG-Fzr (see section 6.2.6) in a thermocycler for 1 h at 30 °C.

   <u>Baculovirus-expressed 6XHIS-TEV-FLAG-Fzr</u>
   20 µl APC/C beads are incubated with 20 µl purified 6XHIS-TEV-FLAG-Fzr (see section 6.2.13.5) in a thermocycler for 1 h at 30 °C.
2) APC-Fzr beads are washed three times with 200 µl IP washing buffer by centrifugation at 1,000 rpm for 1 min at 4 °C. Supernatant is removed using a Hamilton Syringe and APC-Fzr beads are resuspended in 20 µl IP washing buffer.

6.2.12 *Drosophila* S2R+ cells

6.2.12.1 Production of stable S2R+ cell lines

Stable S2R+ cell lines constitutively expressing a protein of interest were established as follows (see Table 31):

Table 31: Timetable for production of stable S2R+ cell line

Time	Procedure
Day 1	S2R+ cells are seeded in a 6-well plate (see section 6.2.12.6).
Day 2	Cells are transfected with 600 ng plasmid DNA containing the expression construct and the *hpt* gene that provides resistance against the antibiotic hygromycin B (see section 6.2.12.8).
Day 5	1) Adherent cells are washed with 3 ml PBS. 2) Cells are incubated in 1 ml Trypsin/EDTA solution for 2 min at room temperature. 3) Cells are transferred into a 15 ml falcon tube, centrifuged off for 2 min at 2,000 rpm and resuspended in 1 ml Schneider's *Drosophila* hygromycin medium. 4) 250 µl are seeded into a new well of a 6-well plate filled with hygromycin cell culture medium (1:4 split).
Day 8	1) Adherent cells are washed with 3 ml PBS. 2) Cells are incubated in 1 ml Trypsin/EDTA solution for 2 min at room temperature. 3) Cells are transferred into a 15 ml falcon tube, centrifuged off for 2 min at 2,000 rpm, resuspended in 12 ml Schneider's *Drosophila* hygromycin medium and transferred into a T25 tissue flask.
From day 9	Schneider's *Drosophila* hygromycin medium is refreshed twice a week. When cells are grown confluently, cells are cultured in Schneider's *Drosophila* complete medium (see section 6.2.12.2).

6.2.12.2 Culturing of S2R+ *Drosophila* cells

The cultivation of S2R+ *Drosophila* cells was performed in 75 cm² tissue flasks containing 12 ml Schneider's *Drosophila* complete medium at 27 °C. Cells were split twice a weak (see section 6.2.12.5).

6.2.12.3 Freezing of S2R+ cell stocks

Culture cells grown in tissue flasks were frozen for long term storage as follows:

1) Adherent cells are washed with 5 ml PBS.
2) Cells are incubated in 5 ml Trypsin/EDTA solution for 2 min at room temperature.
3) Cells are detached from the surface by tapping gently on the side wall of the cell culture flask and by pipetting the Trypsin/EDTA solution several times up and down on the attached cells. The cell suspension is then transferred in a 15 ml falcon tube.
4) Cells are washed in 5 ml Schneider's *Drosophila* complete medium by centrifuging for 2 min at 2,000 rpm.

5) Cells are centrifuged off for 2 min at 2,000 rpm and resuspended in *Drosophila* freezing medium at a density of 0.5 X 10^7 cells/ml (see section 6.2.12.7).
6) 1 ml cell suspension are frozen in cryo vials overnight at -80 °C and stored in liquid nitrogen.

6.2.12.4 Thawing of frozen S2R+ cell stocks

Frozen cells in cryo vials were thawed at 30 °C and washed twice with 5 ml Schneider's *Drosophila* complete medium in a 15 ml falcon before being transferred in a 75 cm² tissue flask.

6.2.12.5 Splitting of cells

In order to provide an appropriate environment for cell growth, culture cells grown in tissue flasks (see section 6.2.12.5) were regularly split twice a week by following protocol:

1) Adherent cells are washed with 5 ml PBS.
2) Cells are incubated in 5 ml Trypsin/EDTA solution for 2 min at room temperature.
3) Cells are detached from the surface by tapping gently on the side wall of the cell culture flask and by pipetting the Trypsin/EDTA solution several times up and down on the attached cells. The cell suspension is then transferred in a 15 ml falcon tube.
4) Cells are centrifuged off for 2 min at 2,000 rpm and resuspended in 4 ml Schneider's *Drosophila* complete medium.
5) 1 ml of the cell suspension is transferred into a new cell culture flask containing 12 ml fresh Schneider's *Drosophila* complete medium.

6.2.12.6 Seeding of cells

Seeding of cells was performed on the same day as the cell culture splitting procedure (see section 6.2.12.5). Depending on the experimental approach, cells were seeded in 6-well or 12-well plates. 6/12-wells were filled with 3/1.5 ml Schneider's *Drosophila* complete medium. 150,000/70,000 cells were seeded per 6/12-well. The volume of cell suspension needed was determined by its cell concentration (see section 6.2.12.7).

6.2.12.7 Determination of cell concentration

The concentration of cells was determined by using the Fuchs-Rosenthal cell counting chamber (16 m² total area, depth 0.2 mm, volume 3.2 µl) consisting of 256 small squares. 20 µl cell suspension mixed with 80 µl Trypan Blue were inserted into the counting chamber. The number of cells in 16 small squares was counted under the microscope. The concentration of cells was calculated by following formula:

Cell concentration = amount of counted cells / 16 x 0.32 / 10e6 [cells/ml]

6.2.12.8 Transfection of cells

Transfection of S2R+ *Drosophila* cells was carried out 24 h after seeding (see section 6.2.12.6) by preparing following transfection mix (see Table 32):

Table 32: Transfection mix

Component	Amount	
	6-well plate	12-well plate
Total plasmid DNA	600 ng	200 – 300 ng
Schneider's *Drosophila* medium	Ad 150 µl	Ad 75 µl
Total volume	**150 µl**	**75 µl**
+ FuGENE HD	**3 µl**	**1 µl**

Transfection was performed using FuGENE HD transfection reagent as follows:

1) The FuGENE HD reagent is vortexed for 10 sec.
2) After adding the indicated amount of FuGENE HD reagent to the transfection mix, the mix is immediately vortexed for 3 sec.
3) The transfection mix is incubated for 15 min at room temperature and subsequently added to the cells while rotating the plate.

When transfected genes were under the control of the metallothionein promoter, $CuSO_4$ was additionally added to the cells to a final concentration of 500 µM.

6.2.12.9 Harvesting of cells

Adherent cells grown in culture flasks were harvested as follows:

1) Cells are scratched off the bottom of the flask in 5 ml PBS using a cell scratcher.
2) Cells are centrifuged off at 2,000 rpm for 10 min at room temperature in a 15 ml Falcon tube.
3) The Falcon tube is frozen in liquid nitrogen and stored at -20 °C.

6.2.12.10 Silencing of genes by RNA interference

RNA interference was mediated by an *in vitro* transcription mix containing dsRNA complementary to the target gene to be downregulated (see section 6.1.13). The mix was added into the cells while rotating the plate. RNAi experiments were scheduled as follows (see Table 33):

Table 33: Timeline for RNAi experiments in S2R+ cells

Time	Procedure
Day 1	Seeding of cells in 12-well plate (see section 6.2.12.6).
Day 2	Transfection (see section 6.2.12.8)
Day 3	Adding of the dsRNA mix (see section 6.1.13), when required $CuSO_4$ induction
Day 4/5	Flow cytometric analysis (see section 6.3.3)

6.2.12.11 *In vivo* APC/C-Fzr activity assay

In vivo APC/C-Fzr activity assays were performed in S2R+ *Drosophila* cells to analyze APC/C-Fzr inhibition by Rca1 *in vivo*. Cells were co-transfected with expressions plasmids encoding for HA-NLS-CycB-S286_K530del-2XGFP (CycB-GFP), a marker for APC/C-Fzr activity, 3XCherry (Cherry) as reference and a Rca1 construct. Cherry was constitutively expressed by the *actin* promoter. CycB-GFP and Rca1 expression was induced by $CuSO_4$ due to control by the metallothionein promoter. APC/C-Fzr activity in absence of endogenous Rca1 was analyzed by treating cells with dsRNA against the 5'- and 3'-UTR of *rca1* (*rca1-UTR* dsRNA). Downregulation of Dap activity was induced by dsRNA complementary to the coding region of *dap* (*dap-CDS* dsRNA). Cell stage, GFP and Cherry fluorescence was analyzed by flow cytometry (see section 6.3.3). APC/C-Fzr activity was quantified by the ratio of GFP and Cherry fluorescent cells in G2 phase. *In vivo* APC/C-Fzr activity assays were scheduled as follows (see Table 34):

Table 34: Timeline for *in vivo* APC/C-Fzr activity assays

Time	Procedure
Day 1	Seeding of cells in 12-well plate (see section 6.2.12.6).
Day 2	Co-transfection (see section 6.2.12.8): 100 ng HA-NLS-CycB-S286_K530del-2XGFP 100 ng 3XCherry (+ Rca1 construct)
Day 3	Adding of 40 nM *rca1-UTR* dsRNA and/or 10 nM *dap-CDS* dsRNA for downregulation of endogenous Rca1 and/or Dap activity (see section 6.1.13), $CuSO_4$ induction to initiate CycB-GFP and/or Rca1 expression
Day 5	Flow cytometric analysis (see section 6.3.3)

6.2.12.12 Preparation of cell extract

Cells seeded in 12-wells were centrifuged for 1 min at 13,000 rpm, resuspended in 40 µl PBS and mixed with 40 µl 2X LSB. Samples were separated by SDS-PAGE (see section 6.2.2) and analyzed by Western-Blot (see section 6.2.4).

6.2.13 Spodoptera frugiperda SF21 cells

6.2.13.1 Maintenance of insect cells

SF21 cells are maintained in 50 ml GIBCO Sf-900 II SFM medium at a cell count of 0.5 – 1 X 10^6 cells/ml in a 500 ml shaker flask shaken at 80 rpm at 27 °C. Cell count was checked every 24 h.

6.2.13.2 Freezing of SF21 cell stocks

A cell culture (not older than 2 weeks) is centrifuged at 2,000 rpm for 5 min. The pellet is resuspended in fresh GIBCO Sf-900 II SFM medium supplemented with 10 % DMSO (v/v) to a cell count of 3 X 10^7 cells/ml. 3 ml aliquots are frozen in 4.5 ml cryo tubes in liquid nitrogen and stored at -80 °C.

6.2.13.3 Thawing of frozen SF21 cell stocks

A 3 ml aliquot is thawed at 37 °C. Cells are centrifuged off at 2,000 rpm for 5 min. The pellet is resuspended in 2 ml GIBCO Sf-900 II SFM medium and transferred into a 50 ml Erlenmeyer flask. Fresh GIBCO medium is added to a cell count of 1 X 10^7 cells/ml. After 4 – 6 days shaking at 80 rpm, cell division occurs every 18 – 24 h and cells are maintained at 0.5 – 1 X 10^6 cells/ml (see section 6.2.13.1).

6.2.13.4 Counting of SF21 cells

The concentration of SF21 cells was determined by the Marienfeld Superior counting chamber (Neubauer system, depth 0.1 mm, largest square 1 mm^2, group square 0.04 mm^2, smallest square 0.0025 mm^2). A drop of cell suspension was injected into the counting chamber according to the manufacturer's instructions. The number of living cells in four large squares consisting of 16 smaller squares was counted under the microscope. The concentration of cells was calculated by following formula:

Cell concentration = Number of cells / 4 X 10e4 [cells/ml]

6.2.13.5 Expression of eukaryotic proteins in baculovirus-infected SF21 cells

Eukaryotic proteins were expressed in SF21 insect cells (cell line derived from *Spodoptera frugiperda*) by the MultiBac system developed by Berger et al. (256-258). The pFastBac HT A transfer plasmid provided by the Bac-to-Bac HT Vector Kit was used for the assembly of a 6XHIS tagged expression construct encoding the protein to be expressed under the control of the insect baculovirus *Autographa californic*a multiple nuclear polyhedrosis virus (AcMNPV) polyhedrin promoter. The expression construct is flanked by TN7 sites that allow transposition into a mini-*att*Tn7 attachment site. Generation of recombinant baculovirus DNA via TN7-mediated transposition was carried out *in vivo* in DH10EmBacY *E. coli* cells that contain the bacmid EMBacY carrying a mini-*att*Tn7 target site for integration of the expression construct into the baculovirus genome, and a helper plasmid providing Tn7 transposition function. The mini-*att*Tn7 attachment site is located in the *lacZα* gene facilitating identification of recombinant clones by blue-white-screening. Recombinant baculovirus was generated by transfecting the recombinant bacmid DNA into SF21 insect cells. High-titer stocks of recombinant baculovirus were used to infect SF21 insect cells for high expression of the recombinant protein of interest. Protein expression was monitored by analyzing the fluorescence signal of YFP expressed from the bacmid EMBacY by the viral polyhedrin promoter.

Heterologous protein expression in baculovirus-infected SF21 cells was performed by following protocol (see Table 35):

Table 35: Timeline for protein expression using the baculovirus expression system

Time	Protocol	Result
Day 1 - 5	Expression construct is cloned into transfer plasmid pFastBac HT A (see section 6.1.1).	Transfer plasmid carrying expression construct.
Day 6	Recombinant transfer plasmid is transformed into chemically competent DH10MultiBac *E. coli* cells. 100 Cells are plated on TYE agar plates containing kanamycin, tetracycline, gentamycin, IPTG and X-gal (see section 6.1.5).	TYE agar plates coated with transformed DH10EmBacY *E. coli* cells. Clones carrying recombinant bacmid DNA appear white.
Day 7	Recombinant clone (white) is incubated overnight at 37 °C in 3 ml 2X TY liquid medium supplemented with kanamycin, tetracycline and gentamycin.	Liquid culture of clone carrying recombinant bacmid DNA.

Time	Protocol	Result
Day 8	1) Cells in 3 ml liquid culture are centrifuged off in a 1.5 ml cup at 14,000 rpm for 1 min. 2) Cells are resuspended in 400 µl Cell Resuspension Solution. 3) 400 µl Cell Lysis Solution is added. Cell suspension is mixed gently by inverting the tube 3 – 5 times. The suspension is incubated for 3 minutes at room temperature. 4) 700 µl Neutralization Solution are added to the lysed cells. Solution is mixed by inverting the tube 3 – 5 times. 5) 900 µl of supernatant are mixed with 800 µl isopropanol to precipitate bacmid DNA. Pellet is washed twice with 250 µl 70 % EtOH. Bacmid DNA is resuspended in 30 µl sterilized H_2O and stored at 4 °C. 6) The quality of purified bacmid DNA (10 µl) is verified by gel electrophoresis (see section 6.1.3). DNA with high molecular weight should appear. 7) Cells of the remaining liquid culture (1 ml) are resuspended in 1 ml 20 % Glycerol by centrifuging in a 1.5 ml cup at 14,000 rpm for 1 min. Cells are stored at -70 °C for isolation of new bacmid DNA. 8) SF21 cells are seeded in a 6-well plate. One well is filled only with medium as control for medium contamination. 9) SF21 cells are transfected with recombinant bacmid DNA as follows: FuGENE HD transfection reagent is vortexed for 10 sec. 2 X 10 µl bacmid DNA are mixed with 5 µl FuGENE HD transfection reagent in 200 µl serum free medium and subsequently vortexed for 2 sec. Following incubation at room temperature for 15 min, both transfection mixes are added in two separate wells while rotating the plate (labeled with A1, A1'). As negativ control, one well is kept uninfected (labeled with C). After transfection, the 6-well plate is sealed with parafilm.	SF21 cells transfected with purified recombinant bacmid DNA.
Day 10	1) After 48 – 60 h, infection of SF21 cells with recombinant baculovirus is checked by analyzing YFP fluorescence under a fluorescence microscope (5 – 10 % cells should be infected). 2) Medium containing initial virus (A1, A1', C) is removed (V_0) and stored in a 15 ml falcon tube at 4 °C. SF21 cells are scratched off in 500 µl PBS using a cell scraper and lysed by sonication for 4 min using 40 % duty cycle and 40 % pulse intensity (Sonopuls HD2070). 50 µl of the lysate are mixed with 50 µl 2XLSB (sample: extract). Another 100 µl of the lysate are centrifuged at 14,000 rpm for 3 min. 50 µl of the supernatant are mixed with 50 µl 2XLSB (sample: soluble fraction). All samples are boiled for 5 min and 40 µl of each sample are subjected to SDS-PAGE (see section 6.2.2). Expression of the protein of interest is analyzed by Western Blot using antibodies specific for the expressed protein (see section 6.2.4). V_0 derived from SF21 cells showing the highest protein expression is used for large scale expression.	First generation of recombinant baculovirus (V_0).

Time	Protocol	Result
From day 12	1) 3 ml V_0 are added to 50 ml freshly diluted SF21 cells at a density of 0.5 X 10^6 cells/ml using a 500 ml shaker flask. Cell count is monitored every 24 h. Cells are split at 24 h intervals to below 1 X 10^6 cells/ml until cell proliferation stops, which is described as date of proliferation arrest (dpa). At that time, cells have grown in size (about twofold). 2) 48 h after dpa, cells are centrifuged off at 2,000 rpm for 5 min and supernatant containing high titer of recombinant baculovirus is collected in a 50 ml Falcon tube (V_1). V_1 is stored at 4 °C. 3) 5 – 10 ml V_1 are added to 400 ml freshly diluted SF21 cells at 5 X 10^6 cells/ml in a 2 l shaker flask. Cell count is monitored every 24 h. Cells are split at 24 h intervals to below 1 X 10^6 cells/ml until dpa. 4) 3 – 4 days after dpa, 1 ml cell suspension is withdrawn from the culture. A lysate is prepared by sonication for 4 min using 40 % duty cycle and 40 % pulse intensity (Sonopuls HD2070). 50 µl of the lysate are mixed with 50 µl 2XLSB (sample: extract). Another 100 µl of the lysate are centrifuged at 14,000 rpm for 3 min. 50 µl of the supernatant are mixed with 50 µl 2XLSB (sample: soluble fraction). All samples are boiled for 5 min and 40 µl of each sample are subjected to SDS-PAGE (see section 6.2.2). Expression of the protein of interest is analyzed by Western Blot using antibodies specific for the expressed protein (see section 6.2.4). SF21 cells are harvested by centrifugation at 2,000 rpm for 5 min. Cells are frozen in liquid nitrogen at -80 °C until being used for purification of the expressed target protein (see section 6.2.7).	SF21 cells containing expressed target protein.

6.3 Flow cytometry of S2R+ *Drosophila* cells

6.3.1 Preparation of living S2R+ *Drosophila* cells

S2R+ *Drosophila* cells grown in a 12-well plate were prepared for flow cytometric analysis as follows:

1) 5 µl Hoechst 33342 (1 mg/ml) are added to the medium in each 12-well filled with 1.5 ml medium (around 3 µg/ml final concentration). Cells are incubated for 30 min at 27 °C.
2) Cells are resuspended in 1 ml Trypsin/EDTA solution supplemented with 3 µg/ml by pipetting up and down several times.
3) The cell suspension in transferred into a 3.5 ml tube and subjected to flow cytometric analysis (see section 6.3.2).

6.3.2 Measurement procedure

Flow cytometric analysis of cells was performed by using the CyFlow space flow cytometer. Following light sources and filter were applied for detection of Hoechst 33342, GFP and Cherry fluorescence signals (see Table 36).

Table 36: Lasers and detection filters for flow cytometric analysis

Fluorophore	Excitation laser	Detection filter
Hoechst 33342	365 nm UV-LED	FL2-Bandpass filter BP 455/50
GFP	488 nm blue solid state laser	FL1-Bandpass filter BP 527/30
Cherry	561 nm yellow laser	FL3-Bandpass filter BP 630/75

S2R+ *Drosophila* cells were identified by their foreward and side scatter after being illuminated by the 488 nm blue solid state laser. The scatter was detected by using the Bandpass filter BP 488.

6.3.3 Analysis of data

Flow cytometric data were analyzed by FCS Express. Detection and quantification of S2R+ *Drosophila* cells and their fluorescence signals were based on defined gates and markers (see Figure 66).

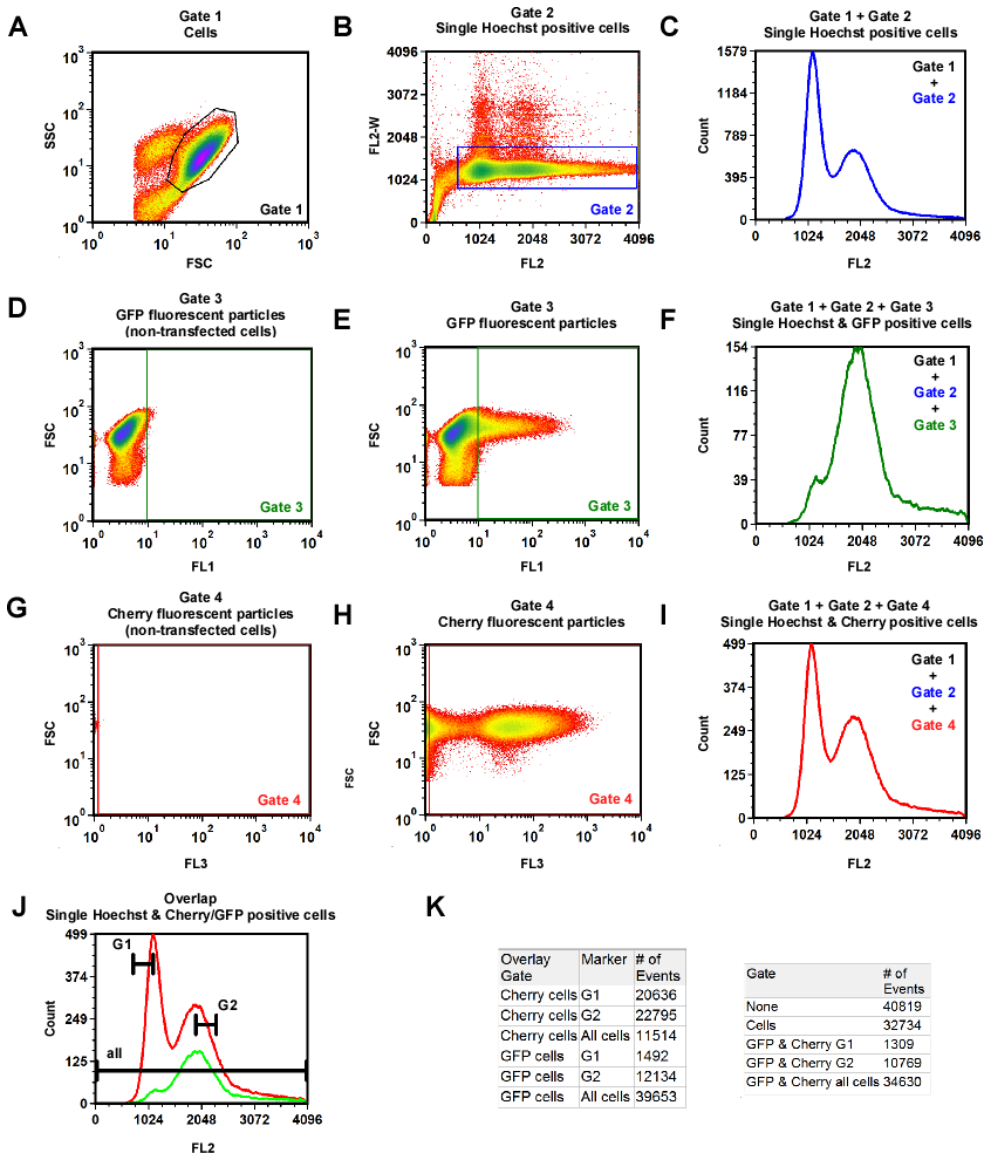

Overlay Gate	Marker	# of Events
Cherry cells	G1	20636
Cherry cells	G2	22795
Cherry cells	All cells	11514
GFP cells	G1	1492
GFP cells	G2	12134
GFP cells	All cells	39653

Gate	# of Events
None	40819
Cells	32734
GFP & Cherry G1	1309
GFP & Cherry G2	10769
GFP & Cherry all cells	34630

Figure 66: Flow cytometric analysis of S2R+ *Drosophila* cells
Gates and histograms applied for the analysis of flow cytometric data are illustrated by an example, as shown above. **(A-C,E,F,H,I,L)** S2R+ cells were co-transfected with a GFP fluorescent construct, HA-NLS-CycB-S286_K530del-2XGFP, and a Cherry fluorescent construct, 3XCherry. **(D,G)** Non-transfected cells were taken as negative control to identify background signals. Cells were stained with Hoechst to quantify DNA content. FSC: forward scatter, SSC: side scatter, FL1: GFP fluorescence, FL2: Hoechst fluorescence, FL2-W: Hoechst fluorescence pulse width, FL3: Cherry fluorescence. **(A,B,D,E,G,H)** Flow cytometric data displayed in density plots. Defined gates were set to analyze the measured data in histograms. **(A)** Measured particles by FSC and SSC. Gate 1 surrounds a region containing intact S2R+ *Drosophila* cells. **(B)** Measured Hoechst fluorescence by FL2 and FL2-W. Gate 2 restricts flow cytometric analyses to single cells. **(D,E)** Measured GFP fluorescent particles by FL1 and FSC. GFP background signals detected by non-transfected cells were excluded by Gate 3 (false GFP positive cells < 0.5 % of measured cells). **(G,H)** Measured Cherry fluorescent particles by FL3 and FSC. Cherry background signals detected by non-transfected cells were excluded by Gate 4 (false Cherry positive cells < 0.5 % of measured cells). **(C,F,I,J)** Histograms representing data subsets defined by the combination of specific gates are shown. **(J)** Overlap of GFP and Cherry positive cells (histogram (F) and (I)). Markers were set to analyze cells in G1 phase (G1), G2 phase (G2) and over the whole cell cycle (all). **(K)** Data resulting from combined gates and markers were summarized in tables.

7 Abbreviations

Table 37: Abbreviations

Abbreviation	Expansion
~	high energy bond
µ	micro
AG	“Arbeitsgruppe” (workgroup)
AMP	adenosine monophosphate
APC/C	Anaphase promoting complex/Cyclosome
ATP	adenosine triphosphate
bp	base pair
C	celsius, centi
cdc	cell division cycle
Cdk	Cyclin dependent kinase
cDNA	complementary DNA
CDS	coding sequence
CKI	Cyclin-dependent kinase inhibitor
CRL	Cullin-RING ubiquitin ligase
CT	C-terminal
C-terminal	carboxy-terminal
CTP	cytidine triphosphate
Cyc	Cyclin
Da	dalton
dATP	deoxyadenosine triphosphate
D-box	destruction box
dCTP	deoxycytidine triphosphate
dFbox	deleted F-box
dGTP	deoxyguanosine triphosphate
DNA	deoxyribonucleic acid
dNTP	deoxynucleotide triphosphate
dPIP	deleted PIP degron
DSHB	Developmental Studies Hybridoma Bank
dsRNA	double stranded RNA
dTTP	deoxythymidine triphosphate
DUB	deubiquitinating enzyme
E. coli	*Escherichia coli*
e.g.	exempli gratia (for example)
et al.	et alii
FBS	fetal bovine serum
FSC	forward scatter
g	gram
G1	gap1
G2	gap2
GFP	green fluorescent protein
GTP	guanosine triphosphate

Abbreviation	Expansion
h	hour
H_2O	Water
HA	hemagglutinin
IP	immunoprecipitation
IR	infrared
k	kilo
l	liter
LB	Luria Broth
LC	liquid chromatography
log	logarithm
m	milli, meter
M	mol per liter
m/z	mass-to-charge ratio
MF	morphogenetic furrow
min	minute(s)
mRNA	messenger RNA
MS	mass spectrometry
n	nano
Ni-NTA	nickel(II)-nitrilotriacetic acid
NLS	nuclear localization signal
NMR	nuclear magnetic resonance
NT	N-terminal
N-terminal	amino-terminal
NTP	nucleotide triphosphate
PAGE	polyacrylamide gel electrophoresis
PBS	phosphate buffer saline
PBT	phosphate buffer saline - tween
PCR	polymerase chain reaction
PIP	PCNA interaction protein
RL	reticulocyte lysate
RNA	ribonucleic acid
RNAi	RNA interference
RNase	ribonuclease
rpm	rounds per minute
SCF	Skp/Cullin/F-box complex
sec	seconds
SEM	standard error of the mean
SSC	side scatter
TAE	Tris/Acetate/EDTA
TE	Tris/EDTA
TEV	Tobacco Etch Virus
tRNA	transfer RNA
Ub	ubiquitin
UBA	ubiquitin-associated
UBC	ubiquitin conjugating enzyme

Abbreviation	Expansion
UBL	ubiquitin-like
UTP	uridine triphosphate
UTR	untranslated region
UV	ultra violette
V	voltage
W	watt
WB	western blot
WT	wild type
ZBR	zinc-binding region

8 Single and three letter code for amino acids

Table 38: Single and three letter code for amino acids

One letter code	Three letter code	Amino acid
A	Ala	Alanine
C	Cys	Cysteine
D	Asp	Aspartate
E	Glu	Glutamate
F	Phe	Phenylalanine
G	Gly	Glycine
H	His	Histidine
I	Ile	Isoleucine
K	Lys	Lysine
L	Leu	Leucine
M	Met	Methionine
N	Asn	Asparagine
P	Pro	Proline
Q	Gln	Glutamine
R	Arg	Arginine
S	Ser	Serine
T	Thr	Threonine
V	Val	Valine
W	Trp	Tryptophan
Y	Tyr	Tyrosine

9 List of figures

10 List of tables

11 References

1. Morgan DO (2007) *The cell cycle : principles of control* (Published by New Science Press in association with Oxford University Press; Distributed inside North America by Sinauer Associates, Publishers, London Sunderland, MA) pp xxvii, 297 p.
2. Hochegger H, Takeda S, & Hunt T (2008) Cyclin-dependent kinases and cell-cycle transitions: does one fit all? *Nat Rev Mol Cell Bio* 9(11):910-U926.
3. Sherr CJ (1993) Mammalian G1 cyclins. *Cell* 73(6):1059-1065.
4. Malumbres M & Barbacid M (2009) Cell cycle, CDKs and cancer: a changing paradigm. *Nat Rev Cancer* 9(3):153-166.
5. Satyanarayana A & Kaldis P (2009) Mammalian cell-cycle regulation: several Cdks, numerous cyclins and diverse compensatory mechanisms. *Oncogene* 28(33):2925-2939.
6. Suryadinata R, Sadowski M, & Sarcevic B (2010) Control of cell cycle progression by phosphorylation of cyclin-dependent kinase (CDK) substrates. *Biosci Rep* 30(4):243-255.
7. O'Farrell PH (2001) Triggering the all-or-nothing switch into mitosis. *Trends Cell Biol* 11(12):512-519.
8. Welcker M & Clurman BE (2008) FBW7 ubiquitin ligase: a tumour suppressor at the crossroads of cell division, growth and differentiation. *Nat Rev Cancer* 8(2):83-93.
9. Yao G, Lee TJ, Mori S, Nevins JR, & You L (2008) A bistable Rb-E2F switch underlies the restriction point. *Nat Cell Biol* 10(4):476-482.
10. Foe VE & Alberts BM (1983) Studies of nuclear and cytoplasmic behaviour during the five mitotic cycles that precede gastrulation in Drosophila embryogenesis. *J Cell Sci* 61:31-70.
11. Rabinowitz M (1941) *Studies on the cytology and early embryology of the egg of Drosophila melanogaster* (Press of the Wistar institute of anatomy and biology, Philadelphia,) p 49 p.
12. Callaini G, Dallai R, & Riparbelli MG (1990) Behavior of Yolk Nuclei during Early Embryogenesis in Drosophila-Melanogaster. *B Zool* 57(3):215-220.
13. O'Farrell PH, Edgar BA, Lakich D, & Lehner CF (1989) Directing cell division during development. *Science* 246(4930):635-640.
14. Tadros W & Lipshitz HD (2009) The maternal-to-zygotic transition: a play in two acts. *Development* 136(18):3033-3042.
15. Foe VE (1989) Mitotic domains reveal early commitment of cells in Drosophila embryos. *Development* 107(1):1-22.
16. Edgar BA, Sprenger F, Duronio RJ, Leopold P, & Ofarrell PH (1994) Distinct Molecular Mechanisms Regulate Cell-Cycle Timing at Successive Stages of Drosophila Embryogenesis. *Gene Dev* 8(4):440-452.
17. Edgar BA & O'Farrell PH (1989) Genetic control of cell division patterns in the Drosophila embryo. *Cell* 57(1):177-187.
18. Edgar BA & O'Farrell PH (1990) The three postblastoderm cell cycles of Drosophila embryogenesis are regulated in G2 by string. *Cell* 62(3):469-480.
19. Bodmer R, Carretto R, & Jan YN (1989) Neurogenesis of the peripheral nervous system in Drosophila embryos: DNA replication patterns and cell lineages. *Neuron* 3(1):21-32.
20. Smith AV & Orr-Weaver TL (1991) The regulation of the cell cycle during Drosophila embryogenesis: the transition to polyteny. *Development* 112(4):997-1008.
21. Edgar BA & Orr-Weaver TL (2001) Endoreplication cell cycles: more for less. *Cell* 105(3):297-306.

22. Suzuki K*, et al.* (2015) Identification of non-Ser/Thr-Pro consensus motifs for Cdk1 and their roles in mitotic regulation of C2H2 zinc finger proteins and Ect2. *Sci Rep* 5:7929.
23. Dowdy SF*, et al.* (1993) Physical interaction of the retinoblastoma protein with human D cyclins. *Cell* 73(3):499-511.
24. Ewen ME*, et al.* (1993) Functional interactions of the retinoblastoma protein with mammalian D-type cyclins. *Cell* 73(3):487-497.
25. Bourne Y*, et al.* (1996) Crystal structure and mutational analysis of the human CDK2 kinase complex with cell cycle-regulatory protein CksHs1. *Cell* 84(6):863-874.
26. Richardson HE, Stueland CS, Thomas J, Russell P, & Reed SI (1990) Human cDNAs encoding homologs of the small p34Cdc28/Cdc2-associated protein of Saccharomyces cerevisiae and Schizosaccharomyces pombe. *Genes Dev* 4(8):1332-1344.
27. Swan A, Barcelo G, & Schupbach T (2005) Drosophila Cks30A interacts with Cdk1 to target Cyclin A for destruction in the female germline. *Development* 132(16):3669-3678.
28. Pearson NJ, Cullen CF, Dzhindzhev NS, & Ohkura H (2005) A pre-anaphase role for a Cks/Suc1 in acentrosomal spindle formation of Drosophila female meiosis. *EMBO Rep* 6(11):1058-1063.
29. Ohtsubo M, Theodoras AM, Schumacher J, Roberts JM, & Pagano M (1995) Human cyclin E, a nuclear protein essential for the G1-to-S phase transition. *Mol Cell Biol* 15(5):2612-2624.
30. Pines J & Hunter T (1991) Human cyclins A and B1 are differentially located in the cell and undergo cell cycle-dependent nuclear transport. *J Cell Biol* 115(1):1-17.
31. Pines J & Hunter T (1994) The differential localization of human cyclins A and B is due to a cytoplasmic retention signal in cyclin B. *EMBO J* 13(16):3772-3781.
32. Jackman M, Firth M, & Pines J (1995) Human cyclins B1 and B2 are localized to strikingly different structures: B1 to microtubules, B2 primarily to the Golgi apparatus. *EMBO J* 14(8):1646-1654.
33. Johnson A & Skotheim JM (2013) Start and the restriction point. *Curr Opin Cell Biol* 25(6):717-723.
34. Bertoli C, Skotheim JM, & de Bruin RA (2013) Control of cell cycle transcription during G1 and S phases. *Nat Rev Mol Cell Biol* 14(8):518-528.
35. McGowan CH & Russell P (1993) Human Wee1 kinase inhibits cell division by phosphorylating p34cdc2 exclusively on Tyr15. *EMBO J* 12(1):75-85.
36. Blagosklonny MV & Pardee AB (2002) The restriction point of the cell cycle. *Cell Cycle* 1(2):103-110.
37. Berthet C, Aleem E, Coppola V, Tessarollo L, & Kaldis P (2003) Cdk2 knockout mice are viable. *Curr Biol* 13(20):1775-1785.
38. Ortega S*, et al.* (2003) Cyclin-dependent kinase 2 is essential for meiosis but not for mitotic cell division in mice. *Nat Genet* 35(1):25-31.
39. Santamaria D*, et al.* (2007) Cdk1 is sufficient to drive the mammalian cell cycle. *Nature* 448(7155):811-815.
40. Geng Y*, et al.* (2003) Cyclin E ablation in the mouse. *Cell* 114(4):431-443.
41. Kozar K*, et al.* (2004) Mouse development and cell proliferation in the absence of D-cyclins. *Cell* 118(4):477-491.
42. Brandeis M*, et al.* (1998) Cyclin B2-null mice develop normally and are fertile whereas cyclin B1-null mice die in utero. *Proc Natl Acad Sci U S A* 95(8):4344-4349.
43. Murphy M*, et al.* (1997) Delayed early embryonic lethality following disruption of the murine cyclin A2 gene. *Nat Genet* 15(1):83-86.
44. Fisher DL & Nurse P (1996) A single fission yeast mitotic cyclin B p34cdc2 kinase promotes both S-phase and mitosis in the absence of G1 cyclins. *EMBO J* 15(4):850-860.
45. Bartek J, Lukas C, & Lukas J (2004) Checking on DNA damage in S phase. *Nat Rev Mol Cell Biol* 5(10):792-804.

46. Wu CL, Zukerberg LR, Ngwu C, Harlow E, & Lees JA (1995) In vivo association of E2F and DP family proteins. *Mol Cell Biol* 15(5):2536-2546.
47. Christensen J*, et al.* (2005) Characterization of E2F8, a novel E2F-like cell-cycle regulated repressor of E2F-activated transcription. *Nucleic Acids Res* 33(17):5458-5470.
48. Di Stefano L, Jensen MR, & Helin K (2003) E2F7, a novel E2F featuring DP-independent repression of a subset of E2F-regulated genes. *EMBO J* 22(23):6289-6298.
49. Lees JA*, et al.* (1993) The retinoblastoma protein binds to a family of E2F transcription factors. *Mol Cell Biol* 13(12):7813-7825.
50. Gaubatz S*, et al.* (2000) E2F4 and E2F5 play an essential role in pocket protein-mediated G1 control. *Mol Cell* 6(3):729-735.
51. Westendorp B*, et al.* (2012) E2F7 represses a network of oscillating cell cycle genes to control S-phase progression. *Nucleic Acids Res* 40(8):3511-3523.
52. Cartwright P, Muller H, Wagener C, Holm K, & Helin K (1998) E2F-6: a novel member of the E2F family is an inhibitor of E2F-dependent transcription. *Oncogene* 17(5):611-623.
53. Eser U, Falleur-Fettig M, Johnson A, & Skotheim JM (2011) Commitment to a cellular transition precedes genome-wide transcriptional change. *Mol Cell* 43(4):515-527.
54. Bracken AP, Ciro M, Cocito A, & Helin K (2004) E2F target genes: unraveling the biology. *Trends Biochem Sci* 29(8):409-417.
55. Xu M, Sheppard KA, Peng CY, Yee AS, & Piwnica-Worms H (1994) Cyclin A/CDK2 binds directly to E2F-1 and inhibits the DNA-binding activity of E2F-1/DP-1 by phosphorylation. *Mol Cell Biol* 14(12):8420-8431.
56. Montagnoli A*, et al.* (1999) Ubiquitination of p27 is regulated by Cdk-dependent phosphorylation and trimeric complex formation. *Gene Dev* 13(9):1181-1189.
57. Carrano AC, Eytan E, Hershko A, & Pagano M (1999) SKP2 is required for ubiquitin-mediated degradation of the CDK inhibitor p27. *Nature Cell Biology* 1(4):193-199.
58. Marti A, Wirbelauer C, Scheffner M, & Krek W (1999) Interaction between ubiquitin-protein ligase SCFSKP2 and E2F-1 underlies the regulation of E2F-1 degradation. *Nature Cell Biology* 1(1):14-19.
59. Dimova DK & Dyson NJ (2005) The E2F transcriptional network: old acquaintances with new faces. *Oncogene* 24(17):2810-2826.
60. Stevaux O*, et al.* (2002) Distinct mechanisms of E2F regulation by Drosophila RBF1 and RBF2. *EMBO J* 21(18):4927-4937.
61. Frolov MV*, et al.* (2001) Functional antagonism between E2F family members. *Gene Dev* 15(16):2146-2160.
62. Meyer CA*, et al.* (2000) Drosophila Cdk4 is required for normal growth and is dispensable for cell cycle progression. *Embo Journal* 19(17):4533-4542.
63. Knoblich JA*, et al.* (1994) Cyclin E controls S phase progression and its down-regulation during Drosophila embryogenesis is required for the arrest of cell proliferation. *Cell* 77(1):107-120.
64. Richardson H, O'Keefe LV, Marty T, & Saint R (1995) Ectopic cyclin E expression induces premature entry into S phase and disrupts pattern formation in the Drosophila eye imaginal disc. *Development* 121(10):3371-3379.
65. Duronio RJ & O'Farrell PH (1995) Developmental control of the G1 to S transition in Drosophila: cyclin Eis a limiting downstream target of E2F. *Genes Dev* 9(12):1456-1468.
66. Zielke N*, et al.* (2011) Control of Drosophila endocycles by E2F and CRL4(CDT2). *Nature* 480(7375):123-127.
67. Moberg KH, Bell DW, Wahrer DC, Haber DA, & Hariharan IK (2001) Archipelago regulates Cyclin E levels in Drosophila and is mutated in human cancer cell lines. *Nature* 413(6853):311-316.
68. Welcker M*, et al.* (2003) Multisite phosphorylation by Cdk2 and GSK3 controls cyclin E degradation. *Mol Cell* 12(2):381-392.

69. Foley E, O'Farrell PH, & Sprenger F (1999) Rux is a cyclin-dependent kinase inhibitor (CKI) specific for mitotic cyclin-Cdk complexes. *Curr Biol* 9(23):1392-1402.
70. Sprenger F, Yakubovich N, & O'Farrell PH (1997) S-phase function of Drosophila cyclin A and its downregulation in G1 phase. *Curr Biol* 7(7):488-499.
71. Hegarat N, Rata S, & Hochegger H (2016) Bistability of mitotic entry and exit switches during open mitosis in mammalian cells. *Bioessays* 38(7):627-643.
72. Mueller PR, Coleman TR, Kumagai A, & Dunphy WG (1995) Myt1: a membrane-associated inhibitory kinase that phosphorylates Cdc2 on both threonine-14 and tyrosine-15. *Science* 270(5233):86-90.
73. Potapova TA, Sivakumar S, Flynn JN, Li R, & Gorbsky GJ (2011) Mitotic progression becomes irreversible in prometaphase and collapses when Wee1 and Cdc25 are inhibited. *Mol Biol Cell* 22(8):1191-1206.
74. Boutros R, Dozier C, & Ducommun B (2006) The when and wheres of CDC25 phosphatases. *Current Opinion in Cell Biology* 18(2):185-191.
75. Pomerening JR, Ubersax JA, & Ferrell JE, Jr. (2008) Rapid cycling and precocious termination of G1 phase in cells expressing CDK1AF. *Mol Biol Cell* 19(8):3426-3441.
76. Ferguson AM, White LS, Donovan PJ, & Piwnica-Worms H (2005) Normal cell cycle and checkpoint responses in mice and cells lacking Cdc25B and Cdc25C protein phosphatases. *Mol Cell Biol* 25(7):2853-2860.
77. Fung TK, Ma HT, & Poon RY (2007) Specialized roles of the two mitotic cyclins in somatic cells: cyclin A as an activator of M phase-promoting factor. *Mol Biol Cell* 18(5):1861-1873.
78. Myer DL, Bahassi el M, & Stambrook PJ (2005) The Plk3-Cdc25 circuit. *Oncogene* 24(2):299-305.
79. Barr FA, Sillje HH, & Nigg EA (2004) Polo-like kinases and the orchestration of cell division. *Nat Rev Mol Cell Biol* 5(6):429-440.
80. Jacobs HW, Knoblich JA, & Lehner CF (1998) Drosophila Cyclin B3 is required for female fertility and is dispensable for mitosis like Cyclin B. *Gene Dev* 12(23):3741-3751.
81. Knoblich JA & Lehner CF (1993) Synergistic action of Drosophila cyclins A and B during the G2-M transition. *EMBO J* 12(1):65-74.
82. Lehner CF & O'Farrell PH (1989) Expression and function of Drosophila cyclin A during embryonic cell cycle progression. *Cell* 56(6):957-968.
83. Lehner CF & O'Farrell PH (1990) The roles of Drosophila cyclins A and B in mitotic control. *Cell* 61(3):535-547.
84. Courtot C, Fankhauser C, Simanis V, & Lehner CF (1992) The Drosophila Cdc25 Homolog Twine Is Required for Meiosis. *Development* 116(2):405-&.
85. Bassermann F, Eichner R, & Pagano M (2014) The ubiquitin proteasome system - implications for cell cycle control and the targeted treatment of cancer. *Biochim Biophys Acta* 1843(1):150-162.
86. Jentsch S, Seufert W, & Hauser HP (1991) Genetic analysis of the ubiquitin system. *Biochim Biophys Acta* 1089(2):127-139.
87. Xu P*, et al.* (2009) Quantitative proteomics reveals the function of unconventional ubiquitin chains in proteasomal degradation. *Cell* 137(1):133-145.
88. Erpapazoglou Z, Walker O, & Haguenauer-Tsapis R (2014) Versatile roles of k63-linked ubiquitin chains in trafficking. *Cells* 3(4):1027-1088.
89. Spence J, Sadis S, Haas AL, & Finley D (1995) A ubiquitin mutant with specific defects in DNA repair and multiubiquitination. *Mol Cell Biol* 15(3):1265-1273.
90. Sun L, Deng L, Ea CK, Xia ZP, & Chen ZJ (2004) The TRAF6 ubiquitin ligase and TAK1 kinase mediate IKK activation by BCL10 and MALT1 in T lymphocytes. *Mol Cell* 14(3):289-301.
91. Maupin-Furlow J (2012) Proteasomes and protein conjugation across domains of life. *Nat Rev Microbiol* 10(2):100-111.

92. Haas AL & Rose IA (1982) The mechanism of ubiquitin activating enzyme. A kinetic and equilibrium analysis. *J Biol Chem* 257(17):10329-10337.
93. Schulman BA & Harper JW (2009) Ubiquitin-like protein activation by E1 enzymes: the apex for downstream signalling pathways. *Nat Rev Mol Cell Biol* 10(5):319-331.
94. Olsen SK & Lima CD (2013) Structure of a ubiquitin E1-E2 complex: insights to E1-E2 thioester transfer. *Mol Cell* 49(5):884-896.
95. Stewart MD, Ritterhoff T, Klevit RE, & Brzovic PS (2016) E2 enzymes: more than just middle men. *Cell Research* 26(4):423-440.
96. Michelle C, Vourc'h P, Mignon L, & Andres CR (2009) What Was the Set of Ubiquitin and Ubiquitin-Like Conjugating Enzymes in the Eukaryote Common Ancestor? *J Mol Evol* 68(6):616-628.
97. Berndsen CE & Wolberger C (2014) New insights into ubiquitin E3 ligase mechanism. *Nature Structural & Molecular Biology* 21(4):301-307.
98. Deshaies RJ & Joazeiro CA (2009) RING domain E3 ubiquitin ligases. *Annu Rev Biochem* 78:399-434.
99. Budhidarmo R, Nakatani Y, & Day CL (2012) RINGs hold the key to ubiquitin transfer. *Trends Biochem Sci* 37(2):58-65.
100. Hegde AN (2010) The ubiquitin-proteasome pathway and synaptic plasticity. *Learn Mem* 17(7):314-327.
101. Metzger MB, Hristova VA, & Weissman AM (2012) HECT and RING finger families of E3 ubiquitin ligases at a glance. *Journal of Cell Science* 125(3):531-537.
102. Spratt DE, Walden H, & Shaw GS (2014) RBR E3 ubiquitin ligases: new structures, new insights, new questions. *Biochem J* 458(3):421-437.
103. Li W*, et al.* (2008) Genome-wide and functional annotation of human E3 ubiquitin ligases identifies MULAN, a mitochondrial E3 that regulates the organelle's dynamics and signaling. *PLoS One* 3(1):e1487.
104. David Y, Ziv T, Admon A, & Navon A (2010) The E2 ubiquitin-conjugating enzymes direct polyubiquitination to preferred lysines. *J Biol Chem* 285(12):8595-8604.
105. Diaz-Villanueva JF, Diaz-Molina R, & Garcia-Gonzalez V (2015) Protein Folding and Mechanisms of Proteostasis. *Int J Mol Sci* 16(8):17193-17230.
106. Tomko RJ, Jr. & Hochstrasser M (2013) Molecular architecture and assembly of the eukaryotic proteasome. *Annu Rev Biochem* 82:415-445.
107. Bar-Nun S & Glickman MH (2012) Proteasomal AAA-ATPases: structure and function. *Biochim Biophys Acta* 1823(1):67-82.
108. Livneh I, Cohen-Kaplan V, Cohen-Rosenzweig C, Avni N, & Ciechanover A (2016) The life cycle of the 26S proteasome: from birth, through regulation and function, and onto its death. *Cell Res* 26(8):869-885.
109. Thrower JS, Hoffman L, Rechsteiner M, & Pickart CM (2000) Recognition of the polyubiquitin proteolytic signal. *EMBO J* 19(1):94-102.
110. Clague MJ*, et al.* (2013) Deubiquitylases from genes to organism. *Physiol Rev* 93(3):1289-1315.
111. Verma R*, et al.* (2002) Role of Rpn11 metalloprotease in deubiquitination and degradation by the 26S proteasome. *Science* 298(5593):611-615.
112. Hamazaki J*, et al.* (2006) A novel proteasome interacting protein recruits the deubiquitinating enzyme UCH37 to 26S proteasomes. *EMBO J* 25(19):4524-4536.
113. Aufderheide A*, et al.* (2015) Structural characterization of the interaction of Ubp6 with the 26S proteasome. *Proc Natl Acad Sci U S A* 112(28):8626-8631.
114. Wilkinson KD*, et al.* (1995) Metabolism of the polyubiquitin degradation signal: structure, mechanism, and role of isopeptidase T. *Biochemistry* 34(44):14535-14546.

115. Sivakumar S & Gorbsky GJ (2015) Spatiotemporal regulation of the anaphase-promoting complex in mitosis. *Nat Rev Mol Cell Biol* 16(2):82-94.
116. Brown NG*, et al.* (2014) Mechanism of polyubiquitination by human anaphase-promoting complex: RING repurposing for ubiquitin chain assembly. *Mol Cell* 56(2):246-260.
117. Wang W & Kirschner MW (2013) Emi1 preferentially inhibits ubiquitin chain elongation by the anaphase-promoting complex. *Nat Cell Biol* 15(7):797-806.
118. Bastians H, Topper LM, Gorbsky GL, & Ruderman JV (1999) Cell cycle-regulated proteolysis of mitotic target proteins. *Mol Biol Cell* 10(11):3927-3941.
119. Treier M, Seufert W, & Jentsch S (1992) Drosophila UbcD1 encodes a highly conserved ubiquitin-conjugating enzyme involved in selective protein degradation. *EMBO J* 11(1):367-372.
120. Mathe E*, et al.* (2004) The E2-C vihar is required for the correct spatiotemporal proteolysis of cyclin B and itself undergoes cyclical degradation. *Current Biology* 14(19):1723-1733.
121. Garnett MJ*, et al.* (2009) UBE2S elongates ubiquitin chains on APC/C substrates to promote mitotic exit. *Nat Cell Biol* 11(11):1363-1369.
122. Lu Y, Wang W, & Kirschner MW (2015) Specificity of the anaphase-promoting complex: a single-molecule study. *Science* 348(6231):1248737.
123. Kelly A, Wickliffe KE, Song L, Fedrigo I, & Rape M (2014) Ubiquitin chain elongation requires E3-dependent tracking of the emerging conjugate. *Mol Cell* 56(2):232-245.
124. Chang L, Zhang Z, Yang J, McLaughlin SH, & Barford D (2015) Atomic structure of the APC/C and its mechanism of protein ubiquitination. *Nature* 522(7557):450-454.
125. Zhang S*, et al.* (2016) Molecular mechanism of APC/C activation by mitotic phosphorylation. *Nature* 533(7602):260-264.
126. Morgan DO (2013) The D box meets its match. *Mol Cell* 50(5):609-610.
127. Pfleger CM & Kirschner MW (2000) The KEN box: an APC recognition signal distinct from the D box targeted by Cdh1. *Genes Dev* 14(6):655-665.
128. He J*, et al.* (2013) Insights into degron recognition by APC/C coactivators from the structure of an Acm1-Cdh1 complex. *Mol Cell* 50(5):649-660.
129. da Fonseca PC*, et al.* (2011) Structures of APC/C(Cdh1) with substrates identify Cdh1 and Apc10 as the D-box co-receptor. *Nature* 470(7333):274-278.
130. Matyskiela ME, Rodrigo-Brenni MC, & Morgan DO (2009) Mechanisms of ubiquitin transfer by the anaphase-promoting complex. *J Biol* 8(10):92.
131. Kramer ER, Scheuringer N, Podtelejnikov AV, Mann M, & Peters JM (2000) Mitotic regulation of the APC activator proteins CDC20 and CDH1. *Mol Biol Cell* 11(5):1555-1569.
132. Shteinberg M, Protopopov Y, Listovsky T, Brandeis M, & Hershko A (1999) Phosphorylation of the cyclosome is required for its stimulation by Fizzy/cdc20. *Biochem Bioph Res Co* 260(1):193-198.
133. Patra D & Dunphy WG (1998) Xe-p9, a Xenopus Suc1/Cks protein, is essential for the Cdc2-dependent phosphorylation of the anaphase- promoting complex at mitosis. *Genes Dev* 12(16):2549-2559.
134. Shteinberg M & Hershko A (1999) Role of Suc1 in the activation of the cyclosome by protein kinase Cdk1/cyclin B. *Biochem Biophys Res Commun* 257(1):12-18.
135. Kraft C*, et al.* (2003) Mitotic regulation of the human anaphase-promoting complex by phosphorylation. *EMBO J* 22(24):6598-6609.
136. Ban KH*, et al.* (2007) The END network couples spindle pole assembly to inhibition of the anaphase-promoting complex/cyclosome in early mitosis. *Dev Cell* 13(1):29-42.
137. Lara-Gonzalez P, Westhorpe FG, & Taylor SS (2012) The spindle assembly checkpoint. *Curr Biol* 22(22):R966-980.
138. Sudakin V, Chan GK, & Yen TJ (2001) Checkpoint inhibition of the APC/C in HeLa cells is mediated by a complex of BUBR1, BUB3, CDC20, and MAD2. *J Cell Biol* 154(5):925-936.

139. Stukenberg PT & Burke DJ (2015) Connecting the microtubule attachment status of each kinetochore to cell cycle arrest through the spindle assembly checkpoint. *Chromosoma* 124(4):463-480.
140. Chao WC, Kulkarni K, Zhang Z, Kong EH, & Barford D (2012) Structure of the mitotic checkpoint complex. *Nature* 484(7393):208-213.
141. Lara-Gonzalez P, Scott MI, Diez M, Sen O, & Taylor SS (2011) BubR1 blocks substrate recruitment to the APC/C in a KEN-box-dependent manner. *J Cell Sci* 124(Pt 24):4332-4345.
142. Herzog F*, et al.* (2009) Structure of the anaphase-promoting complex/cyclosome interacting with a mitotic checkpoint complex. *Science* 323(5920):1477-1481.
143. Izawa D & Pines J (2012) Mad2 and the APC/C compete for the same site on Cdc20 to ensure proper chromosome segregation. *J Cell Biol* 199(1):27-37.
144. Zhang Y & Lees E (2001) Identification of an overlapping binding domain on Cdc20 for Mad2 and anaphase-promoting complex: model for spindle checkpoint regulation. *Mol Cell Biol* 21(15):5190-5199.
145. Foster SA & Morgan DO (2012) The APC/C subunit Mnd2/Apc15 promotes Cdc20 autoubiquitination and spindle assembly checkpoint inactivation. *Mol Cell* 47(6):921-932.
146. Di Fiore B & Pines J (2010) How cyclin A destruction escapes the spindle assembly checkpoint. *Journal of Cell Biology* 190(4):501-509.
147. Wolthuis R*, et al.* (2008) Cdc20 and Cks direct the spindle checkpoint-independent destruction of cyclin A. *Molecular Cell* 30(3):290-302.
148. Hardy T*, et al.* (2014) Multisite phosphorylation of C-Nap1 releases it from Cep135 to trigger centrosome disjunction. *J Cell Sci* 127(Pt 11):2493-2506.
149. Hayes MJ*, et al.* (2006) Early mitotic degradation of Nek2A depends on Cdc20-independent interaction with the APC/C. *Nat Cell Biol* 8(6):607-614.
150. Sedgwick GG*, et al.* (2013) Mechanisms controlling the temporal degradation of Nek2A and Kif18A by the APC/C-Cdc20 complex. *EMBO J* 32(2):303-314.
151. Lesage B, Qian J, & Bollen M (2011) Spindle checkpoint silencing: PP1 tips the balance. *Curr Biol* 21(21):R898-903.
152. Howell BJ*, et al.* (2001) Cytoplasmic dynein/dynactin drives kinetochore protein transport to the spindle poles and has a role in mitotic spindle checkpoint inactivation. *J Cell Biol* 155(7):1159-1172.
153. Yang M*, et al.* (2007) p31comet blocks Mad2 activation through structural mimicry. *Cell* 131(4):744-755.
154. Gligoris T & Lowe J (2016) Structural Insights into Ring Formation of Cohesin and Related Smc Complexes. *Trends in Cell Biology* 26(9):680-693.
155. Jones KT (2010) Cohesin and Cdk1: an anaphase barricade. *Nat Cell Biol* 12(2):106-108.
156. Wurzenberger C & Gerlich DW (2011) Phosphatases: providing safe passage through mitotic exit. *Nat Rev Mol Cell Bio* 12(8):469-482.
157. Jaspersen SL, Charles JF, & Morgan DO (1999) Inhibitory phosphorylation of the APC regulator Hct1 is controlled by the kinase Cdc28 and the phosphatase Cdc14. *Curr Biol* 9(5):227-236.
158. Listovsky T & Sale JE (2013) Sequestration of CDH1 by MAD2L2 prevents premature APC/C activation prior to anaphase onset. *J Cell Biol* 203(1):87-100.
159. Rape M & Kirschner MW (2004) Autonomous regulation of the anaphase-promoting complex couples mitosis to S-phase entry. *Nature* 432(7017):588-595.
160. Gavriilidis P, Giakoustidis A, & Giakoustidis D (2015) Aurora Kinases and Potential Medical Applications of Aurora Kinase Inhibitors: A Review. *J Clin Med Res* 7(10):742-751.
161. Fragkos M, Ganier O, Coulombe P, & Mechali M (2015) DNA replication origin activation in space and time. *Nat Rev Mol Cell Biol* 16(6):360-374.

162. Reber A, Lehner CF, & Jacobs HW (2006) Terminal mitoses require negative regulation of Fzr/Cdh1 by Cyclin A, preventing premature degradation of mitotic cyclins and String/Cdc25. *Development* 133(16):3201-3211.
163. Sigrist SJ & Lehner CF (1997) Drosophila fizzy-related down-regulates mitotic cyclins and is required for cell proliferation arrest and entry into endocycles. *Cell* 90(4):671-681.
164. Zachariae W, Schwab M, Nasmyth K, & Seufert W (1998) Control of cyclin ubiquitination by CDK-regulated binding of Hct1 to the anaphase promoting complex. *Science* 282(5394):1721-1724.
165. Williamson A*, et al.* (2009) Identification of a physiological E2 module for the human anaphase-promoting complex. *Proc Natl Acad Sci U S A* 106(43):18213-18218.
166. Listovsky T*, et al.* (2004) Mammalian Cdh1/Fzr mediates its own degradation. *EMBO J* 23(7):1619-1626.
167. Machida YJ & Dutta A (2007) The APC/C inhibitor, Emi1, is essential for prevention of rereplication. *Gene Dev* 21(2):184-194.
168. Hsu JY, Reimann JD, Sorensen CS, Lukas J, & Jackson PK (2002) E2F-dependent accumulation of hEmi1 regulates S phase entry by inhibiting APC(Cdh1). *Nat Cell Biol* 4(5):358-366.
169. Reimann JD, Gardner BE, Margottin-Goguet F, & Jackson PK (2001) Emi1 regulates the anaphase-promoting complex by a different mechanism than Mad2 proteins. *Genes Dev* 15(24):3278-3285.
170. Skaar JR, Pagan JK, & Pagano M (2013) Mechanisms and function of substrate recruitment by F-box proteins. *Nat Rev Mol Cell Biol* 14(6):369-381.
171. Cenciarelli C*, et al.* (1999) Identification of a family of human F-box proteins. *Curr Biol* 9(20):1177-1179.
172. Jin J*, et al.* (2004) Systematic analysis and nomenclature of mammalian F-box proteins. *Genes Dev* 18(21):2573-2580.
173. Winston JT, Koepp DM, Zhu C, Elledge SJ, & Harper JW (1999) A family of mammalian F-box proteins. *Curr Biol* 9(20):1180-1182.
174. Ganoth D*, et al.* (2001) The cell-cycle regulatory protein Cks1 is required for SCF(Skp2)-mediated ubiquitinylation of p27. *Nat Cell Biol* 3(3):321-324.
175. Hao B*, et al.* (2005) Structural basis of the Cks1-dependent recognition of p27(Kip1) by the SCF(Skp2) ubiquitin ligase. *Mol Cell* 20(1):9-19.
176. Spruck C*, et al.* (2001) A CDK-independent function of mammalian Cks1: targeting of SCF(Skp2) to the CDK inhibitor p27Kip1. *Mol Cell* 7(3):639-650.
177. D'Angiolella V*, et al.* (2012) Cyclin F-mediated degradation of ribonucleotide reductase M2 controls genome integrity and DNA repair. *Cell* 149(5):1023-1034.
178. D'Angiolella V*, et al.* (2010) SCF(Cyclin F) controls centrosome homeostasis and mitotic fidelity through CP110 degradation. *Nature* 466(7302):138-142.
179. Skaar JR, D'Angiolella V, Pagan JK, & Pagano M (2009) SnapShot: F Box Proteins II. *Cell* 137(7):1358, 1358 e1351.
180. Flick K & Kaiser P (2013) Set them free: F-box protein exchange by Cand1. *Cell Res* 23(7):870-871.
181. Pierce NW*, et al.* (2013) Cand1 promotes assembly of new SCF complexes through dynamic exchange of F box proteins. *Cell* 153(1):206-215.
182. Rizzardi LF & Cook JG (2012) Flipping the switch from g1 to s phase with e3 ubiquitin ligases. *Genes Cancer* 3(11-12):634-648.
183. Starostina NG & Kipreos ET (2012) Multiple degradation pathways regulate versatile CIP/KIP CDK inhibitors. *Trends Cell Biol* 22(1):33-41.
184. Lu Z & Hunter T (2010) Ubiquitylation and proteasomal degradation of the p21(Cip1), p27(Kip1) and p57(Kip2) CDK inhibitors. *Cell Cycle* 9(12):2342-2352.
185. Frescas D & Pagano M (2008) Deregulated proteolysis by the F-box proteins SKP2 and beta-TrCP: tipping the scales of cancer. *Nat Rev Cancer* 8(6):438-449.

186. Crusio KM, King B, Reavie LB, & Aifantis I (2010) The ubiquitous nature of cancer: the role of the SCF(Fbw7) complex in development and transformation. *Oncogene* 29(35):4865-4873.
187. Sherr CJ & Roberts JM (1999) CDK inhibitors: positive and negative regulators of G1-phase progression. *Genes Dev* 13(12):1501-1512.
188. Lee MH, Reynisdottir I, & Massague J (1995) Cloning of p57KIP2, a cyclin-dependent kinase inhibitor with unique domain structure and tissue distribution. *Genes Dev* 9(6):639-649.
189. Russo AA, Jeffrey PD, Patten AK, Massague J, & Pavletich NP (1996) Crystal structure of the p27Kip1 cyclin-dependent-kinase inhibitor bound to the cyclin A-Cdk2 complex. *Nature* 382(6589):325-331.
190. Lapenna S & Giordano A (2009) Cell cycle kinases as therapeutic targets for cancer. *Nature Reviews Drug Discovery* 8(7):547-566.
191. Deng C, Zhang P, Harper JW, Elledge SJ, & Leder P (1995) Mice lacking p21CIP1/WAF1 undergo normal development, but are defective in G1 checkpoint control. *Cell* 82(4):675-684.
192. Coats S, Flanagan WM, Nourse J, & Roberts JM (1996) Requirement of p27Kip1 for restriction point control of the fibroblast cell cycle. *Science* 272(5263):877-880.
193. Poon RY, Toyoshima H, & Hunter T (1995) Redistribution of the CDK inhibitor p27 between different cyclin.CDK complexes in the mouse fibroblast cell cycle and in cells arrested with lovastatin or ultraviolet irradiation. *Mol Biol Cell* 6(9):1197-1213.
194. Fero ML*, et al.* (1996) A syndrome of multiorgan hyperplasia with features of gigantism, tumorigenesis, and female sterility in p27(Kip1)-deficient mice. *Cell* 85(5):733-744.
195. Zhang P*, et al.* (1997) Altered cell differentiation and proliferation in mice lacking p57KIP2 indicates a role in Beckwith-Wiedemann syndrome. *Nature* 387(6629):151-158.
196. Urano T*, et al.* (1999) p57(Kip2) is degraded through the proteasome in osteoblasts stimulated to proliferation by transforming growth factor beta1. *J Biol Chem* 274(18):12197-12200.
197. Yan Y, Frisen J, Lee MH, Massague J, & Barbacid M (1997) Ablation of the CDK inhibitor p57Kip2 results in increased apoptosis and delayed differentiation during mouse development. *Genes Dev* 11(8):973-983.
198. Bornstein G*, et al.* (2003) Role of the SCFSkp2 ubiquitin ligase in the degradation of p21Cip1 in S phase. *J Biol Chem* 278(28):25752-25757.
199. Sitry D*, et al.* (2002) Three different binding sites of Cks1 are required for p27-ubiquitin ligation. *J Biol Chem* 277(44):42233-42240.
200. Kamura T*, et al.* (2003) Degradation of p57Kip2 mediated by SCFSkp2-dependent ubiquitylation. *Proc Natl Acad Sci U S A* 100(18):10231-10236.
201. Vlach J, Hennecke S, & Amati B (1997) Phosphorylation-dependent degradation of the cyclin-dependent kinase inhibitor p27. *EMBO J* 16(17):5334-5344.
202. Xu S*, et al.* (2007) Substrate recognition and ubiquitination of SCFSkp2/Cks1 ubiquitin-protein isopeptide ligase. *J Biol Chem* 282(21):15462-15470.
203. Wang W, Nacusi L, Sheaff RJ, & Liu X (2005) Ubiquitination of p21Cip1/WAF1 by SCFSkp2: substrate requirement and ubiquitination site selection. *Biochemistry* 44(44):14553-14564.
204. Ungermannova D, Gao Y, & Liu X (2005) Ubiquitination of p27Kip1 requires physical interaction with cyclin E and probable phosphate recognition by SKP2. *J Biol Chem* 280(34):30301-30309.
205. Nishitani H*, et al.* (2008) CDK inhibitor p21 is degraded by a proliferating cell nuclear antigen-coupled Cul4-DDB1Cdt2 pathway during S phase and after UV irradiation. *J Biol Chem* 283(43):29045-29052.
206. Kim Y, Starostina NG, & Kipreos ET (2008) The CRL4Cdt2 ubiquitin ligase targets the degradation of p21Cip1 to control replication licensing. *Genes Dev* 22(18):2507-2519.
207. Havens CG & Walter JC (2009) Docking of a specialized PIP Box onto chromatin-bound PCNA creates a degron for the ubiquitin ligase CRL4Cdt2. *Mol Cell* 35(1):93-104.

208. Havens CG & Walter JC (2011) Mechanism of CRL4(Cdt2), a PCNA-dependent E3 ubiquitin ligase. *Genes Dev* 25(15):1568-1582.
209. Abbas T*, et al.* (2008) PCNA-dependent regulation of p21 ubiquitylation and degradation via the CRL4Cdt2 ubiquitin ligase complex. *Genes Dev* 22(18):2496-2506.
210. Amador V, Ge S, Santamaria PG, Guardavaccaro D, & Pagano M (2007) APC/C(Cdc20) controls the ubiquitin-mediated degradation of p21 in prometaphase. *Mol Cell* 27(3):462-473.
211. de Nooij JC, Letendre MA, & Hariharan IK (1996) A cyclin-dependent kinase inhibitor, Dacapo, is necessary for timely exit from the cell cycle during Drosophila embryogenesis. *Cell* 87(7):1237-1247.
212. Lane ME*, et al.* (1996) Dacapo, a cyclin-dependent kinase inhibitor, stops cell proliferation during Drosophila development. *Cell* 87(7):1225-1235.
213. de Nooij JC, Graber KH, & Hariharan IK (2000) Expression of the cyclin-dependent kinase inhibitor Dacapo is regulated by cyclin E. *Mech Dev* 97(1-2):73-83.
214. Swanson CI*, et al.* (2015) Expression of an S phase-stabilized version of the CDK inhibitor Dacapo can alter endoreplication. *Development* 142(24):4288-4298.
215. Dui W*, et al.* (2013) The Drosophila F-box protein dSkp2 regulates cell proliferation by targeting Dacapo for degradation. *Mol Biol Cell* 24(11):1676-1687, S1671-1677.
216. Ghorbani M, Vasavan B, Kraja E, & Swan A (2011) Cks85A and Skp2 interact to maintain diploidy and promote growth in Drosophila. *Developmental Biology* 358(1):213-223.
217. Thomas BJ, Gunning DA, Cho J, & Zipursky L (1994) Cell cycle progression in the developing Drosophila eye: roughex encodes a novel protein required for the establishment of G1. *Cell* 77(7):1003-1014.
218. Thomas BJ*, et al.* (1997) roughex down-regulates G2 cyclins in G1. *Genes Dev* 11(10):1289-1298.
219. Reimann JDR*, et al.* (2001) Emi1 is a mitotic regulator that interacts with Cdc20 and inhibits the anaphase promoting complex. *Cell* 105(5):645-655.
220. Miller JJ*, et al.* (2006) Emi1 stably binds and inhibits the anaphase-promoting complex/cyclosome as a pseudosubstrate inhibitor. *Genes Dev* 20(17):2410-2420.
221. Di Fiore B & Pines J (2007) Emi1 is needed to couple DNA replication with mitosis but does not regulate activation of the mitotic APC/C. *Journal of Cell Biology* 177(3):425-437.
222. Hansen DV, Loktev AV, Ban KH, & Jackson PK (2004) Plk1 regulates activation of the anaphase promoting complex by phosphorylating and triggering SCFbetaTrCP-dependent destruction of the APC Inhibitor Emi1. *Mol Biol Cell* 15(12):5623-5634.
223. Frye JJ*, et al.* (2013) Electron microscopy structure of human APC/C(CDH1)-EMI1 reveals multimodal mechanism of E3 ligase shutdown. *Nat Struct Mol Biol* 20(7):827-835.
224. Yamano H (2013) EMI1, a three-in-one ubiquitylation inhibitor. *Nat Struct Mol Biol* 20(7):773-774.
225. Margottin-Goguet F*, et al.* (2003) Prophase destruction of Emi1 by the SCF(betaTrCP/Slimb) ubiquitin ligase activates the anaphase promoting complex to allow progression beyond prometaphase. *Dev Cell* 4(6):813-826.
226. Lau AW, Fukushima H, & Wei WY (2012) The Fbw7 and Beta-TRCP E3 ubiquitin ligases and their roles in tumorigenesis. *Front Biosci-Landmrk* 17:2197-2212.
227. Moshe Y, Boulaire J, Pagano M, & Hershko A (2004) Role of Polo-like kinase in the degradation of early mitotic inhibitor 1, a regulator of the anaphase promoting complex/cyclosome. *P Natl Acad Sci USA* 101(21):7937-7942.
228. Eldridge AG*, et al.* (2006) The evi5 oncogene regulates cyclin accumulation by stabilizing the anaphase-promoting complex inhibitor emi1. *Cell* 124(2):367-380.
229. Dong X*, et al.* (1997) Control of G1 in the developing Drosophila eye: rca1 regulates Cyclin A. *Genes Dev* 11(1):94-105.

230. Grosskortenhaus R & Sprenger F (2002) Rca1 inhibits APC-Cdh1(Fzr) and is required to prevent cyclin degradation in G2. *Dev Cell* 2(1):29-40.
231. Zielke N, Querings S, Grosskortenhaus R, Reis T, & Sprenger F (2006) Molecular dissection of the APC/C inhibitor Rca1 shows a novel F-box-dependent function. *EMBO Rep* 7(12):1266-1272.
232. Morgenthaler C (2013) Der Zellzyklusregulator Rca1 - Inhibitor und Substrat des Anaphase-Promoting-Komplexes in *Drosophila melanogaster*. phD (University of Regensburg, phD Thesis).
233. Letunic I, Doerks T, & Bork P (2015) SMART: recent updates, new developments and status in 2015. *Nucleic Acids Res* 43(Database issue):D257-260.
234. Kosugi S, Hasebe M, Tomita M, & Yanagawa H (2009) Systematic identification of cell cycle-dependent yeast nucleocytoplasmic shuttling proteins by prediction of composite motifs. *Proc Natl Acad Sci U S A* 106(25):10171-10176.
235. Kies M (2011) Analyse von rca1-Allelen und Herstellung von transgenen Drosophila zur Bestimmung von Rca1-Aktivität in vivo. Bachelor (University of Regensburg, Bachelor Thesis).
236. Frank M (2013) Analyse der F-box-Funktion von Rca1 in *Drosophila melanogaster*. phD (University of Regensburg, phD Thesis).
237. Giot L*, et al.* (2003) A protein interaction map of Drosophila melanogaster. *Science* 302(5651):1727-1736.
238. Huntley RP*, et al.* (2015) The GOA database: gene Ontology annotation updates for 2015. *Nucleic Acids Res* 43(Database issue):D1057-1063.
239. Binns D*, et al.* (2009) QuickGO: a web-based tool for Gene Ontology searching. *Bioinformatics* 25(22):3045-3046.
240. Heo J, Eki R, & Abbas T (2016) Deregulation of F-box proteins and its consequence on cancer development, progression and metastasis. *Semin Cancer Biol* 36:33-51.
241. Cardozo T & Pagano M (2004) The SCF ubiquitin ligase: insights into a molecular machine. *Nat Rev Mol Cell Biol* 5(9):739-751.
242. Lee HS, Simon JA, & Lis JT (1988) Structure and expression of ubiquitin genes of Drosophila melanogaster. *Mol Cell Biol* 8(11):4727-4735.
243. Komander D, Clague MJ, & Urbe S (2009) Breaking the chains: structure and function of the deubiquitinases. *Nat Rev Mol Cell Biol* 10(8):550-563.
244. Grasmüller C (2016) Investigation of CKI turnover in Drosophila and human cells using in vivo ubiquitination and protein stability analysis. Master (University of Regensburg, Master Thesis).
245. Raasi S, Varadan R, Fushman D, & Pickart CM (2005) Diverse polyubiquitin interaction properties of ubiquitin-associated domains. *Nat Struct Mol Biol* 12(8):708-714.
246. Mark KG, Simonetta M, Maiolica A, Seller CA, & Toczyski DP (2014) Ubiquitin ligase trapping identifies an SCF(Saf1) pathway targeting unprocessed vacuolar/lysosomal proteins. *Mol Cell* 53(1):148-161.
247. Schrader EK, Harstad KG, & Matouschek A (2009) Targeting proteins for degradation. *Nat Chem Biol* 5(11):815-822.
248. Rubin GM*, et al.* (2000) A Drosophila complementary DNA resource. *Science* 287(5461):2222-2224.
249. Wong YH*, et al.* (2007) KinasePhos 2.0: a web server for identifying protein kinase-specific phosphorylation sites based on sequences and coupling patterns. *Nucleic Acids Res* 35(Web Server issue):W588-594.
250. Havens CG*, et al.* (2012) Direct role for proliferating cell nuclear antigen in substrate recognition by the E3 ubiquitin ligase CRL4Cdt2. *J Biol Chem* 287(14):11410-11421.
251. Peters JM (2006) The anaphase promoting complex/cyclosome: a machine designed to destroy. *Nat Rev Mol Cell Biol* 7(9):644-656.
252. Tian W*, et al.* (2012) Structural analysis of human Cdc20 supports multisite degron recognition by APC/C. *Proc Natl Acad Sci U S A* 109(45):18419-18424.

253. Kies M (2013) Establishment of APC/C activity assays for the analysis of Rca1 as an inhibitor and substrate of the APC/C. Master (University of Regensburg, Master Thesis).
254. Kramer ER, Gieffers C, Holzl G, Hengstschlager M, & Peters JM (1998) Activation of the human anaphase-promoting complex by proteins of the CDC20/Fizzy family. *Curr Biol* 8(22):1207-1210.
255. Camasses A, Bogdanova A, Shevchenko A, & Zachariae W (2003) The CCT chaperonin promotes activation of the anaphase-promoting complex through the generation of functional Cdc20. *Molecular Cell* 12(1):87-100.
256. Berger I, Fitzgerald DJ, & Richmond TJ (2004) Baculovirus expression system for heterologous multiprotein complexes. *Nat Biotechnol* 22(12):1583-1587.
257. Trowitzsch S, Bieniossek C, Nie Y, Garzoni F, & Berger I (2010) New baculovirus expression tools for recombinant protein complex production. *J Struct Biol* 172(1):45-54.
258. Fitzgerald DJ*, et al.* (2006) Protein complex expression by using multigene baculoviral vectors. *Nat Methods* 3(12):1021-1032.
259. Wang Y, Wang F, Wang R, Zhao P, & Xia Q (2015) 2A self-cleaving peptide-based multi-gene expression system in the silkworm Bombyx mori. *Sci Rep* 5:16273.
260. Burton JL, Xiong Y, & Solomon MJ (2011) Mechanisms of pseudosubstrate inhibition of the anaphase promoting complex by Acm1. *EMBO J* 30(9):1818-1829.
261. Tang W, Pavlish OA, Spiegelman VS, Parkhitko AA, & Fuchs SY (2003) Interaction of Epstein-Barr virus latent membrane protein 1 with SCFHOS/beta-TrCP E3 ubiquitin ligase regulates extent of NF-kappaB activation. *J Biol Chem* 278(49):48942-48949.
262. Sorensen CS*, et al.* (2001) A conserved cyclin-binding domain determines functional interplay between anaphase-promoting complex-Cdh1 and cyclin A-Cdk2 during cell cycle progression. *Mol Cell Biol* 21(11):3692-3703.
263. Zielke N (2006) Functional analysis of the cell cycle regulator Rca1 in Drosophila melanogaster. phD (University of Cologne, phD Thesis).
264. Hoogenraad CC & Akhmanova A (2016) Bicaudal D Family of Motor Adaptors: Linking Dynein Motility to Cargo Binding. *Trends Cell Biol* 26(5):327-340.
265. den Dunnen JT & Antonarakis SE (2000) Mutation nomenclature extensions and suggestions to describe complex mutations: a discussion. *Hum Mutat* 15(1):7-12.
266. Kosugi S*, et al.* (2008) Design of peptide inhibitors for the importin alpha/beta nuclear import pathway by activity-based profiling. *Chemistry & biology* 15(9):940-949.
267. Kosugi S*, et al.* (2009) Six classes of nuclear localization signals specific to different binding grooves of importin alpha. *The Journal of biological chemistry* 284(1):478-485.
268. Mullis K*, et al.* (1986) Specific enzymatic amplification of DNA in vitro: the polymerase chain reaction. *Cold Spring Harbor symposia on quantitative biology* 51 Pt 1:263-273.
269. Berghammer H & Auer B (1993) "Easypreps": fast and easy plasmid minipreparation for analysis of recombinant clones in E. coli. *Biotechniques* 14(4):524, 528.
270. Birnboim HC & Doly J (1979) A rapid alkaline extraction procedure for screening recombinant plasmid DNA. *Nucleic acids research* 7(6):1513-1523.
271. Mello CC & Conte D, Jr. (2004) Revealing the world of RNA interference. *Nature* 431(7006):338-342.
272. Gurevich VV, Pokrovskaya ID, Obukhova TA, & Zozulya SA (1991) Preparative in vitro mRNA synthesis using SP6 and T7 RNA polymerases. *Anal Biochem* 195(2):207-213.
273. Laemmli UK (1970) Cleavage of structural proteins during the assembly of the head of bacteriophage T4. *Nature* 227(5259):680-685.

12 Supplement

12.1 Identification of Rca1 interaction partners by mass spectrometry

Table 39: 4XFLAG-Rca1 precipitate from S2R+ cells was analyzed by LC-MS/MS. Raw MS data were searched against the *Drosphila* UniProtKB database. Identified proteins were restricted to proteins involved in cell cycle regulation using the gene ontology browser QuickGo (GO-term "cell cycle"/GO:0007049, releationship settings: is_a, part_of, occurs_in, regulates, positively_regulates and negatively_regulates)

Protein	Biological process (related to GO term "cell cycle")	Score	No. of peptides	SC [%]
cindr	regulation of cytokinesis	1803.0	28	49.2
Rca1	G1/S transition of mitotic cell cycle regulation of mitotic nuclear division negative regulation of meiotic nuclear division negative regulation of ubiquitin-protein ligase activity involved in mitotic cell cycle	1541.9	26	42.1
Skp2	mitotic cell cycle endomitotic cell cycle positive regulation of cell cycle	1076.0	18	33.1
Khc-73	establishment of spindle orientation	951.0	23	15.4
bel	mitotic sister chromatid segregation	938.5	19	37.8
14-3-3epsilon	DNA damage checkpoint regulation of mitotic nuclear division mitotic cell cycle checkpoint mitotic G2 DNA damage checkpoint	917.8	15	51.9
eIF4G1	G1/S transition of mitotic cell cycle mitotic nuclear division mitotic G2 DNA damage checkpoint	898.3	23	20.0
alphaTub84B	mitotic spindle assembly checkpoint	880.6	16	51.1
Dis3	mitotic cell cycle	781.1	20	24.8
pAbp	male meiosis cytokinesis male meiosis	779.9	16	31.4
gammaTub23C	mitotic nuclear division centrosome duplication mitotic sister chromatid separation regulation of cell cycle	779.1	15	37.1
SkpA	mitotic nuclear division mitotic G2 DNA damage checkpoint regulation of centrosome duplication DNA endoreduplication positive regulation of mitotic cell cycle centrosome duplication	776.1	10	72.2
Cul1	mitotic G2 DNA damage checkpoint	738.1	17	26.7
alphaCOP	male meiosis cytokinesis	649.8	17	18.2
RpL10Ab	centrosome duplication	584.3	10	47.9
hyd	male meiosis cytokinesis	525.8	19	8.7

RpL3	centrosome duplication	524.7	9	31.2
Eb1	mitotic spindle elongation mitotic spindle organization establishment of mitotic spindle localization spindle assembly	494.9	9	32.1
me31B	mitotic G2 DNA damage checkpoint	492.4	13	37.3
rump	mitotic nuclear division	459.3	8	15.0
Ote	cell cycle mitotic nuclear division	434.9	8	31.1
Act57B	mitotic cytokinesis	428.8	10	31.9
RpL4	centrosome duplication	412.9	9	23.4
msps	mitotic spindle elongation establishment of mitotic spindle orientation cell cycle mitotic nuclear division female meiotic division meiotic cell cycle	406.5	12	8.2
pont	cell cycle mitotic G2 DNA damage checkpoint mitotic spindle assembly	397.9	10	30.7
REG	regulation of G1/S transition of mitotic cell cycle	382.1	9	37.6
RpL21	centrosome duplication	373.4	9	37.7
gammaCOP	mitotic cytokinesis male meiosis cytokinesis	365.7	8	12.2
mEFTu1	mitotic cell cycle	345.2	7	27.2
CCT4	mitotic spindle organization	343.7	10	25.3
Khc	centrosome separation	342.3	8	11.2
Klp61F	mitotic cell cycle cell cycle mitotic spindle organization mitotic nuclear division mitotic centrosome separation centrosome duplication centrosome separation mitotic spindle assembly	340.5	11	13.3
Spindly	mitotic spindle assembly checkpoint regulation of mitotic metaphase/anaphase transition	320.2	8	16.6
CCT6	mitotic spindle organization mitotic nuclear division centriole replication	302.2	7	16.3
tsr	mitotic cytokinesis actomyosin contractile ring assembly cell cycle meiotic cytokinesis centrosome separation	278.6	5	35.8
RpS6	centrosome duplication	274.1	4	18.1
RpL14	centrosome duplication	264.5	4	26.5
CCT2	mitotic spindle organization centrosome duplication	258.2	9	24.7

DCTN2-p50	spindle organization mitotic spindle organization mitotic nuclear division	256.3	7	24.5
RpL27	centrosome duplication	254.9	5	37.0
l(1)dd4	meiotic spindle organization male meiosis centrosome duplication mitotic spindle assembly	237.5	7	10.9
eIF3-S6	regulation of cell cycle	226.1	5	13.8
CCT7	mitotic spindle organization	222.2	7	17.6
lark	mitotic nuclear division	218.8	6	21.3
RpL23A	centrosome duplication	216.1	5	13.0
Smr	regulation of mitotic cell cycle	209.7	7	2.2
Grip75	spindle assembly involved in female meiosis II mitotic nuclear division male meiosis cytokinesis centrosome duplication mitotic spindle assembly	207.5	4	8.9
rept	mitotic G2 DNA damage checkpoint	206.1	4	10.0
CCT8	mitotic spindle organization	204.2	6	12.3
Caf1	mitotic cytokinesis regulation of mitotic cell cycle	203.9	4	14.7
Cdk2	regulation of cell cycle	196.3	5	24.5
Mcm7	cell cycle mitotic G2 DNA damage checkpoint	193.9	6	11.1
SF2	mitotic G2 DNA damage checkpoint	192.2	6	22.4
RpL8	centrosome duplication	189.1	4	21.9
Kap-alpha3	mitotic G2 DNA damage checkpoint	185.7	3	8.8
Grip71	spindle assembly involved in female meiosis I mitotic nuclear division centrosome duplication regulation of cell cycle	178.5	6	12.1
polo	mitotic cell cycle actomyosin contractile ring assembly spindle assembly involved in female meiosis II mitotic nuclear division male meiosis cytokinesis male meiosis female meiotic division female meiosis II astral microtubule nucleation meiotic spindle midzone assembly attachment of mitotic spindle microtubules to kinetochore	167.9	5	9.4
RpL18A	centrosome duplication	167.0	5	26.6
Mcm6	cell cycle mitotic nuclear division	160.0	5	7.5
RpL6	centrosome duplication	158.4	3	10.3
His2A	centrosome duplication	158.3	3	49.2

spidey	negative regulation of DNA endoreduplication	151.4	4	15.6
shrb	mitotic cytokinesis	142.5	3	24.8
CG30291	regulation of cyclin-dependent protein serine/threonine kinase activity	138.2	5	12.8
Cdc16	mitotic cell cycle mitotic nuclear division regulation of mitotic metaphase/anaphase transition positive regulation of mitotic metaphase/anaphase transition	129.6	4	6.1
RpA-70	mitotic G2 DNA damage checkpoint	116.0	4	8.3
LanA	female meiosis chromosome segregation	113.2	4	1.5
Cul4	mitotic G2 DNA damage checkpoint	108.3	4	5.4
Pen	centrosome duplication	107.3	3	8.0
Cdk1	G1/S transition of mitotic cell cycle G2/M transition of mitotic cell cycle mitotic cell cycle cell cycle mitotic nuclear division mitotic G2 DNA damage checkpoint male meiosis male meiosis I meiotic G2/MI transition mitotic G2/M transition checkpoint regulation of meiotic cell cycle	106.3	3	14.5
cher	mitotic nuclear division	101.5	4	2.8
SmD2	mitotic nuclear division	101.1	4	38.7
CycE	G1/S transition of mitotic cell cycle regulation of cell cycle	100.2	3	6.5
Cdc5	centrosome duplication	99.8	3	6.9
Arp1	mitotic nuclear division	96.8	3	12.0
Mcm5	resolution of meiotic recombination intermediates cell cycle meiotic nuclear division DNA endoreduplication	96.0	3	4.2
dap	regulation of cyclin-dependent protein serine/threonine kinase activity mitotic cell cycle cell cycle arrest regulation of mitotic cell cycle negative regulation of cell cycle negative regulation of G1/S transition of mitotic cell cycle	94.5	3	16.7
CycB	G2/M transition of mitotic cell cycle mitotic cytokinesis cell cycle mitotic nuclear division mitotic chromosome movement towards spindle pole attachment of spindle microtubules to kinetochore syncytial blastoderm mitotic cell cycle	92.8	3	9.2
pic	mitotic G2 DNA damage checkpoint	92.5	4	4.4

Nup43	mitotic nuclear division	91.3	2	8.9
RpL30	centrosome duplication	90.5	3	25.2
mr	regulation of cell cycle	90.4	2	4.1
Jra	regulation of cell cycle	87.5	3	14.9
RpL13A	centrosome duplication	86.5	2	9.3
Fim	female meiosis chromosome segregation	85.4	2	4.2
sti	mitotic cytokinesis actomyosin contractile ring assembly male meiosis cytokinesis regulation of cytokinesis regulation of cytokinesis, actomyosin contractile ring assembly	84.8	4	3.0
Non3	cell cycle mitotic nuclear division mitotic spindle assembly	84.4	2	6.9
RpL19	centrosome duplication	83.2	1	8.4
Su(var)205	mitotic nuclear division	83.0	1	9.2
thoc5	male meiosis	82.8	4	7.8
Tctp	mitotic G2 DNA damage checkpoint intra-S DNA damage checkpoint	82.6	2	12.2
1-Sep	mitotic cytokinesis cell cycle	80.7	1	3.0
CG31687	regulation of mitotic metaphase/anaphase transition	78.5	2	6.3
pzg	positive regulation of mitotic cell cycle	78.1	3	4.5
tum	mitotic cytokinesis regulation of cytokinesis centrosome duplication	76.6	3	5.9
eIF3ga	mitotic nuclear division regulation of cell cycle	75.8	3	9.3
ens	centrosome separation	74.0	3	7.3
RfC38	sister chromatid cohesion	73.1	2	7.3
Nup44A	regulation of mitotic cell cycle regulation of meiotic cell cycle	71.0	2	9.6
SmD3	mitotic nuclear division	68.4	2	12.6
pnut	mitotic cytokinesis actomyosin contractile ring assembly cell cycle	67.3	2	4.1
Rab11	actomyosin contractile ring contraction male meiosis cytokinesis	61.5	2	9.8
M1BP	mitotic G2 DNA damage checkpoint	60.3	1	2.6
Nipped-B	mitotic sister chromatid cohesion	59.9	2	1.1
2-Sep	mitotic cytokinesis cell cycle mitotic nuclear division regulation of cell cycle	58.6	3	10.5
Ras85D	G1/S transition of mitotic cell cycle	57.1	2	11.1
Mcm2	cell cycle	56.6	3	5.0

ebi	cell cycle	54.9	1	2.1
Rae1	mitotic cell cycle male meiosis I regulation of cell cycle regulation of G1/S transition of mitotic cell cycle	53.4	2	7.2
MBD-R2	mitotic G2 DNA damage checkpoint	53.2	2	1.7
Aos1	regulation of mitotic cell cycle	52.9	2	6.2
smt3	mitotic spindle organization syncytial blastoderm mitotic cell cycle	52.7	1	13.3
mor	negative regulation of G1/S transition of mitotic cell cycle	52.6	3	3.3
mgr	spindle assembly involved in meiosis	50.3	2	10.3
mgr	mitotic spindle assembly	50.3	2	10.3
Gl	mitotic nuclear division second mitotic wave involved in compound eye morphogenesis spindle assembly mitotic spindle midzone assembly centrosome separation	49.1	2	1.7
mip120	cell cycle	49.1	1	2.0
pins	establishment of mitotic spindle orientation establishment of mitotic spindle localization establishment of spindle orientation	47.7	1	2.6
RpL35	centrosome duplication	46.9	1	10.6
PCNA	mitotic spindle organization	42.1	1	7.3
emb	centriole replication	40.3	2	2.5
shtd	mitotic nuclear division	40.1	2	2.0
nesd	cell cycle male meiosis cytokinesis meiotic cell cycle	39.3	1	2.0
Rpb5	mitotic G2 DNA damage checkpoint	38.0	1	8.1
RfC3	sister chromatid cohesion	38.0	1	3.0
fzr	regulation of mitotic nuclear division positive regulation of exit from mitosis exit from mitosis	37.5	1	3.3
Cdc37	cell cycle mitotic nuclear division meiotic cell cycle	37.1	1	3.3
geminin	endomitotic cell cycle regulation of syncytial blastoderm mitotic cell cycle	34.2	2	10.4
BubR1	male meiosis sister chromatid cohesion female meiosis sister chromatid cohesion mitotic spindle assembly checkpoint regulation of exit from mitosis male meiosis regulation of mitotic sister chromatid separation meiotic sister chromatid cohesion, centromeric	33.6	1	1.0
tacc	mitotic spindle organization mitotic nuclear division female meiotic division	33.4	2	2.0

CG3436	mitotic nuclear division	32.5	1	3.2
Grip163	mitotic nuclear division meiotic nuclear division centrosome duplication mitotic spindle assembly	31.0	1	0.7
Dlic	mitotic nuclear division	30.5	1	3.8
SelD	cell cycle	29.4	1	3.8
Mink	mitotic cytokinesis establishment of mitotic spindle localization	27.3	1	2.5
Not1	mitotic G2 DNA damage checkpoint	25.9	1	0.6
pelo	meiotic spindle organization cell cycle mitotic nuclear division meiotic nuclear division male meiosis male meiosis I meiotic G2/MI transition meiotic nuclear envelope disassembly meiotic cell cycle	25.0	1	2.5
Bap55	mitotic cytokinesis mitotic nuclear division	24.9	1	2.4
Spc105R	attachment of spindle microtubules to kinetochore	24.4	1	0.4
ida	positive regulation of mitotic metaphase/anaphase transition regulation of cell cycle	23.6	1	1.2
mio	regulation of meiotic nuclear division	23.6	1	1.6
MED17	mitotic G2 DNA damage checkpoint	23.2	1	1.9
Det	mitotic cytokinesis actomyosin contractile ring assembly mitotic spindle organization meiosis I cytokinesis meiosis II cytokinesis meiotic cytokinesis meiotic chromosome segregation spindle assembly mitotic spindle assembly	22.8	1	10.5
TBCD	microtubule cytoskeleton organization involved in mitosis	22.6	1	1.2
mud	establishment of mitotic spindle orientation spindle assembly involved in female meiosis II	22.6	1	0.6
CG5181	mitotic cell cycle checkpoint	22.1	1	4.4
COX4	mitotic cell cycle	21.4	1	6.6
mip130	cell cycle	20.9	1	1.6
Mcm3	mitotic G2 DNA damage checkpoint	20.8	1	2.4
Ctf4	mitotic cell cycle preblastoderm mitotic cell cycle DNA endoreduplication	20.7	1	1.2
Tap42	mitotic spindle organization	19.9	1	4.5
mre11	mitotic G2 DNA damage checkpoint intra-S DNA damage checkpoint	19.4	1	1.8

	meiotic cell cycle			
RpII215	mitotic G2 DNA damage checkpoint	18.8	1	0.5
noi	mitotic nuclear division regulation of cell cycle	18.2	1	1.8
kst	mitotic cytokinesis	17.9	1	0.3
mip40	cell cycle	17.8	1	6.4
Bub3	mitotic spindle assembly checkpoint	17.7	1	2.1
Rbf	cell cycle mitotic G2 DNA damage checkpoint endomitotic cell cycle maintenance of mitotic sister chromatid cohesion DNA endoreduplication regulation of cell cycle regulation of cohesin loading negative regulation of G1/S transition of mitotic cell cycle	17.5	1	1.7
wds	mitotic G2 DNA damage checkpoint	17.3	1	3.9
aub	mitotic chromosome condensation	17.2	1	1.5
CG11839	mitotic nuclear division	16.9	1	4.7
tef	cell cycle male meiosis chromosome segregation male meiosis I male meiosis chromosome separation meiotic cell cycle	16.5	1	1.2
nopo	positive regulation of mitotic cell cycle, embryonic	16.4	1	1.8
pav	mitotic cytokinesis cytokinesis actomyosin contractile ring assembly actomyosin contractile ring contraction mitotic spindle organization female meiosis chromosome segregation centrosome duplication microtubule bundle formation involved in mitotic spindle midzone assembly	16.4	1	2.0
CG8273	regulation of cell cycle	16.1	1	1.4
CycK	positive regulation of cyclin-dependent protein serine/threonine kinase activity	16.0	1	2.2
alph	mitotic cell cycle	15.9	1	2.1
skap	mitotic spindle organization regulation of centrosome duplication	15.8	1	4.9
SMC2	mitotic nuclear division	15.7	1	0.8
slmb	regulation of mitotic nuclear division regulation of centriole replication	15.6	1	2.4
gpp	DNA damage checkpoint regulation of cell cycle	15.5	1	0.4
Asun	cell cycle mitotic nuclear division regulation of mitotic cell cycle meiotic cell cycle	15.4	1	2.8
Sin3A	regulation of mitotic cell cycle	15.4	1	0.6

SCAR	actin filament reorganization involved in cell cycle	15.3	1	2.9
Cog3	male meiosis cytokinesis	15.2	1	0.8
mia	meiotic nuclear division male meiosis I	15.1	1	1.2

12.2 Identification of Dap interaction partners by mass spectrometry

Table 40: 4XFLAG-Dap-dCDI-dPIPa precipitate from S2R+ cells was analyzed by LC-MS/MS. Raw MS data were searched against the *Drosphila* UniProtKB database. Identified proteins were restricted to proteins involved in cell cycle regulation using the gene ontology browser QuickGo GO-term "cell cycle"/GO:0007049, releationship settings: is_a, part_of, occurs_in, regulates, positively_regulates and negatively_regulates)

Protein	Biological process (related to GO term "cell cycle")	Score	No. of peptides	SC [%]
dap	regulation of cyclin-dependent protein serine/threonine kinase activity mitotic cell cycle cell cycle arrest regulation of mitotic cell cycle negative regulation of cell cycle negative regulation of G1/S transition of mitotic cell cycle	1807.4	22	64.5
14-3-3epsilon	DNA damage checkpoint regulation of mitotic nuclear division mitotic cell cycle checkpoint mitotic G2 DNA damage checkpoint	1438.6	23	53.4
cindr	regulation of cytokinesis	1249.9	21	30.5
alphaTub84D	mitotic cytokinesis	837.5	15	49.3
bel	mitotic sister chromatid segregation	617.3	14	27.6
pAbp	male meiosis cytokinesis male meiosis	521.1	12	23.2
gammaTub23C	mitotic nuclear division centrosome duplication mitotic sister chromatid separation regulation of cell cycle	501.3	10	25.5
Dis3	mitotic cell cycle	406.7	13	17.1
Khc-73	establishment of spindle orientation	359.8	12	8.6
RpL10Ab	centrosome duplication	333.1	8	41.0
RpL4	centrosome duplication	331.4	9	23.2
pont	cell cycle	328.0	8	26.5
rump	mitotic G2 DNA damage checkpoint mitotic spindle assembly mitotic nuclear division	298.7	6	10.4
eIF3-S6	regulation of cell cycle	288.9	6	18.9
Ote	cell cycle mitotic nuclear division	278.1	5	19.3
RpL3	centrosome duplication	261.7	5	17.1
Eb1	mitotic spindle elongation mitotic spindle organization establishment of mitotic spindle localization spindle assembly	256.6	5	19.3
eIF4G1	G1/S transition of mitotic cell cycle mitotic nuclear division mitotic G2 DNA damage checkpoint	255.6	10	6.8

RpL30	centrosome duplication	253.6	5	53.2
Khc	centrosome separation	250.3	7	7.9
me31B	mitotic G2 DNA damage checkpoint	246.1	6	19.2
RpS6	centrosome duplication	245.8	5	18.1
CCT4	mitotic spindle organization	232.5	6	22.7
Kap-alpha3	mitotic G2 DNA damage checkpoint	216.3	4	10.3
RpL21	centrosome duplication	215.2	6	27.7
RpL27	centrosome duplication	212.0	4	37.0
SkpA	mitotic nuclear division mitotic G2 DNA damage checkpoint regulation of centrosome duplication DNA endoreduplication positive regulation of mitotic cell cycle centrosome duplication	211.8	4	25.9
rept	mitotic G2 DNA damage checkpoint	208.9	5	12.5
His2A	centrosome duplication	206.7	2	25.8
tsr	mitotic cytokinesis actomyosin contractile ring assembly cell cycle meiotic cytokinesis centrosome separation	200.6	4	23.6
Rca1	G1/S transition of mitotic cell cycle regulation of mitotic nuclear division negative regulation of meiotic nuclear division negative regulation of ubiquitin-protein ligase activity involved in mitotic cell cycle	197.9	5	10.9
Pen	centrosome duplication	189.6	4	10.3
gammaCOP	mitotic cytokinesis male meiosis cytokinesis	178.7	6	7.2
alphaCOP	male meiosis cytokinesis	177.2	6	5.7
RpL14	centrosome duplication	176.8	4	26.5
DCTN2-p50	spindle organization mitotic spindle organization mitotic nuclear division	176.2	5	16.8
Klp61F	mitotic cell cycle cell cycle mitotic spindle organization mitotic nuclear division mitotic centrosome separation centrosome duplication centrosome separation mitotic spindle assembly	174.2	6	7.5
Mcm6	cell cycle mitotic nuclear division	161.4	5	7.8
lark	mitotic nuclear division	149.6	5	17.3

Mcm5	resolution of meiotic recombination intermediates cell cycle meiotic nuclear division DNA endoreduplication	145.9	5	7.8
Caf1	mitotic cytokinesis regulation of mitotic cell cycle	142.6	3	11.6
RpL23A	centrosome duplication	139.3	3	9.0
Cdc5	centrosome duplication	132.0	4	7.6
Rab11	actomyosin contractile ring contraction male meiosis cytokinesis	123.5	3	9.8
Mcm7	cell cycle mitotic G2 DNA damage checkpoint	116.6	4	7.2
Spindly	mitotic spindle assembly checkpoint regulation of mitotic metaphase/anaphase transition	102.6	3	5.8
1-Sep	mitotic cytokinesis	100.9	1	3.0
42979	cell cycle	100.9	1	3.0
ebi	cell cycle	91.5	2	4.6
spidey	negative regulation of DNA endoreduplication	91.1	2	9.7
Ras85D	G1/S transition of mitotic cell cycle	84.4	3	16.9
Pp1-87B	mitotic nuclear division mitotic metaphase plate congression spindle assembly	79.9	2	8.6
Bub3	mitotic spindle assembly checkpoint	79.0	3	12.6
RpA-70	mitotic G2 DNA damage checkpoint	77.8	2	4.0
RpL8	centrosome duplication	77.5	2	10.2
eIF3ga	mitotic nuclear division regulation of cell cycle	76.1	3	9.3
CCT2	mitotic spindle organization centrosome duplication	75.0	2	4.1
REG	regulation of G1/S transition of mitotic cell cycle	72.1	3	15.5
RpL18A	centrosome duplication	68.6	3	16.9
Cdc37	cell cycle mitotic nuclear division meiotic cell cycle	65.2	2	6.2
RfC38	sister chromatid cohesion	62.7	2	6.5
mEFTu1	mitotic cell cycle	61.8	2	8.0
Vps33B	mitotic spindle assembly	60.9	1	1.4
skap	mitotic spindle organization regulation of centrosome duplication	60.0	2	5.5
l(1)dd4	meiotic spindle organization male meiosis centrosome duplication mitotic spindle assembly	55.1	2	2.6
SF2	mitotic G2 DNA damage checkpoint	54.2	2	10.2
ens	centrosome separation	54.0	1	1.7
Arp3	actin filament reorganization involved in cell cycle	49.2	1	2.6

SmD3	mitotic nuclear division	46.7	1	6.6
pzg	positive regulation of mitotic cell cycle	46.2	2	3.3
Su(var)205	mitotic nuclear division	44.6	1	9.2
Mcm3	mitotic G2 DNA damage checkpoint	43.5	1	2.1
CCT6	mitotic spindle organization mitotic nuclear division centriole replication	42.1	2	5.3
RpL6	centrosome duplication	42.0	1	5.8
Cdk1	G1/S transition of mitotic cell cycle G2/M transition of mitotic cell cycle mitotic cell cycle cell cycle mitotic nuclear division mitotic G2 DNA damage checkpoint male meiosis male meiosis I meiotic G2/MI transition mitotic G2/M transition checkpoint regulation of meiotic cell cycle	40.8	2	9.8
SMC5	sister chromatid cohesion	39.9	2	2.6
rl	cell cycle mitotic nuclear division	37.0	1	4.0
RpL19	centrosome duplication	34.6	1	8.4
Cdk2	regulation of cell cycle	34.3	2	7.0
mud	establishment of mitotic spindle orientation spindle assembly involved in female meiosis II	33.5	1	0.6
M1BP	mitotic G2 DNA damage checkpoint	32.8	1	2.6
Cul4	mitotic G2 DNA damage checkpoint	32.6	2	2.4
pelo	meiotic spindle organization cell cycle mitotic nuclear division meiotic nuclear division male meiosis male meiosis I meiotic G2/MI transition meiotic nuclear envelope disassembly meiotic cell cycle	32.1	1	2.5
RpL35	centrosome duplication	31.6	1	10.6
asl	centrosome cycle centriole replication negative regulation of centriole elongation	31.4	1	0.7
Cul1	mitotic G2 DNA damage checkpoint	29.4	1	1.4
Nipped-B	mitotic sister chromatid cohesion	28.4	1	0.5
Rae1	mitotic cell cycle male meiosis I regulation of cell cycle regulation of G1/S transition of mitotic cell cycle	28.1	1	3.5
Arp1	mitotic nuclear division	27.9	1	2.1

Mcm2	cell cycle	27.9	1	1.8
Tctp	mitotic G2 DNA damage checkpoint intra-S DNA damage checkpoint	27.4	1	7.0
mgr	spindle assembly involved in meiosis mitotic spindle assembly	26.5	1	6.2
SmD2	mitotic nuclear division	26.4	1	6.7
kst	mitotic cytokinesis	25.6	1	0.2
Bap55	mitotic cytokinesis mitotic nuclear division	25.5	1	2.4
mip40	cell cycle	24.7	1	6.4
msps	mitotic spindle elongation establishment of mitotic spindle orientation cell cycle mitotic nuclear division female meiotic division meiotic cell cycle	24.5	1	0.6
Grip71	spindle assembly involved in female meiosis I mitotic nuclear division centrosome duplication regulation of cell cycle	24.5	1	2.2
tum	mitotic cytokinesis regulation of cytokinesis centrosome duplication	23.6	1	1.9
CycE	G1/S transition of mitotic cell cycle regulation of cell cycle	22.6	1	2.3
asp	establishment of mitotic spindle orientation cell cycle spindle organization mitotic spindle organization mitotic nuclear division actin filament reorganization involved in cell cycle astral microtubule nucleation establishment of meiotic spindle localization	22.6	1	0.5
Gl	mitotic nuclear division second mitotic wave involved in compound eye morphogenesis spindle assembly mitotic spindle midzone assembly centrosome separation	21.8	1	0.9
JIL-1	female meiosis chromosome segregation	21.5	1	1.2
timeout	DNA damage checkpoint	19.9	1	0.7
CCT7	mitotic spindle organization	19.0	1	2.2
Rpb8	mitotic G2 DNA damage checkpoint	18.4	1	5.4
mip120	cell cycle	18.0	1	2.0
Su(var)2-10	mitotic G2 DNA damage checkpoint	17.7	1	1.9
spd-2	astral microtubule organization	17.6	1	1.2
wake	establishment of mitotic spindle orientation	17.2	1	1.1
CCT8	mitotic spindle organization	16.6	1	1.8

RfC3	sister chromatid cohesion	16.4	1	3.9
mop	spindle assembly	16.3	1	0.4
smt3	mitotic spindle organization syncytial blastoderm mitotic cell cycle	16.2	1	13.3
PCNA	mitotic spindle organization	16.1	1	7.3
Nup44A	regulation of mitotic cell cycle regulation of meiotic cell cycle	15.8	1	3.1
RpL13A	centrosome duplication	15.8	1	5.4
Skp2	mitotic cell cycle endomitotic cell cycle positive regulation of cell cycle	15.8	1	2.0
Spc105R	attachment of spindle microtubules to kinetochore	15.6	1	0.4
Jra	regulation of cell cycle	15.5	1	4.5
CG30291	regulation of cyclin-dependent protein serine/threonine kinase activity	15.3	1	2.0
pds5	sister chromatid cohesion mitotic sister chromatid cohesion mitotic cohesin unloading	15.3	1	1.6
gig	regulation of cell cycle	15.1	1	1.2

13 Zusammenfassung

Der Anaphase-Promoting Complex/Cyclosome (APC/C) vermittelt den Abbau einer Vielzahl an mitotischen Zellzyklus-regulatorischen Proteinen und eine strikte Regulation der APC/C Aktivität spielt eine zentrale Rolle im Zellzyklus. Für den Eintritt in die Mitose ist es wichtig, den APC/C in der G2-Phase inaktiv zu halten; dies geschieht 1) durch Cdk-abhängige Phosphorylierung der APC/C-aktivierenden Untereinheit Fzr, wodurch Fzr nicht mehr mit dem APC/C interagieren kann, und 2) durch direkte Inhibition von APC/C-Fzr mittels Regulator of Cyclin A1 (Rca1). Vorangegangene Studien lassen vermuten, dass neben dem C-terminalen Teil auch die zentral lokalisierte F-box in Rca1 wichtig für die APC/C-Fzr Inhibition ist. F-box Proteine rekrutieren normalerweise Substrate zu SCF Komplexen, was zu deren Polyubiquitinierung und anschließendem Abbau führt. Um solche Substrate zu identifizieren, wurde ein Rca1 Präzipitat von S2R+ Zellen mittels Massenspektrometrie analysiert. Rca1 wurde in Komplex mit SCF Komponenten und anderen Zellzyklus-regulatorischen Proteinen wie Dap und Skp2 gefunden. Rca1 bindet *in vivo* F-box abhängig polyubiquitinierte Substrate, was auf einen funktionalen SCF-Rca1 Komplex hinweist. Um zu analysieren, ob SCF-Rca1 die Proteinstabilität von Dap und Skp2 beeinflusst, wurde eine Methode für die Stabilitätsanalyse von GFP-gebundenen Proteinen während des Verlauf des Zellzyklus von S2R+ Zellen etabliert. Die Dap Stabilität wurde analysiert, indem eine Zellzyklus-inaktive GFP-getaggte Version von Dap verwendet wurde, welche nicht mehr während der S-Phase durch CRL4-Cdt2 destabilisiert wird (GFP-Dap-dCDI-dPIPa). Herabregulation der Rca1 Aktivität mittels RNAi führte zu einer Stabilisierung von GFP-Dap-dCDI-dPIPa. Im Gegensatz dazu, stimulierte die Überexpression von Rca1 F-box abhängig den Abbau von GFP-Dap-dCDI-dPIPa. Überexpression von CycE verstärkte die Interaktion zwischen Rca1 und Dap-dCDI-dPIPa und führte zu einer weiteren Destabilisierung von GFP-Dap-dCDI-dPIPa. Dies zeigt, dass SCF-Rca1 synergistisch mit CycE/Cdk2 agiert um den Abbau von Dap zu vermitteln. Zwei potentielle Cdk Phosphorylierungsstellen in Dap, S205 und S214, wurden mutiert, jedoch beeinflussten diese Mutationen weder die Stabilität, noch störten sie die Interaktion mit Rca1. Interaktionsanalysen mit verkürzten Rca1 und Dap Konstrukten zeigten, dass der N-terminale Teil von Dap und die zentrale Region in Rca1 für deren Interaktion benötigt werden. Solche N-terminal verkürzten Dap-Konstrukte zeigten auch eine starke Stabilisierung von GFP-Dap-dCDI-dPIPa. Durchflusszytometrie-basierte *in vivo* APC/C-Fzr Aktivitäts-Assays in S2R+ Zellen wurden verwendet, um die funktionale Interaktion zwischen SCF-Rca1 und Dap zu analysieren. Ein Verlust der F-box in Rca1 reduzierte dessen APC/C-Fzr-Inhibition. Durch gleichzeitige RNAi-vermittelte Herabregulation von Dap wurde die APC/C-Inhibition zum Teil wiederhergestellt. Zusammengefasst kann aus diesen Studien ein Modell vorgeschlagen werden, in dem Rca1 in einem SCF-Komplex agiert, Dap als Substrat bindet und für den Abbau markiert. Dadurch kann CycE/Cdk2 Aktivität freigesetzt werden, was zur Phosphorylierung von Fzr führt und somit dessen Interaktion mit dem APC/C unterbindet. Um die Inhibition des APC/C durch Rca1 biochemisch zu untersuchen, wurde ein *in vitro* APC/C-Fzr Ubiquitinylierungsassay weiterentwickelt. Frühere Experimente, den *Drosophila* APC/Fzr aus transgenen Embryos zu isolieren schlugen fehl. Aus diesem Grund wurde eine stabile Zelllinie, die die GFP-getaggte APC/C Komponente Cdc16-MYC-TEV-GFP exprimiert, etabliert. Zusätzlich wurde Fzr in Retikulozytenlysat *in vitro* translatiert und von Baculovirus-infizierten SF-21 Zellen aufgereinigt. APC/C-Fzr-abhängige Ubiquitinylierungsaktivität wurde zum gewissen Ausmaß detektiert, wenn ein mit *in vitro* translatierten Fzr behandeltes Cdc16 Präzipitat eingesetzt wurde.

14 Danksagung

Ein großer Dank gilt meinem Doktorvater Prof. Dr. Frank Sprenger, der mich seit Beginn meiner Doktorarbeit bei all meinen Problemen, die doch hier und da mal aufgetreten sind, großartig unterstützt hat. Sehr geschätzt habe ich seine ständige Hilfsbereitschaft und seine Kompetenz, die mir bei meiner Arbeit im Labor und letztendlich beim Anfertigen dieser Dissertation sehr geholfen hat. Vor allem war es aber seine sympathische Persönlichkeit, die mich nie daran hat zweifeln lassen, meine Promotion in seiner Arbeitsgruppe unter seiner Leitung angefangen zu haben.

Ein weiterer Dank geht an meinen Mentor Dr. Yuu Kimata, der mich bei Problemen und Fragestellungen immer unterstützt hat.

Ein Dank geht auch an meinen Doktoranden-Kollegen Thomas Rössler, der mich bei Fragestellungen unterstützt hat und nebenbei immer mal wieder Schwung in den Alltag gebracht hat. Ohne ihn hätte ich wahrscheinlich nie gewusst, wie viel man doch eigentlich im Labor „fluchen“ kann.

Sehr viel Spaß hat mir auch die Zusammenarbeit mit Christiane Sprenger bereitet. Ihre Gespräche haben mich immer sehr amüsiert und waren eine freudige Abwechslung zum Laboralltag. Außerdem hat sie es immer gewusst, mich bei Problemen aufzumuntern und hat zum Glück die Schokolade immer so versteckt, dass man sie immer finden konnte. Zudem hat mich ihre sorgfältige Arbeit im Labor, vorallem in der Zellkultur, sehr bei meinen Experimenten unterstützt.

Nicht zu vergessen sind natürlich Daniel Bergér und Jan Polz, die es verstanden haben, Arbeit mit einer guten Portion Spaß zu verbinden, und ohne sie viele Tage einfach nur langweilig gewesen wäre. Und mit langweilig meine ich: Keine gemütlichen Bierrunden am Balkon (see Figure 67), keine durch angezündete Papier-Reifen springende Spielzeugautos, keine mit Styropor gefüllte Schubläden, kein Eis zum schlecken von der begehrten „Uschi“, keine festgeklebten Laborutensilien, kein duftender Fisch in Jans Weihnachtskalendertürchen, kein unendlich hoher Leberkassemmelkonsum, kein Battlebots, keine Glücksspiele, usw. …

Figure 67 | Gemütliches Feiertagsbierchen am Balkon … nach einem anstrengenden Arbeitstag
Von links nach rechts: Daniel Bergér, Simon Eder (zur richtigen Zeit am richtigen Ort), meine Wenigkeit und Jan Polz.

Des Weiteren bedanke ich mich bei Frau Dr. Astrid Bruckmann (AG Deutzmann), die mir sehr bei der Durchführung meiner MS-Analysen geholfen hat.

Außerdem möchte ich mich noch bei der AG Sterner und AG Medenbach bedanken, die mich bei vielen Fragenstellungen kompetent beraten haben und ohne deren Hilfsbereitschaft und Unterstützung ich viele Experimente hätte nicht durchführen können.

Ein weiterer Dank gilt auch der gesamten Arbeitsgruppe von Herrn Prof. Dr. Seufert, die mich bei Problemstellungen immer unterstützt hat und zudem ein angenehmes Arbeitsklima geschaffen hat.

Besonders bedanken möchte ich mich auch bei Christina Grasmüller für die wundervolle Unterhaltung im Labor, die rege Ablenkung vom Labor und vor allem für die Unterstützung beim Schreiben der Arbeit.

Zum Schluss möchte ich meinen Eltern danken, die mir das Biologiestudium ermöglicht haben und ohne dessen Unterstützung diese Arbeit wahrscheinlich nicht existieren würde.

15 Eidesstattliche Erklärung

Ich erkläre hiermit an Eides Statt, dass ich die vorliegende Arbeit selbstständig verfasst und keine anderen als die angegebenen Quellen und Hilfsmittel benutzt habe. Die aus fremden Quellen direkt oder indirekt übernommenen Gedanken sind als solche gekennzeichnet. Die Arbeit wurde bisher in gleicher oder ähnlicher Form keiner anderen Prüfungsbehörde vorgelegt und auch nicht veröffentlicht.

Regensburg, den 05.05.2017

_____

Matthias Kies